Non-destructive Testing of Metal Ducted Post-tensioned Bridge Beams using Sonic Impact-Echo Techniques

Julia Martin

PhD - The University of Edinburgh - 1997

Abstract

On 25 September 1992 the Department of Transport (DoT) issued a press notice stating that it would not be commissioning any new grouted duct post-tensioned bridges in England. The decision was taken due to fears that existing grouted duct post-tensioned concrete bridges were badly corroded and could be in a state of imminent collapse. The press notice also announced that existing grouted duct post-tensioned bridges were to undergo detailed inspection. Non-Destructive techniques needed to be developed to allow detailed investigation of these structures. The results of these investigations had to be accurate to a high level of confidence as decisions on repair, renovation or destruction would be made on the findings of the investigation.

This thesis will give the reasons for the DoT's decision followed by an overview of possible non-destructive techniques available at the time of issue. The main body of work carried out investigates the use of the Sonic Impact-Echo method of non-destructive testing. This involves the development of suitable testing equipment and preliminary laboratory and field investigation. Detailed numerical simulations were carried out using the Finite Element Method in order to quantify the probable limits of the Sonic Impact-Echo method. Final laboratory investigations were carried out on a model with known defects. Detailed field testing was carried out on test beams manufactured by the Transport Research Laboratory in Crowthorne and by TBV Stanger in Elstree.

Acknowledgements

The author would like to thank the following people for their help and support throughout her research.

The University of Edinburgh

Acknowledgements go to Professor M.C. Forde for his supervision during the undertaking of the research and writing of this thesis and as Head of Department, for making the University facilities available. Thanks are also due to her second supervisor, Dr. M.S.A. Hardy and to Dr. A. Usmani for their help and encouragement. Mr. K. Broughton's unfailing enthusiasm and assistance are also gratefully acknowledged. The support, both professional and personal, of friends and colleagues in the Department of Civil Engineering ensured my period of study was rewarding and enlightening.

Ove Arup and Partners

Ove Arup and Partners provided industrial sponsorship for the EPSRC Case award and their financial assistance is gratefully acknowledged. Thanks are due to Mr. A.M. Paul and Mr. H. Tomsett for their support during the research period and their continuing help during my subsequent employment. Friends and colleagues at Ove Arup and Partners, Transportation Group 1, have been unfailingly encouraging during the writing of this thesis.

The continuing support of family and friends has been invaluable and was a necessary part of these last four years. Special mention must be made of Simon for his unfailing encouragement in the face of seemingly desperate situations.

Table of Contents

Chapter IV - Preliminary Investigation

Chapter V11 - Field Validation of Developed Testing Method

Chapter V111 - Discussion and Recommended Testing Procedure

Table of Figures

Chapter VII

Chapter I

Introduction

Catastrophic failure of post-tensioned bridges due to the corrosion of prestressing tendons is a possibility. The investigation of many existing bridges is necessary requiring the development of efficient non-destructive testing techniques.

The prestressed and post-tensioned design methods offer the engineer an opportunity to create longer span concrete bridges with much smaller concrete sections (Beckett, 1973). The resulting bridges can form a spectacular addition to a landscape rather than intrude upon it due to the size of the reinforced concrete sections. The advent of post-tensioned bridges also allowed greater spans to be crossed using concrete. Figure 1.1 shows views of the Bloukrans bridge in South Africa and the Kocher viaduct Geislingen in Germany (Brown, 1996). The arch bridge is in the style of Robert Maillard who is considered one of best designers of concrete bridges. The use of post-tensioning systems allowed Maillard's concrete arch bridge design to be used on much longer spans without the fine lines of the bridges being lost.

The principle of prestressing and post-tensioning is quite straightforward. Stress is preimposed on a structure in the opposite direction to that caused by the dead load and other superimposed loads. Using the principle of superposition, the resulting stresses in the structural members are therefore much reduced allowing finer sections to be designed. One drawback of this method is that a large percentage of the strength of the bridge is concentrated in the tensioned tendons. In the case of post-tensioned bridges, these tendons are bundled together into a few discrete ducts. These are then tensioned and the ducts grouted up to bond the tendons to the structure and fill any voids surrounding the tendons, thus preventing water ingress and possible corrosion of the tendons. If the grouting is insufficient, voiding occurs in the duct and, if water ingress occurs, corrosion of the tendons is likely. Catastrophic failure of post-tensioned bridges is therefore possible if tendons in a duct lose a significant percentage of their cross-section due to corrosion. If one tendon fails, the load is transferred to the next tendon. This is likely to stress this tendon to failure and so can lead to sequential failure of the tendons across the bridge until the bridge collapses. This sequence of events is thought to have occurred at Ynys-y-Gwas in Wales in 1985 with the collapse mechanism taking a few seconds from failure of the first tendon to collapse of the bridge (Woodward and Williams, 1988). Further details of the design and possible faults in post-tensioned bridges are discussed in Chapter II.

The aim of the work discussed in this thesis is to investigate available non-destructive testing methods and to develop a promising method to investigate metal ducted post-tensioned bridge beams. The planned programme of work is as follows:

a) Bloukrans Bridge, South Africa

b) Kocher Viaduct, Germany

Figure 1.1 Examples of Post-tensioned bridges

- A desk top survey was carried out into the available testing techniques. Many non-destructive testing techniques have been applied to concrete with varying degrees of success. Some methods offer a high degree of accuracy but their implementation is expensive, complex and, in some cases, hazardous to health. Others are quick and relatively inexpensive to implement but the likelihood of success in detecting voided ducts in concrete is remote (Bungey, 1989). There are many post-tensioned bridges in the UK requiring quick and efficient testing. The major factors in developing a suitable testing method were ease of implementation and high enough resolution to detect voids of approximately 100mm diameter in concrete beams.

- Recent research carried out at the University of Edinburgh has involved extensive use of Ground Penetrating Radar, GPR, (Forde, et al, 1992). This testing system was available to the author and was considered a probable method for the detection of duct location and investigation of the condition of the concrete surrounding the ducts. Plastic ducts have been used in some bridges and in these GPR should be able to be used to investigate the internal condition of the tendon ducts. Earlier research at the University of Edinburgh had investigated the use of sonic impact-echo techniques (Chan, 1987). This method has been used recently to test concrete by a research group based at Cornell University, USA (Sansalone and Carino, 1986) and it was considered a very promising technique for investigating the internal duct condition of metal-ducted post-tensioned bridges.

- A test beam was constructed by the Transport Research Laboratory (TRL) at Crowthorne, UK with known defects. Testing houses were then invited to propose and investigate different testing methods on this and two other post-tensioned bridge beams that had been retrieved from demolished bridges. The author participated in investigations carried out by the University of Edinburgh using GPR and Sonic impact-echo techniques.

- Following the preliminary investigations carried out at TRL the Sonic Impact-Echo method seemed the most promising investigation technique for the straightforward testing of metal ducted post-tensioned bridge beams. The sonic method used previously at the University of Edinburgh was not suitable for detecting the small defects (~ 100mm diameter) found in post-tensioned bridge

beams. The method therefore required considerable adaptation to allow effective testing to be undertaken. The main body of this thesis addresses this task.

- The moratorium on the design of post-tensioned bridges caused considerable disruption to bridge designers and constructors. It was therefore necessary to develop a practical testing method. This research was carried out with assistance from Ove Arup and Partners and Tarmac/TBV Stanger. Part of this assistance was the construction of a laboratory model by TBV Stanger with known defects to be tested once a suitable method had been developed. A laboratory model was also constructed at the University of Edinburgh to enable detailed testing of possible instrumentation and other testing configurations to be carried out as the method was developed.

- 2-D Finite Element, F.E., methods were used to investigate the likely range and limits of the Sonic impact-echo technique. Two different F.E. packages were used: ANSYS ver 5.0a, a commercially available program was used for the initial F.E. models and DYNPAK, (Owen and Hinton, 1980) an F.E. code with the pre-processing software written at the University of Edinburgh (Usmani, 19??) was used for more detailed models.

- A second laboratory specimen was constructed at Edinburgh University to validate the F.E.findings. This model was unreinforced and contained a simple void arrangement.

- The test beams at TRL and TBV Stanger were tested using the developed investigation method. Another investigation method, ultrasonic time-of-flight tomography, was used to reinforce these findings at a number of locations.

The research programme led to the development of a recommended testing procedure for the investigation of post-tensioned bridge beams containing ducts of 100mm diameter or greater. Further research is required to achieve improvements in the performance of the system and ease of implementation on site.

The moratorium on the design of continuous post-tensioned bridges was lifted by the Department of Transport in September 1996. The ban remains in place for bridges of a segmental construction without continuous tendon ducts. Segmental construction offers a rapid and often economical construction method and the development of a

reliable investigation technique could result in the ban on post-tensioned design being fully lifted. Never the less, all new post-tensioned bridges should be designed with an appropriate assessment strategy in place. This strategy should allow for testing and possible maintenance.

Chapter II

The Post-tensioned Bridge Problem

Post -tensioned design methods have been used extensively over the last forty years. This method has many advantages but also some inherrant flaws which are discussed in this chapter.

2.1 History of Post-tensioned Concrete Bridge Design

The classical forms for bridges, the beam, arch and chain have remained unchanged for thousands of years (Beckett, 1973). Masonry and timber were the principal materials of construction until the end of the 18th century. However, the completion of the Iron Bridge, spanning the river Severn at Coalbrookdale in Shropshire, in 1779 heralded the beginning of the use of iron and steel as a major bridge building material. The use of cast iron, wrought iron and eventually steel in bridge building was developed in the 19th century by engineers such as Thomas Telford, Isambard Kingdom Brunel, Robert Stephenson, Gustave Eiffel and Benjamin Baker. Steel construction continued to be the dominant material for long span bridges until the early 1950s.

The use of reinforced concrete in construction began towards the end of the 19th century. Its development was rapid and after a period of around fifty years it was being applied to most engineering structures and dominating the field of small and medium-sized bridges (Komendant, 1952). However, steel was still used in the construction of long-span bridges. The reasons for this were:

i. The dead load of a concrete structure increases approximately with the length of the span squared. Therefore, the cost of this design rises sharply once the span reaches a certain length.

ii. Materials cannot be used efficiently in reinforced-concrete members subject to bending. The area of the beam under tension is disregarded as the tensile strength of concrete is approximately a tenth of the compressive strength. This results in only a third of the cross-sectional area being effective in carrying the bending stress while only a sixth of the cross-sectional area is being used efficiently.

iii. A basic principle of reinforced-concrete is the proper transmission of stresses from concrete to steel. This allows the steel to be considered as an integral part of the beam section. This total bond is provided between the two materials by ensuring a sufficient surface area of steel being covered by a sufficient amount of concrete. However, practical observations suggest that the bond between the steel and concrete is generally insufficient with steel bars having a diameter greater than one inch. This is especially true in the case of a large number of round steel bars arranged in consecutive layers and proves a

severe limitation on the use of conventional reinforced-concrete in the construction of long-span bridges.

After World War II there was a shortage of steel. This led to the rapid development in the use of prestressed concrete.Within twenty years, prestressed concrete became the most widely used construction material for bridges in several countries including the United Kingdom.

2.2 Principles of Prestressing and Post-tensioning

The fundamental principle of prestressing is the induction of stesses in a concrete member before the dead and live loads are applied. In a post-tensioned beam the stresses are induced after the member has been constructed. In both cases the induced stresses act in the opposite direction to those developed by the loading. The resulting stresses in the member can be calculated using the Principle of Superposition and are therefore lower than those induced in a conventionally reinforced member. A prestressed or post-tensioned design gives a more economical stress distribution over the cross-section. Depending on the magnitude of the prestress, the tensile stresses in the concrete can be reduced or even eliminated (see figure 2.1).

Another advantage is that, if the design load on a prestressed or post-tensioned member is exceeded and cracks occur they will be closed when the excess load is removed. Therefore, theoretically, when compared to conventional reinforced-concrete, maintenance costs are considerably reduced and the life of the structure is increased. Steel structures incur high maintenance costs and are sensitive to overloading and vibration. Hence prestressed and post-tensioned concrete was considered a suitable alternative for medium-span bridges.

2.3 Methods of Prestressing Beams

A structural member may be prestressed in two ways:

i. Pretensioned: The steel is positioned and tensioned against exterior anchors. The concrete is then poured around the steel. The steel is released from the anchors when the concrete has gained sufficient strength. In most cases the bond between the steel and the concrete is enough to prevent the steel from returning to its original length. However, when this bond is insufficient anchorage plates must be used. This method was mainly used for prestressing simple beams and was developed by Freyssinet, Wettstein and Hoyer in the late 1920s.

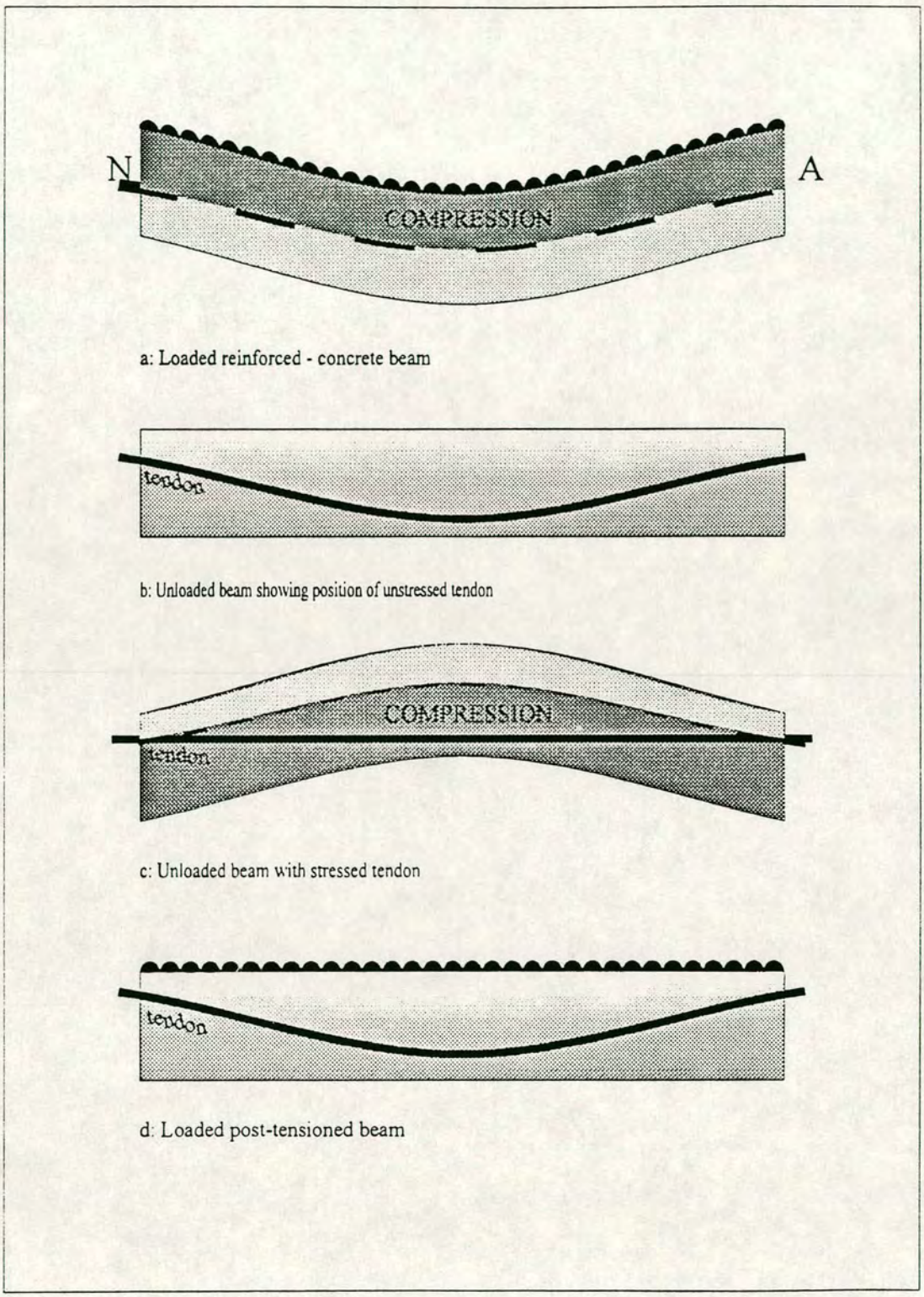

Figure 2.1 Principle of Post-tensioning

ii. Post-tensioned: Ducts or grooves are left in the structural member when the concrete is poured. After the concrete has hardened the prestressing tendons are pulled through these preformed ducts and then tensioned. The ducts are then grouted under high pressure. This is done to establish bond and to prevent corrosion. Another method is to surround the tendons with sheathing prior to pouring. The sheathing prevents a bond forming between the tendon and the concrete. The concrete is then left to cure and, once it is of sufficient strength, the tendon is tensioned using jacks acting against the ends of the member. The steel tendons used in this method usually require specially designed anchorages. The tendons carry large concentrated loads which are transmitted to the concrete member. The transmission of these loads at the anchorage can result in the concrete at this point becoming overstressed. To reduce this effect, large anchorage plates are used. However, the concrete in this area will still be severely stressed and so must be sufficiently reinforced. Post-tensioning was first developed by Dill in 1928 but was developed and implemented mainly by Freyssinet, Wayss and Freytag, Magnel, Roebling Company and Preload Corporation.

2.4 Components in post-tensioned concrete (Waldron 1993)

i. Prestressing Steel. Normally a 7-wire strand up to 15.2mm in diameter is used. These are generally formed into a single cable and threaded and stressed together. A prerequisite for tendons are high strength, large elastic range, low relaxation under loading , reasonable ductility and fatigue resistance.

ii. Anchorages. The steel anchorages are essential in the jacking operation to provide a firm reaction. Once the tendon is tensioned, the anchorages hold the tendon in place if the bond between the tendon and the grout is insufficient. Anchorages tend to be cast within the member to prevent corrosion.

iii. Ducting. Different materials have been used to construct the tendon duct. Corrugated steel ducting is usual in the UK but other metallic and plastic ducts have also been used. The duct must be sufficiently flexible to follow the designed tendon profile and yet robust enough to withstand deformation during the placing of the concrete. The ducting must also be watertight during the initial casting of the concrete. The grout must fill the entire duct and so vents must be

included at any high points along the duct profile to allow for the expulsion of air and water from the tendon duct during the grouting operation.

iv. Grout. The grout must fully cover the tendons to prevent corrosion. Cementitious grout is normally used due to the high alkalinity of the cement which provides better protection against corrosion. Sand is often added to the cement/water mix if the ducts are large. The grout also provides a bond between the concrete and the steel tendon with the ducting thus reducing the stresses induced at the anchorages.

2.5 Advantages and disadvantages of post-tensioned bridge design

The main advantage of this method is that there is no need for a heavy prestressing bed as the tendons are tensioned within the concrete and the jacks act against the actual member being tensioned. The profile of the tendon can be varied along the length of the structure. This is partcularly effective when the beam is continuous over several spans. Post-tensioned members can be manufactured in-situ thus no transportation is required. Much longer spans can therefore be constructed. The concrete is usually much more mature when first loaded, hence the loss of tension due to creep and shrinkage is reduced. The tendons tend to be grouped together so that fewer ducts need be cast and stressed.

This method can create serious defects within the member if the grouting is insufficient and voids are left around the steel tendon. The tendons are usually concentrated into a few ducts resulting in the beam being vulnerable to localised corrosion which could lead to a catastrophc collapse (Waldron, 1993). The high stresses induced in the concrete at the anchorages can also cause defects to form. The detection of defects within post-tensioned beams by non-destructive techniques is the aim of this thesis.

2.6 Problems associated with post-tensioned beams

As mentioned previously voids in the tendon ducts can lead to water ingress to the tendons. The tendons then corrode and, because the strength of the bridge is concentrated in the tendons, severe corrosion can lead to failure of that tendon and possible collapse of the structure. It is likely that this sequence of events led to the collapse of the Ynys-y-Gwas bridge in Wales in 1985.

2.6.2 Collapse of Ynys-y-Gwas post-tensioned concrete bridge

The bridge at Ynys-y-Gwas carried an unclassified road over the River Afan near Port Talbot in Wales (Woodward and Wilson, 1991). It was of single span segmental post-tensioned design (figures 2.2). The bridge deck collapsed without warning at around 7.00am on 4th December 1985. The edge beams carrying the parapet wall and walkway remained in position. There had been no warning signs evident on the structure prior to failure.

2.6.2.1 History and description of bridge

The bridge was constructed in 1953 by the Direct Labour Organisation of the Port Talbot Borough Council. Although unclassified, the bridge was heavily used as it formed an alternative route to a motorway and access to a large housing development. For this reason the bridge was on the West Glamorgan County Council primary winter gritting routes.

The bridge had a clear span of 18.3m and sat on bearing paper on mass concrete abutments. The nine internal beams were of segmental construction - eight precast I-sections made up each beam. The sections were stressed together longitudinally and transversely. The edge box beams were stressed together in a similar fashion. Concrete slabs spanned between the internal beams and the edge beams. The tendon ducts were unlined within each segment but a metal sleeve surrounded the tendons between the segments. The tendon would then have been threaded through the sections and tensioned. The carriageway consisted of a cementitious base with flexible road surfacing. Records show that a bituminous felt waterproofing layer was included in the bridge specification.

2.6.2.2 Inspection history

The bridge had been inspected regularly and thoroughly and no signs of deterioration were recorded. The location of the bridge gave rise to scouring problems and in 1981 was required to carry a load of over sixty tonnes. This accounted for the frequent inspection of the bridge. Thereafter, no problems concerning the structure were identified although the road needed resurfacing and the waterproofing required maintenance.

2.6.2.3 Bridge Collapse

The collapse mechanism is shown in figure 2.3. It can be seen that all nine internal beams failed but the edge beams remained in position despite the forces exerted on them due to the transverse stressing. Most of the transverse tendons failed at the joint between the edge beams and the internal beams. Thus the I-beams failed as a single unit indicating that transverse distribution of the loading occurred up to failure. A detailed investigation into a large section of the bridge was carried out by the Transport and Road Research Laboratory (TRRL).

2.6.2.4 Investigation Findings

Some tendons were found to be severely corroded at the point where they crossed the joints between segments. Chlorides were discovered over the concrete surface and had penetrated into the joints between the segments. The concentration of chloride was lower in the edge beams than in the internal I beams. It was concluded that chlorides from the de-icing salts were the main cause of corrosion of the tendons. The tendons continued to corrode at the joints until the beam could no longer support the imposed load. The strain imposed on the tendon wires would increase as the cross-sectional area reduced. Traffic on the bridge would cause fluctuations in the strain which at times could exceed the failure strain for a wire and cause that wire to fail. The load would then be transferred to adjacent wires.

It is possible that a large vehicle could have caused a number of wires to break bringing that tendon almost to a state of collapse. No vehicle was on the bridge at collapse but if the bridge was left in a state on the brink of collapse it is possible that subsequent creep, bond failure and load redistribution may have caused the tendon to fail. The load on this tendon would then be transferred to an adjacent tendon which could then also fail causing the load to be transferred to the next tendon and so on across the bridge.

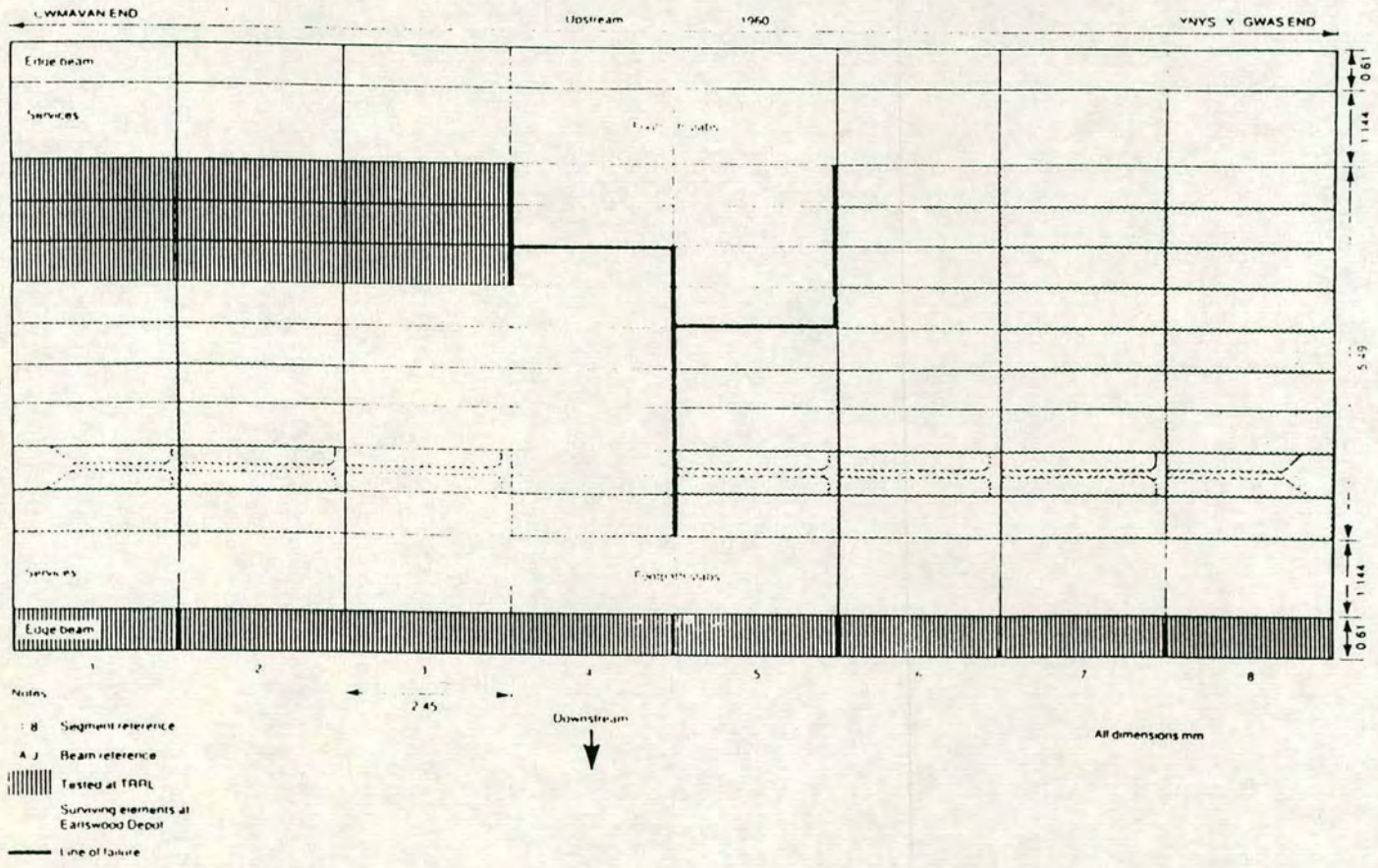

Figure 2-3 Deck Layout of Ynys-y-Gwas bridge showing the line of failure

The bridge failed early in the morning (at approximately 7.00am). The effective bridge temperature would be at a minimum and it is possible that temperature effects may have been the deciding factor. The ends of the beams rested on bearing paper which would give considerable frictional restraint and would act to hold prestress in the structure. As the temperature dropped the beam would shrink and so the prestress would also reduce. Simple calculations showed that a small reduction in temperature (approximately 1 degree centigrade) would be enough to overcome friction. However, any additional restraining effect of the fill behind the beams was not taken into account. A larger drop in temperature may well have been required to overcome the total restraining friction.

2.6.2.5 Consequences of findings

In the case of post-tensioned concrete bridges a Principal Inspection may not be adequate to ascertain the state of the bridge. A principal inspection was carried out at Ynys-y-Gwas and so all parts of the bridge had to be accessed and inspected. However no signs of distress were noticed. A principal inspection requires an estimate of the remaining sectional area of steel to be made. This was not possible on a bridge of that design at that time. It was decided that inspections of post-tensioned bridges should include a check against features similar to those of the bridge at Ynys-y-Gwas. These features included:

- segmental construction
- narrow infilled joints between segments
- no reinforced concrete deck slab
- transverse stressing
- location
- regular winter gritting
- date of construction

One existing method for testing the corrosion risk was to measure the chloride concentrations at and around the joints between segments. However, this did not provide conclusive information and it was recommended that improved testing techniques should be developed. The Dept. of Transport issued a moratorium on the use of post-tensioned beams in the design of bridges it

may commission (DoT press notice, 1992). The initial ban covered all post-tensioned design, however, in September 1996 the total ban was relaxed and continuous post-tensioned design was allowed. The ban on the design of segmental construction with discontinuous ducting remains pending the development of suitable testing or corrosion prevention methods.

2.7 Conclusions

The post-tensioned beam design method offers an effective and economic way of constructing medium span bridges. However, there existed some problems inherent in this method:

i. Voids may occur in the ducts where grouting has been inadequate.

ii. Water and chlorides from deicing salts may have penetrated these voids allowing corrosion of the tendons to take place.

iii. Existing assessment techniques were not adequate to determine the level of structural integrity. It was therefore possible for collapse to take place without any warning.

Chapter III

Post-tensioned Bridge Investigation Techniques

Many non-destructive techniques have been applied to test concete structures with varying degrees of success. An investigation into available methods was undertaken and a promising method for the investigation of post-tensioned bridge beams was identified for further development.

3.1 Introduction

A variety of different investigation techniques have been applied to post-tensioned bridges. The most promising can be categorised under three main headings.

i. Visual inspection and intrusive methods
ii. Electromagnetic investigation methods
iii. Elastic wave methods

Before any investigation method is undertaken all existing information about the bridge construction and past inspections should be researched. A detailed visual inspection is also required (Tomsett and Millar, 1995). Obvious signs of distress can be discovered although one of the major problems with post-tensioned bridges is that no signs of distress may be visible despite the fact that the bridge may be in a state of dangerous disrepair. However, any signs of chloride ingress or other problems in the bridge sections should be carefully monitored as these may indicate possible problems within the tendon ducts.

3.2 Intrusive methods

Endoscopy is an intrusive method that has been widely applied. The tendon ducts are identified and an access channel for the endoscope carefully drilled (Johnson, M.A.E. and Fifield, B.E. 1993). The endoscope is then fed along the duct and any defects noted. The main advantage of this method is that the state of the steel tendons can be directly investigated. Any corrosion is instantly identified. However, this method is intrusive and requires specialist drilling and investigation. Great care must be taken to avoid damaging the tendons. The above difficulties result in this method being time consuming and expensive.

3.3 Electromagnetic investigation techniques

Two methods have been widely applied to investigating post-tensioned bridges:

i. Ground Penetrating Radar
ii. Radioactive Techniques

Ground penetrating radar has been successfully used by the author and Nyall McCavitt of Edinburgh University to test unducted and plastic ducted post-tensioned bridge beams for TRL (Transport Research Laboratory). This method has also been applied to the testing of segmental post-tensioned bridges (Cooke et al, 1993).

3.3.1 Ground Penetrating Radar (GPR)

The term Ground Penetrating Radar refers to the range of electromagnetic techniques for the identification of buried objects or interfaces in the upper surface of the earth. The subject is largely applications-oriented and different types of equipment have been developed suitable for use with different types of target and covering material.

Ground penetrating radar theory is reasonably well understood and there have been many papers written on the subject (Daniels, et al. 1988; Ulriksen, 1982; McCavitt and Forde, 1992; Bungey et al. 1993).

3.3.1.1 Basic Radar Theory

The antenna transmits an electromagnetic wave which travels into the structure. The velocity of the wave depends upon the material through which it is travelling. If the wave reaches a material interface, produced by adjacent materials with different electrical properties, a proportion of the wave will be reflected and a proportion transmitted. The amount of reflection and transmission is dependent on the relative electromagnetic properties of the two materials. The moisture content of the material can greatly affect the electromagnetic properties. Most Civil Engineering materials encountered are, with the exception of metals, low-loss dielectrics, i.e. non-magnetic materials.

The velocity of propagation of the wave through a medium is given by:

$$_m = \frac{C}{\sqrt{\varepsilon_r \mu_r}} \qquad (3.1)$$

where: V_m = Vel. of propagation
C = Vel. of electromagnetic wave in Free Space
ε_r = Relative dielectric constant
μ_r = Relative magnetic permeability = 1 for low-loss dielectrics

The amount of reflection and transmission at an interface is given by:

$$R = \frac{\sqrt{E_1} - \sqrt{E_2}}{\sqrt{E_1} + \sqrt{E_2}}$$

$$T = \frac{2\sqrt{E_1}}{\sqrt{E_1} + \sqrt{E_2}}$$

$$\sigma_q = E\varepsilon_q = E\frac{\partial u_q}{\partial q}$$

σ_q = stress in q direction
E = modulus of elasticity
ε_q = strain in q direction

(3.2)

where R = Reflection Coefficient

$$T = \frac{2\sqrt{E_1}}{\sqrt{E_1} + \sqrt{E_2}} \qquad (3.3)$$

where T = Transmission Coefficient

3.3.1.2 Antenna

Antennae of different frequency are used for different testing requirements. A high frequency signal will produce a detailed survey but will not penetrate deeply into the material. A lower frequency signal will give a less detailed survey but will penetrate further. Detailed surveys are required when testing post tensioned beams. The beams tend to be fairly small with the cover to the tendons usually less than 300 mm. This enables high frequency antennae, 900 MHz and 1 GHz, to be used.

Concrete is an inhomogeneous material. Signal clutter can arise due to small, scattered reflections from the larger aggregates. To the reduce this effect, the antenna selected should be have a dominant signal wavelength at least five times the size of the largest aggregate (Padaratz and Forde, 1995).

Steel has a much higher electromagnetic impedance than concrete and results in a reflection of opposite phase to the incident wave. Air has a relatively lower electromagnetic impedance than concrete and results in a reflection of the same phase as the incident wave. Total reflection occurs at a boundary with steel. If the tendon ducts are made of steel the electromagnetic wave will be totally reflected and no energy will penetrate the duct. It will therefore be impossible to determine the condition of the grouting and tendons within the duct.

Metallic ducts can also be located accurately under certain concrete reinforcement conditions. If the rebar is spaced closely together and a radar antenna of a frequency resulting in a wavelength longer than the bar spacing is used, the rebar layer will appear to give a total reflection of the wave, the position and condition of the duct will therefore not be distinguishable. If there are many layers of rebar the large reflections from these may result in insufficient energy propagating into the region of the duct and then being reflected back through the reinforcement for detection. The area around the anchorages is likely to be heavily reinforced and so location in this area is unlikely.

Ground penetrating radar is a suitable technique for investigating plastic-ducted and unducted tendon ducts but most post-tensioned bridge beams contain metallic ducts and so its use is severely restricted.

3.3.2 Radiographic Techniques

Electromagnetic radiation investigation methods have been applied to post-tensioned bridge inspection with considerable success (Kear, P. and Leeming, M. 1994). The frequencies used are very high (between 10^{18} Hz and 10^{24} Hz)(Sears, F.W. et al 1982) and the wavelengths correspondingly short so particle theory is applicable rather than wave theory. The radioactive rays can then be considered to pass through the structure. The testing set-up can be in the form of a through test or an echo-test. The intensity of the radiation decays exponentially with distance, x travelled giving: (Jones, R. 1962);

$$S(x) = S_0 e^{-\alpha x} \qquad (3.4)$$

where $S(x)$ = Intensity of radiation at x

S_0 = Intensity at source

α = Mass coefficient of absorption (mass per unit area)

For materials such as concrete, the important form of absorption is due to the loss of energy of the radiation to the outer electron of the atom. The amount of energy loss is maximum for radiation scattered back towards the source. In practice, the source - detector geometry is designed to ensure the intensty of the back-scattered radiation decreases approximately linearly with increasing material density.

Gamma-radiography was first used to test concrete by Whiffin in 1954, in which reinforcement position was determined. In 1958 Forrester developed a basic technique for investigating the condition of concrete and the position of the reinforcement that is still used today. A source was held a set distance from the front face of the concrete and a standard X-ray film was held against the back surface. The radiation travelling through the structure then developes the film. The amount of radiation penetrating the structure at a particular section will govern the amount of development on the film at that point. The radiation is electromagnetic and so will be reflected by a metallic boundary, however, total reflection does not occur at the thin steel ducts (approximately 1mm thick) as some particles will penetrate the ducting by passing between the steel molecules. A particle counter may be used instead of a film to detect the radiation penetrating the structure. The exposure time required is dependent on the strength of the source and the thickness of the structure. A two-dimensional picture of the section is then produced. One limitation of this method is that if a voided duct is situated behind a sound tendon duct, the voided duct would not be detected (Stain and Dixon, 1993). However, three-dimensional representation can be produced using orthogonal planes. Individual strands of the tendon can usually be identified and any loss of section caused by corrosion detected.

In France the system, SCORPION, has been developed which is fitted to a vehicle and can be lowered over the side of bridges to be inspected. This system uses a high energy gamma source which reduces the necessary exposure time. However, the radiation hazard involved are considerable and extensive safety precautions are necessary. This will almost certainly involve

bridge and surrounding road closure - a 250m exclusion zone is required with this method (Leeming et al, 1995). The equipment is large, cumbersome and specialist knowledge is required to use the system safely and effectively which results in this method being very expensive.

A lower energy source, the BETATRON has undergone trial investigations of post-tensioned bridges. The safety precautions, although considerable, are less extensive than for the SCORPION - the exclusion zone with this source is 70 m. This system is much smaller and therefore more mobile, the source can be carried by two people and access to difficult bridge geometries is possible. However, the exposure times involved are much longer and for exposures greater than 600mm (which requires approximately 30 minutes exposure), the exposure time approximately doubles for every extra 100mm penetration. It has also been necessary to rigidly attach the equipment to the structure to avoid blurred images which makes the technique more time consuming and cumbersome. Specialist knowledge is also required and road closure would be necessary for most bridge inspections. Again this system is relatively expensive.

The health risks and the cost involved in both systems make these techniques unsuitable for the majority of inspections but could be very useful under specific circumstances. A bridge on a major road thought to be in a critical state of disrepair could be investigated using this method. It is especially suitable for investigating structural members containing dense reinforcement.

3.4 Elastic Wave Investigation

Elastic waves of different frequency can be introduced into a structural member using mechanical impact, vibrating mass or sound source. This type of investigation can be divided into two separate methods: ultrasonic investigation, similar to medical techniques and; sonic investigation, which has been successfully used to non-destructively investigate pile foundations since the 1970s (Davis and Dunn, 1974). Elastic wave investigation comprises of the introduction of an excitation force into a structural member and subsequent measurement of the structural response. The arrangement of excitation force and response transducer can be configured in one of three ways: direct transmission; indirect transmission or; impact-echo (see figure 3.1).

3.4.1 Ultrasonic Investigation

Ultrasonic investigation introduces a narrow frequency-band input using a vibrating source. The frequencies used typically range from 50kHz to 300kHz. Ultrasonic investigation is successfully used to investigate homogeneous materials such as metals and the use of high frequency enables accurate measurements to be made. However, the inhomogeneous nature of concrete introduces noise due to 'grain scatter' (Langenberg et al, 1995) at high frequency which can mask the measured response. The effect of this scatter is subject to debate but is thought to be exaggerated in concretes with large diameter aggregate (up to 32mm). Simple ultrasonic investigation systems are readily available.

PUNDIT (or digital testers) can be used in any of the testing arrangements and the travel time of the wave from transmitter to reciever gives an indication of the condition of the concrete. Tomographic techniques can now also be used to give a more detailed picture of the condition (Gheshlaghi et al, 1995).

Recently more sophisticated ultrasonic investigation systems have been developed including movable scanning devices and transducer arrays (Gaydecki, Glossop and Burdekin, 1995). Sophisticated signal processing is available to reduce any noise caused by scatter and two and three dimensional plots (B- and C- scans) can be produced (Schickert, 1995) which give readily analysed information. However, high frequency signals suffer a high degree of attenuation and so the depth of penetration is reduced. Currently, penetration up to about 400mm can be achieved.

3.4.2 Sonic investigation

Sonic investigation introduces a broad band frequency input at lower frequencies (0Hz to 30 kHz) and mechanical impactors offer the most popular method of excitation. Impactors of different masses are used depending upon the size and geometry of the structure to be tested. A large impactor will introduce a force of high energy but low frequency and would be used to test large structures for large defects. A smaller impactor would introduce an excitation of lower energy but containing higher frequencies and would be used to test smaller structures where smaller defects were to be identified.

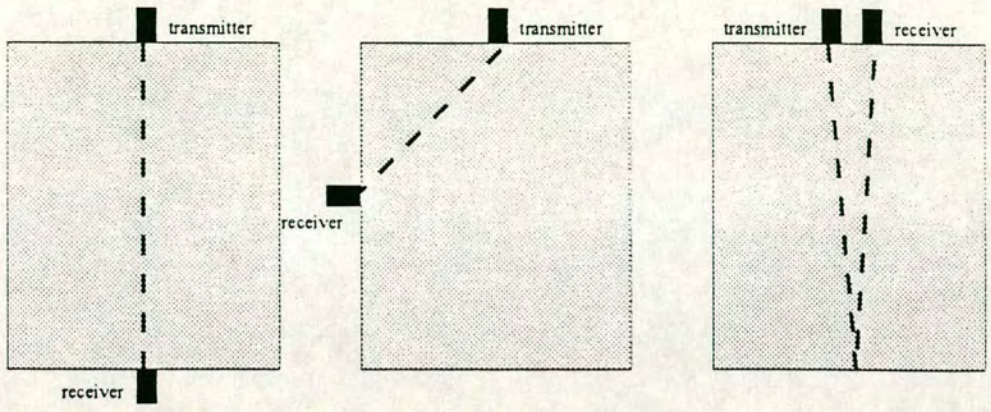

Figure 3.1 Transducer arrangements for stress wave testing

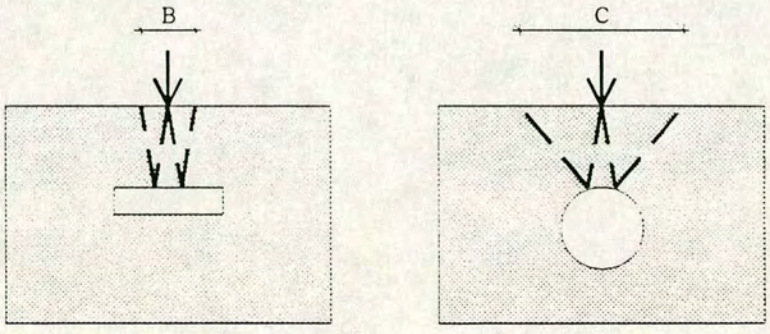

Figure 3.2 Effect of wave scattering from circular defect

As with ultrasonic investigation, sonic investigation can be carried out as a transmission test, indirect test or impact-echo test. Much research into sonic impact-echo testing of concrete has been carried out at Cornell University, Ithaca, USA since the 1980s (Carino and Sansalone, 1984). This research has resulted in an impact-echo system, the DOCter, being developed for commercial testing by Germann Instruments. Sonic impact-echo has been found to be very successful in the investigation of planar defects and in determining the geometry of concrete structures (Carino, Sansalone and Hsu, 1986, Sansalone, M. and Carino, N.J. 1989). Research into the use of impact-echo as an investigation technique for void detection in tendon ducts of post-tensioned bridges has been carried out with some success (Sansalone, M. and Carino, N.J. 1988). It was discovered that reflections from voids could be identified by this method and a subsequent study was commissioned by the National Bureau of Standards into possible investigation techniques for post-tensioned bridges (Ghorbanpoor, 1993) at the University of Wisconsin-Milwaukee. The most promising investigation method was found to be sonic impact-echo, although several different conclusions were drawn from this research when compared to that at Cornell. This research concluded that, due to the cylindrical nature of the ducts, the incident elastic waves would be widely scattered and so no reflection directly from the surface of the void would be detected at the impacting surface (see figure 3.2).

Voids can be detected by analysing the signal reflected from the base of the beam. The longer the time until the arrival of the wave reflected from the base, the larger the void within the duct. This assumes the surrounding concrete to be in a uniform condition throughout the structural member. It was felt that sonic impact-echo offered a promising investigation technique for metal-ducted post-tensioned bridge beams but that considerable research was required to determine the suitablilty of this method and to determine its limitations. The remainder of this thesis is dedicated to this task.

3.5 Elastic Theory of Wave Propagation in a solid medium

3.5.1 Stress Waves in Infinite Solids

Materials behave elastically when loading conditions result in stresses below the yield point (Zukas et al, 1982). Elegant mathematical solutions have been produced for specific loading conditions in the elastic region.

In the classical theory of impact, stereomechanics, colliding objects are regarded essentially as single points, i.e. both objects are instantaneously subjected to the same change of motion as the result of an impact (Goldsmith, 1960). However, in reality, the disturbance generated at the point of impact propagates through the colliding bodies with a finite velocity. It is reflected at material boundaries which produce oscillation or vibration in the objects. Local transient deformations and stresses created by this disturbance cannot be calculated using stereomechanics and so must be investigated using wave theory.

This is developed by firstly examining the impact of objects with simple geometries. Only the transfer of mechanical energy will be discussed. The effects of light, heat and sound produced at impact are ignored as these terms account for a small fraction of the total energy involved in the process.

Stereomechanical theory is seriourly in error when a significant proportion of the energy involved is converted into vibrations. The impact-echo investigation technique arises by studying wave phenomena resulting from an impact on the test object. It is initially assumed that the stresses introduced to the test specimen are small and so the wave behaviour is that in an elastic solid.

3.5.2 Wave Transmission in an Elastic Solid

The mathematical formulation of one-dimensional wave transmission in a solid is dependent on the geometry and material properties of the colliding objects. The elastic solid is regarded as a linear spring with stress proportional to strain:

$$\sigma_q = E\varepsilon_q = E\frac{\partial u_q}{\partial q} \tag{3.5}$$

where

σ_q = stress in q direction

E = modulus of elasticity

ε_q = strain in q direction

The modulus of elasticity has been found to be nearly independent of the rate of loading (Sternglass, 1953).

The wave equations are derived by a combination of three dimensional stress-strain relations, compatibility conditions and the equations of motion. The sum of the three orthogonal normal strains is termed the dilatation, Δ, representing unit volume expansion. In addition, rotation generally results in shearing strain, γ_{ij}, being produced (see figure 3.3).

The shear strain is the total angular deformation and for small deformations:

$$\gamma ij = \frac{\partial u_i}{\partial q_j} + \frac{\partial u_j}{\partial q_i} \quad i,j = 1,2;\ 2,3;\ 3,1 \tag{3.6}$$

The corresponding shear stress, τ_{ij} is linearly related to this shear strain by G, the modulus of shear rigidity.

For a rectangular coordinate system x,y,z the normal strains, shear strains, dilatation and rotations are;

$$\varepsilon_x = \frac{\partial u_x}{\partial x} \qquad \varepsilon_y = \frac{\partial u_y}{\partial y} \qquad \varepsilon_z = \frac{\partial u_z}{\partial z}$$

$$\gamma_{xy} = \frac{\partial u_y}{\partial x} + \frac{\partial u_x}{\partial y} \qquad \gamma_{yz} = \frac{\partial u_z}{\partial y} + \frac{\partial u_y}{\partial z} \qquad \gamma_{zx} = \frac{\partial u_x}{\partial z} + \frac{\partial u_y}{\partial x}$$

$$\Delta = \frac{\partial u_x}{\partial x} + \frac{\partial u_y}{\partial y} + \frac{\partial u_z}{\partial z}$$

$$2\varpi_x = \frac{\partial u_z}{\partial y} - \frac{\partial u_y}{\partial z} \qquad 2\varpi_y = \frac{\partial u_x}{\partial z} - \frac{\partial u_z}{\partial x} \qquad 2\varpi_z = \frac{\partial u_y}{\partial x} - \frac{\partial u_x}{\partial y}$$

(3.7)

The relationship between stress and strain for homogeneous isotropic media will contain only two independent elastic parameters:

$$\sigma_i = \lambda\Delta + 2G\varepsilon_i \tag{3.8}$$

$$\tau_{ij} = \tau_{ji} = G\gamma_{ij} = G\gamma_{ji} \tag{3.9}$$

where λ and G are Lamé constants.

$$\lambda = \frac{\nu E}{(1+\nu)(1-2\nu)} \tag{3.10}$$

The equations of motion are then derived from a force balance of the stresses on an elemental volume.

For the situation with no body forces;

$$\begin{aligned}
\frac{\rho\partial^2 u_x}{\partial t^2} &= \frac{\partial\sigma_x}{\partial x} + \frac{\partial\tau_{xy}}{\partial y} + \frac{\partial\tau_{xz}}{\partial z} \\
\frac{\rho\partial^2 u_y}{\partial t^2} &= \frac{\partial\tau_{yx}}{\partial x} + \frac{\partial\sigma_y}{\partial y} + \frac{\partial\tau_{yz}}{\partial z} \\
\frac{\rho\partial^2 u_z}{\partial t^2} &= \frac{\partial\tau_{zx}}{\partial x} + \frac{\partial\tau_{zy}}{\partial y} + \frac{\partial\sigma_z}{\partial z}
\end{aligned} \tag{3.11}$$

The displacement equations of motion can be determined by substitution of the above;

$$\begin{aligned}
\frac{\rho\partial^2 u_x}{\partial t^2} &= (\lambda + G)\frac{\partial\Delta}{\partial x} + G\nabla^2 u_x \\
\frac{\rho\partial^2 u_y}{\partial t^2} &= (\lambda + G)\frac{\partial\Delta}{\partial y} + G\nabla^2 u_y \\
\frac{\rho\partial^2 u_z}{\partial t^2} &= (\lambda + G)\frac{\partial\Delta}{\partial z} + G\nabla^2 u_z
\end{aligned} \tag{3.12}$$

where $\nabla^2 \equiv \left[\frac{\partial^2}{\partial x} + \frac{\partial^2}{\partial y} + \frac{\partial^2}{\partial z}\right]$ the second Laplacian operator.

If initial and boundary conditions are known, the solution of the above equations determines the history of the disturbance at any point.

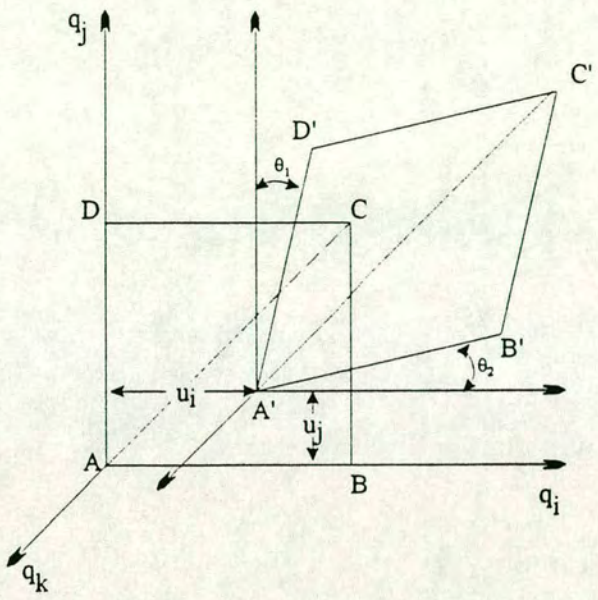

Figure 3.3 Shear strain in a plane element

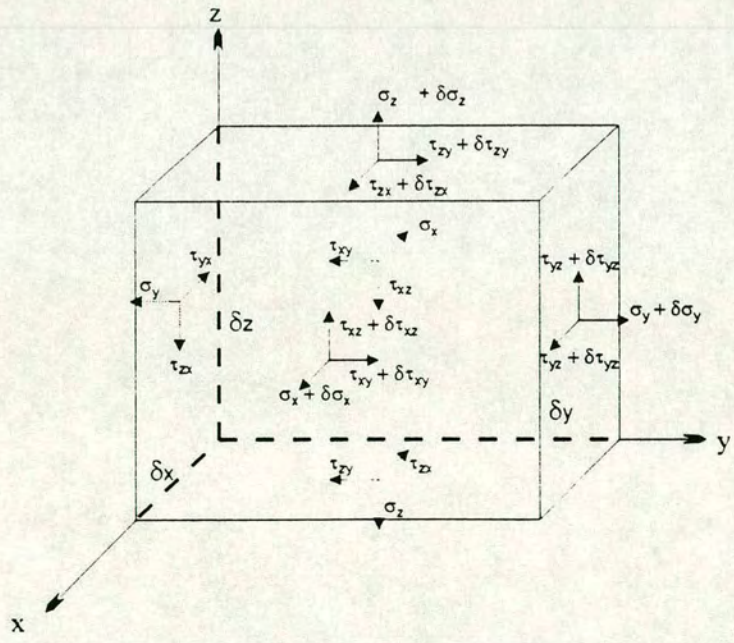

Figure 3.4 Stresses acting on an Element of Volume

If both sides of the above equations are differentiated with respect to x, y and z respectively and the results added, the following equation is obtained (Love, 1944):

$$\rho\delta^2\Delta/\delta t^2 = (\lambda + 2G)\nabla^2\Delta \quad \text{or} \quad \delta^2\Delta/\delta t^2 = V_c^2\nabla^2\Delta \tag{3.13}$$

where $_c^2 = (\lambda + 2G)/\rho$

Therefore, Δ is propagated with velocity V_C. That is, the dilatational wave (compression wave) travels at velocity, V_C.

Expressing the displacement equations of motion in terms of rotation yields the following;

$$\rho\delta^2\varpi_i/\delta t^2 = G\nabla^2\varpi_i \quad \text{or} \quad \delta^2\varpi_i/\delta t^2 = V_s^2\nabla^2\varpi_i \tag{3.14}$$

where $_s^2 = G/\rho$ i = x, y, z.

Therefore, the rotation (shear wave), ϖ_i, is propagated with velocity V_S.

The above shows that elastic waves can propagate with two different speeds in an unbounded and homogeneous solid. The 'characteristic equation' for elastic wave propagation in solids is:

$$\delta^2\phi/\delta t^2 = V^2\nabla^2\phi \tag{3.15}$$

where $^2 = (\lambda + 2G)/\rho$ for dilatational waves and $^2 = G/\rho$ for rotational waves.

Rewriting the above velocity equations in terms of ν and E gives:

$$_c^2 = E(1-\nu)/[\rho(1+\nu)(1-2\nu)] \tag{3.16}$$

and

$$_s^2 = E/[2\rho(1+\nu)] \tag{3.17}$$

For normal weight concrete, $\nu = 0.2$. This gives the ratio of V_S to V_C as 0.612. That is the shear wave travels at 61.2% of the velocity of the compression wave.

There exist three idealised shapes of wavefronts which may travel through a structure: planar, spherical and cylindrical. Planar waves are produced by a flat vibrating mass, mounted on a rigid platform. Such waves would radiate on a liquid surface. For a point impact dilatational and rotational waves propagate into the solid on spherical wavefronts and a line source will produce cylindrical wavefronts radiating from this source (Love, 1944). Spherical and cylindrical wavefronts diverge as they propagate through the medium and at a distance from the source the wavefronts appear nearly planar and exhibit the acoustic characteristics of a planar wave.

3.5.3 Surface Waves

In addition to waves propagating into a solid after impact, stress waves are set up across the surface of the solid. These surface waves, Rayleigh Waves, propagate at a velocity related to the shear wave velocity of propagation (Ghorbanpoor, 1993):

$$V_R = k_1 V_S \tag{3.18}$$

where

$$k_1^6 - 8k_1^4 + (24 - 16\alpha_1^2)k_1^2 + (16\alpha_1^2 - 16) = 0 \tag{3.19}$$

and

$$\alpha_1^2 = \mu/(\lambda + 2\mu) = (1 - 2\nu)/[2(1 - \nu)] \tag{3.20}$$

$\nu \approx 0.2$ for normal weight concrete. This gives $k_1 = 0.911$, i.e. surface waves travel at 91.1% of shear waves.

Rayleigh wave propagation causes elliptical particle displacement. The period of this displacement is the same as that of the impact signal. This result is important in determining the duration of the impact signal and therefore the cut-off frequency if the actual impact is not directly measured. An

approximation of the contact time can be made from the resulting response of the structure. This phenomenon will be investigated more fully in chapters V and VI. The amplitude of the displacement caused by Rayleigh wave propagation decreases exponentially with depth in the direction normal to the surface. Higher frequency Rayleigh waves attenuate more rapidly with depth than lower frequency waves.

3.5.4 Wave propagation across a material boundary

Incident waves on a material interface can be considered in the same manner as light rays. The stress waves can be visualised as travelling along ray paths and reflection and refraction occur as for a light ray propagating across a material boundary (Carino and Sansalone, 1984). See Figure 3.5.

Spherical stress waves are reflected as spherical waves. The angle of refraction, β, is dependent on the angle of incidence, θ, and the relative wave velocities in the different materials. This relationship is given by Snell's law.

$$\sin\beta = (C_1/C_2)\sin\theta \tag{3.21}$$

where C_1 and C_2 are the wavespeed through material 1 and 2 respectively.

An unusual property of stress waves is that the mode of propagation can change completely or partially upon reflection at an interface. Depending upon the angle of incidence, compression waves can be partially reflected as both compression and shear waves, or even as a surface wave. Shear waves travel at a lower velocity than surface waves and so the angle of reflection of an incident compression wave which has been mode converted will be smaller than that of an incident compression wave which has not been mode converted. If the angle of incidence is zero, i.e. normal incidence, no mode conversion takes place (Ghorbanpoor, 1993).

The amount of reflection at a material boundary is dependent on the relative difference in material properties, the angle of incidence, the dimensions of the interface and the orientation of the interface. A large reflection will occur if there is a large difference in material properties and a small reflection will occur if there is a small difference in material properties (Ghorbanpoor 1993).

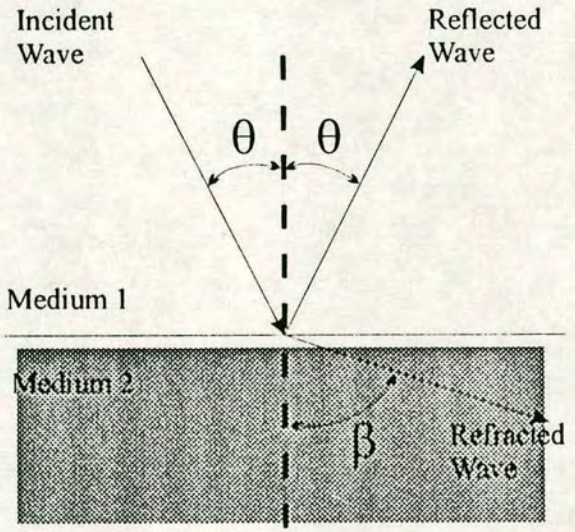

$$\frac{\sin\theta}{C_1} = \frac{\sin\beta}{C_2}$$

(a) Reflection and Refraction

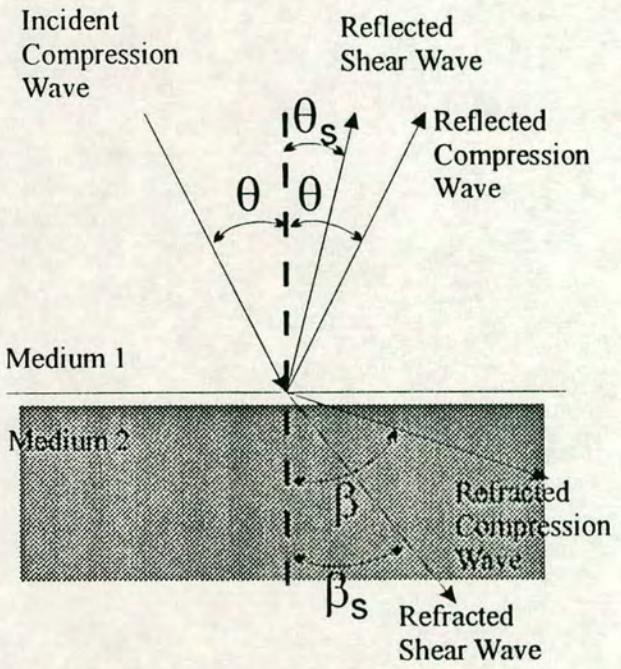

$$\frac{\sin\theta}{C_{p1}} = \frac{\sin\beta}{C_{p2}} = \frac{\sin\theta_S}{C_{s1}} = \frac{\sin\beta_S}{C_{s2}}$$

(b) Mode Conversion

Figure 3.5 Behaviour of elastic waves at a material interface

Total reflection will occur at a solid boundary with air as the difference in material properties is very large. For normal incidence of pure compression or pure shear waves on an infinite, flat boundary,

$$A_R = A(\rho_2 C_2 - \rho_1 C_1)/(\rho_2 C_2 + \rho_1 C_1) \qquad (3.22a)$$

and

$$A_T = A(2\rho_1 C_1)/(\rho_2 C_2 + \rho_1 C_1) \qquad (3.22b)$$

where

A = Initial wave amplitude
A_R = Amplitude of reflected wave
A_T = Amplitude of transmitted wave
$\rho 1$ = Mass density of initial material
$\rho 2$ = Mass density of second material
C_1 = Wavespeed through initial material
C_2 = Wavespeed through second material

3.5.5 Effect of angle of incidence

As the angle of incidence increases the relative reflections change. Figure 3.6 shows the relationship between different reflections and the angle of incidence for a plane wave at concrete/air interface (Carino and Sansalone, 1984). Although these figures are not directly applicable to the wave propagation produced by a point impact a good indication of the effect of the angle of incidence is given. The figures show the following information:

Top left graph:	Amplitude of reflected wave of same mode
Bottom right graph:	Amplitude of reflected mode converted wave
Top right graph:	Angular relationship between incident wave and reflected, mode converted wave. (Snell's law)

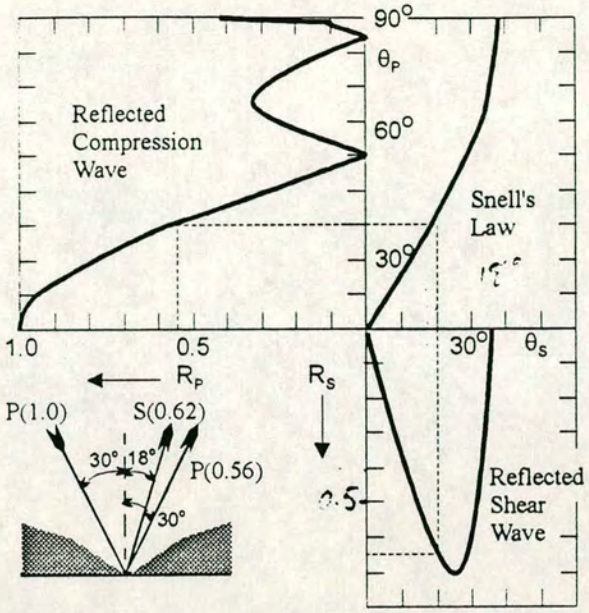

Figure 3.6a Reflection coefficients for an incident compression wave

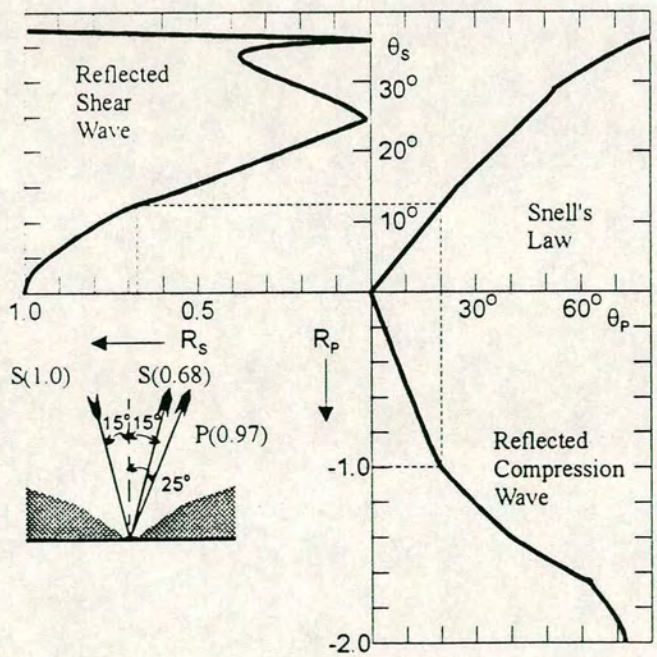

Figure 3.6b Reflection coefficients for an incident shear wave

It can be seen that for an incident dilatational wave, the maximum reflected dilatational wave occurs if the angle of incidence is zero. The maximum reflected mode converted (shear) wave occurs with an incident angle of approximately 45°. The relative amplitude and angle of all the waves reflected at an interface can be estimated from the figures.

3.5.6 Diffraction and Scattering

The above section describing reflection is applicable to plane boundaries. If however, the material interface is not planar, diffraction and scattering of the wave can occur, that is, the wavefronts will not follow the paths expected with refraction and reflection. Diffraction occurs when the incident wave intersects the sharp edge of a discontinuity, e.g. a rigid barrier or a crack tip. In this case, spherical waves are produced with their origin at the crack tip, see figure 3.7 (Sommerfield diffraction problem). Compression waves and shear waves produce both spherical diffracted compression and shear waves when incident on a crack tip or similar situation. It should be noted that the zone directly beneath the discontinuity can be penetrated by the diffracted waves. These waves have been shown to exist using photoelasticity. Research has shown that the magnitude of diffracted waves produced at a crack tip are approximately one tenth of the magnitude of reflected waves. However, they can still be detected and are a useful method for detecting cracks in concrete which are orientated at an unfavourable angle for detection by reflected waves (Graff, 1973). Figure 3.2 shows how scattering occurs when waves are incident upon a non-planar surface; when the interface is planar the energy reflected from the portion of the incident wave shown in the figure is dispersed over a region of width B. However, if the interface is circular in section, the energy reflected from the same region of the incident wave is scattered and is now dispersed over the region C. C is a much larger region than B and so the energy reaching the response transducer on the surface from the circular interface is much less than that detected at the response transducer from a planar interface. In some cases, insufficient energy may be reflected for detection at the surface. Most ducts used in post-tensioned bridge beams are circular in section and so detection of these ducts and of possible flaws within the ducts is made more difficult.

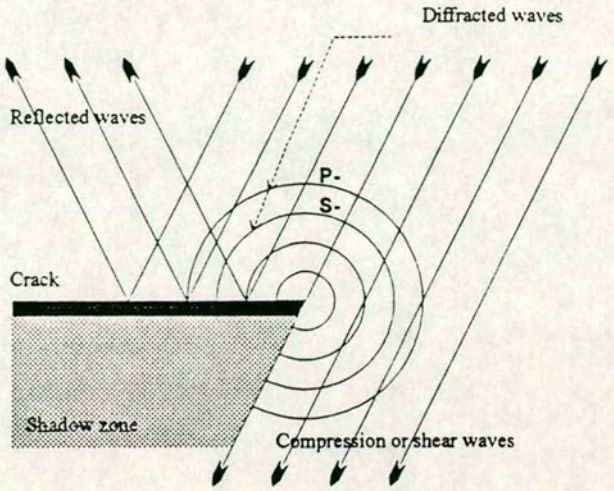

Figure 3.7 Diffracted waves at crack tip

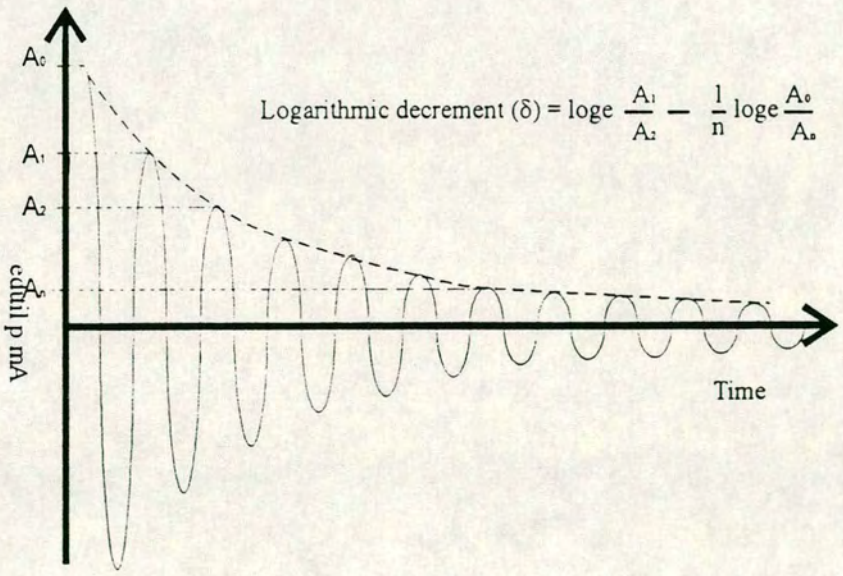

Figure 3.8 Coefficient of Attenuation

3.5.7 Attenuation and Divergence

As elastic waves propagate through a solid medium they lose energy due to attenuation and divergence. Attenution is caused by scattering and absorption of the stress wave. Concrete is an inhomogeneous material. It is made up of aggregate bound by cement paste. The individual pieces of aggregate generally have a higher density and elastic modulus than the cement paste. This gives rise to reflection, refraction, diffraction and mode conversion occuring at the interfaces between the aggregate pieces and the cement paste. The aggregate pieces do not offer smooth, planar surfaces to the incident stress waves and so the reflections are scattered in a similar manner to that shown in figure3.2. If the wavelength of the incident stress pulse is smaller than the aggregate particle size the waves are scattered at every aggregate - cement paste interface and it is highly unlikely that any usable response will be detected at the response transducer (Steinbach and Vey, 1975). If the cement paste is denser and has a higher elastic modulus the difference in acoustic impedance between the cement paste and the aggregate is reduced and so the scattering effect is also reduced. However, in most pulse-echo evaluations of concrete, lower frequencies are used to reduce the attenuation of the wave due to scattering from the aggregate - cement paste interface. The use of a lower frequency excitation will, however, reduce the sensitivity of the method, i.e. small defects will not be detected - see below for details.

For heterogeneous materials, the attenuation is mainly due to the effects mentioned above. However, absorption also occurs by internal friction at a molecular level, causing a loss of signal energy in the form of heat (material damping). In homogeneous solids, attenuation is mainly due to material damping.

Attenuation causes the amplitude of the displacement produced by a stress pulse to decrease exponentially with distance travelled by the pulse (Jones, 1962).

$$A = A_o e^{-\alpha x} \tag{3.23}$$

where A = Amplitude at distance x

A_O = Original amplitude

κ = Coefficient of attenuation

The value of the coefficient of attenuation is dependent on the material properties of the concrete and the cut-off frequency of the impact, since the amount of scattering depends on the wavelength of the stress pulse. Values for concrete are not readily available and it is usual to estimate the coefficient of attenuation from the measured response from a transducer by measuring the apparent response envelope as shown in figure 3.8.

3.6 Application of Theory

3.6.1 Detection of flaws within a test specimen

The velocity, V, of a stress wave is related to the frequency and wavelength as shown below (Sears, 1982):

$$V = f\lambda \tag{3.24}$$

where f = frequency / Hz

λ = wavelength / m

If the pulse velocity through the specimen is known and the time to the arrival of a reflection from within the specimen is measured, then the distance to the target can be calculated using equation 3.25.

$$2d = Vt \tag{3.25}$$

where d = depth to target

V = P-wave (compression wave) velocity

t = time to reflection

The highest frequency input (the cut-off frequency) will determine the smallest defect that can be detected and the minimum depth at which a target can be detected. Stress waves will diffract around the edges of discontinuities that offer a profile that is too small for reflection to occur. The actual minimum size of defect detectable by reflection is subject to debate. The most conservative estimate is that the defect should be approximately the same size

or greater than the wavelength of the stress wave to allow reflection to occur (Carino and Sansalone, 1986). In some homogeneous materials, such as steel, it is assumed that a discontinuity which presents a profile greater than a seventh of the minimum wavelength contained in the incident stress pulse will cause reflection. However, due to the inhomogeneous nature of concrete the profile must be greater in size than half the minimum wavelength of the incident stress pulse (Jackson and Tweeton, 1994).

3.6.2 Sonic Impact-Echo Test Procedure and Instrumentation

The surface displacement of the test specimen is measured near to the impact point. This is to give the smallest interference from the surface wave, which will pass the measurement transducer, before the first reflections from within the test object arrive back at the transducer. Problems may occur if the test object is narrow. The reflection of the surface wave from the edge of the specimen may arrive at the transducer at the same time as reflections from material boundaries within the specimen and distort or swamp the results.

The stress pulse is produced by mechanical impact with a hammer. The hammer may be instrumented which allows measurement of the impact. If the impact is measured for each test, signal processing can be carried out to normalise each test and allow the direct comparison of different tests. However, investigation of post-tensioned bridges requires high frequency impacts and instrumented hammers of sufficiently high frequency and input energy may not be available at present to test post-tensioned bridges adequately. Ballbearings can also be used to produce a mechanical impact. It is not currently possible to instrument these and so each test response cannot be normalised. This makes analysis of the results more complicated as different test results cannot be directly compared. It is also more difficult to detect a poor quality impact. Stress-wave reflections are measured using a displacement, velocity or acceleration transducer. Results for simple specimen geometries can be analysed in the time domian. However, for most practical investigations, the response in the time domain becomes very complicated and analysis is nearly impossible. In these instances it is beneficial to analyse the response trace in the frequency domain. This is done by performing a Fast Fourier Transform (FFT) on the data (see figure 3.9).

3.7 Signal Processing

3.7.1 Fourier Analysis

The Fourier transform is the basis of frequency analysis. The assumption is made that the time signal is made up of up to an infinite number of sinusoidal components with various frequencies at different amplitudes and initial phases (Papoulis, 1977). The Fast Fourier Transform (FFT) is a highly efficient algorithm for computing the Discrete Fourier Transform and was first developed in the 1960s by Cooley and Tukey (Lynn and Fuerst, 1989).

3.7.2 General Form of Fourier Series

The purpose of calculating a fourier series is to represent a function by a trigonometrical series as shown (Stroud, 1984):

$$f(t) = A_0 + a_1 \cos t + a_2 \cos 2t + a_3 \cos 3t + \ldots\ldots$$
$$+ b_1 \sin t + b_2 \sin 2t + b_3 \sin 3t + \ldots\ldots \quad (3.27)$$

For a signal of period T, the above can be written in the form :

$$f(t) = \tfrac{1}{2} a_0 + \sum (a_n \cos \omega t + b_n \sin \omega t) \quad (3.28)$$

where

$$\alpha_0 = \int a$$

&

$$a_0 = \frac{2}{T} \int_0^T f(t)dt = \frac{\omega}{\pi} \int_0^{\frac{2\pi}{\omega}} f(t)dt \quad (3.29)$$

$$a_n = \frac{2}{T} a_n = \frac{2}{T} \int_o^T f(t) \cos n\omega t dt = \frac{\omega}{\pi} \int_0^{\frac{2\pi}{\omega}} f(t) \cos n\omega t dt \quad (3.30)$$

$$b_n = \frac{2}{T} \int_0^T f(t) \sin n\omega t dt = \frac{\omega}{n} \int_0^{\frac{2\pi}{\omega}} f(t) \sin n\omega t dt \quad (3.31)$$

and

$$T = \frac{2\pi}{\omega} \quad (3.32)$$

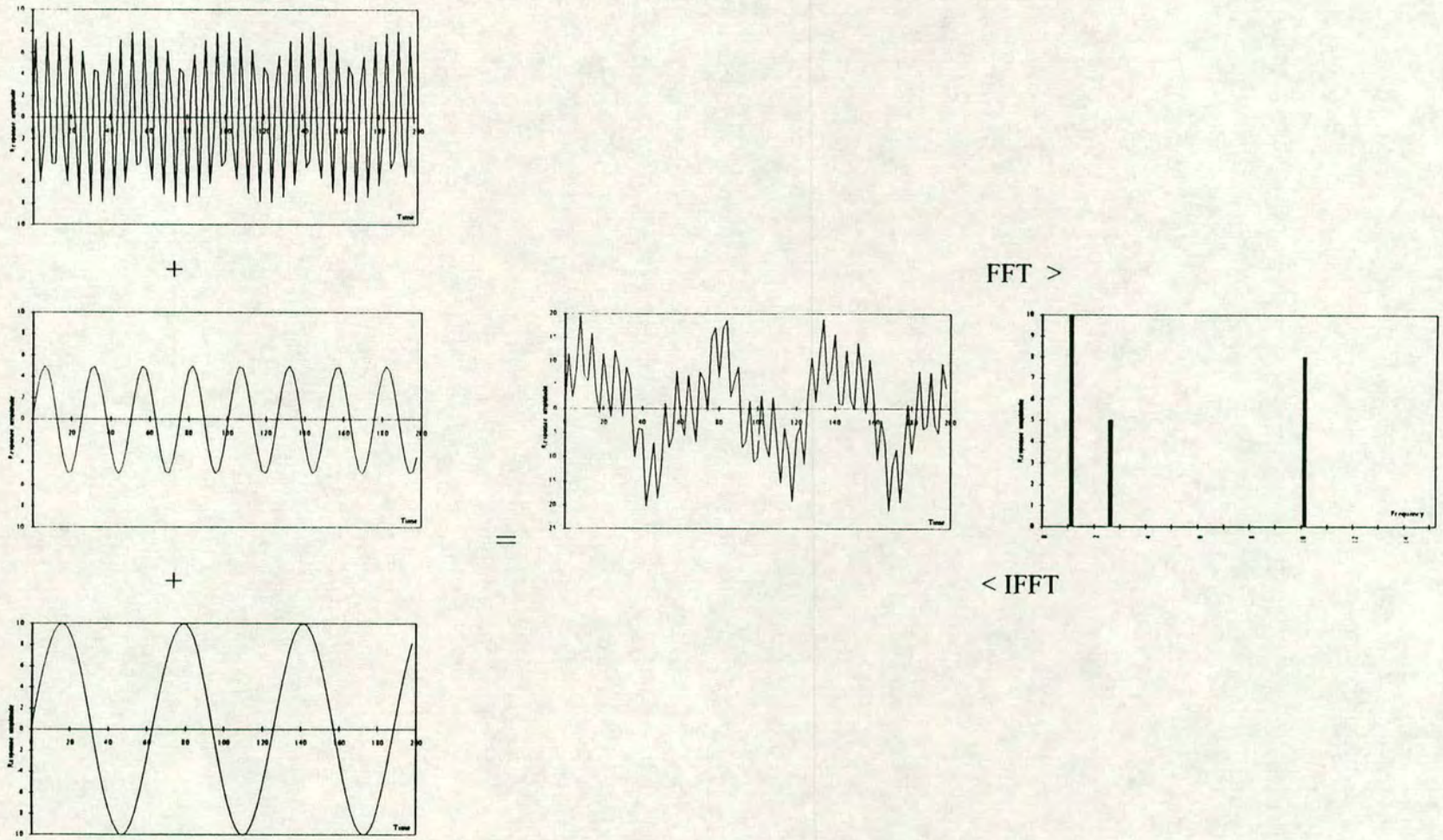

Figure 3.9 Principle of the Fourier Transform

3.7.3 Discrete Fourier Transform (DFT)

The impact and response of an impact-echo test are measured on a digital analyser, i.e. the signals are sampled in the time domain. Most analysers allow the signal to be measured in the frequency domain. This is also a discrete signal. The corresponding time domain trace can be calculated using the Inverse Discrete Fourier Transform or IDFT (McDonnell, E. 1993). The forward transform is now of the form;

$$X[k]=\sum_{n=0}^{N-1} x[n]e^{\frac{-j2\pi kn}{N}} \qquad k = 0, 1, 2, ..., N-1 \tag{3.33}$$

The inverse transform takes the form;

$$x[n]=\sum_{k=0}^{N-1} x[k]e^{\frac{-j2\pi kn}{N}} \qquad n = 0, 1, 2, ..., N-1 \tag{3.34}$$

3.7.4 Possible Sources of Error with FFT

The limitations of this process are due to the sampled nature of the signals. Because the impact and response must be sampled at specific intervals, a degree of averaging must take place. Independent of the actual impact and response of the beam, the analyser will only measure the signal over a finite time interval. Theoretically, this represents one period in an infinitely long periodic signal when the FFT is calculated.

3.7.5 Aliasing

If a signal is undersampled, i.e. the time interval between samples provides insufficient detail to accurately represent the impact or response (see figure 3.10). This produces an overlap in the frequency domain and can result in high frequency components appearing as lower frequencies. If a signal is sampled at a frequency, fs, then the highest frequency that can be represented is half this sampled frequency. Sampling a signal at a given frequency results in the spectrum of the original signal being repeated around multiples of this sampling frequency. If the sampling frequency is lower than twice the highest frequency component of the signal then aliasing errors can again occur (Ewins, 1984). Aliasing effects are shown in figure 3.10. Most analysers used in practice will use anti-aliasing filters before the signal is measured to ensure

that any frequency components higher than twice the sampling frequency are highly attenuated. Therefore if any aliasing occurs the resulting distortion of the measured signal is negligible.

If anti-aliasing filters are not available, the aliased frequencies can be determined as shown;

$$f_{alias} = 2kf_{Nyquist} \pm f_{true} \text{ for } k \geq 1 \tag{3.35}$$

where $f_{Nyquist} = \frac{f_s}{2}$

3.7.6 Window Effects

Windowing techniques involve taking a signal and multiplying it by a 'window signal' of finite duration i.e.

$$z[n] = x[n]w[n] \tag{3.36}$$

This results in $z[n]$ being of finite duration. This is important in signal analysis as the impact and response are measured over a finite time interval (the time window) and therefore the actual signal available for analysis is:

$$z[n] = \begin{cases} x[n] & -M \leq n \leq M \\ 0 & otherwise \end{cases} \tag{3.37}$$

where -M ≤ n ≤ M is the time window.
If

$$w[n] = \begin{cases} 1 & -M \leq n \leq M \\ 0 & otherwise \end{cases} \tag{3.38}$$

w[n] is a rectangular window in the time domain. In the frequency domain this is represented as a complex sin*cx* function. The time domain multiplication shown above is equivalent to a frequency domain convolution of the respective Discrete Fourier Transforms (DFT) of the functions. If a rectangular window is used the resulting transform of the impact or response will be the convolution of the actual signal and a complex sin*cx* function:

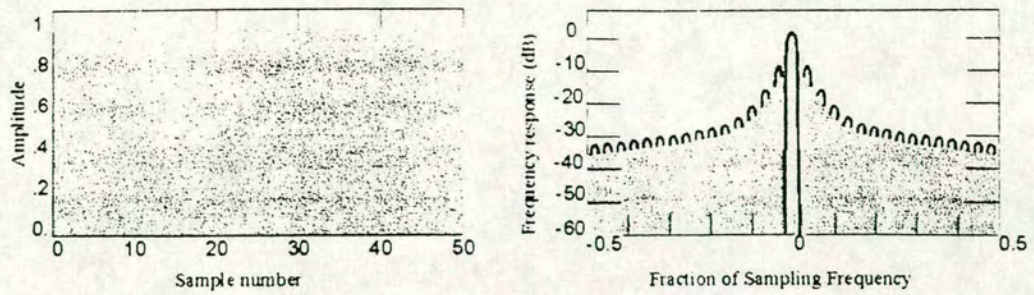

(a) Rectangular window

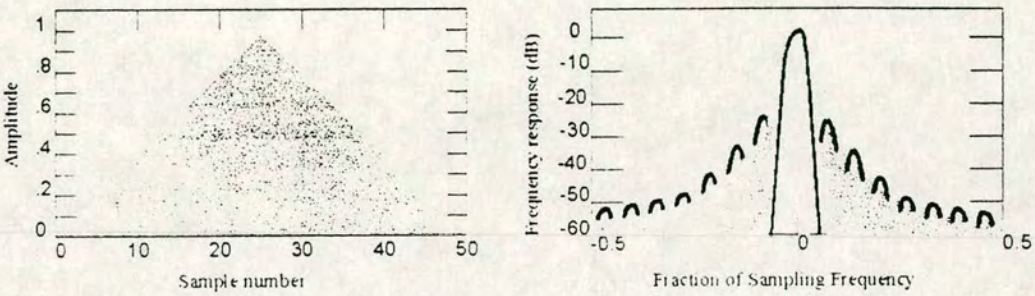

(b) Triangular window

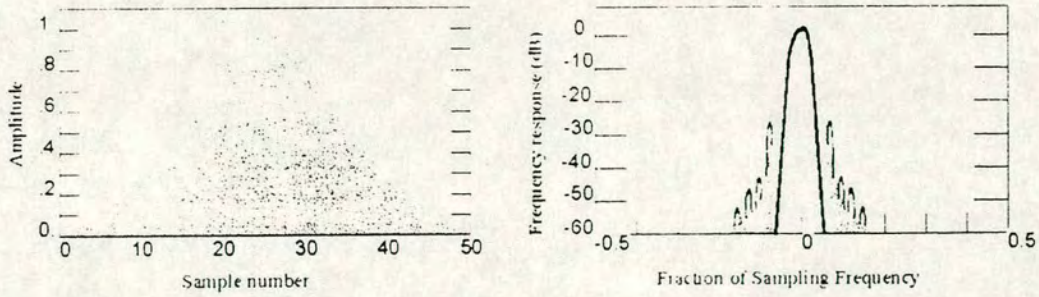

(c) Hanning window

Figure 3.11 Window signals and their DFT

$$Z[k]= X[k]W[k] \tag{3.39}$$

For most signal analysis this is an inappropriate window to use. It is better to use a window with the amplitude equal to zero at either end and varying smoothly along its length. Figure 3.11 shows some available window signals and their DFT.

3.7.7 Leakage

The side lobes shown on the window spectra cause the signal spectra to 'leak'. That is, signal energy which might have been concentrated at a single frequency on the spectrum is spread across many frequency bands. This will be a problem if a small amplitude frequency component exists at a frequency close to that of a high amplitude component. The small amplitude component may be completely overshadowed by leakage and therefore will not be detected. Leakage is particularly high with a rectangular window (See Figure 3.11). If leakage is thought to be a serious problem a window signal with small side lobes should be chosen. However, the smaller the side lobes, the wider the main lobe. This results in a lower frequency resolution which may result in two distinct frequency components being depicted as a single component. A compromise must be reached between required resolution and minumum interference from leakage. Usually leakage problems are kept to a munimum.

3.7.8 'Picket Fence' Effect

A DFT results in the signal in the frequency domain also being sampled. The sample points are spaced at multiples of f_S / N, where f_S is the temporal sampling frequency and N is the number of points sampled. If the signal being sampled has a whole number of cycles per sampling block no error will occur. However, the 'picket fence' effect arises if the signal contains frequencies other than at the discrete sampling frequencies. The actual frequency will be seen by the discrete sampled frequencies on either side (due to leakage). It is termed the picket fence effect as it is analogous to looking at a signal through the gaps in a fence (see figure 3.12).

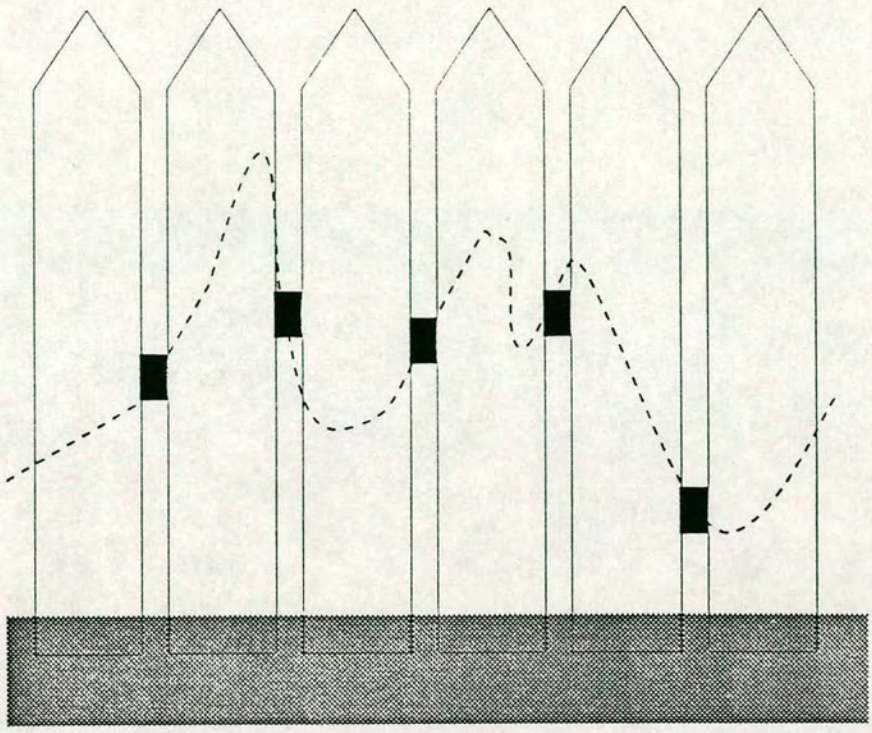

Figure 3.12 Picket fence effect

3.7.9 Frequency Resolution

The ability of a process to distinguish between the main lobes of two frequency components is termed the frequency resolution, δf, defined as:

$$\delta f = \beta \frac{f_s}{N} \tag{3.42}$$

where β is a coefficient which reflects the effect of the window signal on the effective bandwidth of each frequency component. δf is the smallest frequency interval available on the spectrum. If $x[n]$ contains two components with frequencies closer than δf they will not be resolved as distinct components.

It is the aim of this thesis to develop practical investigation techniques for post-tensioned bridges using sonic impact-echo. The available instrumentation will be investigated and conclusions made as to the suitability of different set-ups for testing.

3.8 Conclusions

1. Possible investigation techniques were assessed, namely, visual inspection and endoscopy, ground penetrating radar, radiography, ultrasonic investigation and sonic impact-echo.

2. The investigation technique judged most promising for widespread and economical application was sonic impact-echo and this method will be applied and discussed throughout this thesis.

3. The majority of ducting used during construction of post-tensioned bridges was cylindrical steel. This may cause difficulties during sonic investigation as incident waves will be scattered when reflected. This results in less energy being returned to the response transducer than would be measured from a reflection created by a plane material boundary.

4. Current research would suggest that sonic impact-echo may be a powerful investigation technique for post-tensioned bridges however there is some disagreement about whether voids may be detected directly by reflection from

the top boundary of the void or that the frequency of the reflection from the base of the structure will give an indication of the presence of voiding.

5. If the base reflection must be measured to detect voiding, problems may arise if the structure is deep and small voids are required to be detected. A high cut-off frequency is required to detect a small void. To input a high cut-off frequency a small impactor must be used. The energy input into the structure is therefore low and attenuation of the signal high. In a deep beam it may not be possible to input a signal of high enough frequency to detect the void and high enough energy to propagate to the base. The signal must also be sampled appropriately to allow adequate resolution of the response in the frequency domain.

Chapter IV

Preliminary Investigations

A laboratory specimen was constructed with known defects. Various testing procedures were investigated and a test configuration suitable for the field testing of post-tensioned bridge beams was developed.

4.1 Introduction

In response to the Department of Transport issuing a moratorium on the design of post-tensioned bridge beams, the Transport Research Laboratory invited tenders from testing houses to investigate post-tensioned beams on its Crowthorne site in November 1992.

Preliminary investigations were carried out at TRL using ground penetrating radar and sonic impact-echo. It was discovered that ground penetrating radar could be used to successfully investigate the condition of the tendon ducts and overall condition of the post-tensioned concrete beams if the ducts were formed using a non-metallic casing. If metallic ducts were used, no indication of the internal condition of the tendon ducts could be gained. However, radar was found to be a useful method for locating the position of the ducts.

The preliminary sonic impact-echo investigations carried out at TRL seemed to give disappointing results. However, the results did show that certain features of the beams could be detected. The instrumentation and field testing set-up required considerable assessment to improve the quality of results. Instrumentation available commercially was investigated and adjustments made to increase the suitability to the specific application of non-destructive testing of concrete. A laboratory model was constructed to investigate different testing configurations. Known defects were included in this model.

One major limitation of sonic impact-echo testing of concrete is producing an impact of relatively high frequency and high energy. Concrete is assumed to behave elastically and so Hertz theory of impact is used to calculate the appropriate cut-off frequencies (Goldsmith, 1960). However, instrumented hammers were used initially to provide the impact. It was noted that the expected cut-off frequencies were not achieved and a study was carried out to investigate the effect of concrete strength and mix ratios on the cut-off frequency obtained from two different instrumented hammers, one with a relatively low expected cut-off frequency (~7.5 kHz) and one with a relatively high expected cut-off frequency (~13 kHz).

An alternative sonic impact-echo technique which did not require such high frequencies was also investigated. This testing method involved testing along the length of the ducts. It is similar to pile testing (Davis and Dunn, 1974). The end of the tendon duct had to be exposed and anchorage details could impede testing in this

way. However, lower cut-off frequencies are required as the distance travelled by the pulse is longer.

4.2 Post-tensioned Beams at TRL

The beams to be investigated consisted of a motorway I-beam containing a single unducted tendon, a box beam footbridge containing metal ducted tendons and a test beam constructed at TRL.

4.2.1 Beam 1 : Billingford Bridge Beam

This beam had been part of a skewed motorway bridge constructed in 1949. It was joined to the other beams by means of ties that were threaded through preformed ducts. See figure 4.1. The tensioning came from a single unducted cable. There was some concern over the anchorages of the cable. Other defects in the beam had also been included.

4.2.2 Beam 2 : Bank Lane Footbridge

A section of this footbridge was transported to TRL for testing. It was built to a post-tensioned concrete box-beam design and contained four metal-ducted tendons. The cross-section of the beam at two locations and the profile of the tendons is shown in figure 4.2. All four tendons run along the lower flange of the beam at the centre. The two outer tendons rise up the side flanges of the beam towards the supports to prevent tension occuring at the top surface of the beam across the supports. The boxed-out section gradually reduces towards the supports and the two inner tendons also rise slightly over the supports.

4.2.3 Beam 3 : Test Beam

The test beam had a span of 10m and contained three tendons, two with metal ducts and one which was half plastic ducted and half metal ducted. The tendons ran along the centre of the beam, one above the other. The top and bottom tendons had a horizontal profile and the middle tendon sloped downwards towards the centre of the span as shown in figure 4.3. The diameter of each duct was 40 mm. Voids and other defects (mainly tendon breaks) were included in the test beam during construction and their location noted.

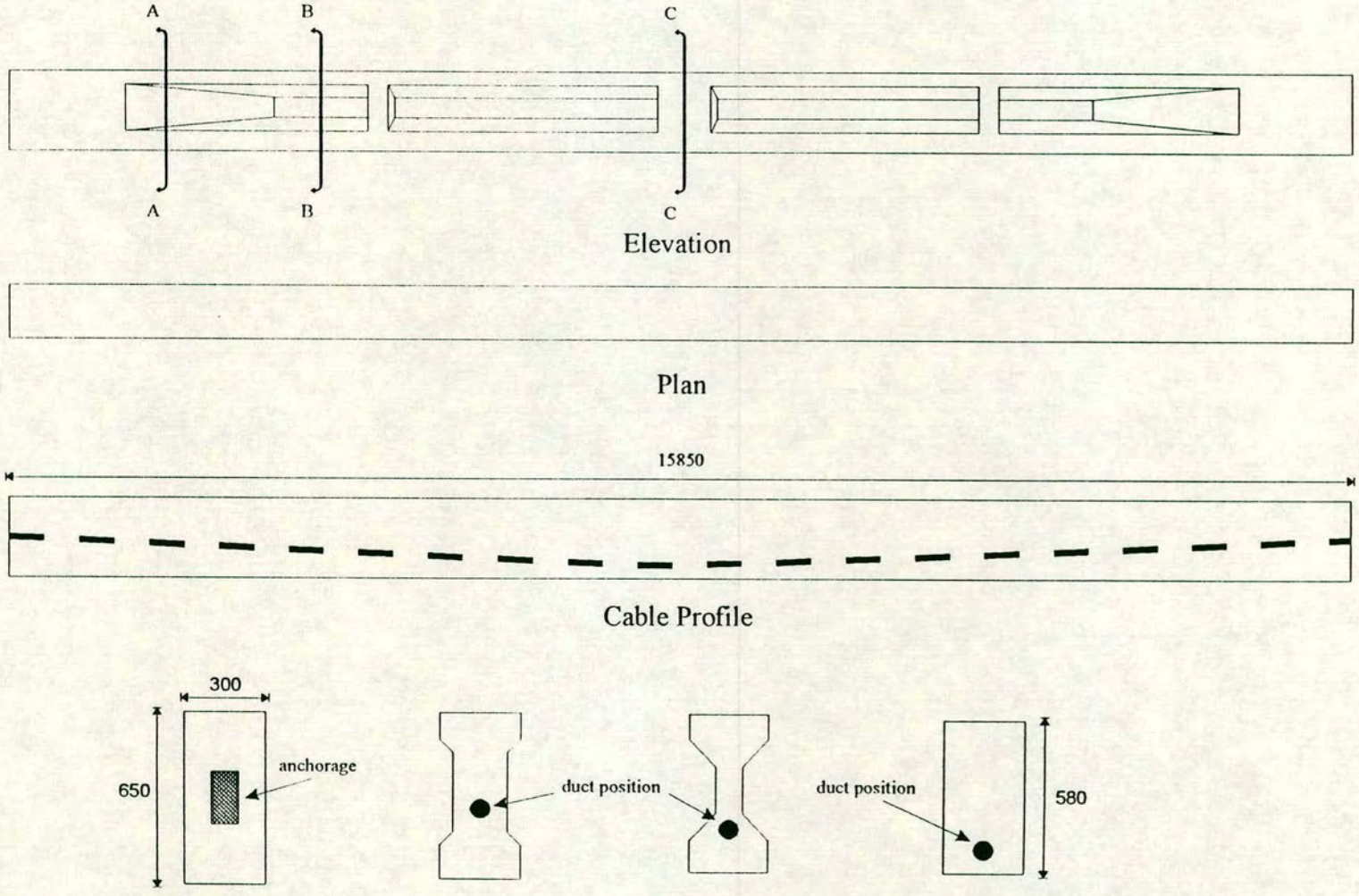

Figure 4.1 TRL beam 1: Billingford bridge beam

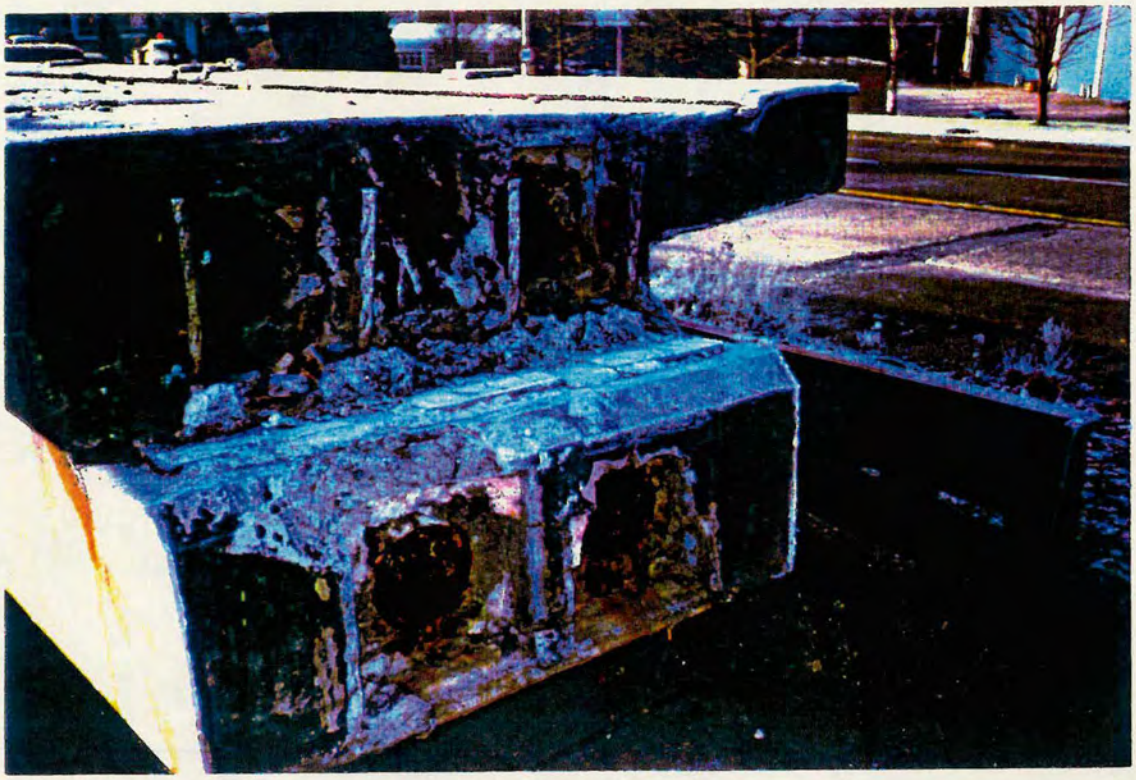

a) Photograph

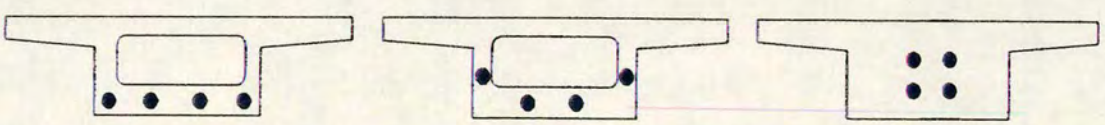

b) Duct location at midspan

c) Duct location at quarter span

d) Duct location at supports

Figure 4.2 TRL Beam 2: Bankend Footpath

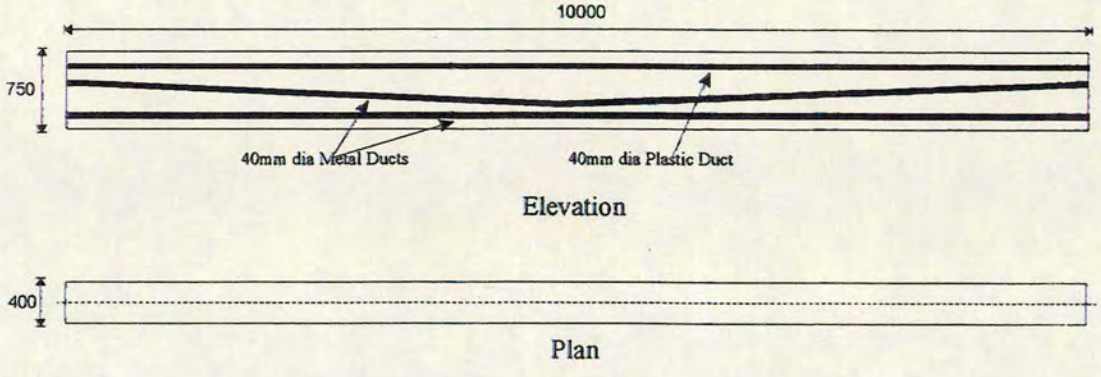

Figure 4.3 TRL Beam 3: Test Beam

The University of Edinburgh was awarded a contract to investigate the beams using radar and sonic impact-echo techniques. The author participated in the group which tested the beams. The group consisted of the author, Prof. M.C. Forde, Mr. N. McCavitt and representatives from the site investigation company Holequest Limited, Galashiels.

4.3 TRL Radar results

The GPR system used in all the field work reported in this report was the GSSI Sir System 10. This system involves digital radar pulsing and recording. The data from the antenna is transformed from an analogue signal to a digital signal using a 16 bit analogue-digital converter. This gives high resolution for subsequent data processing. The data is displayed on site on a high resolution colour monitor. Following visual inspection it is then stored digitally on tape for subsequent analysis and signal processing. These files are then downloaded onto a PC. Post processing was undertaken using GSSI RADAN III software. The many techniques available allow the raw data to be filtered and different features highlighted which enable much more detailed analysis.(RADAN MANUAL)

The three post tensioned beams at TRL were tested. The radar antennae used were a 1 GHz and two 900 MHz antennae.

4.3.1 Beam 1: Billingford bridge beam

The radar surveys on this beam were the most successful. Figure 4.4 shows a radar trace of a 900 MHz antenna being dragged along the top surface of the beam. The beam is 'I' shaped towards the centre and the extent of this is clearly seen. The tendon and the tie ducts can also clearly be identified. On this trace only large defects can be detected. Two large defects occur where the tendon begins to slope upwards. This is to be expected as the tendon is unducted and was encased in concrete when tensioned. The largest movement of the cable will be at these points. This may cause voiding and, if water ingression takes place, corrosion.

Figure 4.5 shows a trace taken along the base of the beam with a 1 MHz antenna. This trace has been filtered horizontally. This filtering removes any horizontal features. In this case the reflections from the flange and most of the

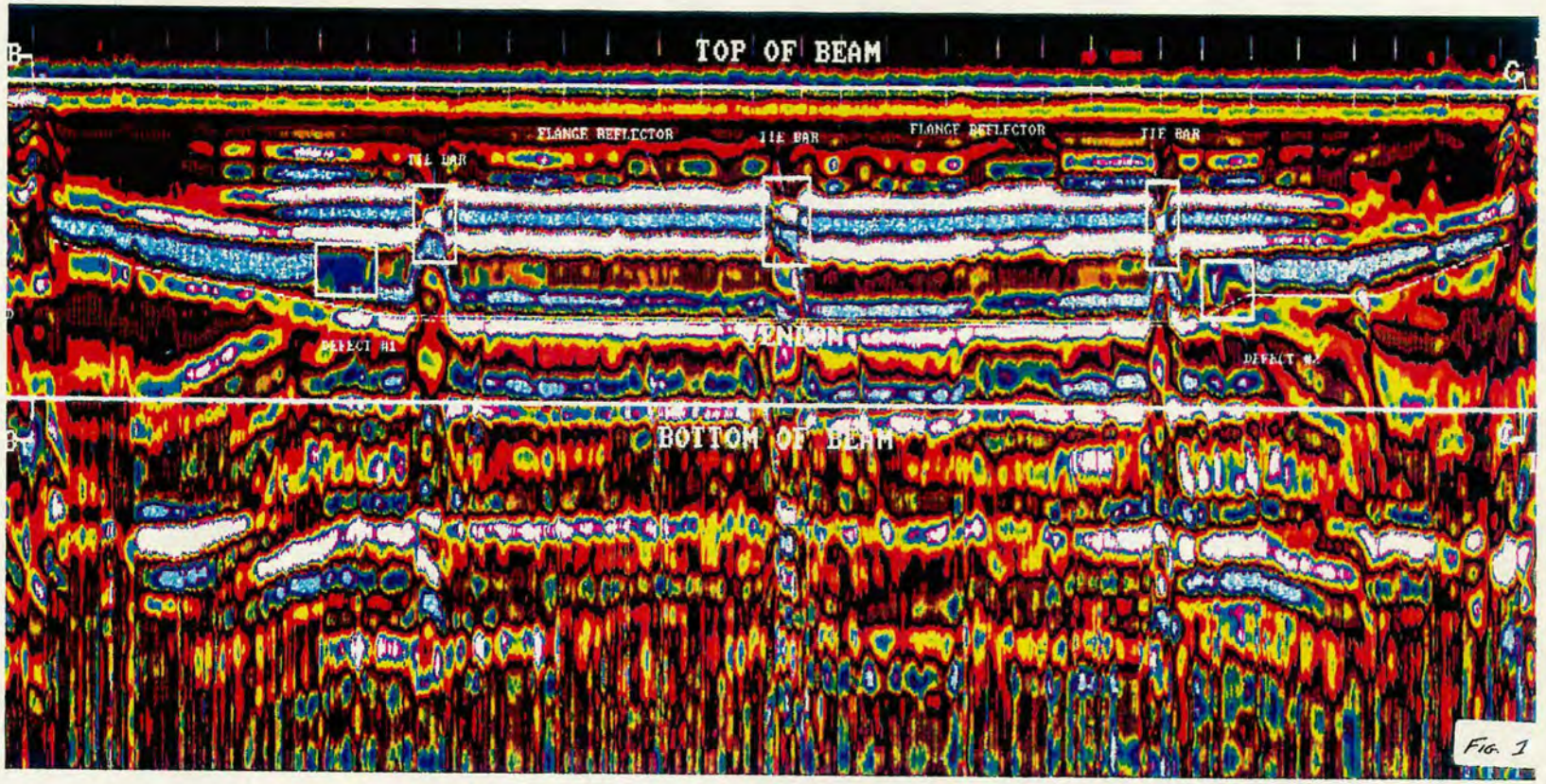

Figure 4.4 Billingford bridge beam, radar plot - 900 MHz antenna along top surface of the beam

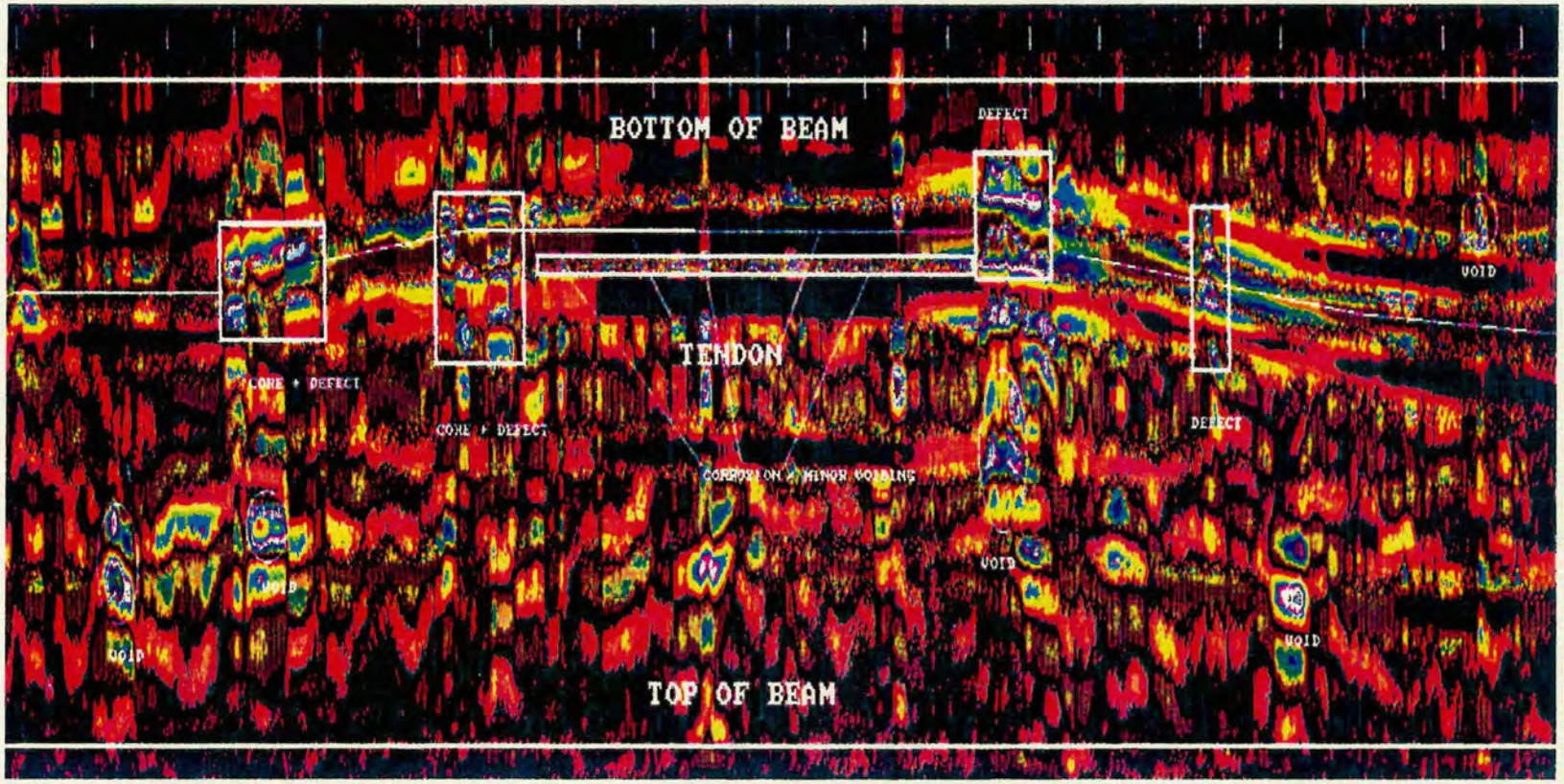

Figure 4.5 Billingford bridge beam, radar plot - 1 GHz antenna along bottom surface of the beam

reflections from the actual tendon have been removed. This allows more possible defects to be detected. Voiding within the concrete is shown on the trace. It can be seen that generally, the condition of the tendon is worst where the tendon changes direction. The lowest portion of the tendon is also quite badly voided. This may occur if water can get to the tendon. When the tendon was tensioned the concrete immediately surrounding it would be crushed slightly. This could allow any water getting to the tendon to travel down along the tendon and collect at the centre (which forms a low point) thus giving conditions under which corrosion could occur.

4.3.2 Beam 2 : Bank Lane Footbridge, Bury

A section of this post tensioned concrete box beam was surveyed. The post tensioning system consisted of four separate tendons formed using steel ducts. Therefore it was not possible to investigate the condition of the actual tendons using the radar system as the electromagnetic wave was totally reflected by the steel ducting. The position of the cables could be found from surveys on the base of the beam, figure 4.6a (taken near the centre of the span with a 1 MHz antenna). However, because of the shape of the beam, it was more difficult to locate the outer tendons as they rose up the sides of the box beam. Although it was not possible to determine the condition of the tendons inside the metal ducts some voiding around the ducts was detected, see figure 4.6b (taken 5 m from the end of the span with a 1 MHz antenna.)

4.3.3 Beam 3: Test Beam

A rectangular beam was constructed at TRL for the investigation. Certain defects were included, e.g. voiding, tendon breaks, etc. Half of the top duct was formed using plastic and so the actual tendon should be seen. The bottom two ducts were formed by steel ducts and, as before, it could only be possible to determine the position of the ducts using the radar.

The tendons could be detected but it was not possible to determine where the duct of top tendon changed from plastic to metal. This is because the tendon itself is metal and so will give a similar signal to the metal duct. The plastic duct has similar electrical properties to concrete and so will be almost 'invisible' to the signal. The plastic is thin and so the reflection from the

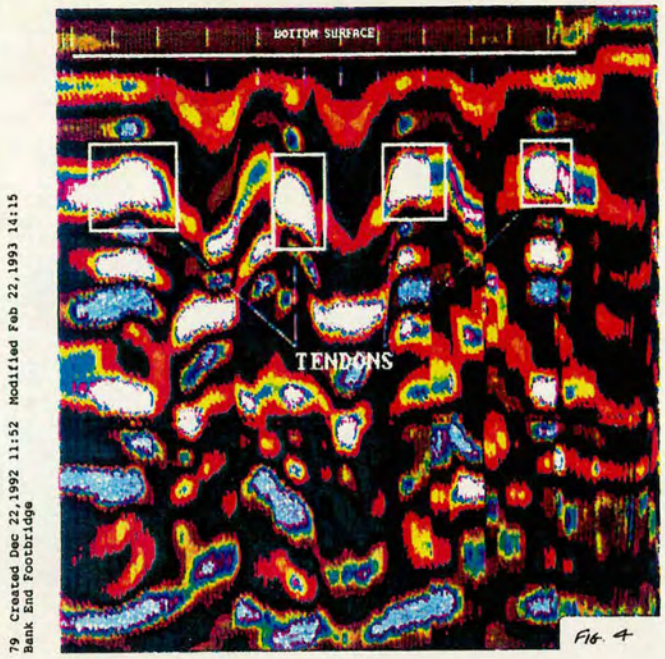

a) Unfiltered data, section across the base of the beam

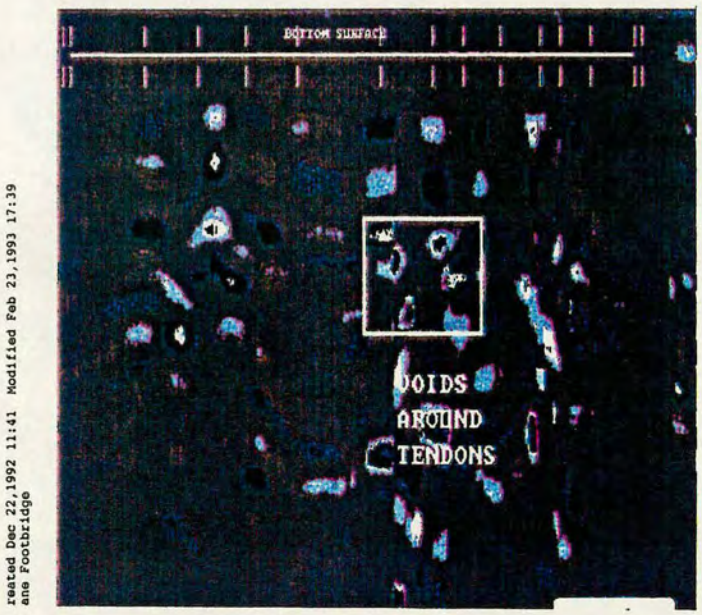

b) Filtered Data, section across the base of the beam

Figure 4.6 Bank lane footbridge radar plots

tendon will not be resolved from the reflection from the metal duct. Figure 4.7 shows a trace taken along the side of the beam with the 1 GHz antenna. It is not possible to determine exactly what the defect is but areas of interest can clearly be identified. This beam was tested shortly after the defects were constructed in the beam. The concrete would therefore be 'green' and this could lead to reflections from the new concrete which could mask more defect specific reflections.

4.3.4 Conclusions on TRL Radar Investigation

It was found that some of the defects included in the beams were discovered and others not. The frequency of the antenna is a factor in determining the minimum size of defect that can be detected. The vertical resolution is considered to be a quarter of the wavelength (Padaratz and Forde, 1995). The inhomogeneity of concrete can give rise to clutter - i.e. the electromagnetic wave is reflected at boundaries of aggregate pieces if the wavelength is less than or equal to the aggregate size. Together, the above properties determine the resolution achievable on a radar test. Some other limitations of radar testing of post-tensioned bridge beams were noted:

i. Radar testing is not suitable for determining the internal condition of metallic ducts as the electromagnetic wave is virtually totally reflected at a concrete - metal interface.

ii. In areas of dense reinforcement, e.g. aroung the anchorages, the wave is reflected from all the reinforcement and so less energy penetrates to the tendons. This may result in the tendon not being detected.

4.4 TRL Impact Echo results

4.4.1 Instrumentation

The sonic equipment used was a Zonic A&D 3525 FFT Analyser, a DJB A/20 T accelerometer and a ball bearing was used as the impactor. The expected cut-off frequency for the ball bearing was 8 kHz. A number of individual tests were carried out at each test point to ensure that the response recorded was representative for that position.

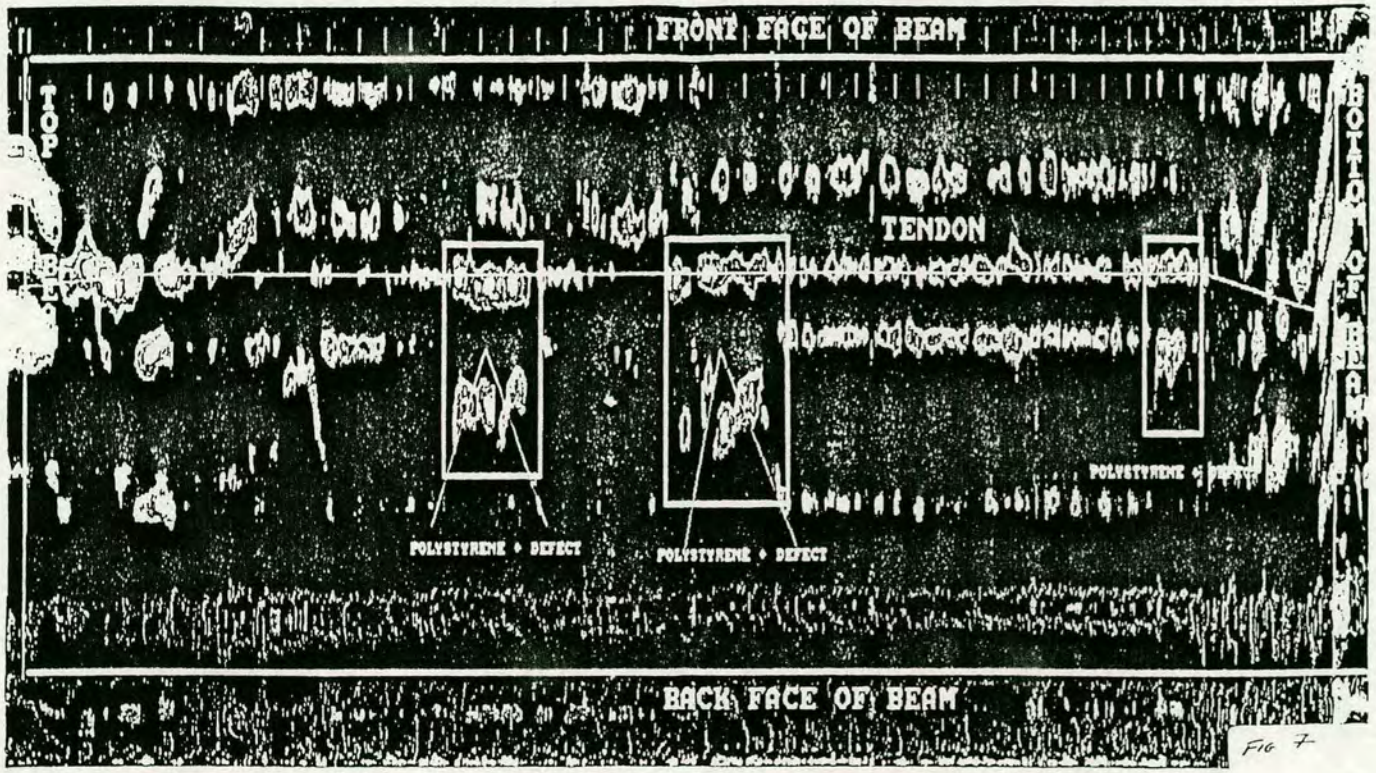

Figure 4.7 TRL test beam, radar plot down side of beam

4.4.2 Beam 1: Billingford Beam

This beam was tested at 1m intervals along the centreline of the top surface. The beam section varied along its length and further tests were carried out at positions of interest. Figure 4.8 shows a typical response in the time domain. It shows the acceleration of the beam at 1.0m from the end. The time traces are quite difficult to analyse and so an FFT is performed to allow the response to be analysed in the frequency domain.

Figure 4.9 shows the frequency spectra for the first 6m of the beam. The spectra change as the beam geometry changes. The beam is approximately 600mm deep and so, assuming a compression wave velocity in concrete of 4000m/s the base reflection is expected at 4000/(2*0.6) = 3.3 kHz. The base frequency would be lower if the compression wave velocity was lower, i.e. the concrete quality was poor or the wave had to diffract around a defect causing a longer wavepath and therefore lower frequency. The cut-off frequency is rather lower than expected for these tests and the reflection from the base cannot be detected on all the traces. The relative amplitude of this reflection is much lower than expected on all the results because of this. The complicated geometry of this beam also results in less reflected energy travelling back to the testing point.

In some of the traces small reflections can be seen at higher frequencies. These reflections may be due to defects within the beam or from the geometry of the beam. However, the results are not conclusive in these tests as the cut-off frequency is too low to detect defects within the beam.

4.4.3 Beam 2: Bankend Footpath

This footpath was constructed to a post-tensioned concrete box beam design. Having previously tested Billingford beam it was decided to test one cross-section in detail rather than try to test the whole beam. The aim of this testing was to identify the internal structure of the box beam and to identify the tendon ducts if possible. It was unlikely than the individual ducts could be identified as the cut-off frequency of the impactor was considered to be very low, estimated as an average of 5 kHz. Therefore the minimum defect that could be identified would be approximately 400mm. Defects smaller than this can be identified but it is not possible to say that no defects exist if none are detected.

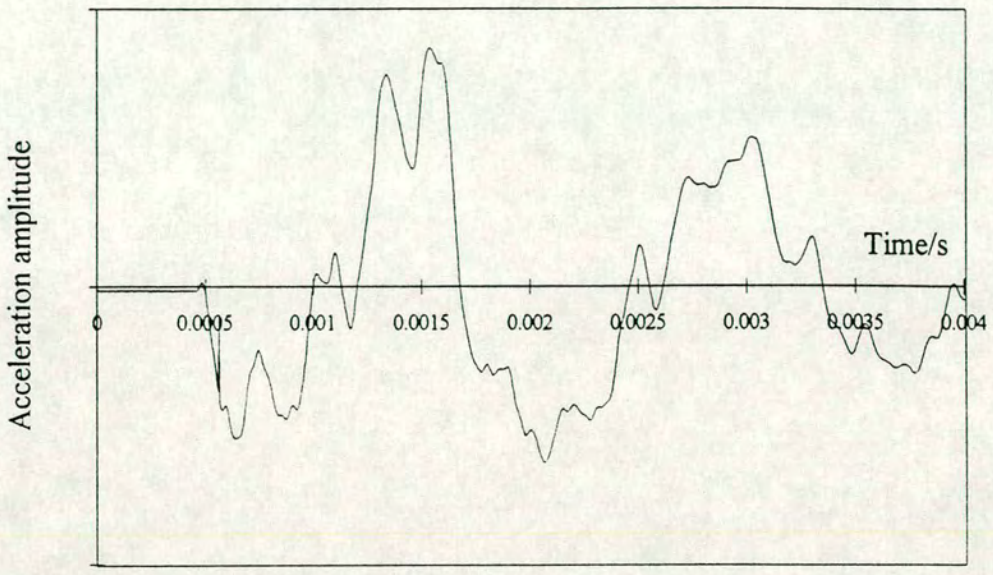

Figure 4.8 **Time domain impact - echo response. TRL Beam 1, Billingford Bridge**

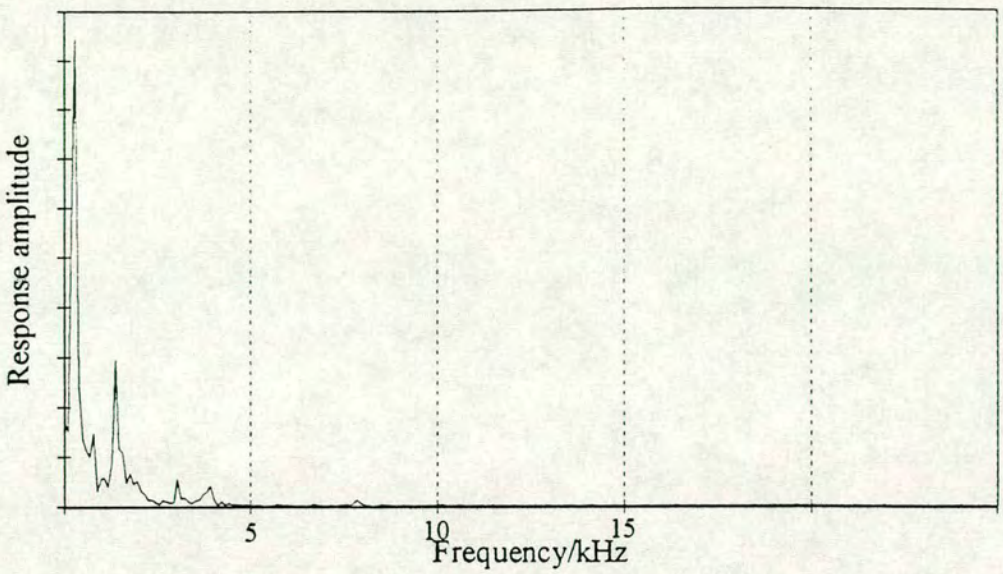

Fig 4.9a 1.0m from track end

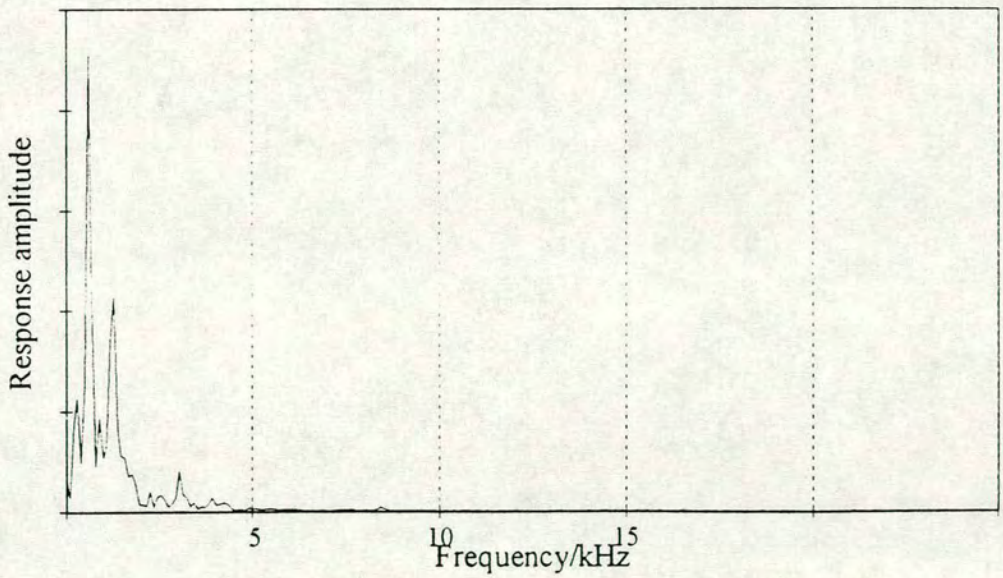

Fig 4.9b 2.0m from track end

Figure 4.9 Frequency Response Spectra for TRL beam 1 for Billingford Bridge

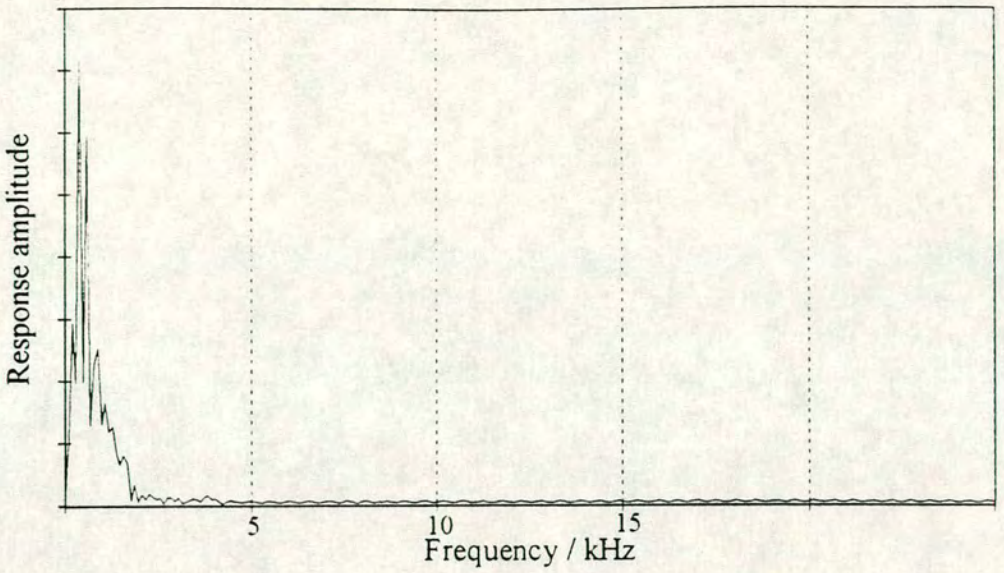

Fig 4.9c 3.0m from track end

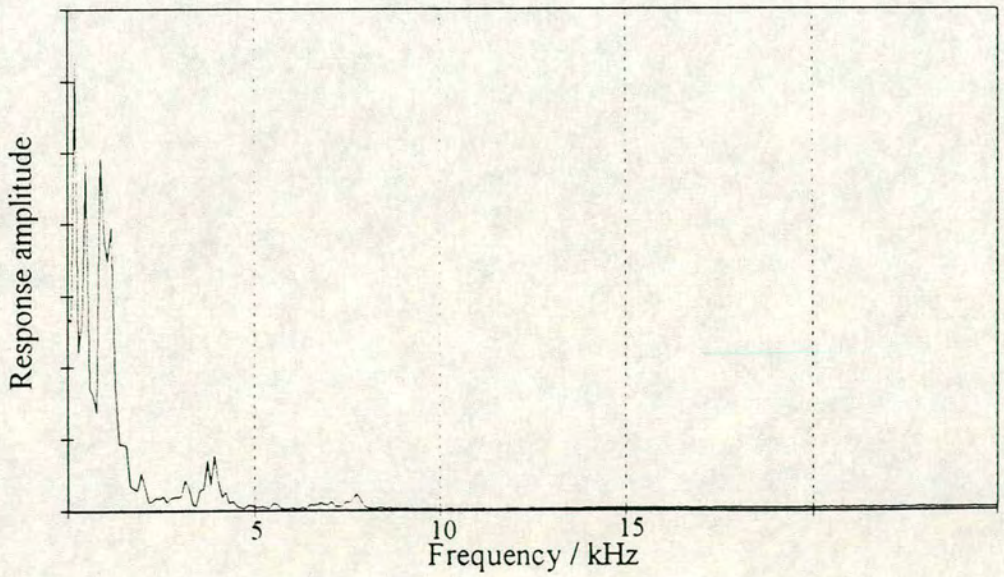

Fig 4.9d 4.0m from track end

Figure 4.9 (cont.) Frequency Response Spectra for TRL beam 1 for Billingford Bridge

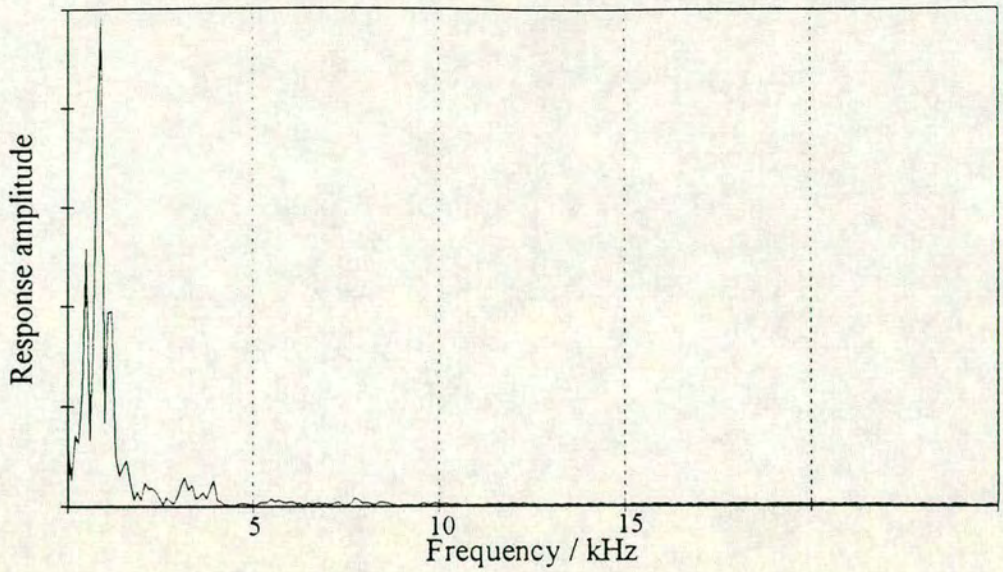

Fig 4.9e 5.0m from track end

The section of the beam to be tested was 5m from the anchorage. The beam was tested at 10cm intervals across the underside. At this point the boxed out section of the bridge reduces. This results in the lower flange of the beam being thicker than the 300mm specified along the main portion of the span. At this point the tendons are not all lying in the same plane. The profiles of the outer tendons rise towards the anchorage to prevent the top section of the beam going into tension.

The response spectra from four positions are shown in figure 4.10. The response at position 1.1m does not show the peak at approximately 4 kHz that is apparent on all the other traces shown. It seems likely that this peak corresponds to the reflection from the boxed out section. If a velocity of 4000m/s is assumed in this beam then the thickness of the section is approximately 500mm. The beam is in fairly poor condition and so it is likely that the actual compression wave velocity is slightly lower than 4000m/s. This would result in the depth at this section being less than 500mm. The response spectra at 1.1m does not show this peak as this position is outside the boxed out section.

The peak at approximately 1.8 kHz may correspond to a reflection from the top surface of the beam, giving a compression wave velocity of 3600m/s. However, other peaks exist on all traces around this frequency and the results are not conclusive. The response at 0.3m shows a distinct peak at 7.5 kHz. This could be a reflection from a voided tendon duct or other defect near the tendon duct within the beam. It is not possible to say what this peak corresponds to without further investigation. Having a response at this frequency would suggest that an elastic impact occured at this point and the resulting cut-off frequency was higher than in the other cases. However, other phenomena arising from the instrumental set-up could cause spurious reflections as detailed above.

4.4.4 Beam 3: Test Beam

The test beam was tested at 1m intervals along the top surface of the beam. The concrete was 'green' at the time of testing and so the velocity of the compression wave through the beam will be lower than expected, i.e. less than 4000m/s.

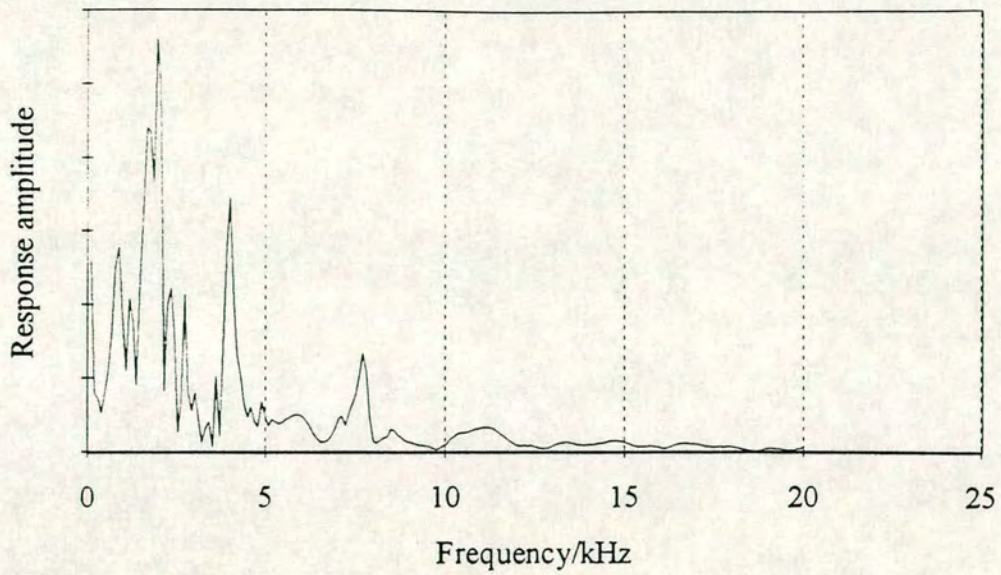

Fig 4.10a 5m from anchorage, 0.3m from edge

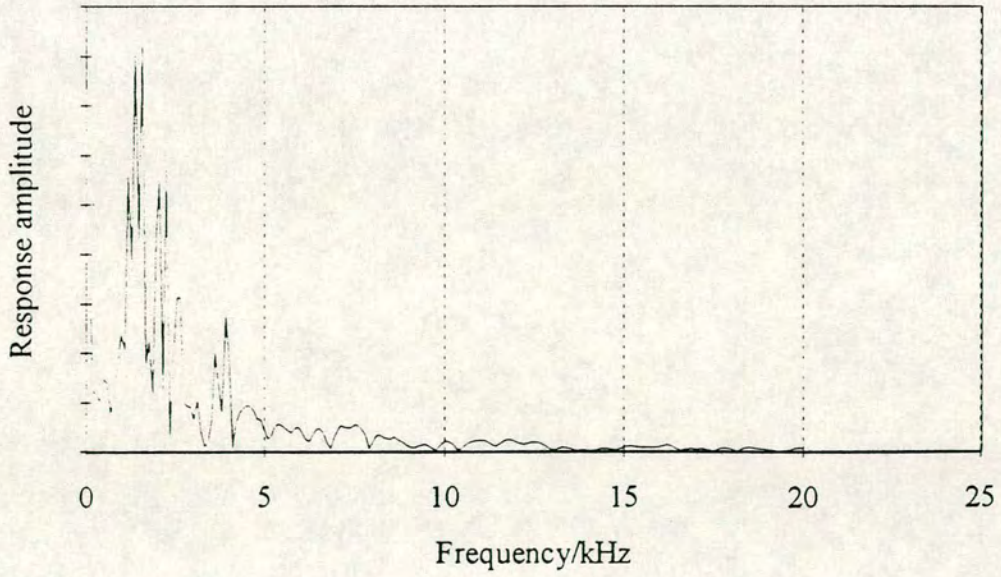

Fig 4.10b 5m from anchorage, 0.5m from edge

Figure 4.10 Frequency response spectra for TRL beam 2, Bankend footpath

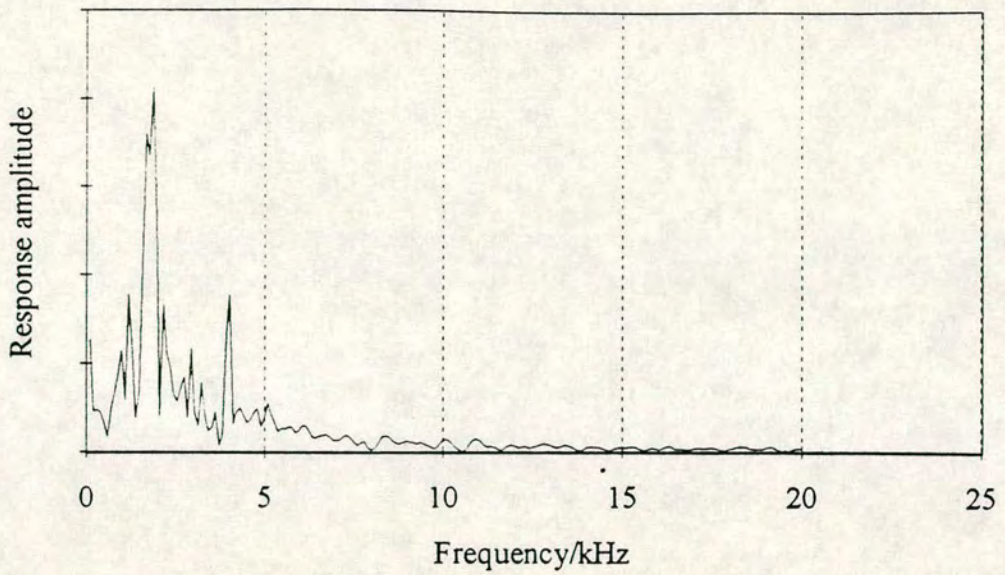

Fig 4.10c 5m from anchorage, 0.9m from edge

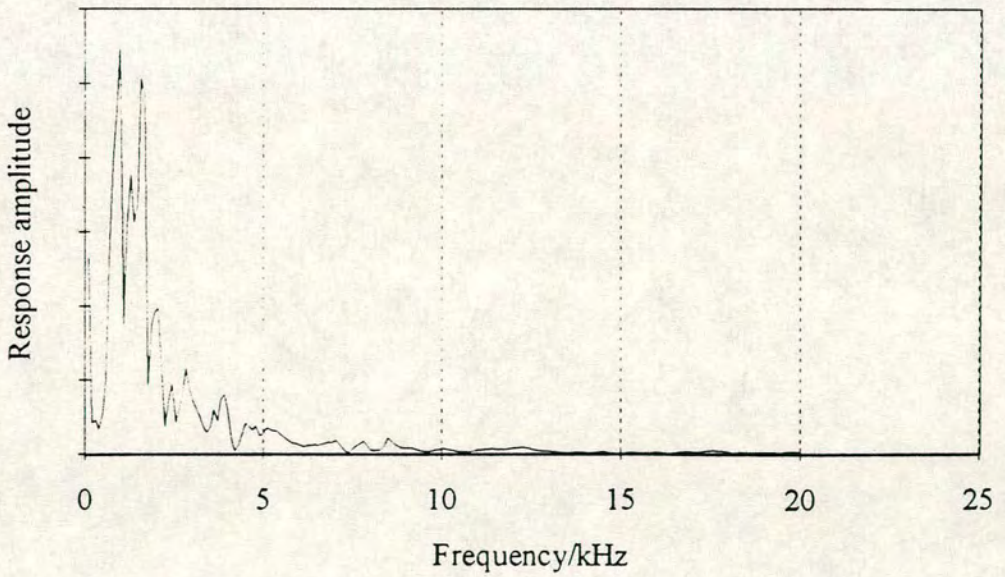

Fig 4.10d 5m from anchorage, 1.1m from edge

Figure 4.10 (cont.) Frequency response spectra for TRL beam 2, Bankend footpath

The test beam is 750mm deep. This would result in an expected reflection from the base at 2.7 kHz or less as the compression wave velocity is likely to be less than 4000m/s. Figure 4.11 shows the response spectra for four positions along the beam, 1m, 5m, 6m and 9m from end 1. The frequency response of interest, i.e. that corresponds to reflections from within the beam is that above approximately 1.75 kHz. This allows for the velocity being lower than 4000m/s. From the figure, a distinct peak can be seen at approximately 2 kHz on each trace. This was assumed to be the reflection from the base. The average frequency was 1.9 kHz giving an average compression wave velocity of 2850m/s.

The response at 5m was not typical. At this point the accelerometer and impact were positioned off centre of the beam. This was because of poor surface conditions at the centre. It is likely that the condition of the concrete was still relatively poor at the test point and could have resulted in a poor impact. This would result in a lower cut-off frequency than that achieved at the other test points and so the resulting response spectrum would not contain the higher frequency components found in the spectra from other test points.

The spectra from positions 1m, 6m and 9m contain a peak at approximately 4 kHz. This corresponds to a target at half the depth of the beam. Other peaks occur on the spectra which relate to targets within the beam. However, the investigation was not detailed enough to give accurate predictions of the position of defects.

Compression and shear waves are hemispherical in profile and so reflections from targets not directly beneath the testing position are detected. A series of tests along a survey line or area are required to give better information as to the actual position of a defect. In this instance, the cut-off frequency of the impact was too low to give accurate information concerning all but large defects. It was therefore not considered worthwhile to carry out further testing until improvements had been made to the testing instrumentation and method.

4.4.5 Discussion on TRL Impact-Echo Investigation

From the results given it can be seen that, although inconclusive for these tests, the impact-echo technique provided a promising investigation method

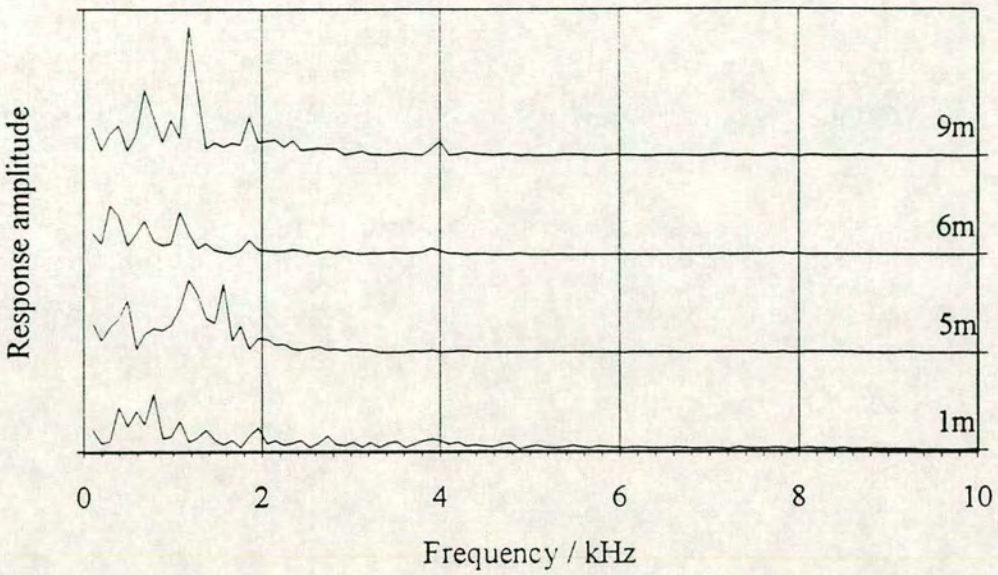

Figure 4.11 Frequency response spectra, TRL beam 3, test beam

for post-tensioned bridges with metallic ducts. Reflections from the base of the beam could be detected. Targets within the beam could not generally be detected as the peak frequency of excitation, the cut-off frequency, was not sufficiently high. A ballbearing of diameter 25mm was used. The expected cut-off frequency for an impact on concrete using elastic theory (Goldsmith, 1960) is 8 kHz. In the field, the cut-off frequency, while not measured directly, could be estimated from the resulting fast fourier transform of the response. This varied slightly throughout the testing as it is dependent on the individual impact. The average cut-off frequency achieved was approximately 5 kHz. This is considerably lower than that expected from elastic impact theory.

The concrete surface suffers some plastic deformation and this reduces the cut-off frequency achieved by impact. The accelerometer was bonded to the structure using water pump grease. In some areas of the beams the concrete was in a poor condition and coupling of the accelerometer was difficult. At these points the accelerometer was held against the structure by hand. This can result in spurious vibrations being set up which will be recorded as part of the beam's response.

Water pump grease is not an ideal coupling material for the accelerometers used as it is rather course and a thick layer is required to bond the acceleromer to the concrete. It is difficult to maintain the same coupling at each test point as the thickness of the grease will change as will the force with which the accelerometer is coupled. This can again result on spurious frequencies appearing on the response trace. It is unlikely to be possible to eradicate resonances arising due to coupling a transducer to concrete since a concrete surface is rarely smooth and dust free. However, it should be possible to couple the transducer sufficiently to ensure these resonances are at higher frequencies that those expected to arise from defects within the test structure. It is also desirable to have the same coupling effects at each test point to allow them to be identified on the response trace and therefore ignored in the analysis.

4.4.6 Conclusions from TRL Impact-Echo Investigation

Sonic impact-echo testing should provide a useful testing method for non-destructive testing of post-tensioned concrete bridges. The method would be

applicable to testing both metallic and non-metallic tendon ducts. However, further research is required to enable this technique to be used with confidence in the field. The testing equipment requires extensive investigation to produce the most efficient set-up. The limitations of this technique also need to be discovered and understood. A laboratory model was constructed to allow detailed investigations of different test set-ups to be made.

4.5 Sonic Impact-Echo Instrumentation Requirements

Any testing system can only be as accurate as the least accurate component. It is therefore necessary to investigate the individual components of the test set-up. A sonic impact-echo set-up consists of an impactor, a response transducer and an analyser with associated connections and power supplies. Each component will be discussed and the requirements detailed. The coupling of the response transducer was also shown to be important and this will be discussed in section 4.8.

4.5.1 Frequency Range of Impactor

The range of the impactor must be sufficiently high to allow the compression wave to 'see' the target. It was decided that in order for a target to be seen in concrete the impactor must be able to input frequencies at half the expected frequency peak. Opinions vary as to how high a frequency is required. In some materials a frequency of 1/7 peak can still identify the target but in concrete 1/2 peak is considered more likely to be successful. This means that the hammer must be able to input an excitation of 10 KHz to detect a defect at a depth of 200mm.

The Brüel and Kjær Hammer Type 8208 has a frequency range of 0 - 7 KHz. See figure 4.12. This is slightly too low to 'see' a 200mm target. A PCB mini hammer 086C80 has a frequency range of 0 - 15 KHz, see figure 4.13. This should therefore be able to detect targets down to 133mm in size. In practice tendon ducts have a wide range of diameters from around 40mm to over 100mm. It is therefore unlikely that either hammer could be used with much success on beams with all but the largest tendon ducts. The energy input by the mini hammer is also low. Problems may occur with achievable depth of penetration with this impactor.

Calibration Chart for Impact Hammer Type 8202

Brüel & Kjær

Serial No. 1352913

Type 8202 includes Force Transducer Type 8200 serial no 1365694
(see individual calibration chart)

Sensitivity at output of hammer 0,99 pC/N
(includes the built-in attenuation of approx 12 dB)

	Force Range (N)	Duration Range (ms)	Approx Frequency Range (-10 dB) (Hz)
Rubber tip	100 - 700	5 - 1.5	0 - 500
Plastic tip	300 - 1000	1 - 0.5	0 - 2000
Steel tip	500 - 5000	0.25 - 0.2	0 - 7000

The additional mass decreases frequency range approx 30%

Temperature dependence of pulse length using rubber tip

Temp °C	-10	+5	+25	+40	+55
Duration ms	1.1	1.6	2.0	2.1	2.2

DC 0157 13

Weight of the hammer 280 g

Materials anodized aluminium, stainless steel, titanium, neoprene rubber

Weight of the additional mass	122 g
Weight of the plastic tip	3.9 g
Weight of the rubber tip	4.1 g
Weight of the steel tip	10.3 g

Dimensions (mm)

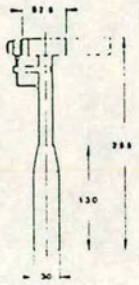

Date 87. 07. 06 Signature J. D.

Figure 4.12 Bruel and Kjaer impact hammer type 8202 specification

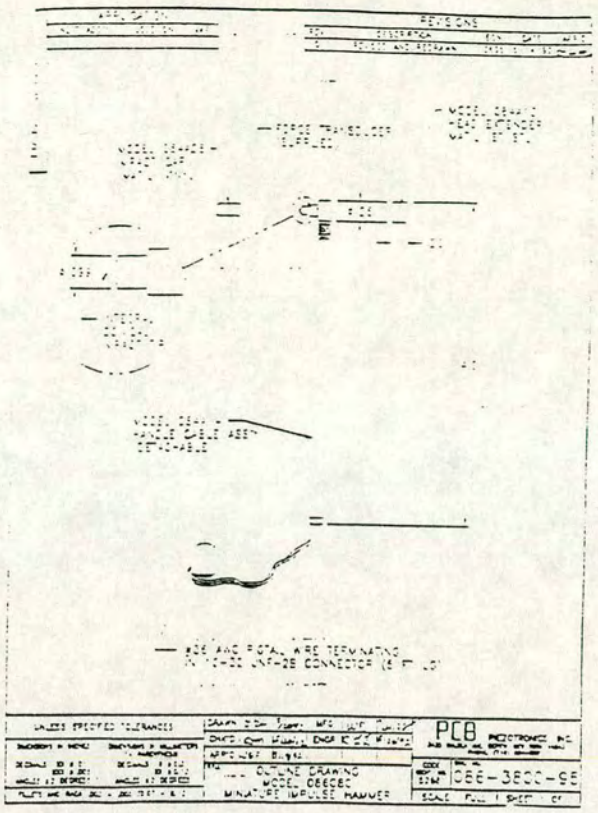

a) PCB mini hammer outline drawing

PCB PIEZOTRONICS

SPECIFICATIONS

IMPULSE HAMMER

REVISIONS

-E- Rev# 3695

SHEET 1 OF 1

MODEL NO. 086C80

Frequency Range	kHz	15
Hammer Range (5V output)	lb (N)	50 (220)
Hammer Sensitivity (approx)	mV/lb (mV/N)	100 (22.5)
Resonant Frequency	kHz	100
Hammer Mass	oz (gram)	0.44 (12.5)
Head diameter	inch (cm)	0.25 (0.63)
Tip Diameter	inch (cm)	0.10 (0.25)
Hammer Length	inch (cm)	0.80 (2.0)
Connector (coaxial)		10-32
Tip Set	Model No.	084A03
Head Extender	Model No.	084A10
Case	Model No.	001A02

b) PCB mini hammer specification

Figure 4.13 PCB mini hammer, 086C80, specification

4.5.2 Frequency Range of Response Tranducer

The accelerometer must be sufficiently sensitive to measure a high frequency response. Two accelerometers which have been used in investigations of large structures by the University of Edinburgh are the PCB A/30 Triaxial accelerometer and PCB A/20/T accelerometer. However, as shown in figure 4.14, these accelerometers have resonant frequencies in the normal direction of 27 KHz and 28 KHz respectively. The triaxial accelerometer has a nominal flat frequency response to 500 Hz and the A/20/T has a nominal flat frequency response to 2 KHz. However, on the calibration certificate for the A/20/T, figure 4.14b, it can be seen that there is still no deviation in the response at 4 KHz.

Manufacturers of accelerometers agree that a reasonable level of accuracy can be attained at 1/3 resonant frequency. Both accelerometers mentioned above are still not sensitive enough at higher frequencies. However, the PCB 303A03 accelerometer has a resonant frequency of 77 KHz. The calibration certificate, figure 4.15, also shows a relatively flat frequency response at 10 KHz. It was decided that this accelerometer would be sufficiently sensitive to measure frequencies up to 20 KHz for preliminary laboratory testing.

4.5.3 Frequency Range of Analyser

A high frequency analyser is necessary because it offers high resolution. A sampling rate of 100 KHz is desirable as the intention of the experiment was to determine the smallest defect that could be resolved. To allow accurate resolution of a signal with a frequency ΔF, a sampling rate $>\Delta F$ must be used. When the analysers used are set to 100 KHz they sample at 256 KHz. A 100 KHz signal corresponds to a depth in concrete of 40 mm. This means that a defect 20 mm wide should be resolved by the analyser. A Zonic A&D 2 Channel FFT Analyser was used throughout the experimentation. This analyser has a maximum frequency range of 100 kHz but can be set to a number of different frequency ranges. Figure 4.16.

The use of instrumented hammers and two channel analysers enable extensive signal processing to be carried out. Instrumented hammers measure the actual impact on the beam using an inbuilt load transducer. The analyser can then

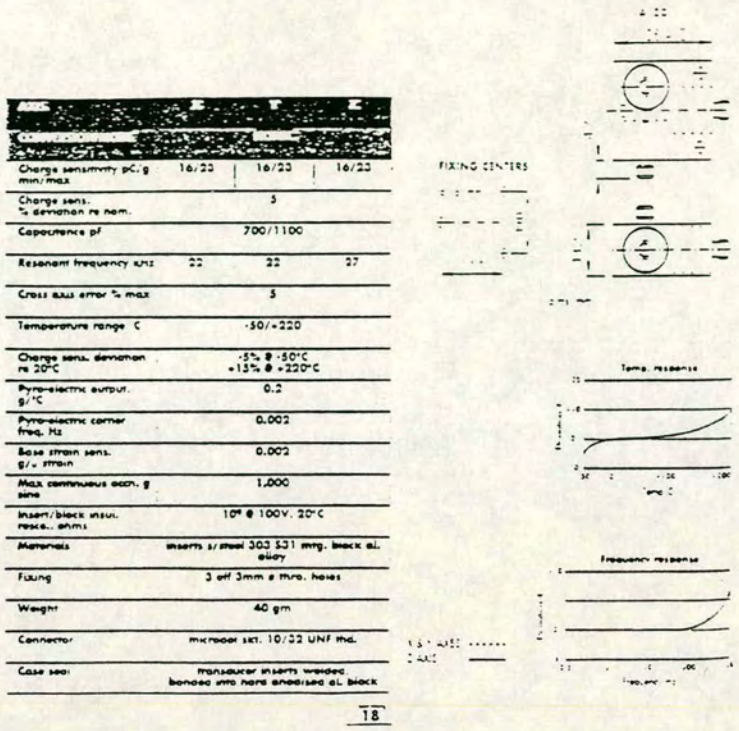

Charge sensitivity pC/g min/max	16/23	16/23	16/23
Charge sens. % deviation re nom.		5	
Capacitance pf		700/1100	
Resonant frequency kHz	22	22	27
Cross axis error % max		5	
Temperature range C		-50/+220	
Charge sens. deviation re 20°C		-5% @ -50°C +15% @ +220°C	
Pyro-electric output g/°C		0.2	
Pyro-electric corner freq. Hz		0.002	
Base strain sens. g/μ strain		0.002	
Max continuous accn. g sine		1,000	
Insert/block insul. resce., ohms		10^8 @ 100V, 20°C	
Materials		inserts s/steel 303 S31 mntg. block al. alloy	
Fixing		3 off 3mm ø thro. holes	
Weight		40 gm	
Connector		microdot skt. 10/32 UNF thd.	
Case seal		transducer inserts welded bonded into hard anodised al. block	

18

Fig 4.14a PCB A/30 accelerometer specification

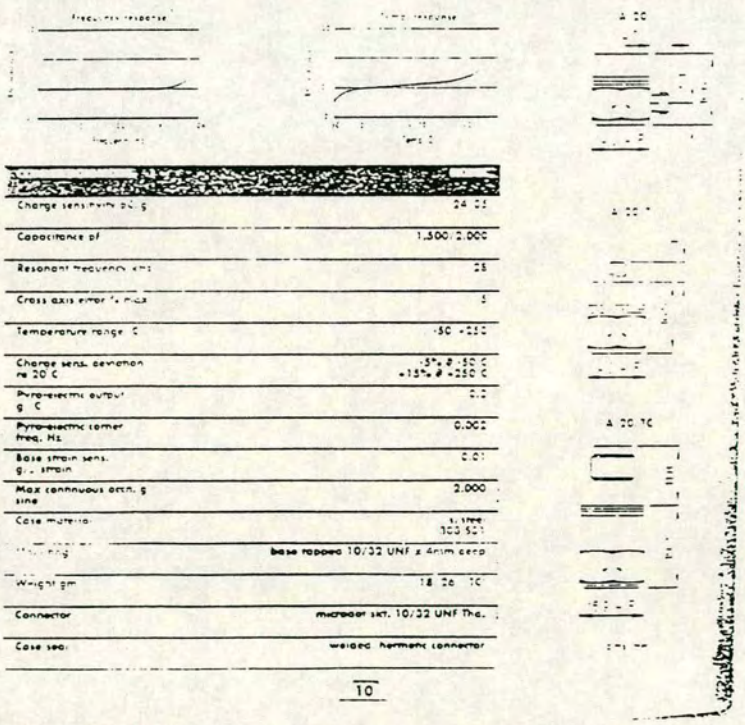

Charge sensitivity pC/g	24
Capacitance pf	1,500/2,000
Resonant frequency kHz	28
Cross axis error % max	5
Temperature range C	-50 +250
Charge sens. deviation re 20 C	-5% @ -50 C +15% @ +250 C
Pyro-electric output g C	0.2
Pyro-electric corner freq. Hz	0.002
Base strain sens. g/μ strain	0.01
Max continuous accn. g sine	2,000
Case material	s/steel 303 S21
Mounting	base tapped 10/32 UNF x 4mm deep
Weight gm	18 2a 1C
Connector	microdot skt. 10/32 UNF Thd.
Case seal	welded hermetic connector

10

Fig 4.14b PCB A/20/2 accelerometer specification

Figure 4.14 Accelerometer specifications

PCB

PIEZOTRONICS

CALIBRATION DATA
ICP ACCELEROMETER (per ISO RP 37.2)
Model No. 303A03
Serial No. 12235

By

Date 11/13/96

Voltage sensitivity:	10.30	mV/g	Resonant frequency:	77	kHz
Transverse sensitivity:	3.4	%	Time constant:	0.5	s
Resolution:	0.01	g	Maximum temperature:	250	°F
Output bias level:	10.9	V	Range:	500	± g

The Calibration procedure of PCB Piezotronics
is in compliance with MIL STD 45662.

Freq. Hz	10	15	30	50	100	300	500	1000	3000	5000	7000	10000
Deviation %	-.7	.3	0.0	-.2	0.0	.6	1.4	1.5	1.4	3.5	3.7	4.2

Calibration traceable to NBS through project no. 737/236905

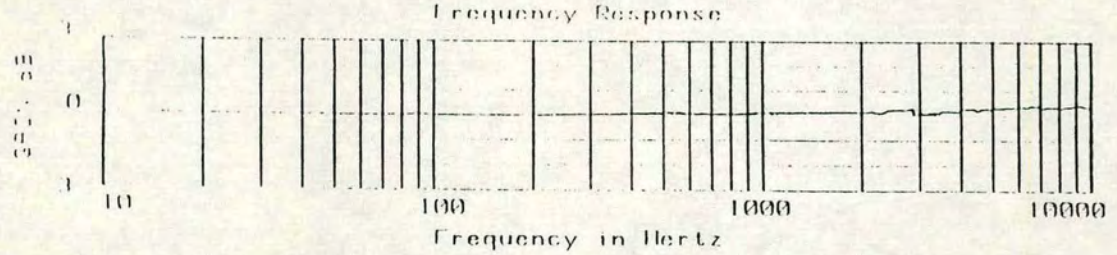

PCB PIEZOTRONICS, INC. 3425 Walden Avenue Depew, New York 14043-2495

Figure 4-15 PCB accelerometer, 303A03 calibration data

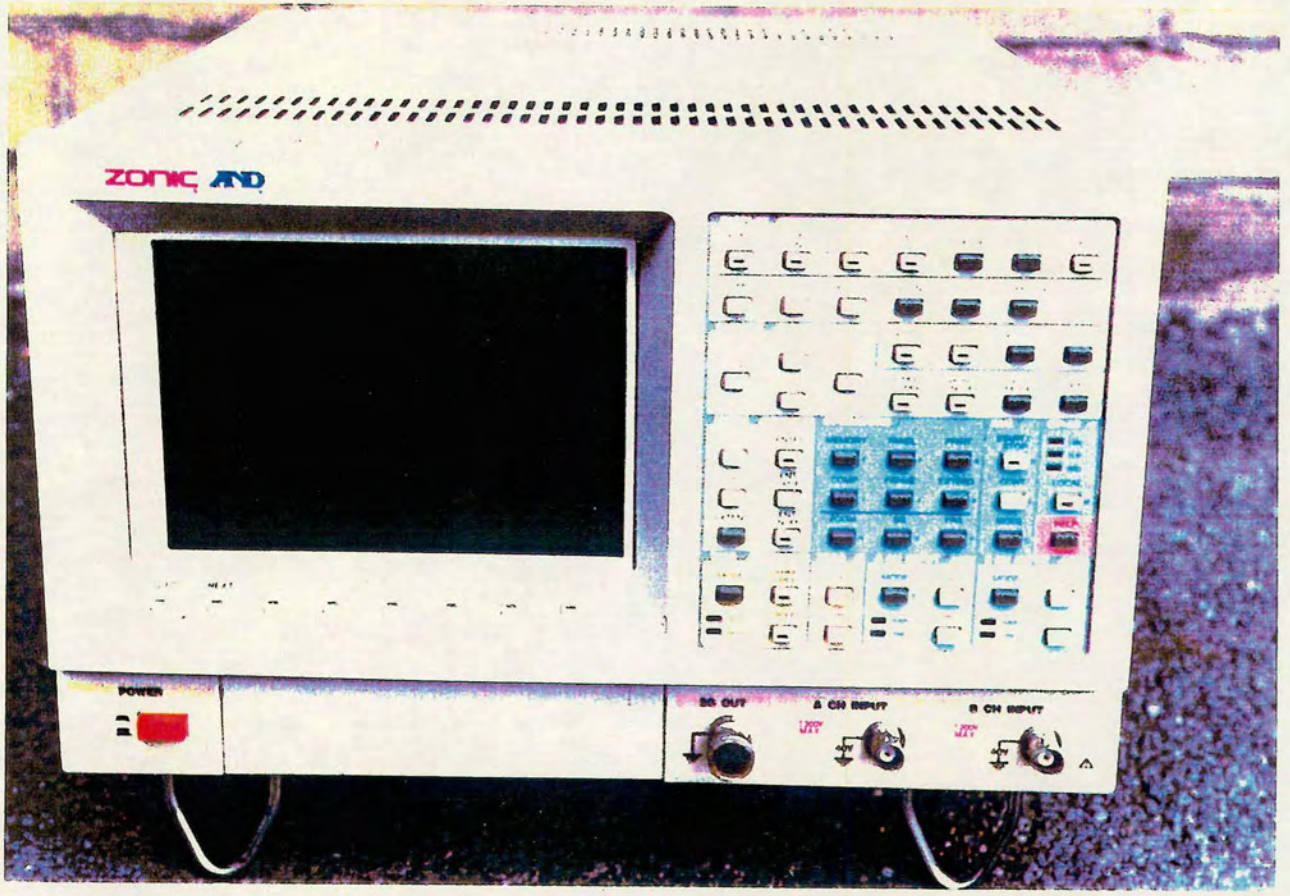

Figure 4.16 Zonic A & D 3525 dual channel FFT analyser

perform an FFT on this time signal and so the actual input could be measured in the frequency domain. The range of usable frequency is measured as the frequency at which the input drops by 10 dB from the 0 Hz reading. The frequency response function (FRF) for each position is calculated using the analyser. The FRF is the FFT of the response from the accelerometer divided by the FFT of the hammer blow. This allows direct comparison of responses at different testing positions to be made as each response can be normalised.

4.6 Laboratory Model

A test beam was constructed containing three tendons. See figure 4.17 for details. All the ducts were formed using spiral metal tubing which was approximately 1mm thick. Two tendons were 75mm in diameter and the third was 100mm in diameter. The model was 2000mm long, 1000mm wide and 700mm deep. Light reinforcement was included to prevent cracking. The 75mm diameter ducts contained steel tendons but the 100mm duct did not. Voids of various size were formed using polystyrene and a delamination was included on the upper 75mm tendon (figure 4.18). Two 75mm tendons were placed one above the other. This was to investigate the vertical resolution with different testing configurations as, in practice post-tensioned beams are often designed with multiple tendons. The minimum depth to a 75mm diameter tendon was 100mm and the depth to the 100mm diameter tendon was 150mm. Experimental compression wave velocities were calculated during the curing of the beam and these will be used to give accurate estimations of expected peaks on the response specta.

4.7 Influence of Concrete properties on Impact

As mentioned previously the size of defect and minimum depth to defect that can be detected depends upon the cut-off frequency of the impact. The higher the cut-off frequency, the smaller the defect that can be detected. It is usual for the cut-off frequency for an impact hammer that is not instrumented to be calculated using Hetzian elastic theory (Goldsmith, 1960, Carino et al, 1986). Assumptions are made as to the average Modulus of Elasticity and Poisson's ratio for concrete and the impactor material. However, concrete is an inhomogeneous material and there will be local variations throughout a concrete structural member. This will affect the actual cut-off frequency obtainable at each point.

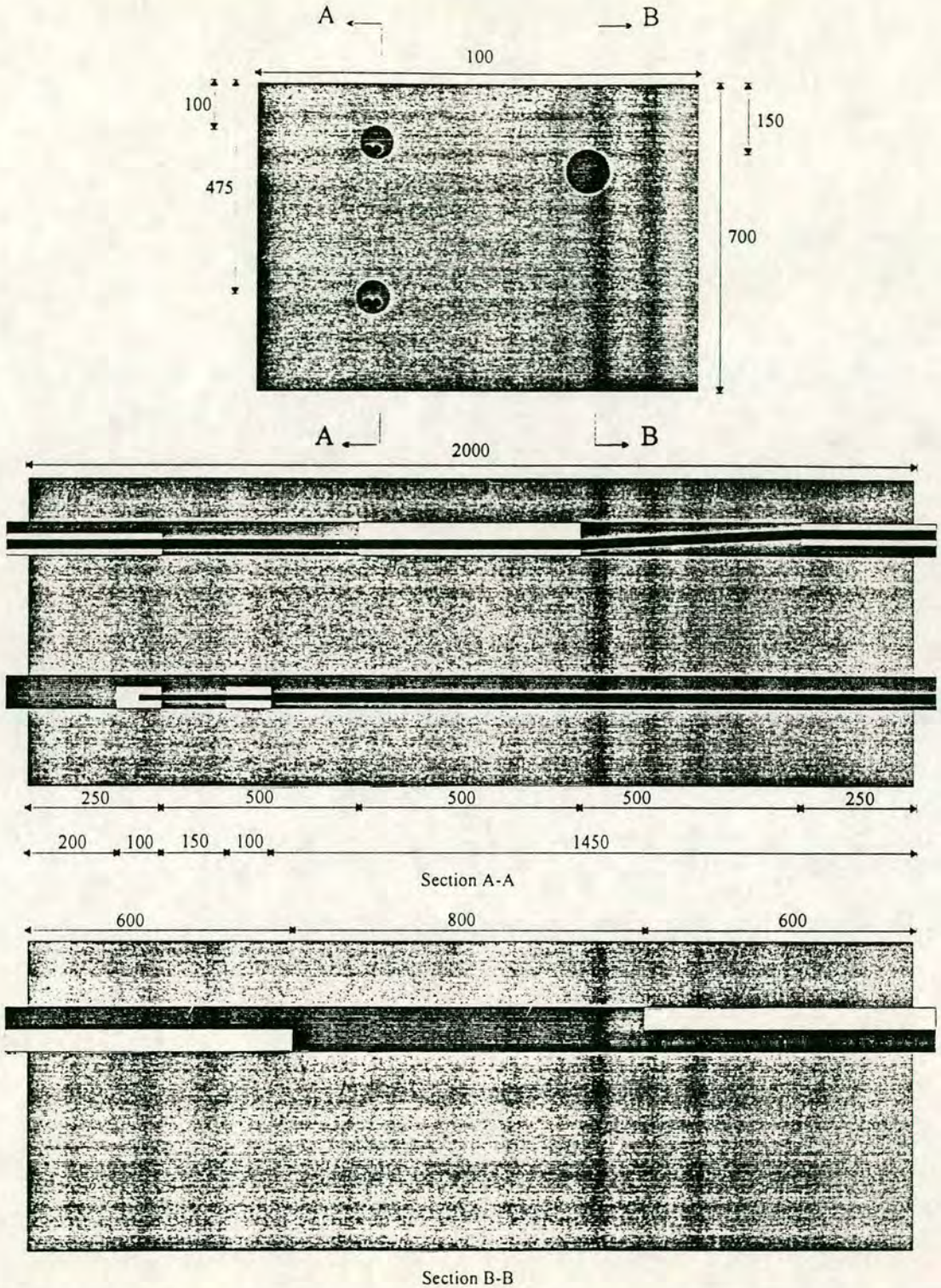

Figure 4.17 Laboratory model 1

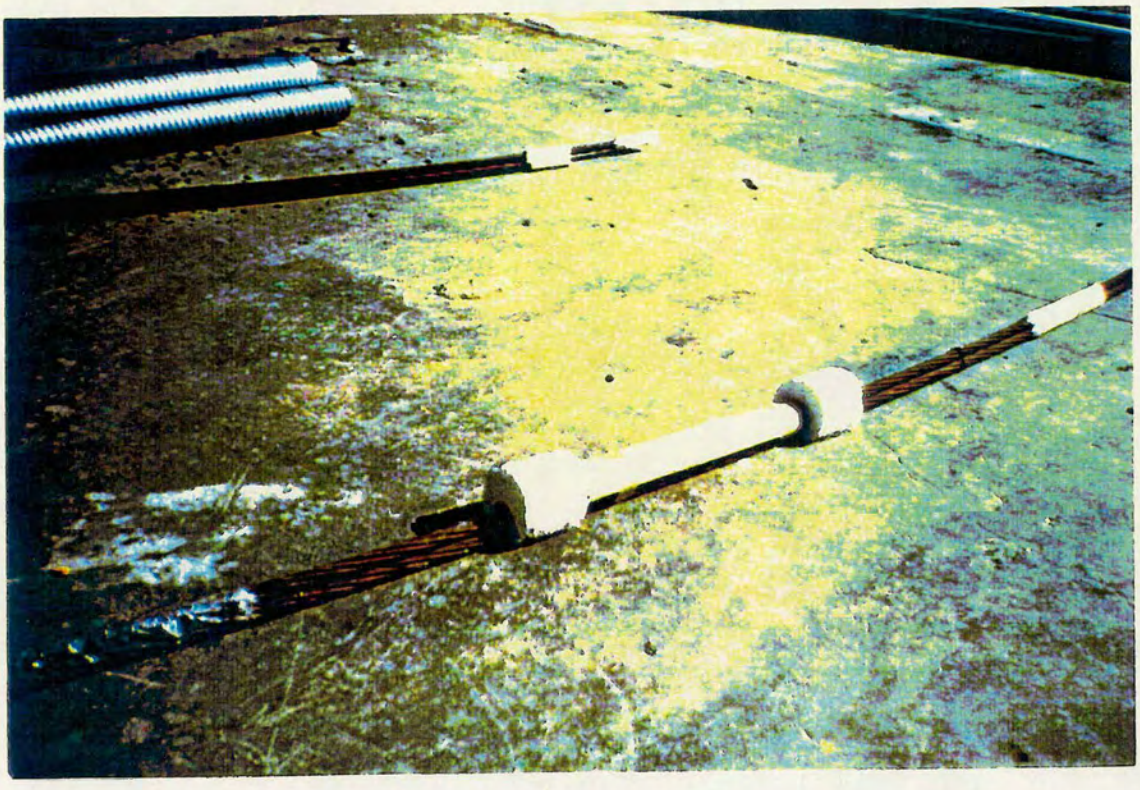

Figure 4.18 Photograph showing void construction

Elastic theory is not fully applicable to impact on concrete as local crushing of the concrete can occur at impact. The amount of crushing will vary according to the force of the impact, the contact area of the impactor and the local compression strength of the concrete. Crushing of the concrete will act to greatly reduce the actual cut-off frequency obtained which will have a detrimental effect on the detection of defects.

An investigation was undertaken into this effect. The compression wave was introduced using instrumented impact hammers. The contact time of the hammer and specimen determines the smallest target that can be located. As the test specimen becomes more complex the response of the specimen becomes difficult to analyse in the time domain. It is more useful to look at the response in the frequency domain. The impact can also be analysed in the frequency domain, the shorter the contact time, the higher the maximum frequency input. The maximum frequency input into the test object therefore determines the smallest target that can be detected and the smallest depth to target. In this study, the maximum frequency of input was taken as the point at which the frequency spectrum of the impact had decreased by 10dB from the 0Hz value (Corelli and Brown, 1984). This value was termed the Cut-off Frequency.

Most impactors used in investigations at present are not instrumented and so no direct measurement of the impact is made. It is therefore not possible to obtain the frequency content of the impact at each test. Some work has been carried out to determine the input force-time function using deconvolution (Hsu, Chen and Sansalone, 1987). The displacement of a point on the beam is measured with time: the displacement-time function. This function is considered the convolution of the input force-time function with an impulse response function (corresponding to the beam). The input force-time function, and therefore the cut-off frequency, can then be determined by deconvolution of the measured displacement-time function with the impulse response function. However, no account is taken of the condition of the concrete in determining the impulse response function.

This study examines the effects that the mix and condition of the concrete have on the cut-off frequency and velocity obtained as the concrete cures over 28 days. The cut-off frequency and pulse velocity are dependent on the density, ρ, Elastic modulus, E, and Poisson's Ratio, ν, of the concrete. Different mixes of concrete will

have different values of r and E. For example, as the cement:aggregate ratio increases the density will decrease (for most aggregates) and the results will be affected accordingly. Previously work has been carried out using the variation in compression wave (p-wave) velocity as concrete ages to determine setting time and strength (Pessiki and Carino, 1988). It was considered worthwhile to determine the p-wave velocity for each set of cubes to investigate the relationship between the development of this and the development of the cut-off frequency.

4.8 Experimental Procedure

4.8.1 Concrete Mixes

Two mixes of concrete were made: one containing sand and granite (10-20mm dia rough granite chips -concrete) and the other sand only -mortar. The mix proportions are shown below.

	Concrete	Mortar
	(kg)	(kg)
Sand	30	60
Gravel	37.5	-
Cement	15	20
Water	7.5	10

Table 4.1 Mix Proportions

Sets of 100mm cubes were cast. On each testing day three cubes of each mix were tested.

4.8.2 Determining the pulse velocity.

It was not possible to accurately measure the p-wave velocity of a sonic wave through each cube by impact-echo or transmission test. i.e. by impacting on one side and measuring the response on the other side. The cut-off frequency was not high enough to pick up the edge of the small cubes in an impact echo test. The cubes were also too small for the time delay to be sufficiently large to measure on the trace in a transmission test. The pulse velocity of an ultrasonic wave was then calculated using two 54kHz transducers. See figure 4.19. The tester is calibrated before being used on the cubes by firstly

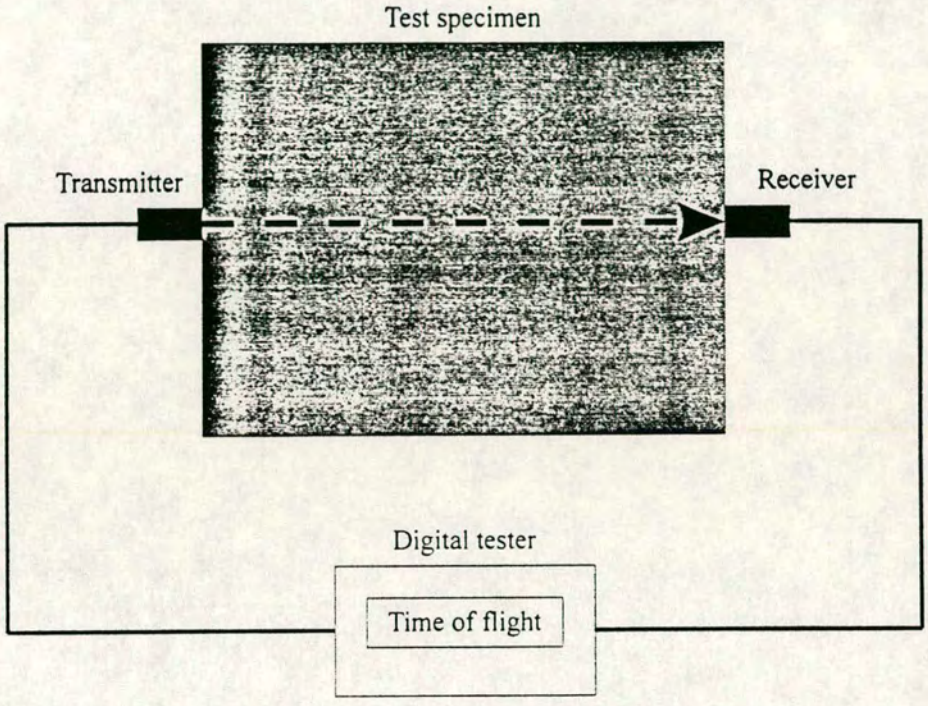

Figure 4.19 Ultrasonic pulse velocity calculation set-up

measuring the time of transmission along a calibration cylinder with a known transmission time and then adjusting the tester to read the correct time.

The 54kHz transducers were placed on opposite sides of the cube, ensuring that both sides were against the smooth sides of the mould when the cubes were cast. This ensured the best coupling. Water pump grease was used to couple the transducers to the cube. One transducer was used as a transmitter and the other as a receiver and the time of flight of the pulse from the transmitter to the receiver, through the concrete, was recorded on the digital tester.

This procedure is repeated three times and the average time calculated. The cube is then measured and the ultrasonic pulse velocity calculated. The ultrasonic pulse velocity was then calculated for the other two cubes, from which the average result for that age of concrete was calculated. Previous research has found that compression wave velocities obtained using ultrasonic pulse-velocity methods were higher than those obtained from sonic impulse-echo methods (Carino, Sansalone and Hsu, 1986). It was therefore considered necessary to investigate the difference between the ultrasonic pulse velocity calculated through a concrete beam using the same method as descibed above and the pulse velocity calculated from a transmission test and also an impact-echo test using an impact hammer and receiving transducer.

4.8.3 Converting Ultrasonic Pulse Velocity to Sonic Pulse Velocity

The ultrasonic pulse velocity was calculated through four locations on a 1m wide concrete beam using the method discussed above. A transmission test and impulse echo test were then carried out at the same locations using the 280g hammer. This hammer gives a high enough cut-off frequency to pick up the back surface and also inputs sufficient energy for the wave to be reflected from the back of the beam and return to the front side for measurement by the accelerometer in the impulse-echo test. See figures 4.20 and 4.21

4.8.4 Impact hammers

Two steel tipped hammers were used. The 280g hammer has an expected cut-off frequency on steel of 7 kHz and the 1.25g mini hammer has an expected cut-off frequency on steel of 15 kHz. Both hammers contained a force transducer allowing the force impact to be measured with time.

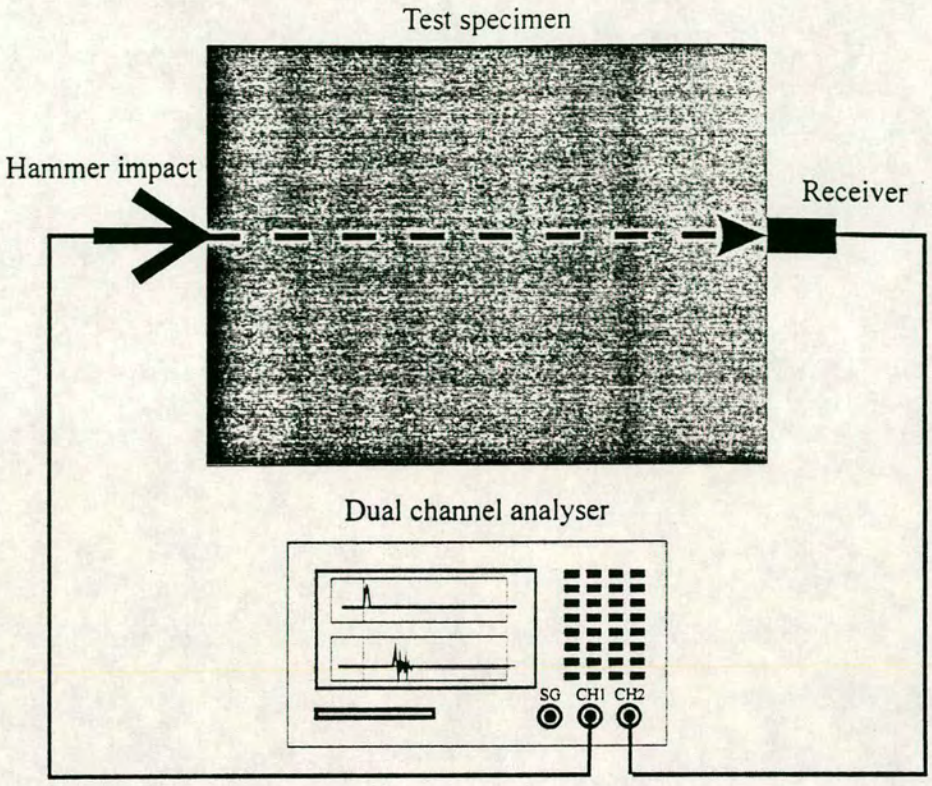

Figure 4.20 Sonic transmission test to determine pulse velocity

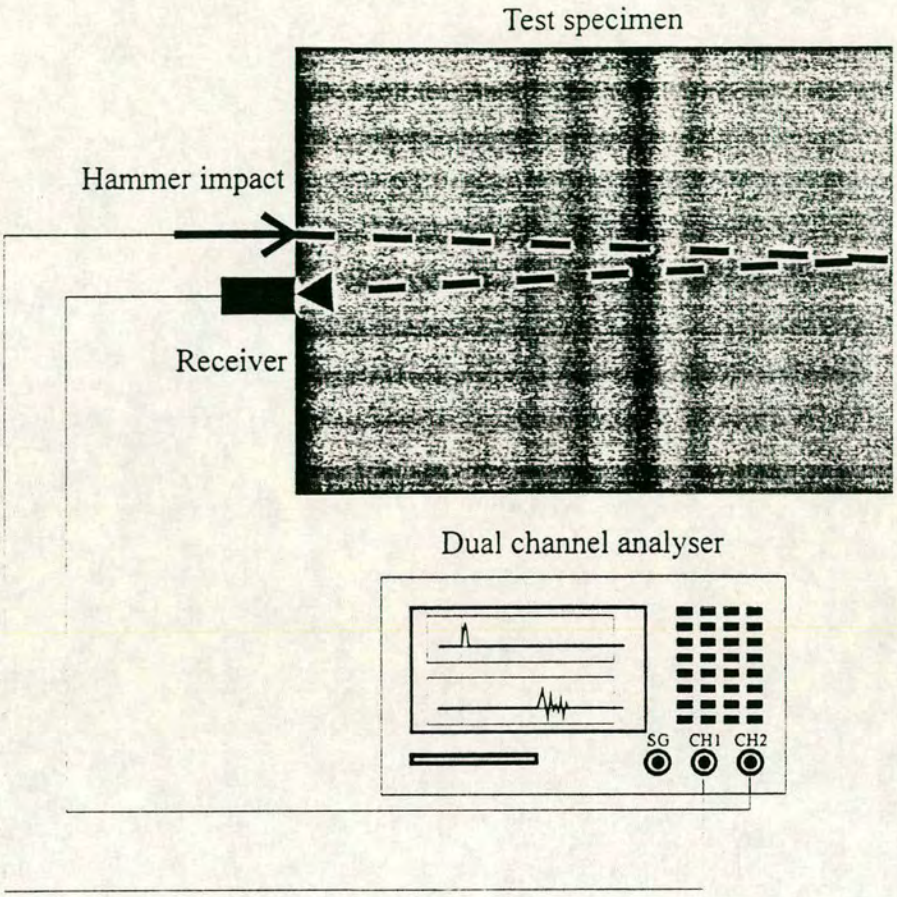

Figure 4.21 Sonic impact-echo test to determine pulse velocity

4.8.5 FFT Analyser

The Zonic A and D dual channel FFT analyser was used. The analyser has built in anti-aliasing filters and so the actual sampling rate is 256 kHz. This gives a good resolution of the impact.

All the tests were performed on a side of the cube that was cast against the smooth metal sides of the cube mould. This ensured similar surface conditions for all the tests. An average of five impacts was taken on each cube with the 1.25g mini-hammer. The impact was recorded in the time domain (figure 4.22a) initially, as it was then instantly obvious if a mishit had occurred. The five impacts were then averaged and an FFT performed which gave the average impact in the frequency domain. (figure 4.22b) The cut-off frequency was then noted for each of the three cubes and an average calculated. The above procedure was then repeated using the 280g hammer. (figure 4.23). The mass, dimensions and compressive strength of the cubes were then measured and the average calculated. This was then repeated on both the concrete and mortar cubes as the cubes aged.

4.8.6 Results

4.8.6.1 Pulse Velocity Determination.

It was expected that the ultrasonic compression wave speed would be greater than the sonic wave speed. However, this was not found to be the case. The results are shown in Table 4.2.

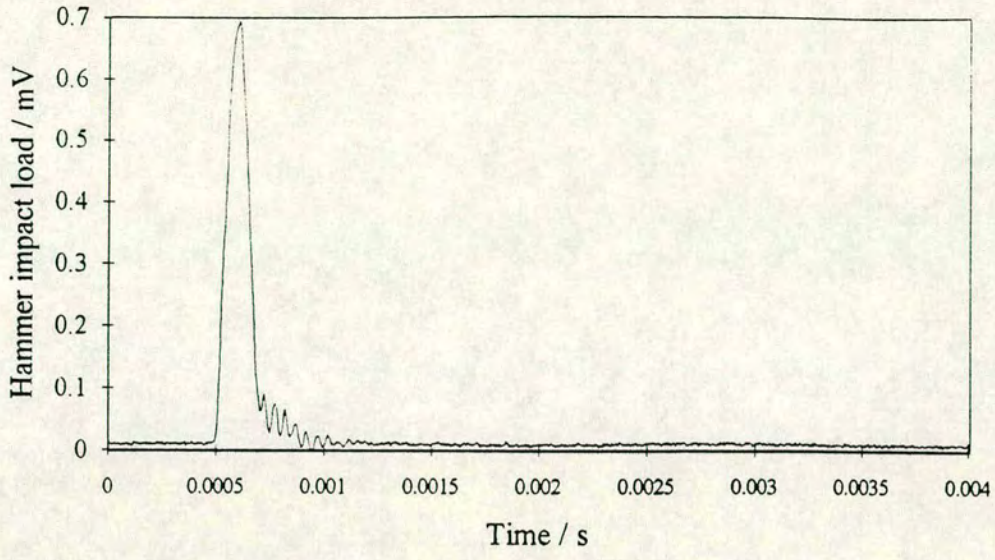

Fig 4.22a Time domain

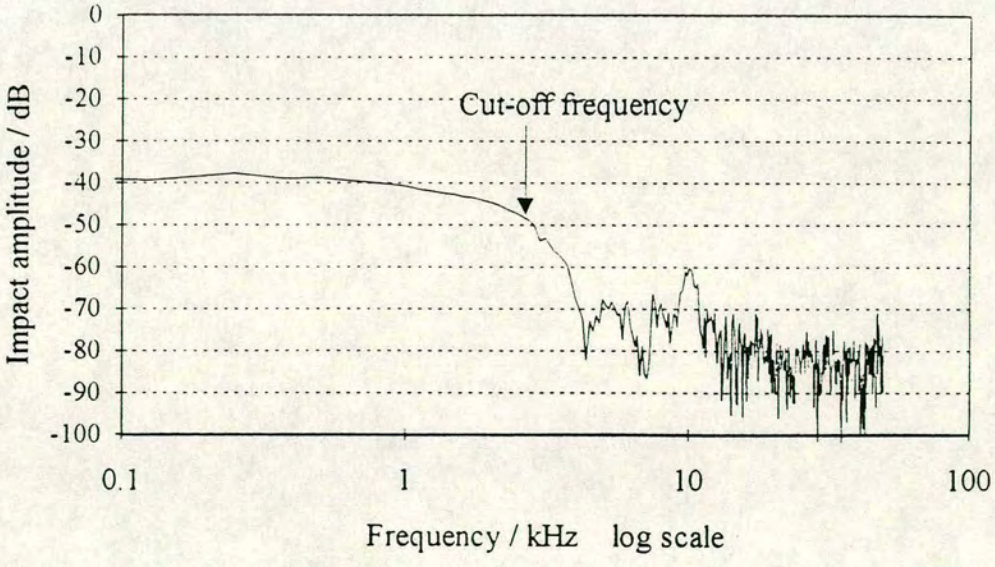

Fig 4.22b Frequency domain

Figure 4.22 Cut-off frequency determination, B&K hammer (280g)

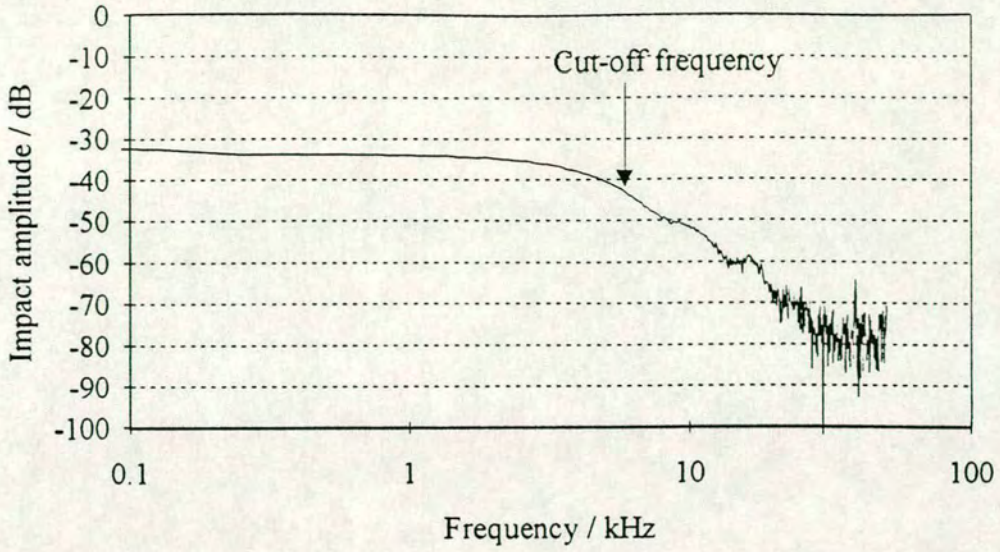

Figure 4.23 Cut-off frequency determination, PCB hammer

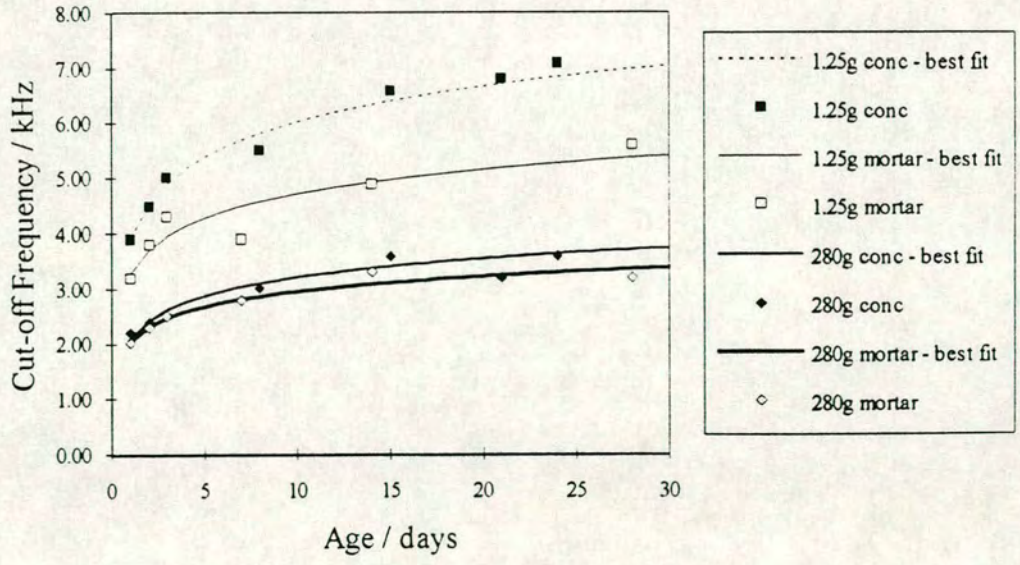

Figure 4.24 Cut-off frequency data

Sonic I-E Test	Position	Peak Frequency (kHz)	Distance (m)	Velocity (m/s)
	1	2.000	2	4000
	2	1.925	2	3850
	3	2.075	2	4150
	4	2.075	2	4150
			Average	4040
	Position	Time ($\times 10^{-6}$s)	Distance (m)	Velocity (m/s)
Sonic Transmission Test	1	254	1	3937
	2	260	1	3846
	3	243	1	4115
	4	246	1	4065
			Average	3991
54kHz Transmission Test	1	248	1	4039
	2	252	1	3971
	3	250	1	3997
	4	250	1	4002
			Average	4002

Table 4.2: Transmission Test Results

As can be seen, the results from the Sonic Transmission test and the Ultrasonic Transmission test (54kHz) are very similar. The results from the Sonic Impact Echo test (sonic I-E test) are slightly higher than expected. However, there is a considerable spread of calculated velocities within each series. It was therefore not considered worthwhile to factor the velocities calculated on the cubes using the ultrasonic digital tester.

The reason the results were very similar was that the frequency of excitation of the ultrasonic tester was relatively low for ultrasonic testing, (54kHz - whereas most ultrasonic testing is undertaken on metals using transducers

with an excitaion frequency greater than 200kHz) and the cut-off frequency of the impulse hammers was relatively high (2 - 8kHz - most sonic testing undertaken to date use hammers with a cut-off frequency less than 1.5kHz). Note:

- Pundit gave an ultrasonic p-wave velocity of 4002 m/s.
- The transmission tests gave a p-wave velocity of 4000 m/s
- The Impact-Echo test gave a p-wave velocity of 4040m/s
- This gives a factor of 1 for velocity results.

4.8.6.2 Defect Identification

Figure 4.24 shows that there is a significant difference in the cut-off frequency obtained between the concrete and mortar cubes with the 1.25g hammer and a detectable difference between the concrete and mortar with the 280g hammer. These results are an average of readings taken for three test cubes. The results are repeatable and individual cut-off frequencies obtained are shown in Table 4.3. At 28 days the cut-off frequency obtained with the 1.25g hammer is 7kHz on the concrete cube and 5.25kHz on the mortar cube - a difference of 25%. The difference in the cut-off frequency obtained with the 280g hammer on the two sets of cubes is much less (approximately 15%). This would suggest that as the cut-off frequency increases the sensitivity to the concrete mix also increases. A 25% drop in cut-off frequency could have a significant effect on an investigation e.g. a cut-off frequency of 10 kHz is expected when testing a concrete beam. Using Eqn. 2 and assuming a pulse velocity of 4000m/s the profile of the smallest target that should be detectable is 200mm. However, if the cut-off frequency is actually 7.5kHz, the profile of the smallest target detectable would be 267mm. If the investigation is required to find voids greater than 200mm it could be possible to conclude that the test object was sound when voids were actually present. Thus the commonly adopted null hypothesis, 'If no defect is identified, none exist' is invalid.

Impact-echo testing of concrete frequently requires cut-off frequencies much higher than 10kHz. If an impact generating frequencies up to 50kHz is expected, the actual cut-off frequency may be very much lower which could have a very serious effect on the results of an investigation if the mix proportions of the specimen have not been investigated. The results indicate

that as the expected cut-off frequency increases the influence of concrete mix also increases. The greater the volume and density of aggregate the greater the cut-off frequency obtained using the same impactor.

As can be seen in figure 4.25 the pulse velocity increases with age for both concrete and mortar as the cubes cure. The cubes are hardening over this period and therefore the pulse velocity increases. The pulse velocity is higher through the concrete cubes as expected. The concrete contains granite chips and the pulse velocity through these is higher than that through the sand and the cement paste. As the size of the chips increases it would be expected that the pulse velocity would also increase towards that of solid granite. A difference of 150 m/s was found. This could lead to a defect being detected in a test specimen but because the assumed velocity was wrong, the expected location of the defect would also be wrong - see figure 4.26.

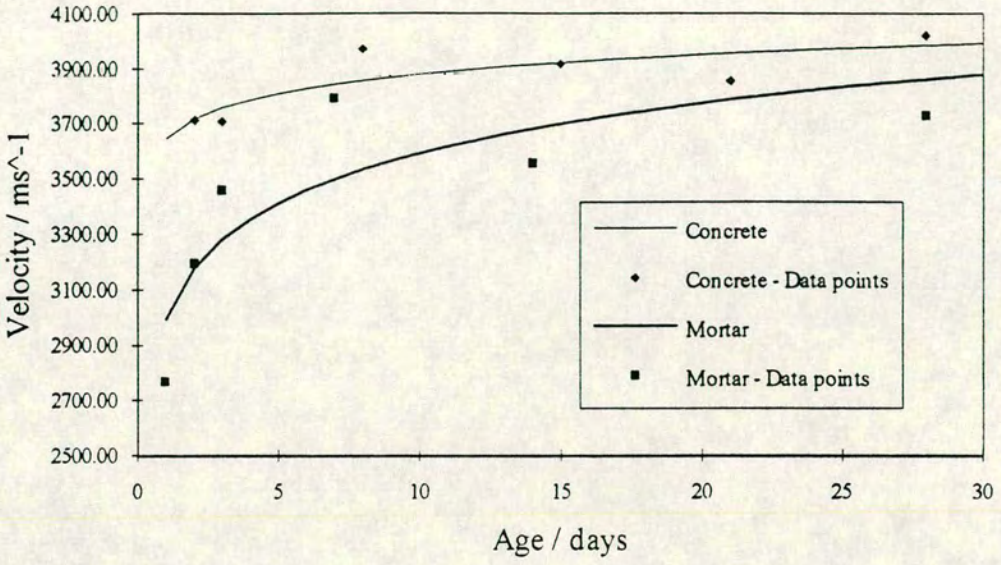

Figure 4.25 Pulse velocity data

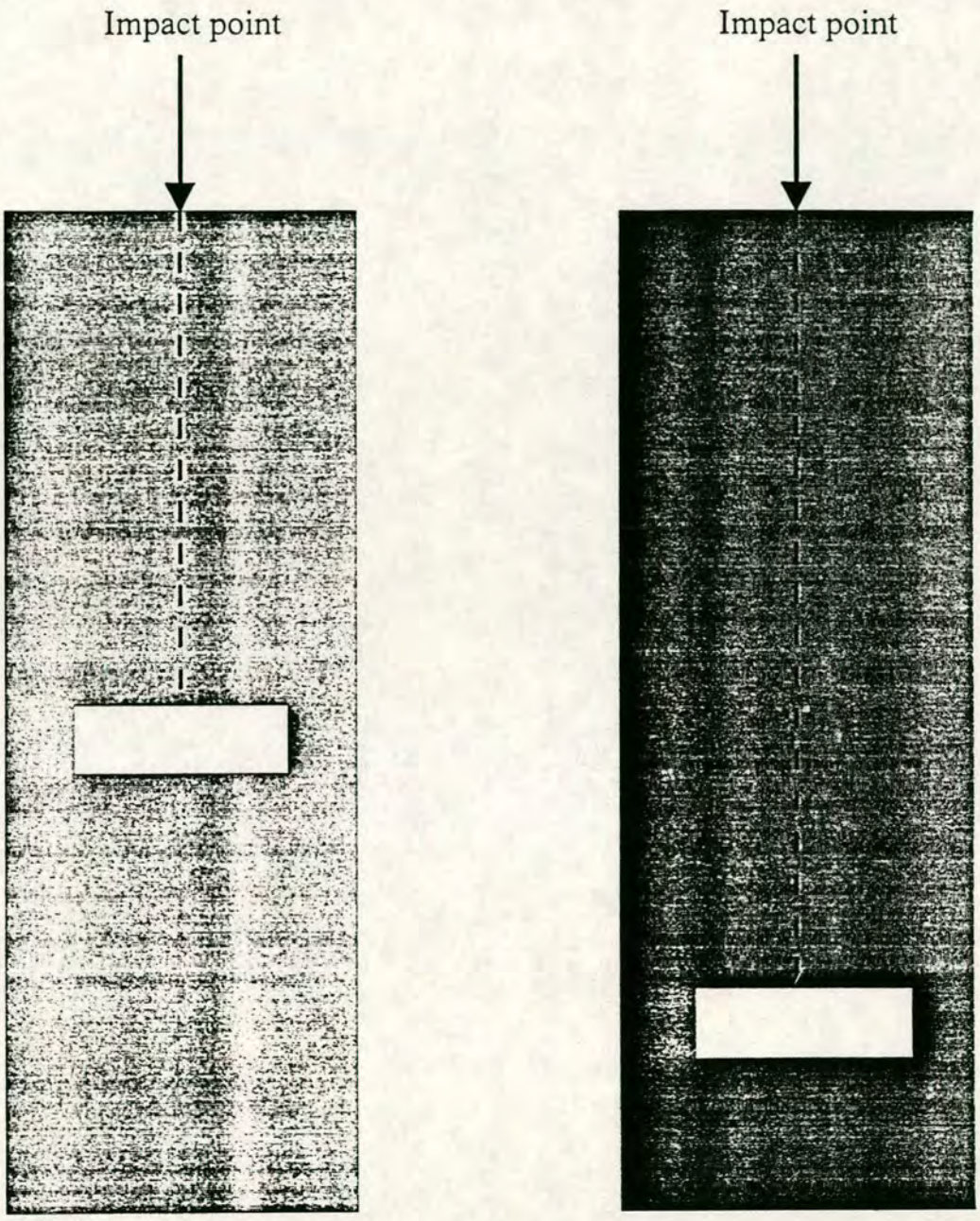

Figure 4.26 Faults in defect location due to incorrect assumption of velocity

Concrete Cube Data				Mortar Cube Data			
Age	Cube No	280g Hammer Cut-off Freq.	1.25g Hammer Cut-off Freq.	Age	Cube No.	280g Hammer Cut-off Freq.	1.25g Hammer Cut-off Freq.
(days)		(kHz)	(kHz)	(days)		(kHz)	(kHz)
1	1	2.375	3.5	1	1	2	2.75
	2	2.25	4.25		2	2	3.25
	3	2	4		3	2	3.5
2	1	2.375	4.5	2	1	2.5	3.5
	2	2.375	4.5		2	2.25	4
	3	2.5	4.5		3	2.25	4
3	1	2.5	4.75	3	1	2.5	2.5
	2	2.5	5		2	2.5	4.5
	3	2.5	5.25		3	2.5	4
8	1	2.75	4.75	7	1	2.75	4
	2	3	6		2	2.75	3.5
	3	3.25	5.75		3	2.75	4.25
15	1	3.25	6.5	14	1	2.75	3.125
	2	2.75	6.75		2	3.5	5.25
	3	4.875	6.5		3	3.5	4.5
21	1	3.25	6	28	1	3.25	6.5
	2	3	7.375		2	3	5.125
	3	3.275	7		3	3.25	5.25
24	1	4	7				
	2	3	7.5				
	3	3.875	6.75				
28	1	4	6.25				
	2	4.25	7				
	3	4	6.75				

Table 4.3 Experimental Data

Figure 4.27 shows the change in compressive strength for the two sets of cubes over 28 days. These results are quite similar as the water:cement ratio is the same for the mortar and concrete mixes (Neville and Brooks, 1987) The concrete has a slightly higher compressive strength. This is expected as it has been found, for a constant water:cement ratio, a mix with proportionately less cement paste has a higher compressive strength. This is due to a reduction in

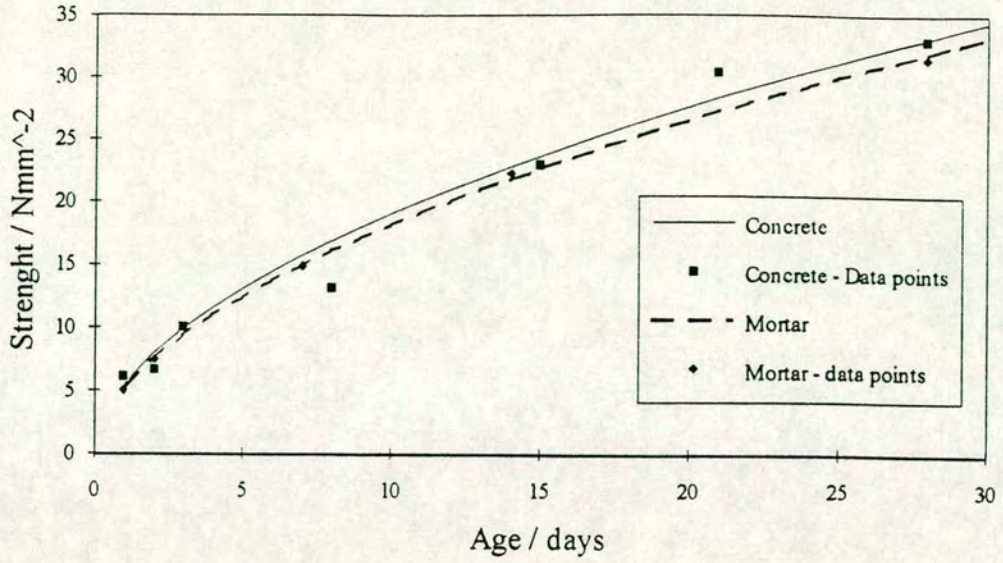

Figure 4.27 Strength data

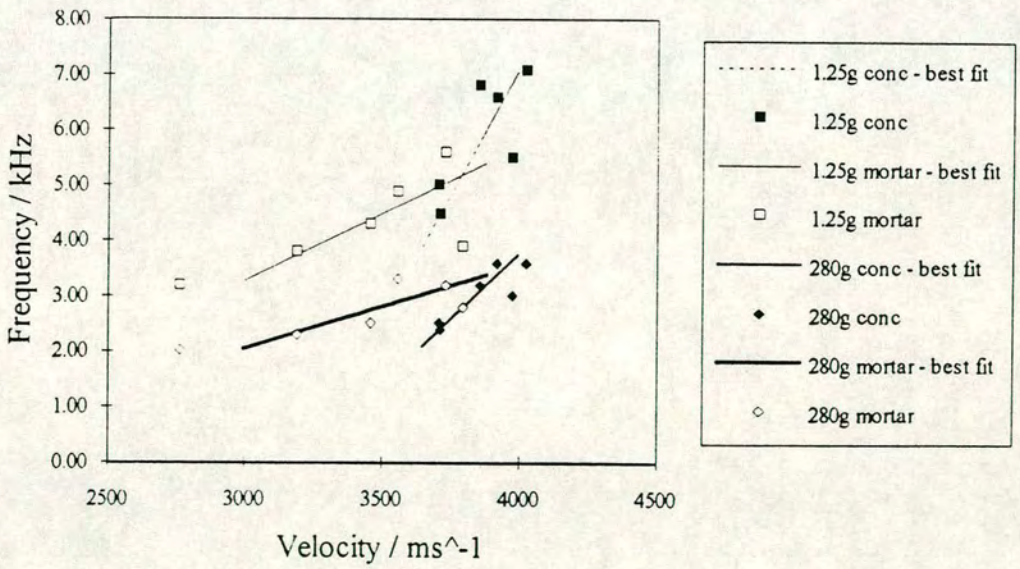

Figure 4.28 Velocity vs. Cut-off frequency

the porosity of the concrete which would give rise to an increased strength (assuming no voids in the aggregate).

4.8.6.3 Influence of Aggregate on Cut-off Frequency

The pulse velocity and the cut-off frequency are both related to the Elastic modulus, density and Poisson's ratio of the material. The values for each were then compared (figure 4.28) to determine their relationship. The surface condition also affects the cut-off frequency but is not that important when determining the pulse velocity as the measurement is taken through the whole structure. However, the cubes were constructed in the same way and the tests were carried out to ensure as similar surface conditions as possible.

The graph shows an approximately linear relationship between pulse velocity and cut-off frequency. The mortar cubes seem to give rise to better results with both hammers than the concrete cubes. This could be because the mortar cubes are more homogeneous than the concrete cubes i.e. there are no granite chips present. With the concrete cubes it would be possible that sometimes a granite chip would be located just under the impact point thus giving a slightly harder surface relative to a point where the granite chip was further from the surface. See figure 4.29. This would give rise to a higher cut-off frequency. The pulse velocity is calculated through the whole cube and any local variations in granite chip density will be averaged out throughout the whole path length. However, a relationship can be seen and with specific research it may be possible to determine the cut-off frequency obtainable with a certain impactor for a specific mix proportions of concrete.

4.8.6.4 Implications for Assessment of Compressive Strength

The relationship between strength and cut-off frequency is linear as shown in figure 4.30. As the strength increases, so the surface hardness and density increases and therefore the cut-off frequency will increase.

The graph indicates that using lower frequency impacts the mix does not greatly affect the cut-off frequency obtained. Also, as the concrete ages and gains strength, the variation in cut-off frequency obtained is not great. Using the 280g hammer, over a strength gain of 25 N/mm^2, the cut-off frequency increases by 1kHz.

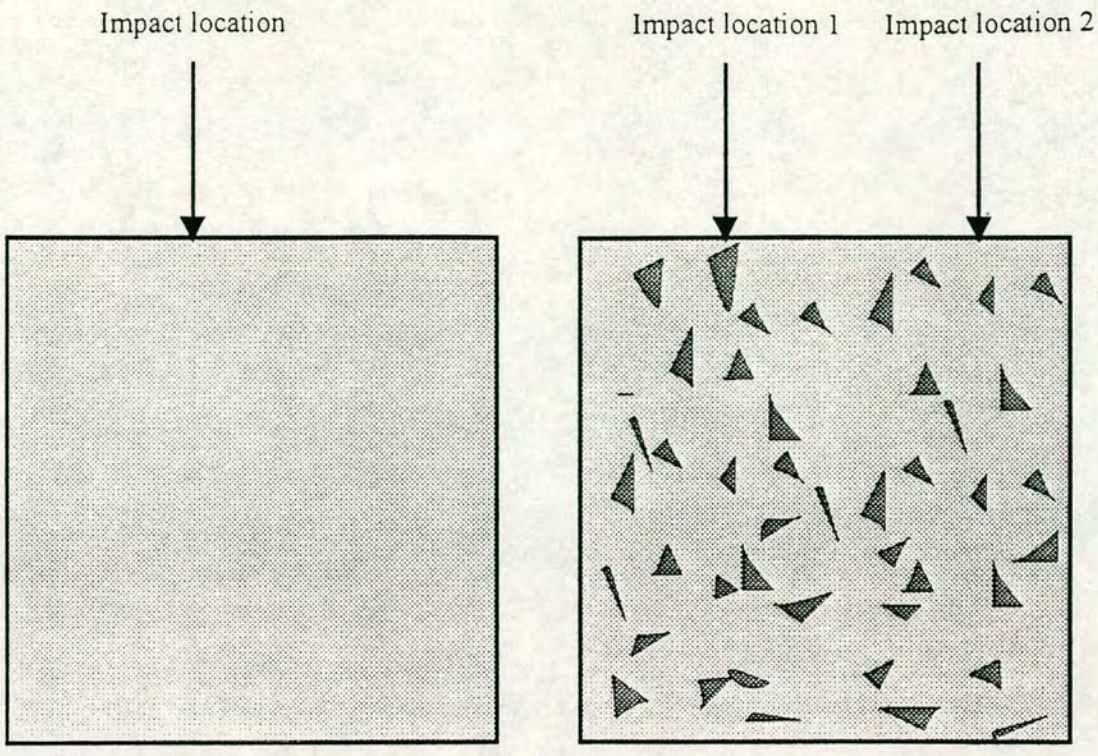

a) Grout specimen

b) Concrete specimen

Figure 4.29 Effect of material structure on impact characteristics

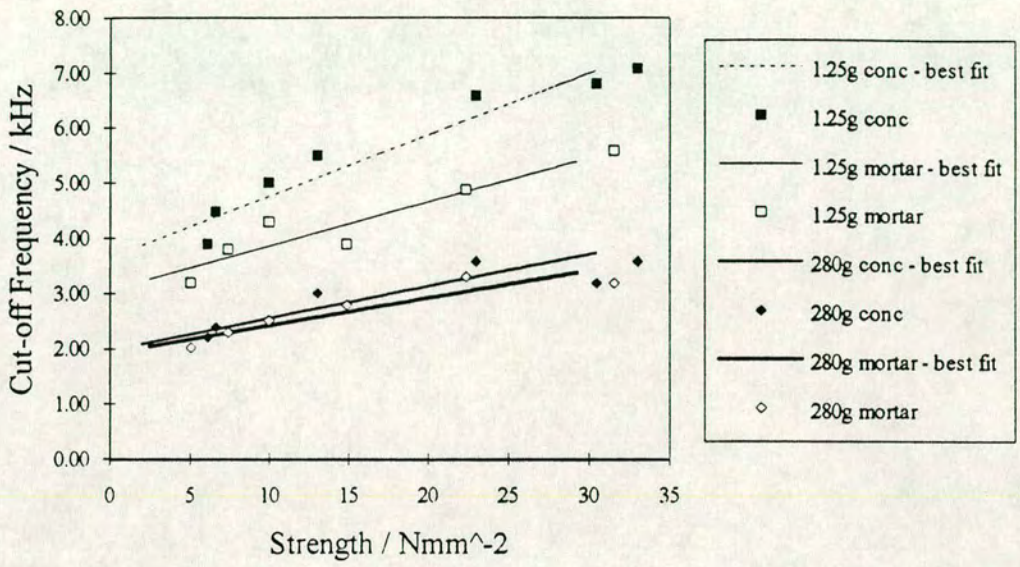

Figure 4.30 Strength vs. cut-off frequency

The results from the 1.25g hammer show a much clearer difference for mix type. With mortar the slope of the line obtained using the 1.25g hammer is greater than that for the 280g hammer. For an increase in strength of 25 N/mm^2, the cut-off frequency increases by 2kHz. The largest slope was found using the 1.25g hammer on concrete (the hardest material tested). In this case over an increase in strength of 25 N/mm^2, the cut-off frequency increases by 3.1kHz. The above results indicate that an insitu testing method for concrete could be developed using high frequency hammers.

A database could be set up with different mixes of concrete and standard curves calculated for each mix of compressive strength against cut-off frequency. The structure could then be tested and the cut-off frequency obtained compared to the curve of strength versus frequency for that particular mix of concrete. Alternatively, a more simple approach would be to cast cubes from a delivery of concrete. The cut-off frequency would be measured for, say, three cubes and the compression strength measured at any given age. The cut-off frequency could then be measured at different points on the structure and compared to those obtained on the cubes. Any areas on the structure resulting in a low cut-off frequency would indicate the concrete in that area had a lower strength and care should be taken, eg. in the removal of formwork. This method would require minimum equipment and many readings could be taken very quickly making this a very economical method for non destructive testing of concrete structures.

4.8.7 Conclusions on Experimental Procedure

1. The mix proportions of a concrete and mortar have a significant effect on the cut-off frequency obtained by an impact hammer. The higher the percentage of aggregate, the higher the cut-off frequency obtained. A difference of almost 2kHz was noted for the same hammer on a mortar and concrete mix.

2. The cut-off frequency obtained increases with age, i.e. as the concrete cures.

3. The higher the modally tuned cut-off frequency of the impactor the greater the effect of mix proportions on the actual cut-off frequency obtained.

4. The pulse velocity increases as the concrete cures. The pulse velocity is higher for concrete and mortar with higher percentages of aggregate. A difference in pulse velocity of 150m/s was noted for the mortar and concrete mixes at the same age.

5. The compressive strength of the concrete and mortar increases as the concrete and mortar cures. The compressive strength of the concrete and mortar is comparable as the water:cement ratio is constant. However, the strength of the concrete is slightly higher as the proportion of paste is lower than that of the mortar.

6. The pulse velocity can be related to the cut-off frequency obtainable for an impulse hammer on a mix of concrete and mortar.

7. There is a linear relationship between compressive strength of a concrete and a mortar mix and the cut-off frequency obtainable. It should be possible to determine the strength of a concrete or mortar mix using an instrumented hammer of high frequency (>5kHz). This would be simple to carry out on site and could be used to determine formwork striking times.

8. There is therefore significant potential for the use of instrumented impulse hammer techniques in the non-destructive evaluation of concrete.

4.9 Alternative Test Configuration

It has been shown that the cut-off frequency of an impact determines the detail achievable by an impact-echo test and that this cut-off frequency is related to the condition and constituents of the concrete upon which the impact occurs. The cut-off frequency obtainable by commercially available instrumented hammers is rather low for impact-echo testing of post-tensioned concrete bridges. Another consideration is the energy introduced to the beam at impact. The highest frequency hammers available do not introduce high energy to penetrate a deep beam fully and allow measurement of the signal reflected from the base.

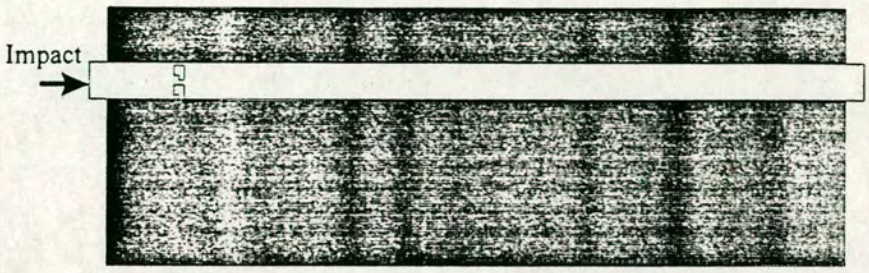

Figure 4.31 Small voids forming a delamination across duct

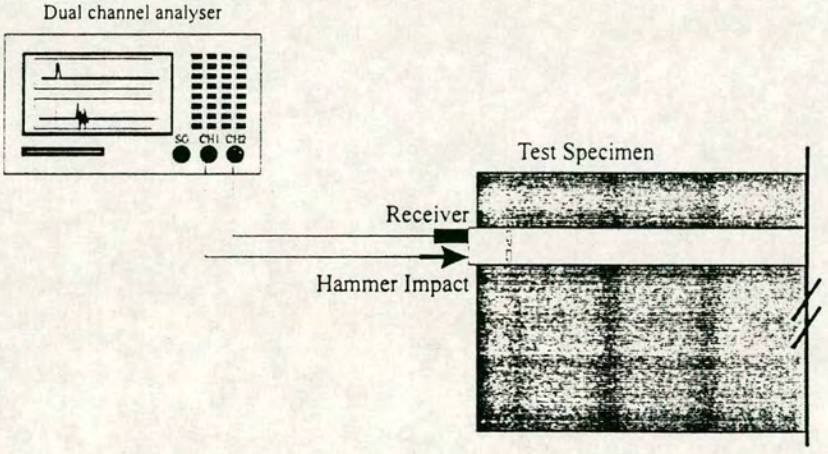

Figure 4.32 Pile-type testing procedure

Target	Distance	Calculated Frequency Peak	Experimental Frequency Peak	Notes
	(m)	(kHz)	(kHz)	
DUCT 1 - Front		(v = 3700 m/s)		
end void 1	0.35	5.3		cof = 2.25 kHz
end delam	0.6	3.1	2.9	
start void 2	0.85	2.2	2.0	
end void 2	1.35	1.4	1.5	
start void 3	1.85	1.0		
end beam	2.2	0.8		
DUCT 1 - Back				
start void 3	0.35	5.3		cof = 2.15 kHz
end void 2	0.85	2.2	2.35	
start void2	1.35	1.4		
end delam	1.6	1.2	1.2	
end void1	1.85	1.0		
start beam	2.2	0.8		
Duct 2 - Front				
start void 1	0.3	6.2		cof = 4.7 kHz
end void 1	0.4	4.6	4.6	
start void 2	0.55	3.4	3.3	
end void 2	0.65	2.8		
end beam	2.2	0.8		
Duct 2 - Back				
end void 2	1.55	1.2		
start void 2	1.65	1.1		
end void 1	1.8	1.0		
start void 1	1.9	1.0		
start beam	2.2	0.8		
Duct 3 - Front				
end void 1	0.7	2.6	3.0 - 3.4	
start void 2	1.5	1.2	1.5	
end beam	2.2	0.8		
Duct 3 - Back				cof = 3.25 kHz
start void 2	0.7	2.6	2.6	
end void 1	1.5	1.2	1.2	
start beam	2.2	0.8		

Table 4.3 Summary of Results

4.9.3 Discussion on Alternative Test Configuration

Table 4.3 gives a summary of the results. Only peaks corresponding to those expected have been shown on the table. A number of other frequency peaks occur on each response spectrum. This will make interpretation more

difficult. Figure 4.33 shows the actual response spectra for a number of tests. The assumed compression wave velocity is 3700m/s. This figure was calculated for grout cubes cast using grout of similar mix proportions. The tendon ducts are each approximately 2.2m in length. A compression wave velocity of 3700m/s would result in a reflection from the far end of the duct occuring at 0.8 Hz. It can be seen on these graphs that the reflection from the far end of the tendon is not evident in any of the responses using the 280g hammer. A response from the end of the tendon duct is not expected from duct 1 as the centre portion of the duct is completely ungrouted. The compression wave would therefore be unable to propagate through this section. Tendon ducts 2 and 3 are at least partially grouted over their entire length. However, both ducts contain voids which cover at least half the duct cross-section. The attenuation within the tendon duct is high and so the stress pulse does not contain sufficient energy to allow reflections from the far end to be detected on the accelerometer.

4.9.3.1 Duct 1

Figure 4.33a shows the response spectrum obtained testing the front of duct 1. The cut-off frequency was 2.225 kHz and so it should be possible to measure frequencies up to 4.45 kHz. It may therefore not be possible to measure the reflection from the end of void 1. This was found to be the case. The response contains many peaks and is difficult to analyse, however, the dominant peak at 1.9 kHz would seem to correspond to the start of void 2. There are many defects within this tendon and it is possible that the actual position of the voids altered slightly during construction. This would result in peaks appearing on the response spectrum at slighlty different frequencies from those expected. It is also possible that the quality of the grout changes throughout the tendons. The amount of vibration each tendon received may not have been consistent and grouting the ducts was quite difficult and it is possible voids occured in positions other than those designed.

The accelerometer must be coupled to the end of the tendon. The available area for the accelerometer to be positioned is small and space must also be left for the hammer impact. The ends of the ducts were not smoothed off during construction and the grout surface is uneven. Duct 1 contained steel tendons which were longer than the steel duct. These acted to further reduce the available area for coupling the accelerometer.

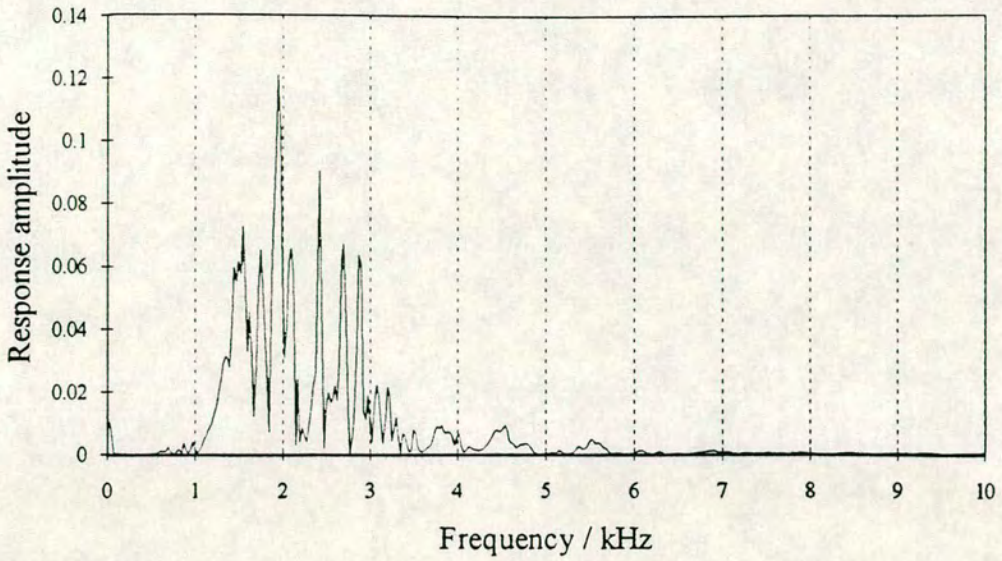

Fig 4.33a Duct 1 - front

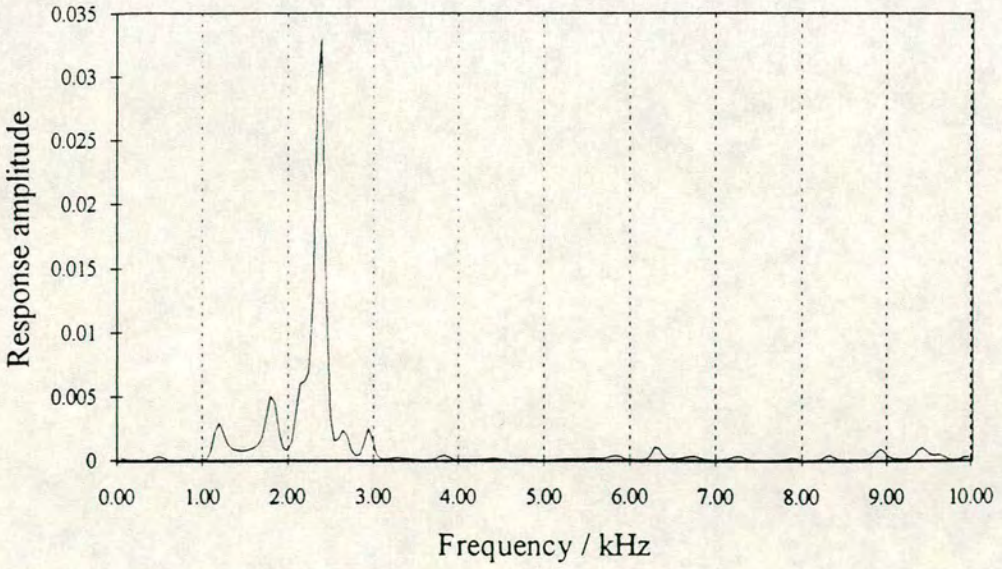

Fig 4.33b Duct 1 - back

Figure 4.33 Pile-type sonic impact-echo frequency response spectra

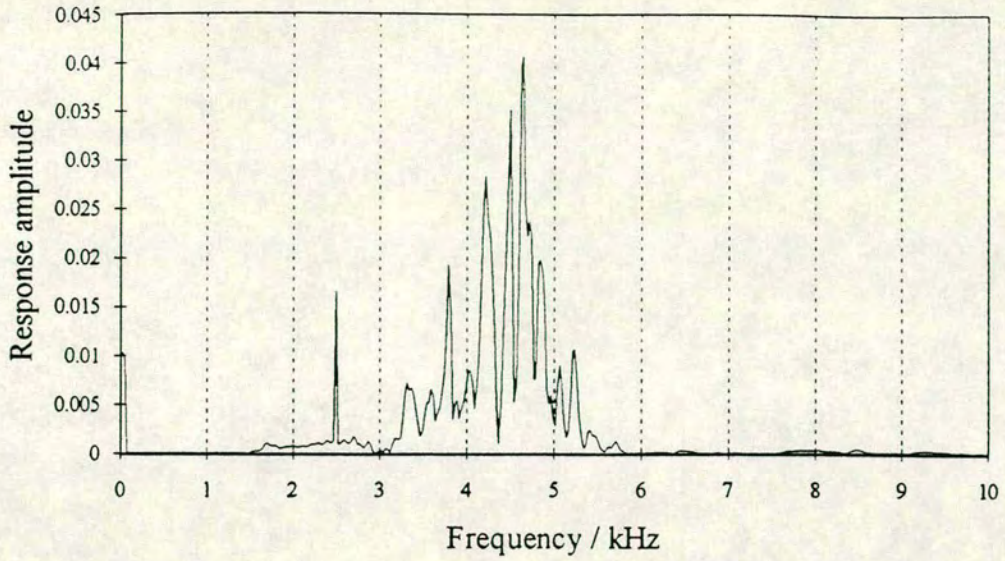

Fig 4.33c Duct 2 - front

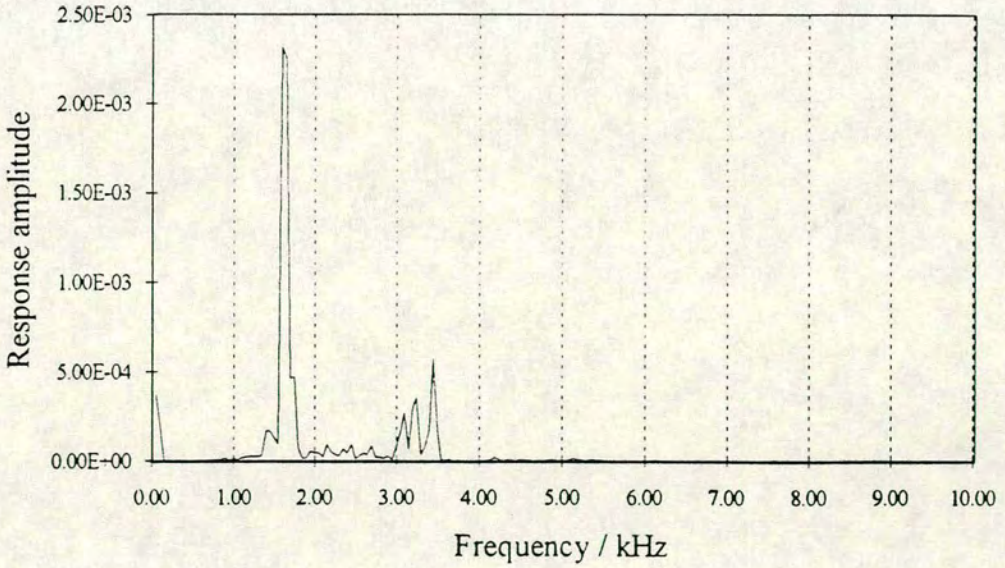

Fig 4.33d Duct 3 - front

Figure 4.33 (cont.) Pile-type sonic impact-echo frequency response spectra

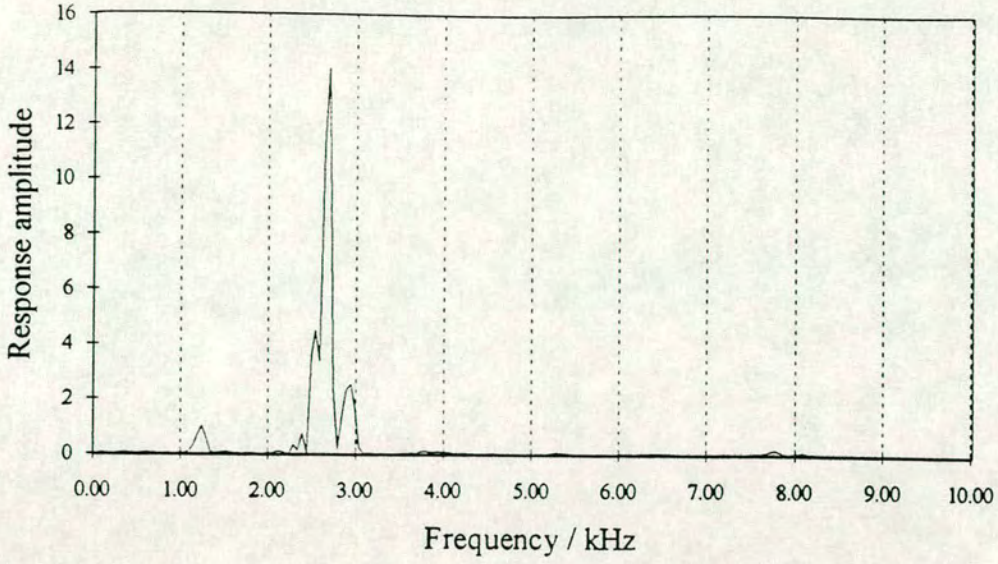

Fig 4.33e Duct 3 - back

Figure 4.33 (cont.) Pile-type sonic impact-echo frequency response spectra

The response spectrum obtained at the back end of duct 1 is shown in figure 4.33b. The dominant peak at 2.35 kHz seems to correspond to the end of void 2. This void covers the entire cross-section of the duct and would be expected to produce a dominant peak. The actual frequency of the peak is higher than expected. However, if the wave speed is still assumed to be 3700m/s, the peak at 2.35 kHz corresponds to a depth of 0.79m which is very close to the design depth of 0.85m. Slight differences in grout condition and placement of voids during construction could easily account for this difference. The response achieved from the back of duct 1 is much cleaner than that achieved at the front. This is because the surface of the grout is smoother at the back end of the duct. This allows a better coupling of the accelerometer and a clean impact with the instrumented hammer.

The voids in Duct1 were formed by attaching polystyrene cylinders and spacers to the steel tendons. The duct was grouted in two stages, firstly from the front end and then, once that grout was dry, from the back end. The grout placed first may have pushed the void formers further along the tendons, i.e. towards the back of the duct. This would account for the lower than expected frequencies from the front end and the higher than expected frequency peaks on the response spectrum from the back end.

4.9.3.2 Duct 2

The back end of duct 2 is very rough and there is little space to attatch the accelerometer. No results were obtained here which could be analysed. The front end of the duct was very smooth as this duct was cast in one pour. The duct was clamped vertically and the steel tendons with attatched void formers postioned inside. The back end of the duct was sealed to prevent grout escaping before it had hardened. This resulted in a smooth surface which allowed good coupling of the acclerometer and a good impact. The cut-off frequency obtained was 4.7 kHz. The voids within this duct are small and so the relative amplitude of reflections will be reduced. However, two peaks occur on this trace that correspond very well with those expected from the end off void 1 and the start of void 2. (Figure 4.33c).

4.9.3.3 Duct 3

Duct 3 contained no steel tendons and so was easier to fill with grout and then smooth off the ends of the duct. The duct was clamped vertically with the back end at the base. The back end of the duct is therefore very smooth. The front end is also quite smooth as the grout settled fairly level since there were no tendons. However, as the grout settled, the level dropped from the end of the steel tendon duct and so the distance to the voids was less than that designed. This settling also caused problems when coupling the accelerometer and creating the impact as the steel ducting was not flush with the end of the grout.

Figures 4.33d and 4.33e show the spectra from the front and the back end of the beam. Two distinct peaks can be seen on each spectrum. On the spectrum from the back of the beam the peaks correspond exactly to the expected peaks from the start of void 2 and the end of void 1 at 2.65 kHz and 1.2 kHz. The actual distance to these voids will not change during the pouring of the grout as mentioned above. The grout in duct 3 was poured at one time and was all from the same mix. It is likely that the compression wave velocity will therefore be consistent throughout the duct, (a slight increase in velocity may be expected at the back end due to the grout being denser at that end after settling).

The spectrum from the front of duct 3 shows a peak at 1.55 kHz which corresponds to a distance of 1.2m. The second peak on this trace ranges from 2.9 kHz to 3.4 kHz which corresponds to a distance of 0.65m to 0.55m. If settling of the grout reducing the actual distance to target is taken into account then these results are consistent with reflections from the start of void 2 and the end of void 1. A similar situation arises from each end of duct 3 and so similar results would therefore be expected.

Overall, this method was judged to be successful for testing post-tensioning ducts in concrete beams. Depending upon the cut-off frequency obtained the nearest defect could be detected. In most cases the first two defects could be detected. This compares well with pile testing using this method. Sonic impact-echo testing of piles can consistently detect the distance to the first defect (or base of the pile). This is considered sufficiently accurate as any defect in the pile would render it unusable. A similar reasoning can be used in

tendon duct testing. If any sizeable defects are detected in a duct then strengthening and repair work would be required.

The reflection from the far end of the duct could not be detected on any of the spectra. The reason for this was the number and size of the defects included in each tendon. Further work would be required to ensure that the penetration of the stress wave was sufficient to propagate the entire duct. If this was not possible then the anchorages of the tendons would need to be exposed at both ends and the grouting tested from either end.

The surface condition of the grout is also important in determining the quality of the results. Coupling of the response transducer is very important in ensuring that a usable response is measured. If the exposed surface is rough then steps would need to be taken to smooth this off. Similarly a reasonably smooth surface is required to produce an impact of the expected cut-off frequency. A rough contact surface can result in considerable local crushing which acts to reduce the cut-off frequency achieved and therefore the minimum size of and depth to defect that can be detected is increased.

This method can be used with considerable success. However, the practicalities involved render it unsuitable in the majority of cases. Exposing the ends of the ducts is unlikely to be possible and, if possible would involve considerable preliminary intrusive investigation. This is likely to make this method very expensive and impractical.

4.9.4 Conclusions on Alternative Test Configuration

1. Sonic impact-echo testing from the exposed ends of tendon ducts can be used to detect defects within the ducts.

2. The cut-off frequencies required are lower than for impact-echo testing from the surface of the beams and so longer distances can be penetrated. The likely orientation of defects within tendon ducts result in this method successfully detecting defects which cannot be detected using the same impactor on the surface of the beam.

3. As with pile testing, only the nearest one or two defects can be detected using this method. However, this is sufficient to determine whether a tendon duct is sound or not.

4. Although theoretically a possible testing method, this test configuration is unlikley to be practical due to the considerable intrusion required to expose the tendon duct ends. This would result in this method being very expensive and other methods, eg gamma radiation, would probably be more appropriate.

4.10 Coupling of Response Transducer to Concrete

The PCB 303A03 accelerometer has an internal resonance of 77 kHz and so it is expected that this accelerometer, if mounted correctly should be able to detect frequency components reasonably accurately up to at least 26 kHz. However, work revealed that the mounted resonance of the accelerometer was much lower than the value expected and was masking any responses from the beam. This effect was found by repeating an impact at a position and pressing the accelerometer to give a better acoustic bond with the concrete. Some of the peaks on the FRF were then seen to move to slightly higher frequencies.

Figure 4.34 shows the FRF of an impact in the centre of the beam. In this case the accelerometer is mounted using a thick layer of grease. There are few reflections on the graph and the largest peak frequency occurs at 16 kHz. Figure 4.35 shows the FRF of an impact at the same position. This time the accelerometer is mounted using the same grease but with the accelerometer weighted to ensure a better bond with the concrete. This graph shows more peaks and the peak which seems to correspond to the peak in figure 4.34 occurs at 18 kHz. One reason for the apparent movement of this response is that it shows the mounted resonance of the accelerometer.

The accelerometer itself resonates at 77 KHz but if it is not coupled adequately to the structure the mounted system may resonate at a much lower frequency. The better the coupling, the higher the mounted resonant frequency. If the accelerometer is coupled perfectly to the structure, the only resonant frequency measured from the accelerometer would be at 77 KHz. The grease that was being used to mount the

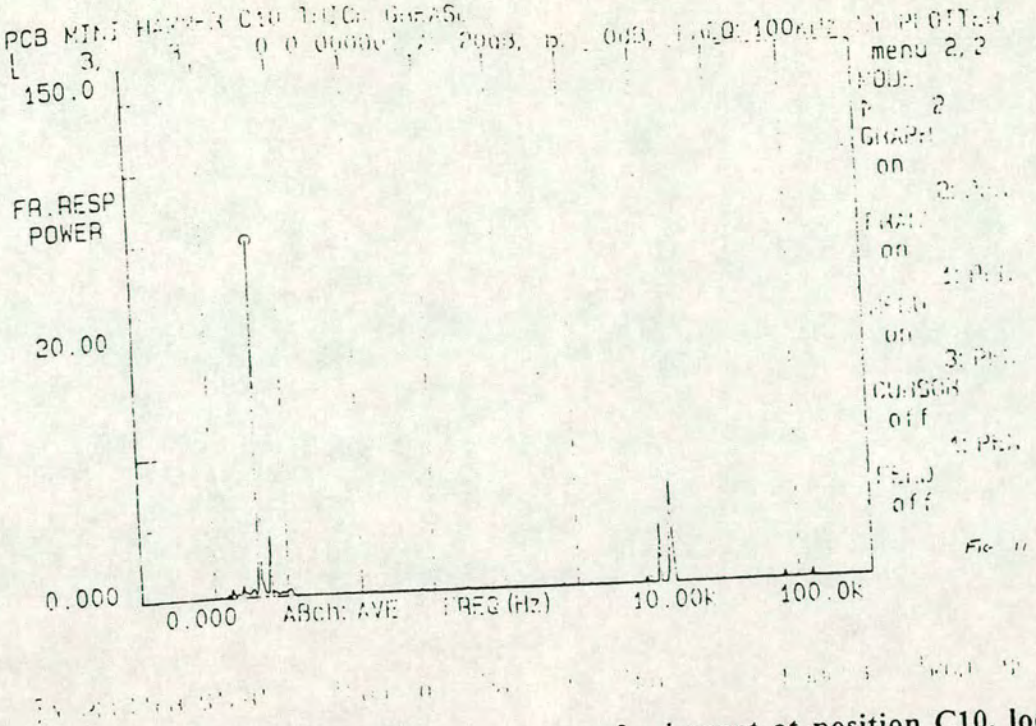

Figure 4.34 Frequency response spectrum for impact at position C10, loosely coupled accelerometer using water pump grease

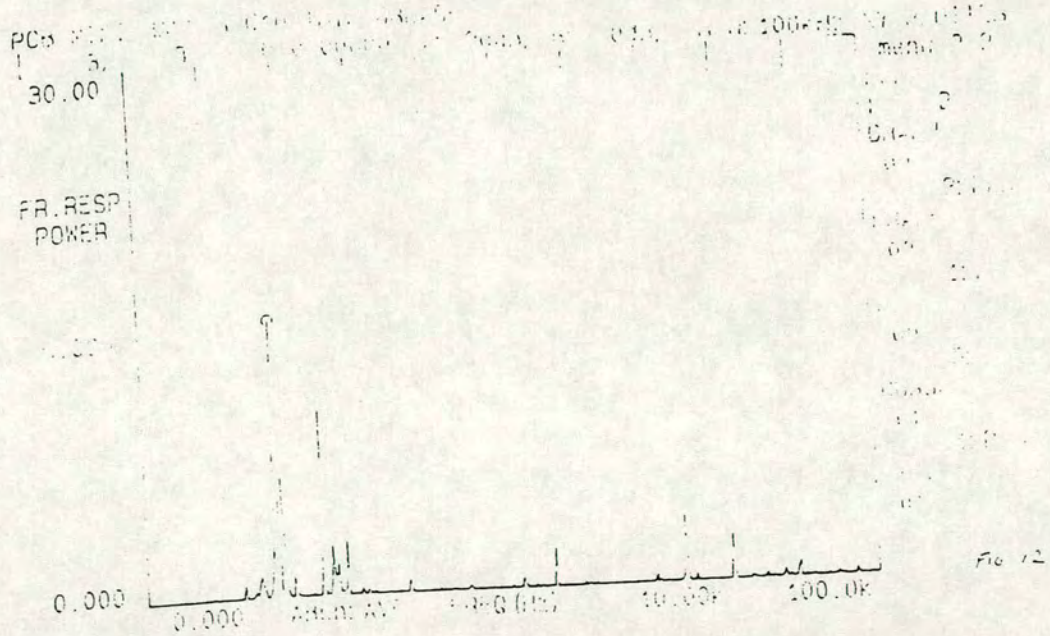

Figure 4.35 Frequency response spectrum for impact at position C10, securely coupled accelerometer using water pump grease

accelerometer had to be in a fairly thick layer to allow for the roughness of the beam's surface. It was not possible to mount the accelerometer using petrowax™ which was recommended for this as the concrete surface was too rough and dusty.

It is also not possible to grind the surface of the concrete as the sand particles and the aggregate particles are too large to give a smooth surface. Small metal discs were then attatched onto the surface of the beam using a variety of bonding agents.

4.10.1 Experimental Work and Discussion

Some discs were bonded with dental plaster which has similar acoustic properties to cement paste. This paste is very quick drying and can easily be removed after testing. However, it is quite brittle so other discs were bonded on using araldite rapid epoxy glue and chemical metal, a metallic epoxy. These took a considerable time to dry (8 hrs to full strength for araldite rapid epoxy and 24hrs for chemical metal) and will also be difficult to remove. The accelerometer can then be mounted on the discs using a thin film of beeswax. This should hopefully mean that the mounted resonance of the accelerometer will be at a much higher frequency than the response from the beam.

Representative results are shown in figures 4.36 to 4.39. Figures 4.36 and 4.37 show the spectra obtained for all the couplants using the 280g hammer and the 1.25g mini-hammer respectively. Figure 4.38 shows a clear reflection from the base using each couplant. No unexpected high frequency components can be seen on the spectra obtained with epoxy glue or chemical metal. However, the spectra obtained using dental plaster contain high frequency components. It is likely these components are due to the mounted accelerometer resonance. The frequency component at position E9 is at 17 kHz and the component at position C10 is at 24 kHz. A difference in mounted resonance can occur for the same coupling material as the exact mounting conditions cannot be repeated. For example, the condition of the surface of the beam will be different as might the thickness of couplants applied. However, these frequency components occur at frequencies of interest when analysing the beam and so metal discs bonded to the beam with dental plaster do not provide a suitable mounting.

Figure 4.37 shows the spectra obtained using the 1.25g mini hammer and metal discs bonded with thin grease, dental plaster and chemical metal at

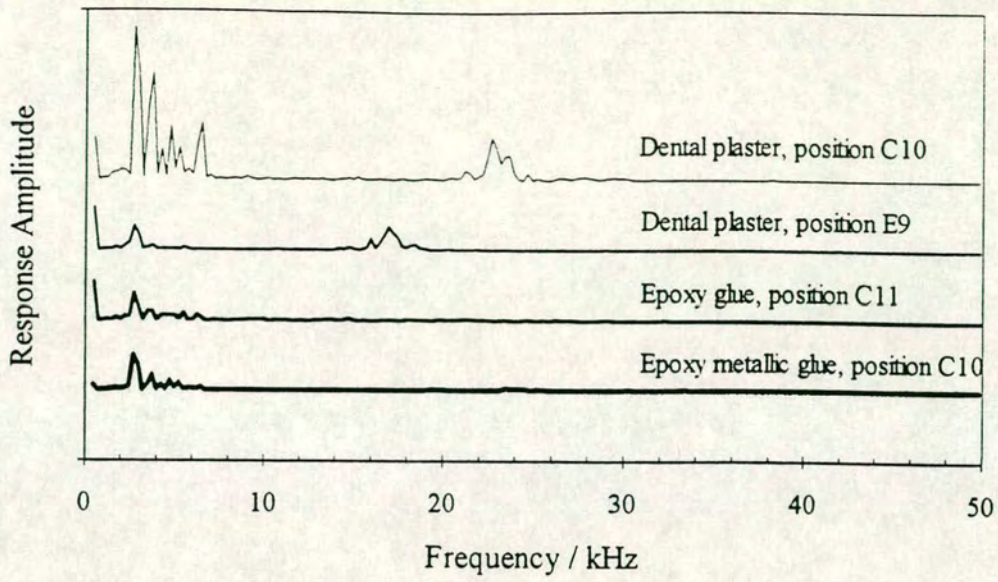

Figure 4.36 B&K hammer - coupling spectra

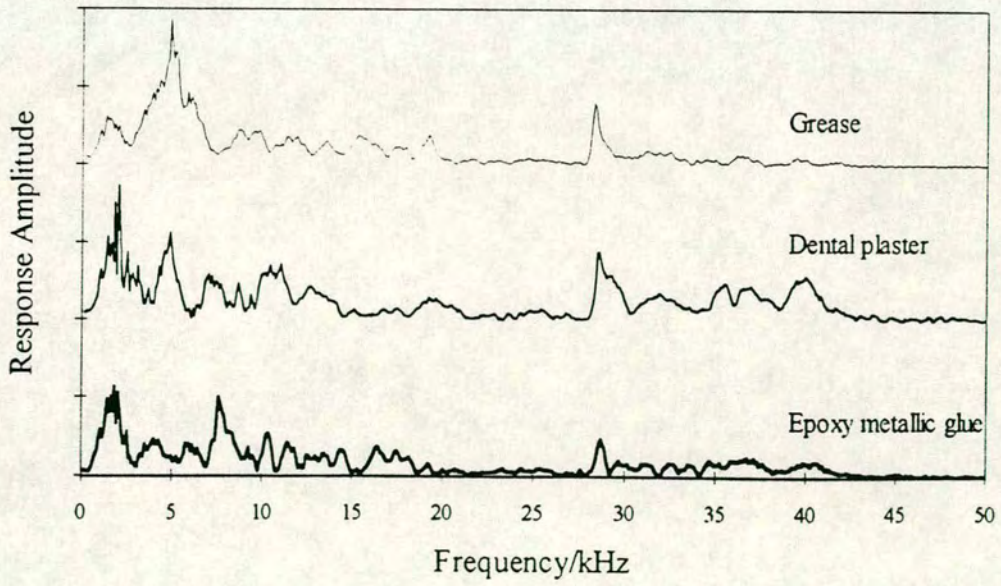

Figure 4.37 PCB mini-hammer, position C10

position C10. A resonance can be detected at approximately 29 kHz on all the spectra. This occurs at a frequency higher than expected from the cut-off frequency and so is likely to be due to the mounting of the accelerometer.

The resonance occuring on the spectrum obtained using a chemical metal coupling was of a much lower amplitude than those obtained using thin grease and dental plaster coupling. Chemical metal coupling was then used at a number of positions and the results are shown in figure 4.38 for the 280g hammer and figure 4.39 for the 1.25g hammer. The spectra shown in figure 4.38 contain high frequency components between 20 and 30 kHz. It is likely these occur due to mounting resonances and again may act to dominate responses from targets within the beam. The spectrum from position E9 shows a distinct peak at 74 kHz corresponding to the internal resonance of the accelerometer. Figure 4.39 shows the spectra obtained using the 1.25g mini-hammer. A high frequency component, 30 kHz, is evident in the responses at positions C10 and E10. This response is not evident in the spectrum obtained at E11.

4.10.2 Conclusions on Coupling of Response Transducer to Concrete

1. The mounting of the accelerometer to the test specimen is important in carrying out impact-echo tests. The accelerometer may have a high resonant frequency but, if not mounted properly, the mounted resonance may be at a considerably lower frequency which can interfere with responses from targets within the specimen.

2. Mounting the accelerometer using the recommended petrowax™ is only possible on concrete if metal discs are firstly attatched to the surface. Epoxy adhesives form a better couplant between the discs and the concrete than brittle pastes, eg cement paste or dental plaster.

3. The PCB 303A03 accelerometer cannot be coupled sufficiently to the beam to allow high frequency testing (>15 kHz) to be carried out with confidence. This results in it being unsuitable for testing all but the largest bridge beams and will not be practical for investigating the internal condition of tendon ducts.

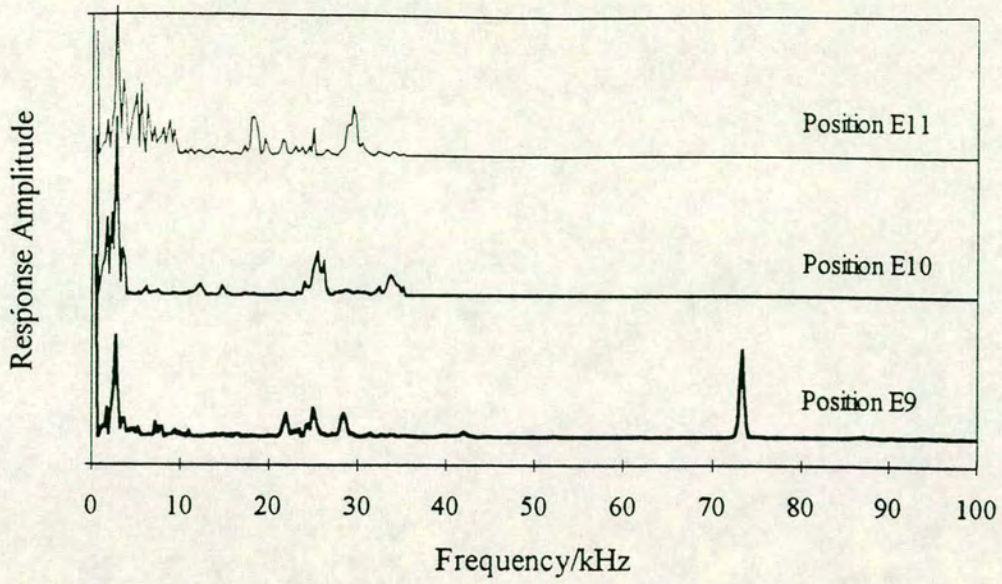

Figure 4.38 B&K hammer - chemical metal coupling

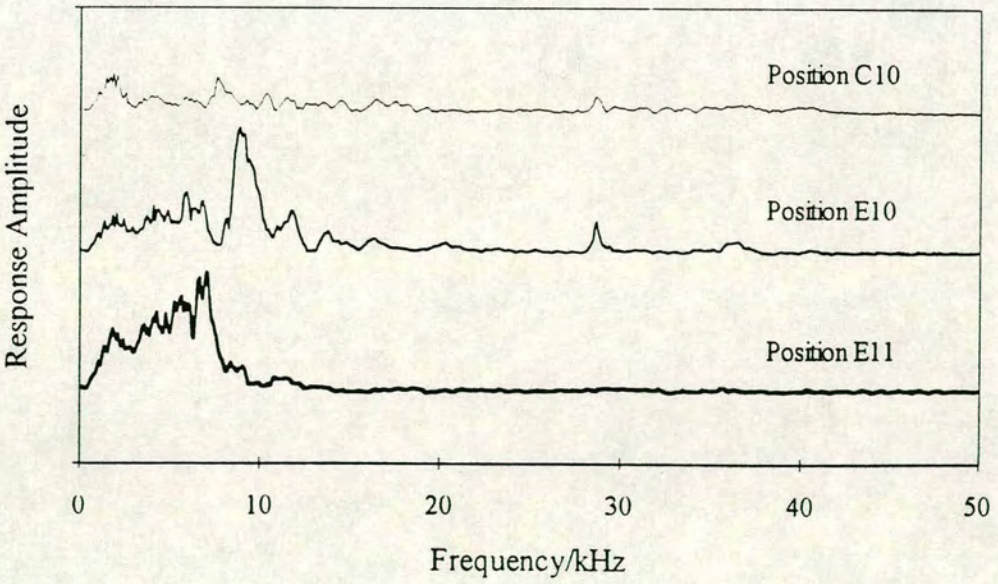

Figure 4.39 PCB mini-hammer - chemical metal coupling

4.11 Optimum Experimental Set-up

Many different experimental configurations have been investigated with different degrees of success. Promising results have been produced using various methods but the deciding factor in the application of sonic impact-echo non-destructive testing of post-tensioned concrete bridges is the performance of the testing components at high frequency, i.e. at frequencies from 10 kHz to 30 kHz. The Zonic A and D dual channel FFT analyser is designed to perform up to 100 kHz and so is suitable for use. Problems have arisen in the cut-off frequency obtainable by the impact hammers and the usable frequency range of the accelerometers available. These testing components are discussed in more detail below.

4.11.1 Response Transducer

The PCB 303A03 accelerometer used in the preliminary testing was not calibrated above 10 kHz. This was sufficient for the initial experimantation but if frequency components up to 30 kHz were to be measured with confidence a response transducer with higher frequency capabilities was required. A NIST conical reference transducer was acquired (figure 4.40). The calibration chart is shown in figure 4.41. This transducer measures the displacement of the beam as opposed to the acceleration and has a flat response to 1 MHz. There was some doubt concerning the response at low frequency (<5 kHz) and so initial tests were carried out to investigate the performance of the transducer at lower frequencies.

Figure 4.42 shows the spectra obtained at position G16 using the pcb mini-hammer as an impactor. A distinct peak can be seen at 2.4 kHz corresponding to the reflection from the base of the beam. This indicates that the NIST transducer is more sensitive than the accelerometers previously used as the base reflection was not usually detected when the pcb mini-hammer was used as the impactor. An estimate of the contact time and therefore the cut-off frequency can be made using the response measured by the NIST transducer. The initial downwards displacement corresponds to the contact time. This is investigated in detail in the following chapters. The NIST transducer was used throughout the majority of the laboratory testing and used to verify the results obtained during the field testing.

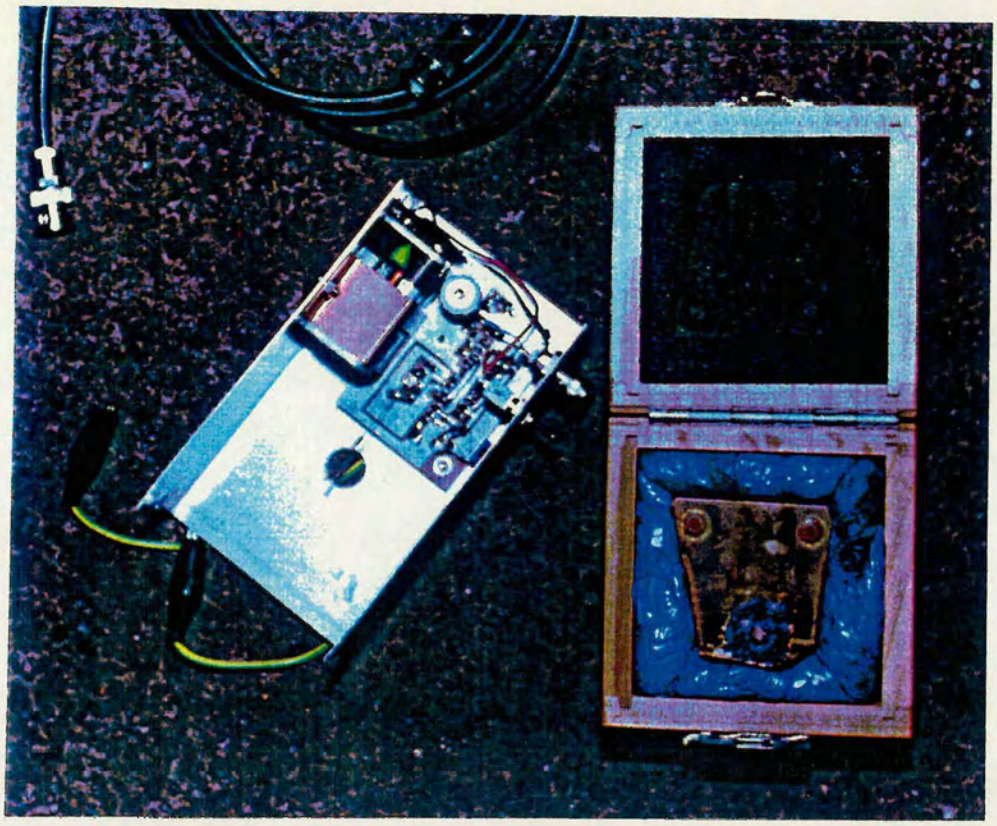

Figure 4.40 NIST displacement transducer components - housing and power supply on left, transducer on right

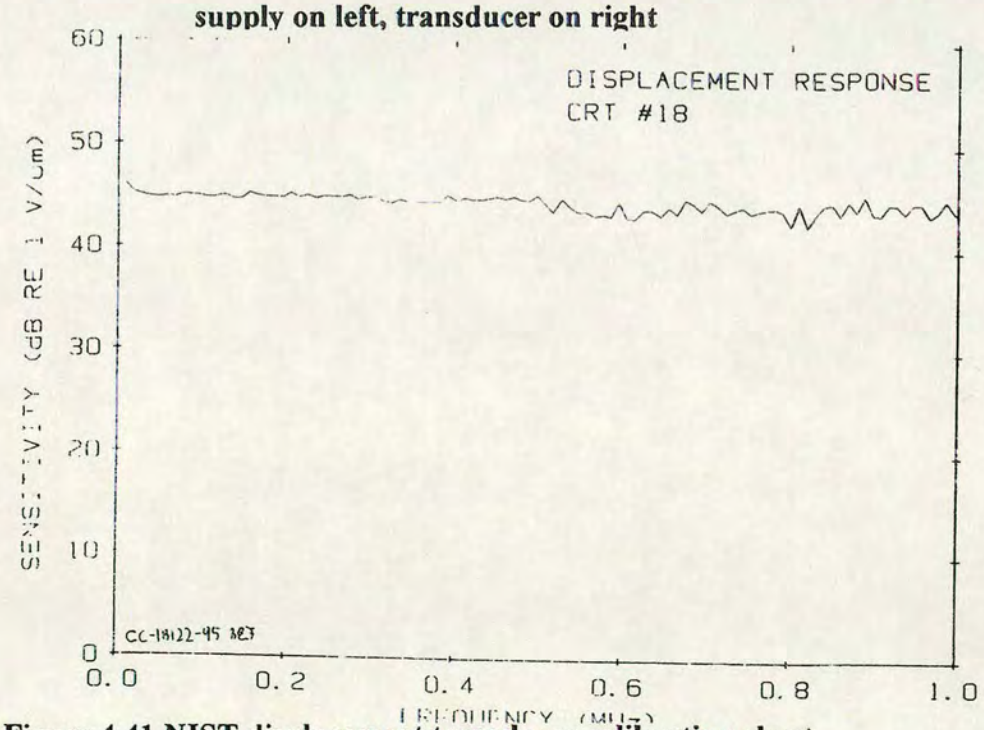

Figure 4.41 NIST displacement transducer calibration chart

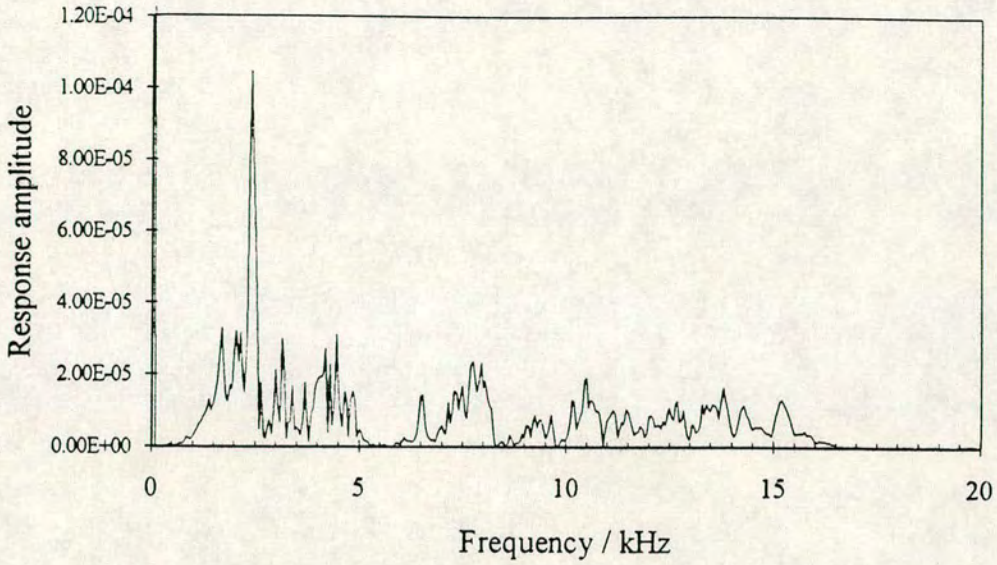

Figure 4.42 Frequency response measurement using NIST transducer, laboratory test beam 1, position G16

4.11.2 Impact Hammers

There was doubt that the mini hammer could regularly produce an impact of high enough energy to transmit through the beam. Figure 4.39 shows the response of the test beam to impacts from the 1.25g mini-hammer. Figure 4.38 shows the response of the test beam to impact from the 280g hammer. The expected peak from the base of the beam is at 2.75 KHz. This peak is not clear on the response spectra from the mini-hammer but is the dominant peak on the spectra from the 280g hammer. This suggests that the impact from the mini-hammer does not produce high enough energy. The attenuation is too great and insufficient energy propagates through the beam and reflects from the base to be detected by the accelerometer.

The average cut-off frequency obtainable on the concrete model is 5.5 kHz. Assuming frequencies up to twice the cut-off frequency can generally be detected, the mini-hammer can be used to detect frequency components up to 11 kHz. This is too low a frequency to resolve most of the defects within the beam.

An alternative impactor was required to produce both a higher frequency excitation and an impact of greater energy. It would be preferable to use an instrumented impactor to enable the actual impact to be measured. However, if sonic impact-echo testing is to be applicable to the non-destructive testing of post-tensioned concrete beams higher energy, higher frequency impactors must firstly be developed. Response spectra can be produced and compared for unmeasured impacts. Care must be taken to ensure that the results produced are representative for that impactor and location by carrying out a number of tests and either comparing each test and recording a typical response or taking an average of a number of responses. If an average is to be taken it is important that the impact occurs in the same place at the same distance from the response transducer for each test.

Different impactors were investigated including hardened steel ball bearings of different diameters attatched to darts. These darts were then fired at the beam with different forces using a cross bow. Elastics of different lengths were used to control the force of the impact. High energies could be achieved using this method but the impact tended to damage the surface of the beam indicating that a plastic impact had occured and therefore the cut-off

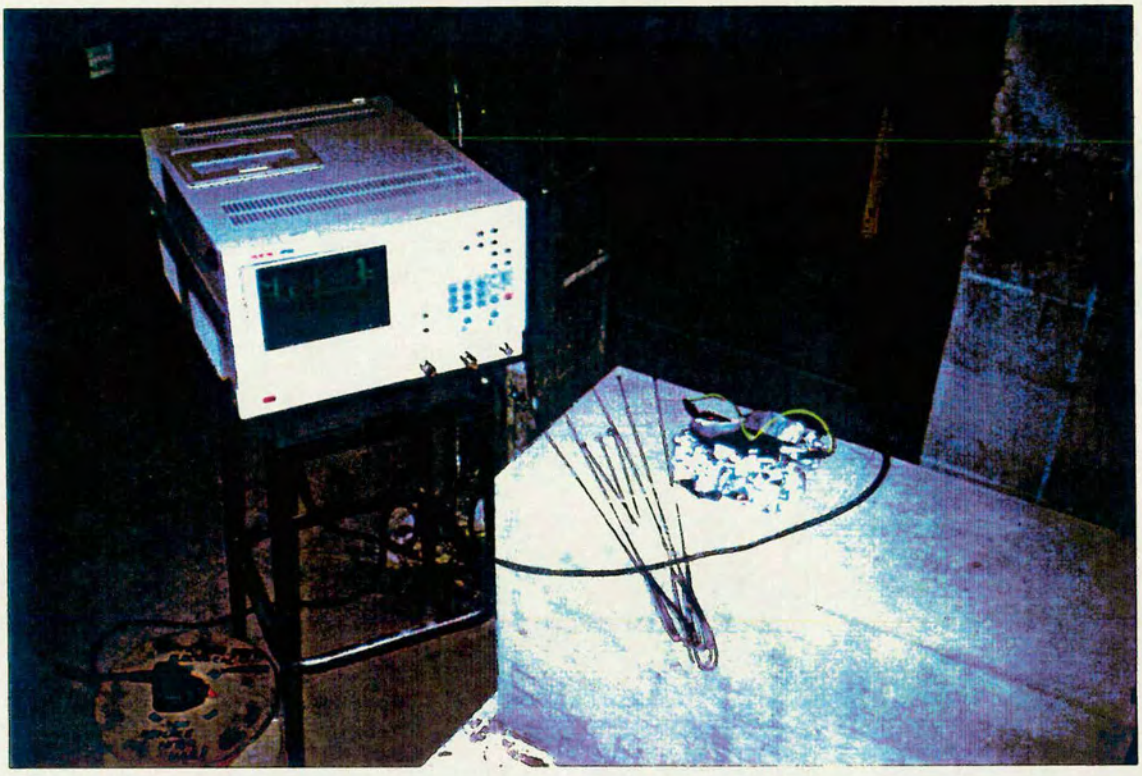

Figure 4.43 Impact-echo set-up showing the range of ball bearing hammers

frequency obtained was much lower than expected. The contact time of the impact is also dependent on the length of the dart as the impact is straight on. At impact, a compression wave is set up in the dart. This wave must travel to the far end of the dart and back to the impacting end before it can bounce off the beam (Fegen 1985). As the diameter of the ball bearing reduces the length of the dart becomes the deciding factor in the cut-off frequency obtainable by that impactor. A similar configuration was investgated. In this instance the ball bearing was set in the cross bow and a flat ended dart fired at it. The dart hit the ballbearing and propelled it along a directing tube to the beam. The dart was stopped before hitting the beam. This method was rather unreliable and could only be used in a horizontal orientation and was impractical for site use.

Ball bearings of different diameters were attatched to lengths of wire (figure 4.43). These were found to give an impact of sufficient energy to penetrate the test specimen and a wide range of sizes were readily available to produce impacts of different cut-off frequency. The expected cut-off frequency obtainable was calculated using Hertz's theory and then the actual cut-off frequency was estimated from the response as detailed in chapters five and six. The theoretical and experimental cut-off frequencies obtained are shown in table 6.1 for impact on a smooth concrete surface. The experimental cut-off frequencies obtained are, as expected, considerably lower than those calculated. However, much higher cut-off frequencies could be achieved using these hammers than using the instrumented hammers used in all the previous experimental work. These ballbearing hammers were used throughout the remainder of the experimental work.

4.12 Conclusions of Preliminary Investigations

1. Ground penetrating radar investigation can be successfully applied to detect defects within the tendon ducts of post-tensioned bridges with non-metallic ducts. It also provides a useful method of locating metallic ducts within a concrete beam. Problems may occur in areas of dense reinforcement.

2. Preliminary field testing showed sonic impact-echo testing to be a promising investigation technique for post-tensioned concrete beams with metallic ducts. Detailed investigation into equipment requirements and limitations was required to allow this method to be applied successfully.

3. A laboratory model was constructed to allow detailed investigation of testing set-ups to be made. The model contained three metallic tendon ducts and contained known defects.

4. The condition and mix design of concrete determines the cut-off frequency that can be obtained by an impactor. The cut-off frequency obtained can vary across a single specimen depending on local inhomogeneities within the specimen. Specifically, for newly cast concrete:
   - The cut-off frequency increases as the concrete cures
   - The higher the expected cut-off frequency expected the greater the influence of mix proportions and condition on the actual cut-off frequency obtained.
   - The pulse velocity increases as the concrete cures and is higher for concrete and mortar with higher percentages of aggregate.
   - The pulse velocity is related to the cut-off frequency obtainable.
   - There is a linear relationship between the compressive strength and the cut-off frequency obtainable. This could easily investigate the strength of concrete on site and be used to determine formwork striking times.

5. An alternative testing configuration was investigated. For this study the tendons were excited and the response measured from the exposed ends.
   - This test configuration can successfully detect the nearest one or two defects.
   - A major disadvantage of this method is the impracticality of exposing the ends of the tendon ducts.

6. The coupling of an accelerometer to a test specimen is very important. Incorrect coupling can result in a mounted resonance that masks the expected frequency components resulting from defects within the test specimen. The coupling of the PCB 303A03 accelerometer to concrete was investigated with the following results;
   - The acclerometer can only be mounted as recommended on a metal surface. Metal discs were therefore attatched to the test specimen. The most succesful method of attatching the metal discs to the specimen was using epoxy bonding agents. However, mounted resonances still occurred at the higher frequencies of interest.

Chapter V

Finite Element Analysis

The finite element method offers a useful method of investigating the potential of a testing technique. Detailed analysis can be carried out using this method and the results validated using a few laboratory specimens. The number of test specimens to be constructed is therefore greatly reduced.

5.1 Introduction

The finite element method derives from classical structural analysis techniques. Rather than manipulating the governing equations into differential form and then solving numerically, this method divides the domain of the solution into a finite number of simple sub domains, elements, and constructs an approximation of the solution over the collection of elements (Becker, 1981). The method has been used with remarkable success in many fields because of the generality of the underlying principles.

The finite element method consists of eight basic steps (Desai, 1979):

Step 1: Discretise and select element configuration
Step 2: Select approximation models of functions
Step 3: Define strain-displacement and stress-strain relationships
Step 4: Derive element equations
Step 5: Assemble element equations to obtain global or assemblage equations and introduce boundary conditions
Step 6: Solve for the primary unknowns
Step 7: Solve for derived or secondary quantities
Step 8: Interpretation of results

Two-dimensional finite element analyses have been carried out on concrete with various 'targets' included in the model. Two finite element codes were used. ANSYS version 5.0a, developed by Swanson Analysis Systems, Inc. of Houston, Pennsylvania was used to perform the analysis of plane voids and lined and unlined ducts. DYNPAK(Owen and Hinton 1980) was used to perform the analysis of beams with spherical voids.

5.2 Finite Element Simulation using ANSYS Ver. 5.0a

ANSYS Ver. 5.0a was used initially to determine if finite element methods could be applied successfully to model sonic impact-echo testing of concrete. The ANSYS license available limited the detail of analysis possible but was adequate to verify that finite element methods were appropriate in modelling this method and could easily and efficiently be used to investigate the applications and limitations of sonic impact-echo testing of concrete. For the analyses carried out a 50mm 8 noded quadratic element was used and it was assumed that the material is perfectly elastic, isotropic and homogeneous. These assumptions will mean that the results achieved in the models will be better than those that can be expected in practical testing. Therefore, if

the result of Finite Element analysis under these idealised, well controlled conditions does not indicate that impact-echo investigation techniques can be used for detecting defects within post-tensioned bridge beams it is unlikely that this technique will be suitable in practice.

5.3 Finite Element Analysis using DYNPAK

More detailed analyses were carried out using DYNPAK. The code used is given in Owen and Hinton (1980). Dr. A. Usmani of Edinburgh University wrote a preprocessor to be used with DYNPAK allowing detailed two-dimensional explicit transient dynamic analysis to be carried out. A brief introduction to the program is given below but full details are given in Owen and Hinton (1980).

DYNPAK utilises a popular and easily implemented explicit, forward-difference scheme. Little computational effort is required for each time step but the method is conditionally stable and so often very small time steps are required resulting in relatively large run-times for analysis. Eight noded quadratic elements were used with a minimum mesh size of 10mm. The computer time required did not pose significant problems and the program was very suitable for carrying out finite element analyses on various cross-sections of concrete beam containing different sizes of voids.

5.4 Initial Analysis

Two sets of models were constructed to determine whether defects in the beam models could be detected using the finite element method. ANSYS version 5.0a was used for these analyses.

The following assumptions were made throughout the finite element analysis:

- Concrete behaves as an homogeneous, isotropic and elastic material. Modulus of elasticity = 31.9 GN/m^2. Poison's ratio = 0.2. Mass density = 2214 kg/m^3. The concrete grout used in the ducts has the same properties.

- Steel behaves as an homogeneous, isotropic and elastic material. Modulus of elasticity = 210 GN/m^2. Poison's ratio = 0.3. Mass density = 7800 kg/m^3.

The first series models were constructed of a concrete beam of width 1000mm and depth 300mm. These are illustrated in figure 5.1. The first model was of a solid concrete beam, the second containing a 50mm delamination at 150mm, the third a 400mm wide, 50mm deep void at 150mm, the fourth a 200mm wide, 50mm deep void at 150mm and the fifth a 150mm diameter circular void at 125mm. The time step used was 5μs and the force impulse was a 50μs duration half sine wave. A full transient dynamic analysis was carried out on each model.

The second series investigated the effect of a 5mm steel liner on a 400mm wide, 50mm deep plane duct on the results of a finite element analysis. Four models were constructed with the same mesh density. The first model was of a fully grouted unlined duct, the second a fully grouted steel lined duct, the third an ungrouted unlined duct and the fourth model was of an ungrouted steel lined duct. These are illustrated in figure 5.2. The time step used was 5μs and the force impulse was again a 50μs half sine wave. Again, a full transient dynamic analysis was carried out on each model.

The third series of analyses was carried out using DYNPAK. Reflections from circular voids were investigated. The dimensions of the beam was again 1000mm wide by 300mm deep. The time step used throughout was 0.75μs and a total of 4096 steps were calculated. This series was divided into three distinct sets:

Set 1: Investigation of contact time of impulse. A model was constructed with a 100mm diameter void at 125mm depth. Finite element analyses were carried out with half sine wave impulses of 30μs, 50μs and 70μs duration.

Set 2: Investigation of void size detectable. A half sine wave impulse of 30μs duration was used throughout this set. The top of each void was 125mm from the top surface of the beam. The first model contained a 75mm diameter void, the second a 100mm diameter void and the third a 125mm diameter void.

Set 3: Investigation of depth to void. As in set 2, a half sine wave impulse of 30μs duration was used throughout this set. The void in each model was 100mm in diameter. The first model contained the void at 100mm from the surface, the second at 125mm from the surface and the third at 150mm from the surface.

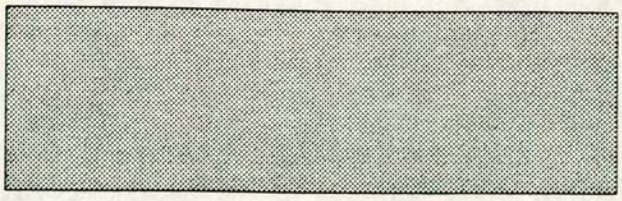

a) Solid Concrete Beam

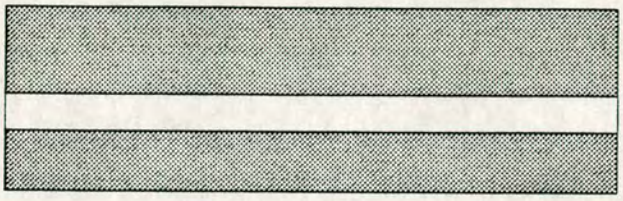

b) Beam with delamination at 150mm

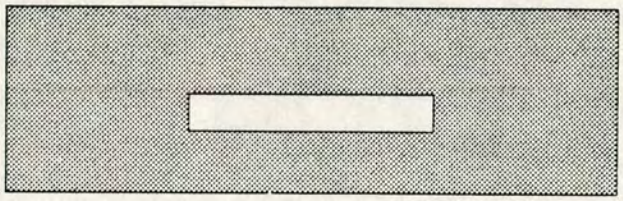

c) Beam with 400mm square void

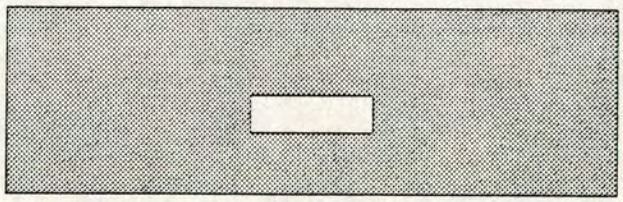

d) Beam with 200mm square void

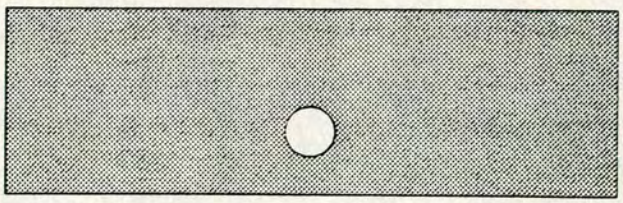

e) Beam with 150mm dia void at 150mm

Note: All models 1000mm * 300mm

Figure 5.1 Finite element models - series 1

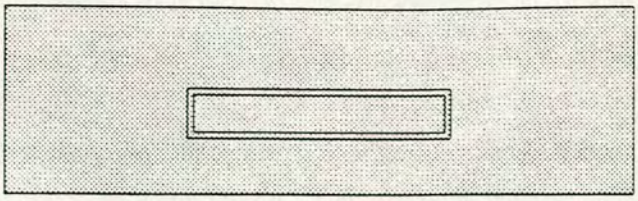

a) Solid Concrete Beam

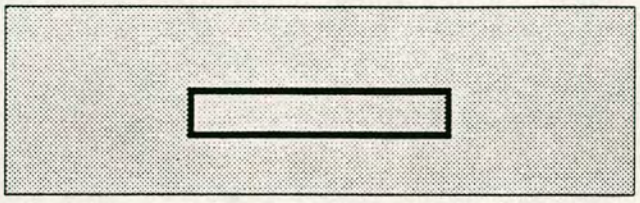

b) Grouted Duct with Steel Liner

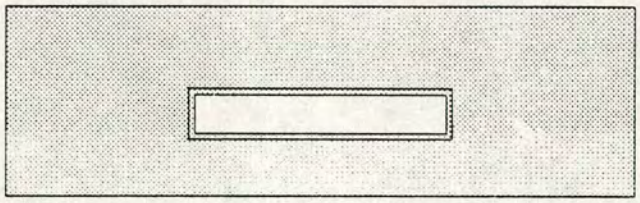

c) Ungrouted Unlined Duct

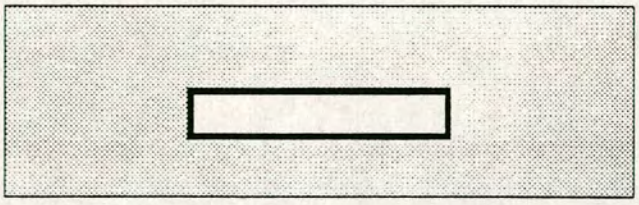

d) Ungrouted Duct with Steel Liner

Note: All models 1000mm * 300mm

Figure 5.2 Finite element models - series 2

5.5 Results

5.5.1 Initial Analyses using ANSYS Ver. 5.0

5.5.1.1 Series 1

Figure 5.3 shows the vertical displacement-time traces for the first two models - the solid concrete beam and the beam with a delamination at 150mm. The traces are quite difficult to analyse and a vertical drift is apparent in each case. This drift is present because the model is unrestrained in the vertical direction. Therefore, the whole model starts moving downwards when the load is applied. The results are more easily analysed if the frequency spectrum is calculated (figure 5.4). This was done using Microsoft Excel version 4.0. A 512 point FFT was carried out.

The spectrum of the solid beam, figure 5.4a, shows a clear peak at the frequency corresponding to the base of the beam, 6.7kHz. This peak cannot be seen on the spectrum of the results from the model containing a delamination at 150mm, figure 5.4b. This plot shows a peak at the frequency corresponding to the frequency of a reflection from the delamination, 13.3kHz.

Figure 5.4c shows the spectrum obtained from the model containing a 400mm wide void at 150mm depth. Again a peak is clearly visible corresponding to the frequency expected from the void, 13.3kHz. The peak from the base is difficult to identify on this plot.

Figure 5.4d shows a similar spectrum plot. This was obtained from the model containing a 200mm wide void at 150mm depth. The frequency peak corresponding to the reflection from the void is still visible but is not as well defined as in the previous two cases. The frequency peak corresponding to the base reflection is easier to identify than in the previous case.

The final plot from series 1 (figure 5.4e) shows the spectrum obtained from the model containing a 150mm diameter circular void at 125mm. The base reflection can be identified on this plot and is at a slightly lower frequency than that shown in figure 5.4a. This is as expected as the wave must travel around the void to reach the base of the beam, thus travelling a greater distance and so reducing the frequency of the reflection. A series of peaks can be seen in the region of the frequency expected from the void but limitations

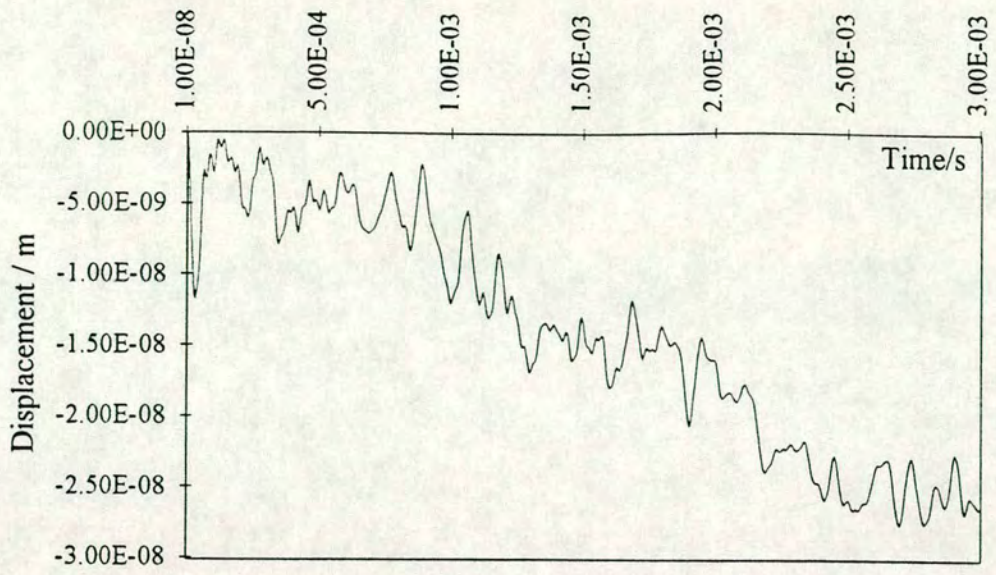

Fig 5.3a Solid 300mm deep beam - Time Domain

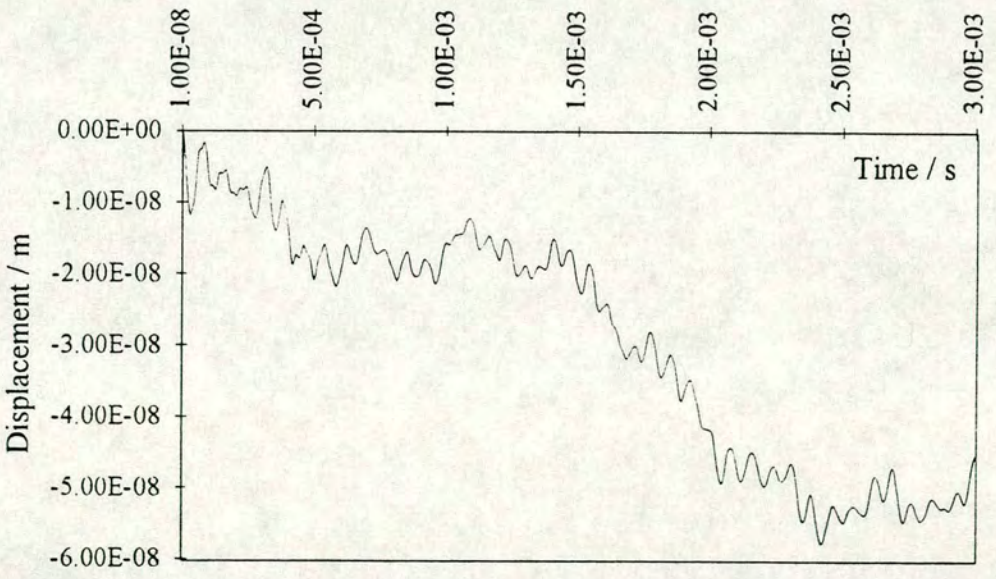

Fig 5.3b Delamination at 150mm - Time Domain

Figure 5.3 Series1 Displacement / Time Traces

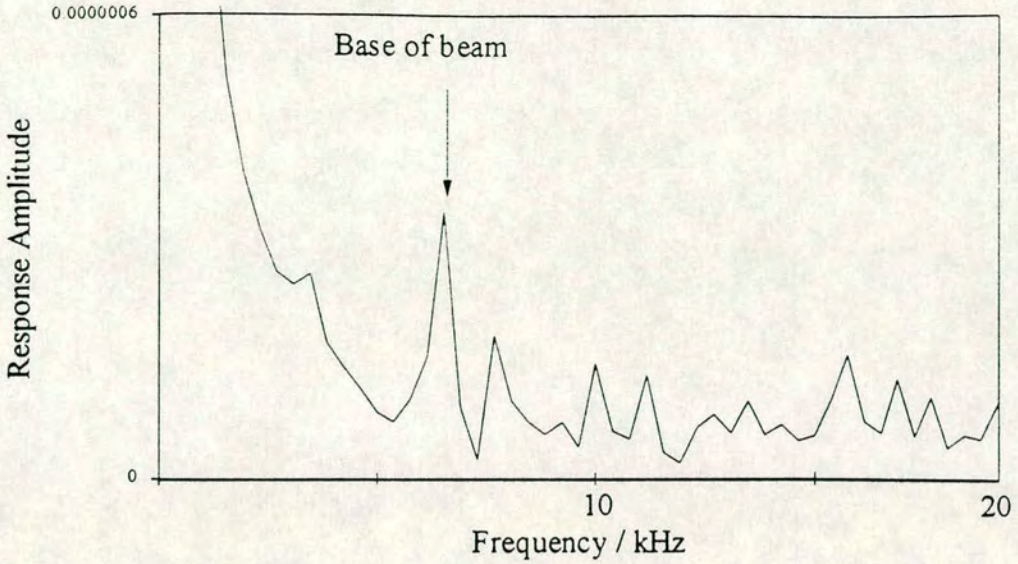

Fig 5.4a Solid 300mm deep beam - 20 kHz

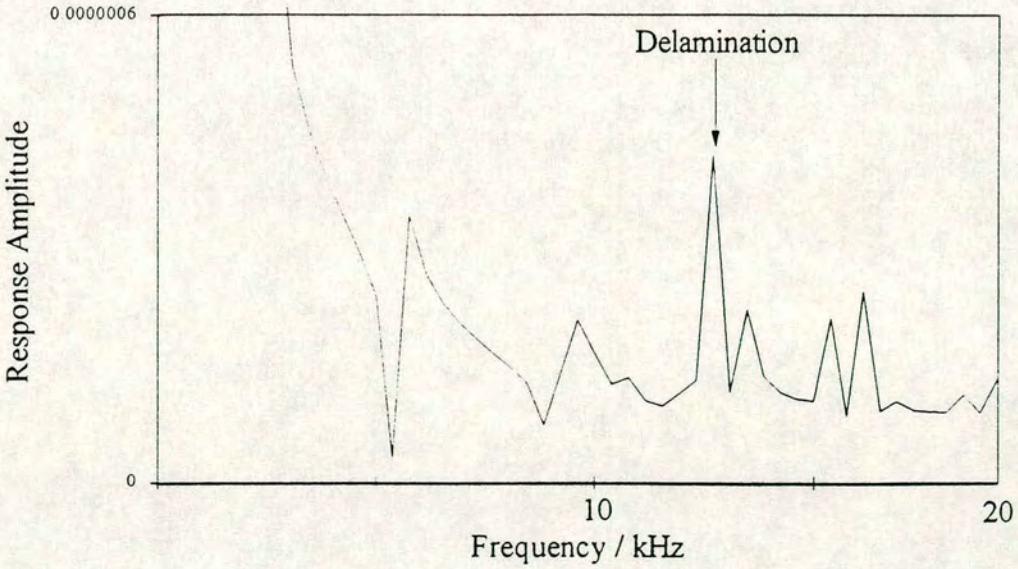

Fig 5.4b Delamination at 150mm - 20 kHz

Figure 5.4 Series1 Frequency Traces

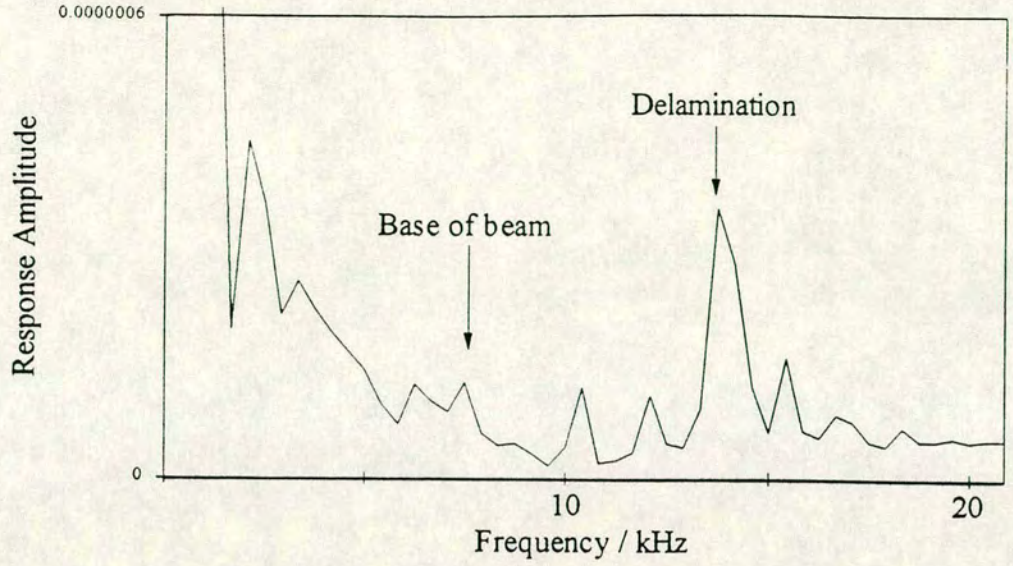

Fig 5.4c 400mm wide void at 150mm - 20kHz

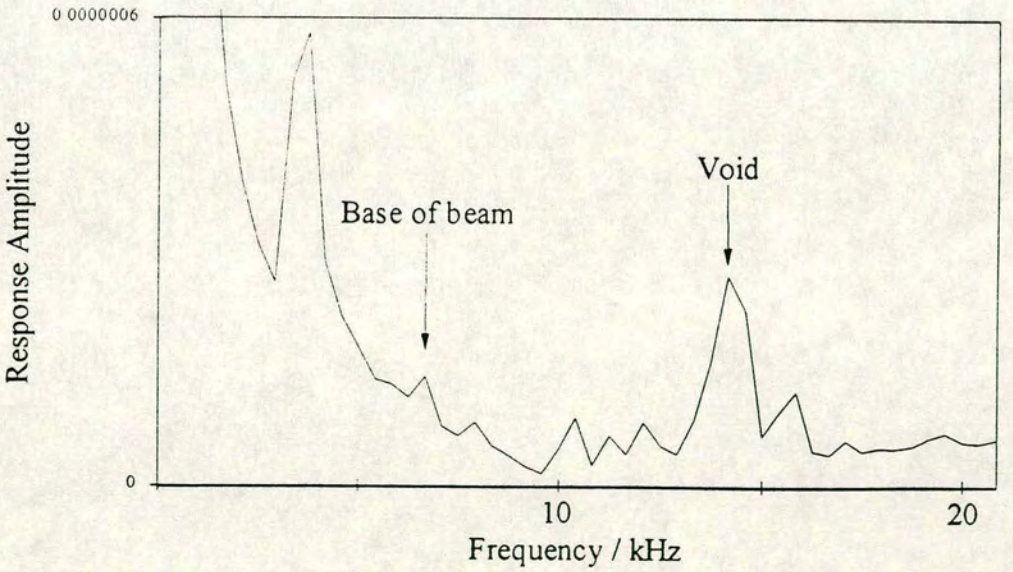

Fig 5.4d 200mm wide void at 150mm -20kHz

Figure 5.4 (cont.) Series 1 Frequency Traces

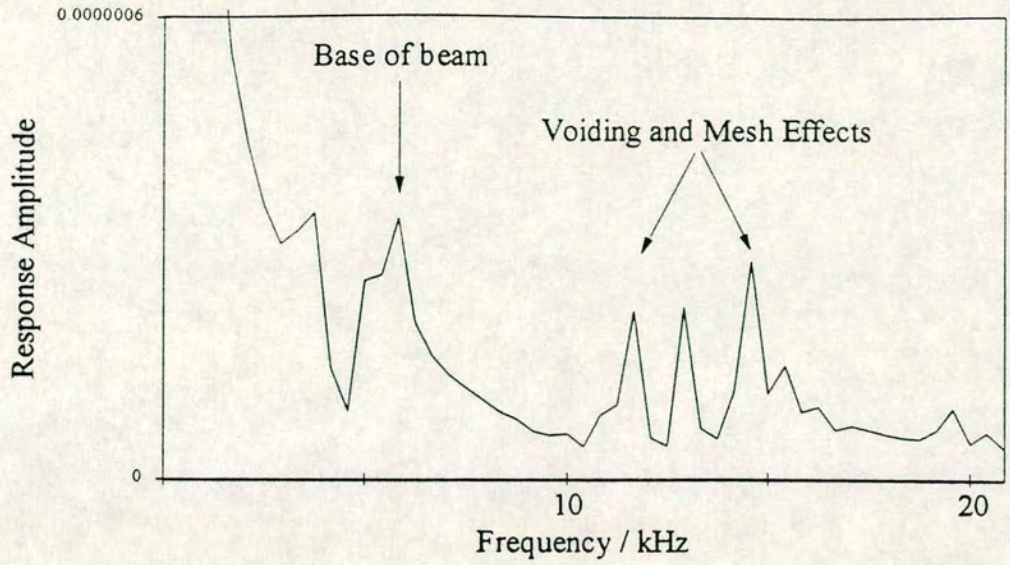

Fig 5.4e 150mm diameter void at 125mm - 20 kHz

Figure 5.4 (cont.) Series 1 Frequency Traces

in the finite element method software used prevented more detailed analysis of this.

5.5.1.2 Series 2

The vertical displacement-time traces from each analysis are shown in figure 5.5. It can be seen that the presence of the steel liner has little effect on the displacement of the beam surface. Similarly to the first series of models, the traces from the ungrouted ducts (figures 5.5b and 5.5d) show a vertical component of displacement at a higher frequency than the traces from the grouted ducts (figures 5.5a and 5.5c).

Figure 5.6 shows the frequency spectrum for each of the above models. As expected, the plots from the models with grouted ducts show the base reflection at approximately 6.7kHz (figures 5.6a and 5.6b). The base reflection is not visible on the plots from the ungrouted ducts but a peak at the frequency corresponding to the top of the void is clearly visible on both plots (figures 5.6c and 5.6d).

5.5.2 Series 3

DYNPAK was used to carry out these analyses to allow more detailed analysis. No vertical drift is shown on the displacement/time traces as this program requires the model to be constrained.

5.5.2.1 Set 1

Figure 5.7 shows the vertical displacement-time traces for the model containing a 100mm diameter void at 125mm from the beam surface - figure 5.7a with an impulse of contact time=30μs, figure 5.7b with contact time=50μs and figure 5.7c with an impulse of contact time=70μs.

The expected arrival time of the compression wave from the base of the beam is approximately 160μs causing the surface of the beam to drop at this time. This can be seen on each displacement-time trace. A compression wave reflected from the top surface of the void would be expected to reach the surface of the beam at 60μs. This wave arrival would again cause the surface of the beam to drop. The plot shown in figure 5.7a shows a clear drop in the surface at the expected time. Figure 5.7b also shows a definite drop in the

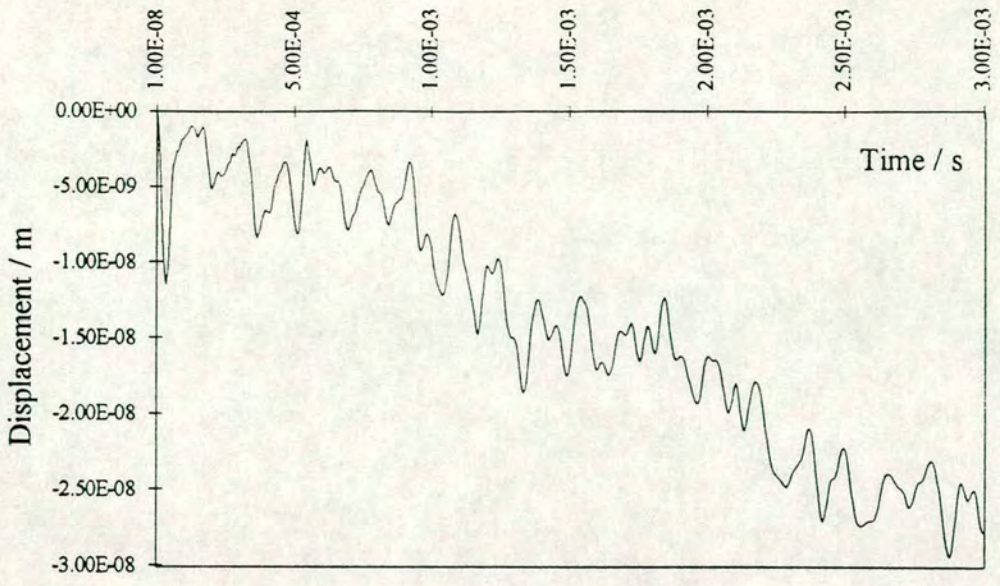

Fig5.5a Solid 300mm deep beam - Time Domain

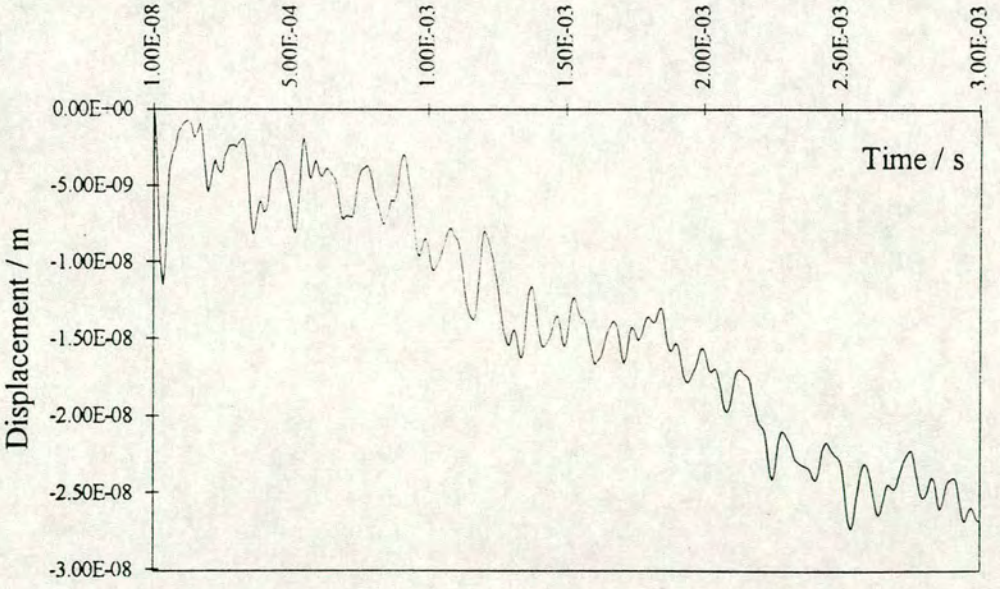

Fig 5.5b Grouted duct with steel liner - 400mm void at 150mm - Time Domain

Figure 5.5 Series 2 Time Domain

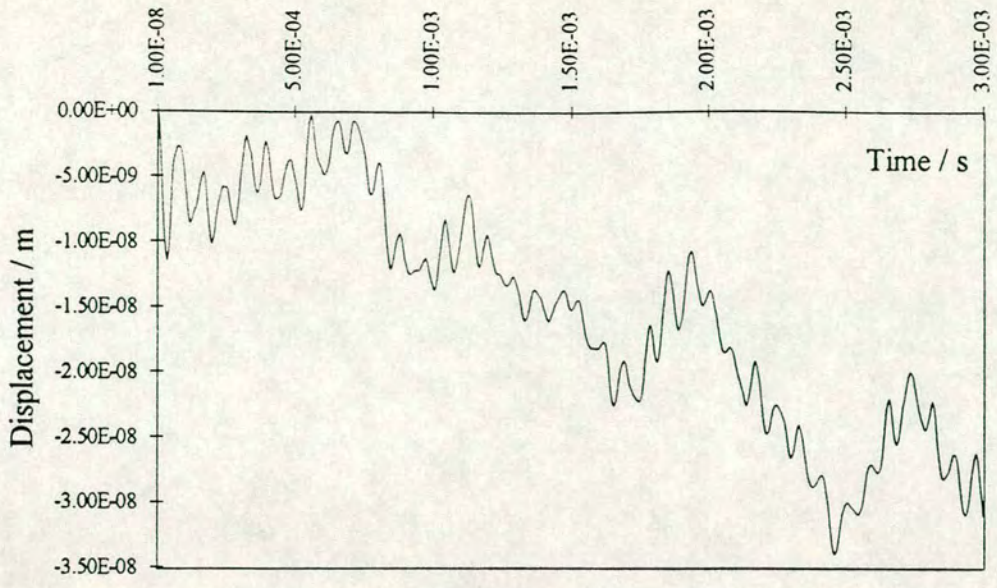

Fig 5.5c Ungrouted duct - unlined - 400mm void at 150mm - Time Domain

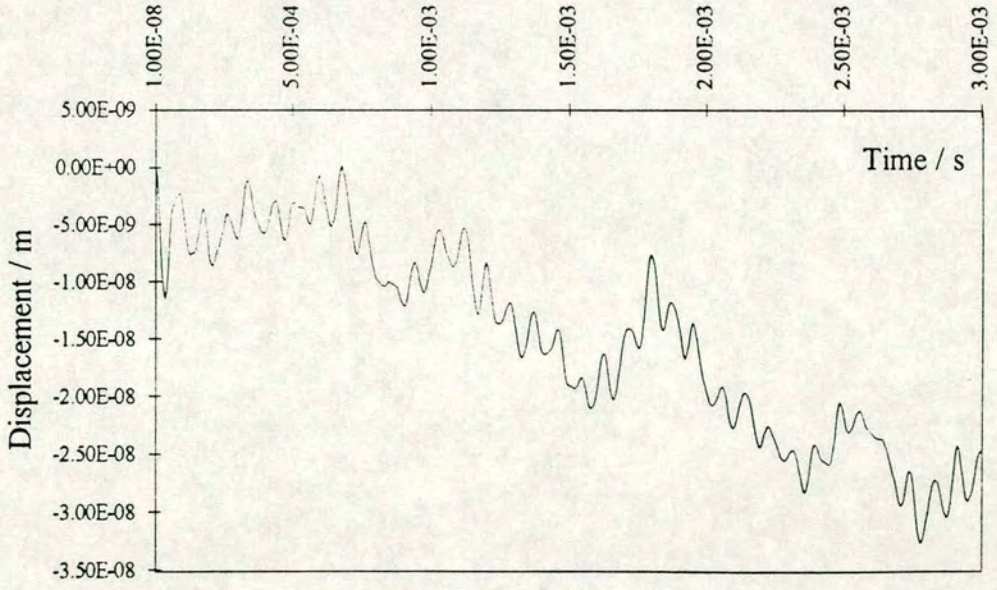

Fig 5.5d Ungrouted duct with steel liner - Time Domain

Figure 5.5 (cont.) Series 2 Time Domain

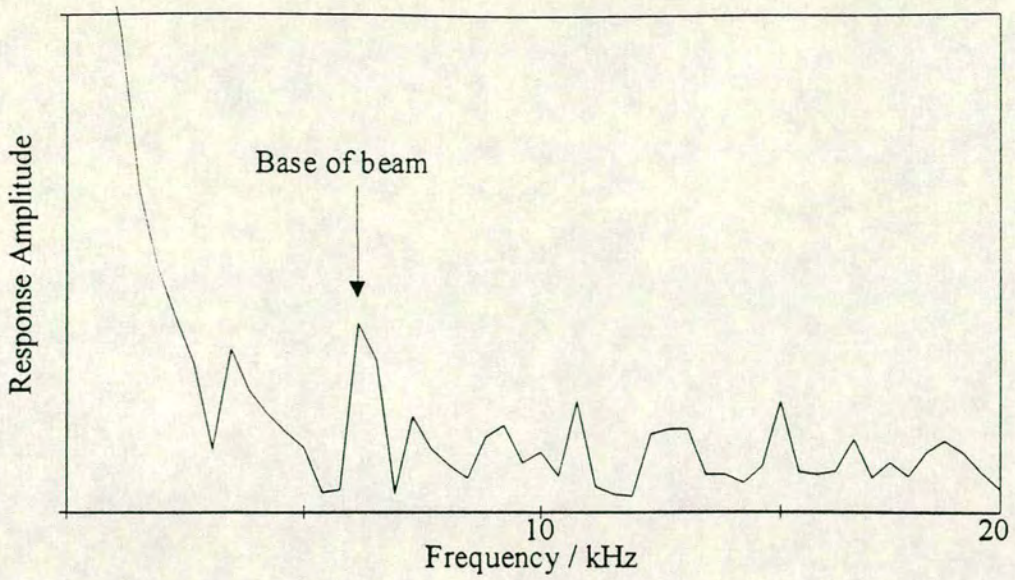

Fig 5.6a Grouted duct - unlined

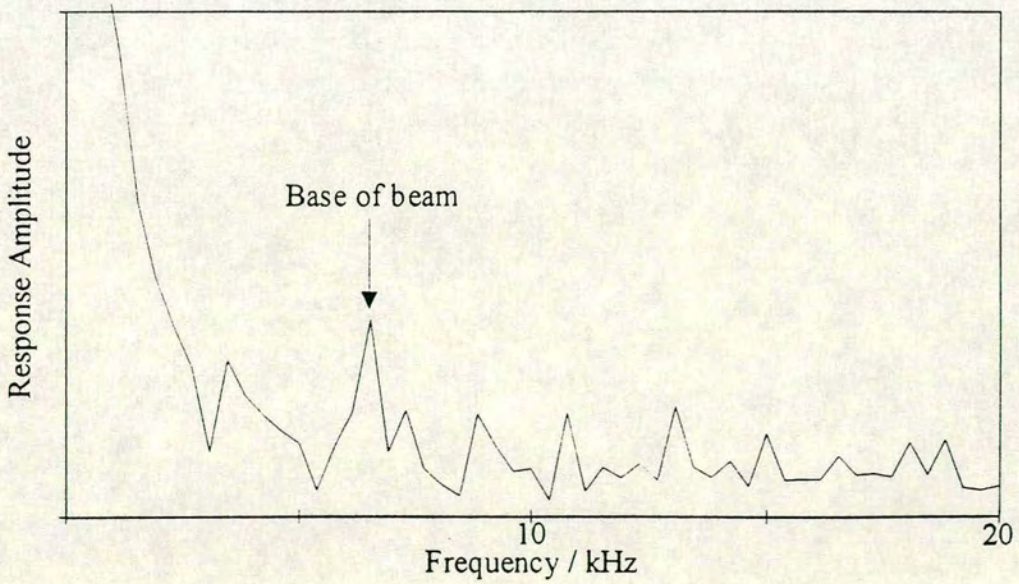

Fig5.6b Grouted duct - lined

Figure 5.6 Series 3 Frequency Traces

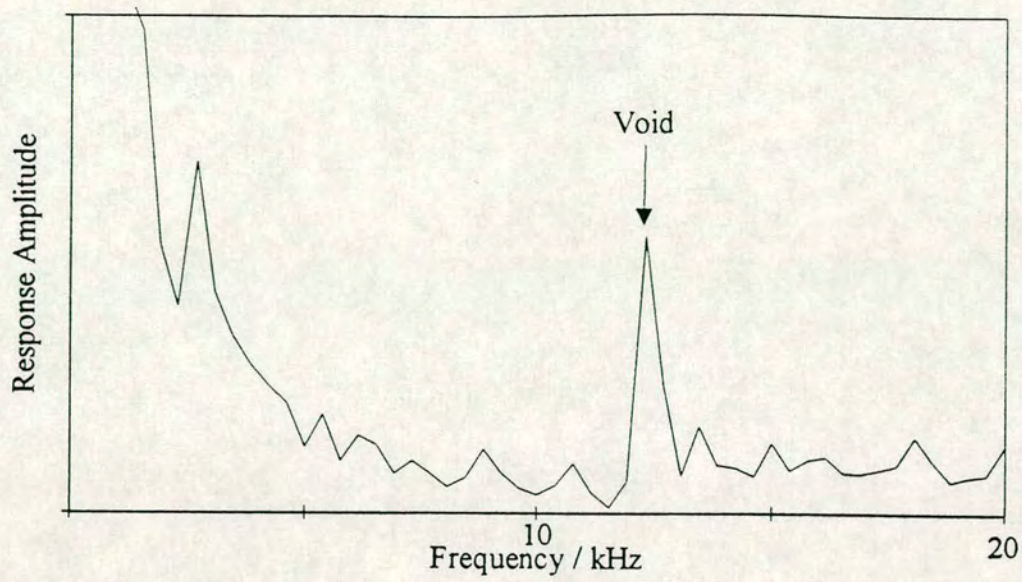

Fig 5.6c Ungrouted duct - unlined

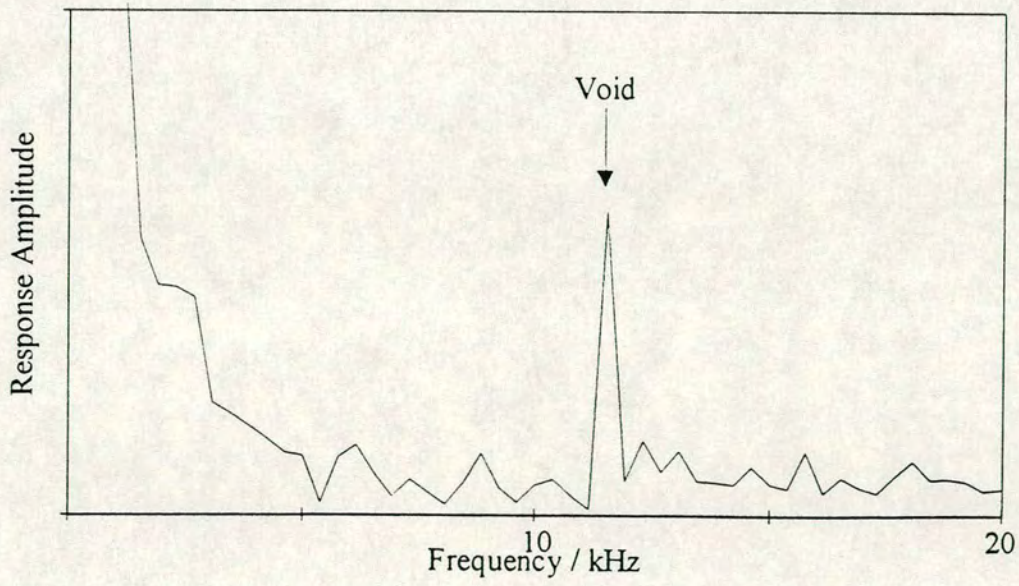

Fig 5.6d Ungrouted duct - lined

Figure 5.6 (cont.) Series 3 Frequency Traces

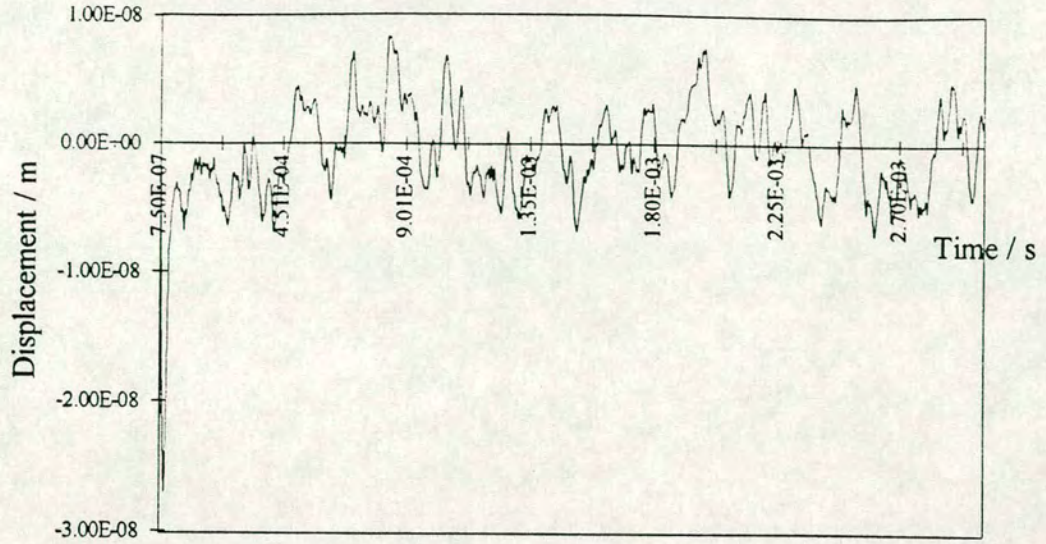

Fig 5.7a Contact Time = 30μs

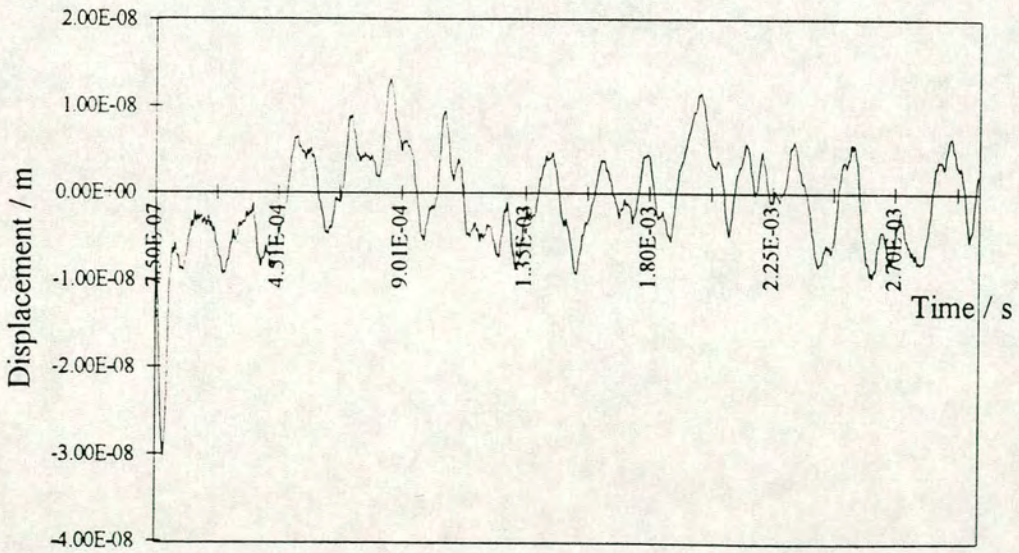

Fig 5.7b Contact Time = 50μs

Figure 5.7 Series 3, Set 1 Time Traces

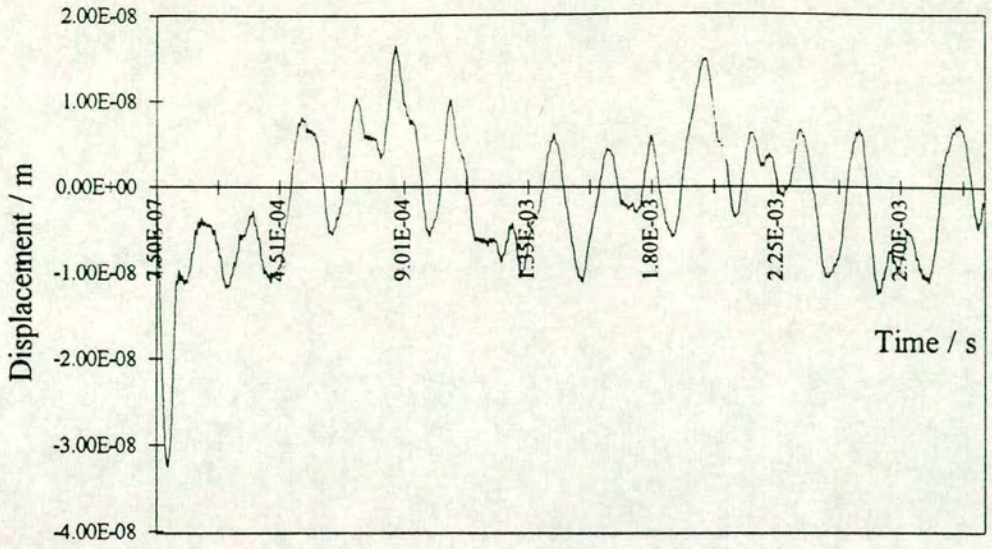

Fig 5.7c Contact Time = 70μs

Figure 5.7 (cont.) Series 3, Set 1 Time Traces

beam surface but it is not as large as that with a 30μs impulse. The plot shown in figure 5.7c shows a discontinuity at about 70μs but the magnitude is much reduced.

Frequency spectrum plots were also calculated for this analysis. This was done by performing a four point moving average on the results from the finite element analysis, extracting every 4th point and performing a 1024 point FFT on the data using Microsoft Excel version 4.0. The spectrum plots are shown in figure 5.8. The frequency peak corresponding to the base reflection can clearly be seen on each plot. The peak corresponding to the reflection from the void can be seen at approximately 14.5kHz. This peak is clearly seen in figure 5.8a, can be seen in figure 5.8b and is difficult to identify in figure 5.8c. This is because the longer pulse length does not input sufficient energy at these higher frequencies.

5.5.2.2 Set 2

The frequency spectra are shown for each of the models constructed for Set 2 (figure 5.9). The traces were constructed in the same way as those described for Set 1.

Figure 5.9a shows the plot obtained from the model containing a 75mm void at 125mm depth. This trace is quite difficult to interpret. The base reflection can be seen at approximately 6.0kHz. A frequency peak can also be seen at approximately 14.5kHz but it is difficult to separate from peaks around that value.

The plot obtained from the model containing a 100mm diameter void at 125mm is shown in figure 5.9b. The frequency peak corresponding to the base reflection can clearly be identified. This is at a slightly lower frequency than that shown in figure 5.9a. The peak corresponding to the reflection from the void can also be identified (14.5kHz).

Figure 5.9c shows the plot obtained from the model containing a 125mm void at 125mm. Again the peak from the void can be seen. The peak corresponding to the base reflection is clearly visible, again it is at a slightly lower frequency than that shown in figure 5.9b.

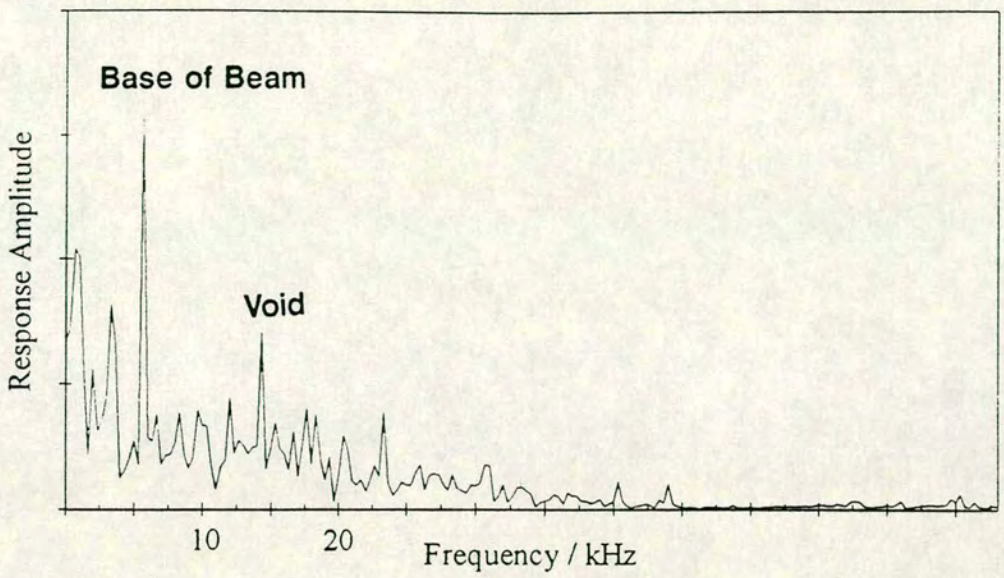

Fig 5.8a Contact Time = 30 μs

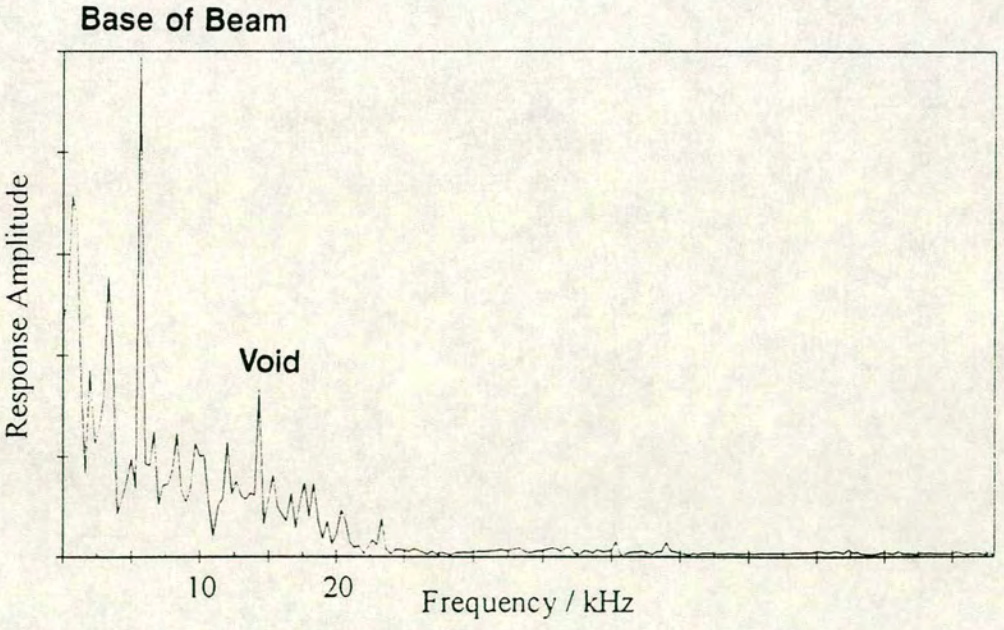

Fig 5.8b Contact Time = 50 μs

Figure 5.8 Series 3, Set 1 Frequency Traces

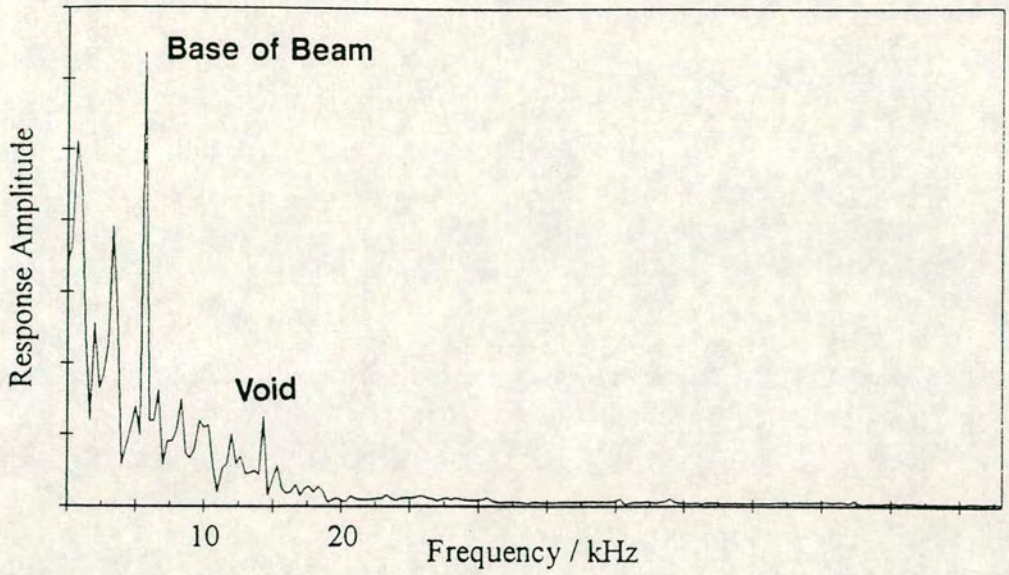

Fig 5.8c Contact Time = 70 μs

Figure 5.8 (cont.) Series 3, Set 1 Frequency Traces

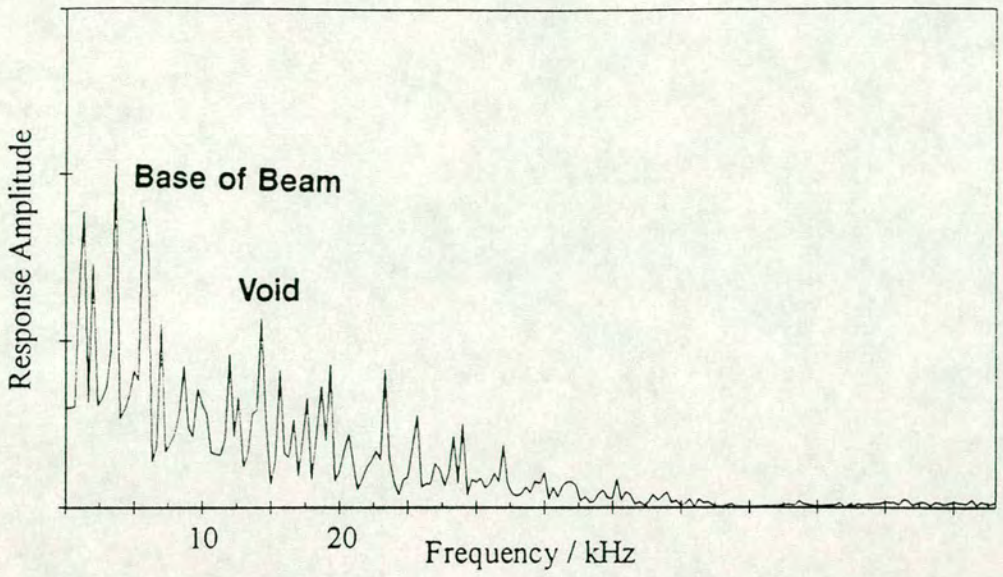

Fig 5.9a 75 mm void

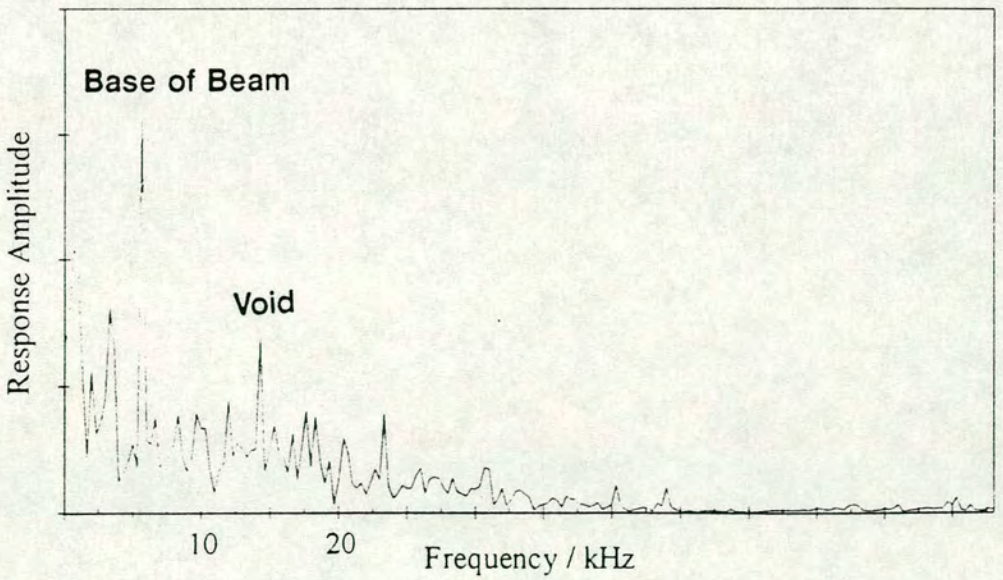

Fig 5.9b 100 mm void

Figure 5.9 Series 3, Set 2 Frequency Traces

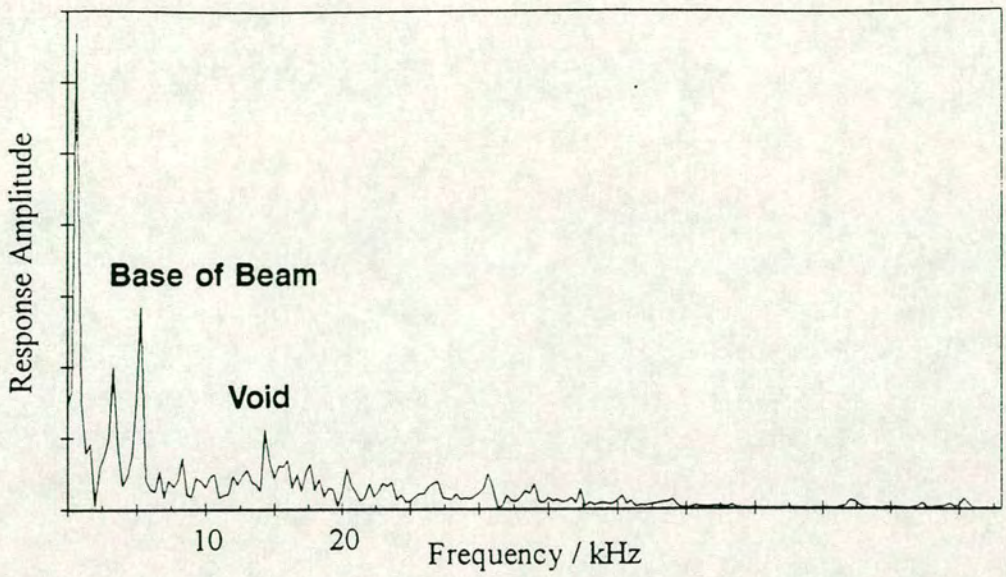

Fig 5.9c 125 mm void

Figure 5.9 (cont.) Series 3, Set 2 Frequency Traces

5.5.2.3 Set 3

The vertical displacement-time traces for Set 3 are shown in figure 5.10. The downwards displacement of the beam surface due to the arrival of the reflected wave from the void can be seen on each trace. The time of arrival varies as expected: the reflection from the void at a depth of 100mm arrives at approximately 60μs, the reflection from the void at a depth of 125mm arrives at approximately 70μs and the reflection from the void at a depth of 150mm arrives at approximately 85μs.

The frequency spectrum plots were constructed as before. The frequency peak corresponding to the reflection from the void at 100mm is difficult to distinguish in figure 5.11a. Figure 5.11b shows a clear peak at approximately 14.5kHz corresponding to the reflection from the void at 125mm. The peak on the frequency spectrum corresponding to the reflection from the void at 150mm can be seen with difficulty in figure 5.11c. The peak corresponding to the reflections from the base (at 6.0kHz) can be clearly seen on all plots.

5.6 Analysis and Discussion

5.6.1 Series 1

The finite element method can be used to analyse structures containing planar flaws quickly. The results from series 1 show that even with the limited mesh density available with the software, planar defects can easily be identified. The size of the defect can be estimated by comparing the frequency of the base reflection with that from a solid beam section. The larger the defect, the lower the frequency of the base reflection. Circular voids are more difficult to detect and require a much finer mesh. However, circular voids of a reasonable diameter can be detected.

As with a planar void, the base reflection occurs at a lower frequency since the wave must propagate around the void to reach the base. Large circular voids may give rise to peaks on the frequency spectrum. As the diameter of the void increases the amount of scattering reduces since the void provides a flatter profile to the wave-front.

5.6.2 Series 2

Similar results are produced with ducts that are lined and unlined. The frequency spectra for the ungrouted ducts clearly show a peak corresponding

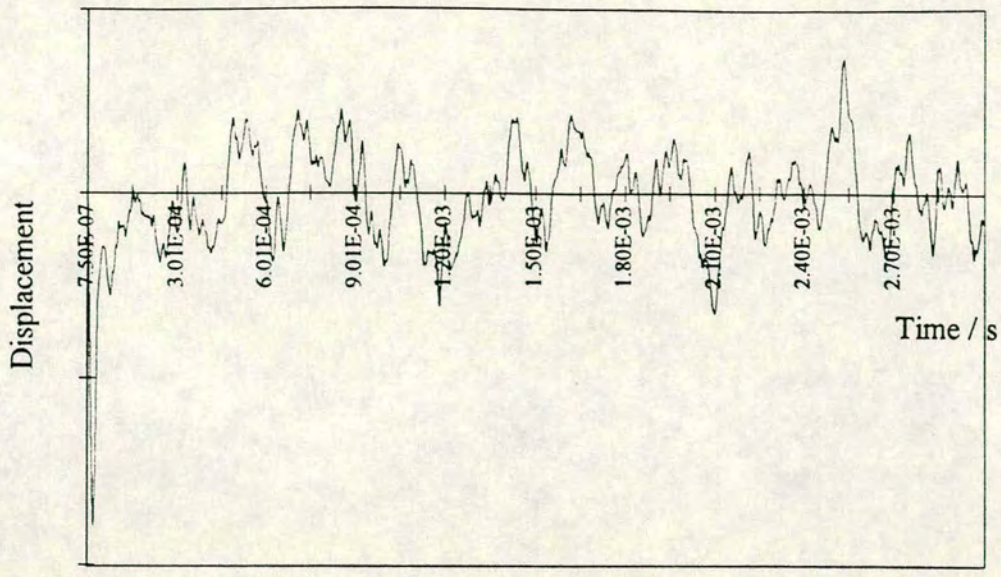

Fig 5.10a 100mm void at 100mm depth

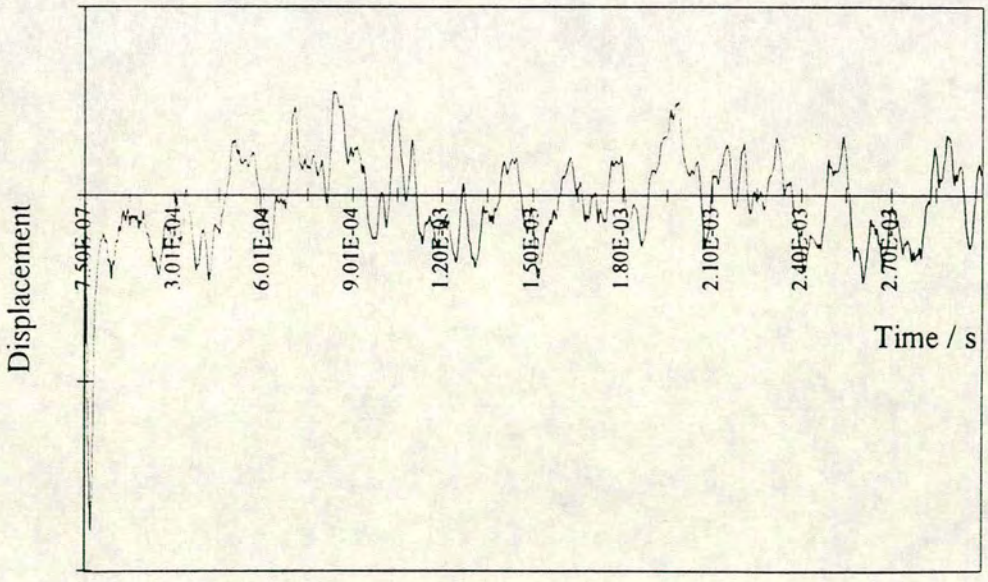

Fig 5.10b 100mm void at 125 mm depth

Figure 5.10 Series 3, Set 3 Time Traces

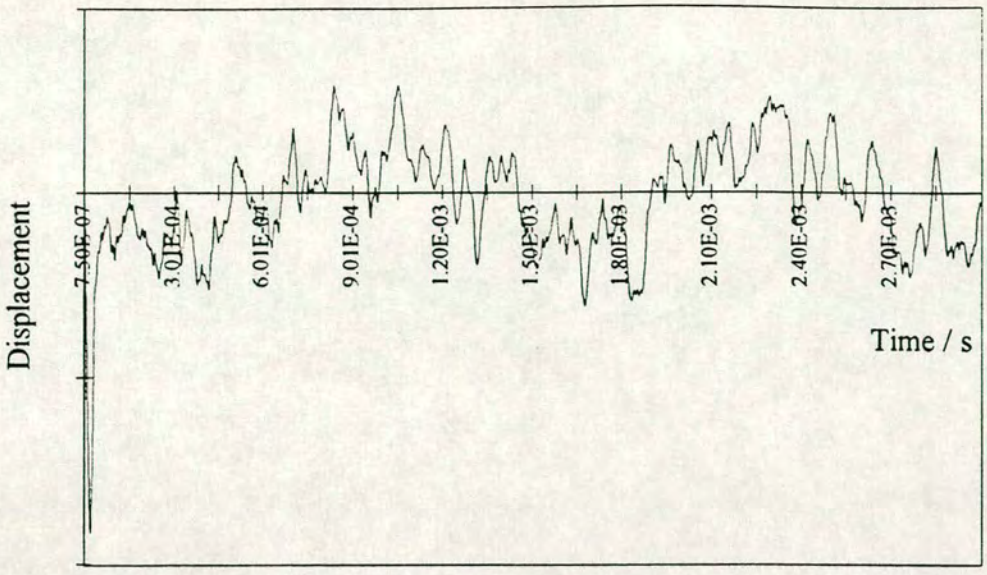

Fig 5.10c 100mm void at 150mm depth

Figure 5.10 (cont.) Series 3, Set 3 Time Traces

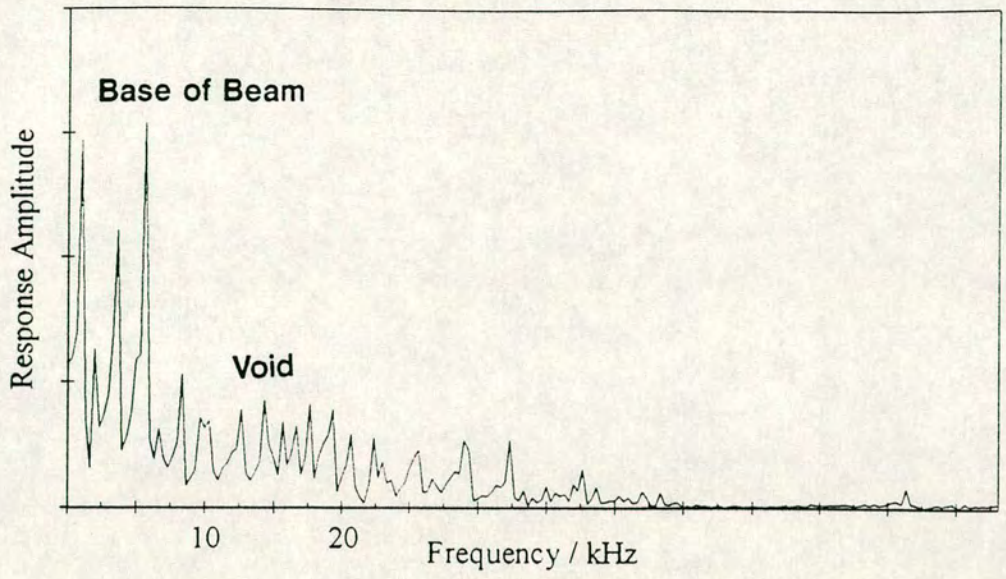

Fig 5.11a 100mm void at 100mm depth

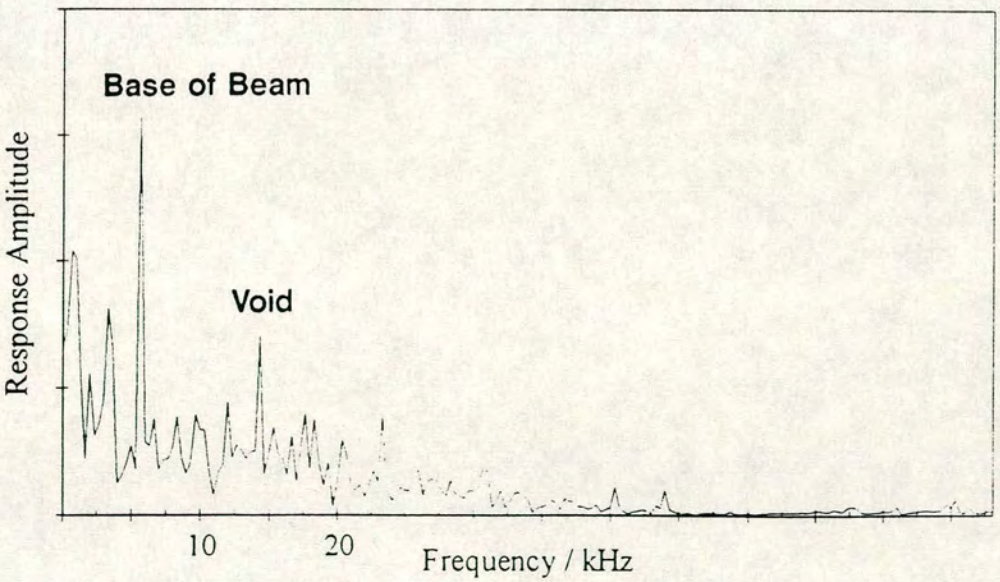

Fig 5.11b 100mm void at 125mm depth

Figure 5.11 Series 3, Set 3 Frequency Traces

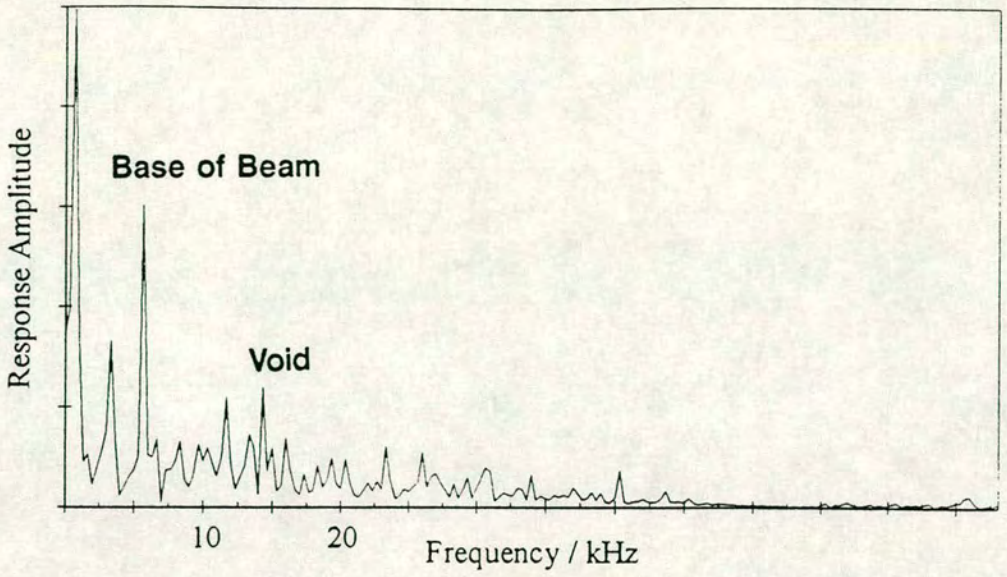

Fig 5.11c 100mm void at 150mm depth

Figure 5.11 (cont.) Series 3, Set 3 Frequency Traces

to a reflection from the void. This peak is missing from the spectra from the grouted ducts. The thin steel liner has very little effect on the results as the wavelength of the highest frequencies contained in the impulse are much greater than the thickness of the steel.

Consider a thin steel layer bonded on to concrete (representing an ungrouted, steel lined duct). No stress occurs at the air-steel interface and, since the steel is thin, virtually no stress will occur at the steel-concrete interface. If the thin steel layer, of greater rigidity, was bonded between two layers of concrete, with the same rigidity, (representing a grouted steel lined duct) the thin layer would not interfere with the stress wave propagation and so the waves will travel directly through the layer (Carino, Sansalone and Hsu, 1986a).

5.6.3 Series 3

It has been shown that the shorter the contact time, the smaller the defect that can be detected. The assumed maximum usable frequency input to the beam and minimum target profile and depth to target detectable are shown below (Sansalone et al, 1986):

$$f_c \approx 1/(1.5T_c) \tag{5.1}$$

where

f_c=Max. frequency input (cut-off frequency) /Hz

T_c=Contact time of impulse /s

and

$$d_{min} \approx \lambda/2 \tag{5.2}$$

where

d_{min}= minimum profile or depth to target detectable/m

$\lambda = v_c / f_c$ /m

From the results obtained this appears to be rather conservative. However, the analyses carried out are on two-dimensional models, with concrete assumed to behave as a linear, isotropic and homogeneous material. This should lead to clearer results than those obtained from real concrete specimens.

Set 1 shows that as the contact time of the impulse increases, the 100mm void at 125mm depth becomes more difficult to detect. The 100mm diameter is the

critical parameter for detection in this case and, using equations 5.1 and 5.2and assuming a compression wave velocity of 4000m/s the critical impulse duration would be:

$f_c = 4000/(2*0.1) = 20\ 000$ Hz
$T_c = 1/(1.5*20000) = 33\mu s$

It should therefore be possible to detect the void in model 3 only. However, as mentioned above, the model is a simplified version of a real concrete structure and so the void could be detected with an impulse of 50μs but could not be detected with an impulse of 70μs duration.

The results from Set 2 agree with the expected results. Using equation 5.1 and 5.2, the minimum profile that could be detected with an impulse of 30μs duration is 90mm. Therefore it will be possible to detect a 100mm void and a 125mm void at a depth of 125mm but it will not be possible to detect a 75mm void at the same depth. The frequency of the reflection from the base also reduced as the void diameter increased. This was as expected and could be used to determine the relative size of the voids.

The models constructed in Set 3 investigated the influence of the depth to a void on the resulting displacement-time traces and frequency spectra. If a cylindrical void is at a depth close to the minimum depth at which defects become detectable the defect may not be detectable, as occurred in figure 5.11a. Scattering may also adversely affect the detection of a void at greater depth (figure 5.12). In this case, the deeper the void, the more severe the scattering.

The results from Set 3 are summarised in Table 5.1 below. The assumptions made in equations 5.1 and 5.2 seem rather conservative and so a further comparison with a quarter of the minimum input wavelength is also made.

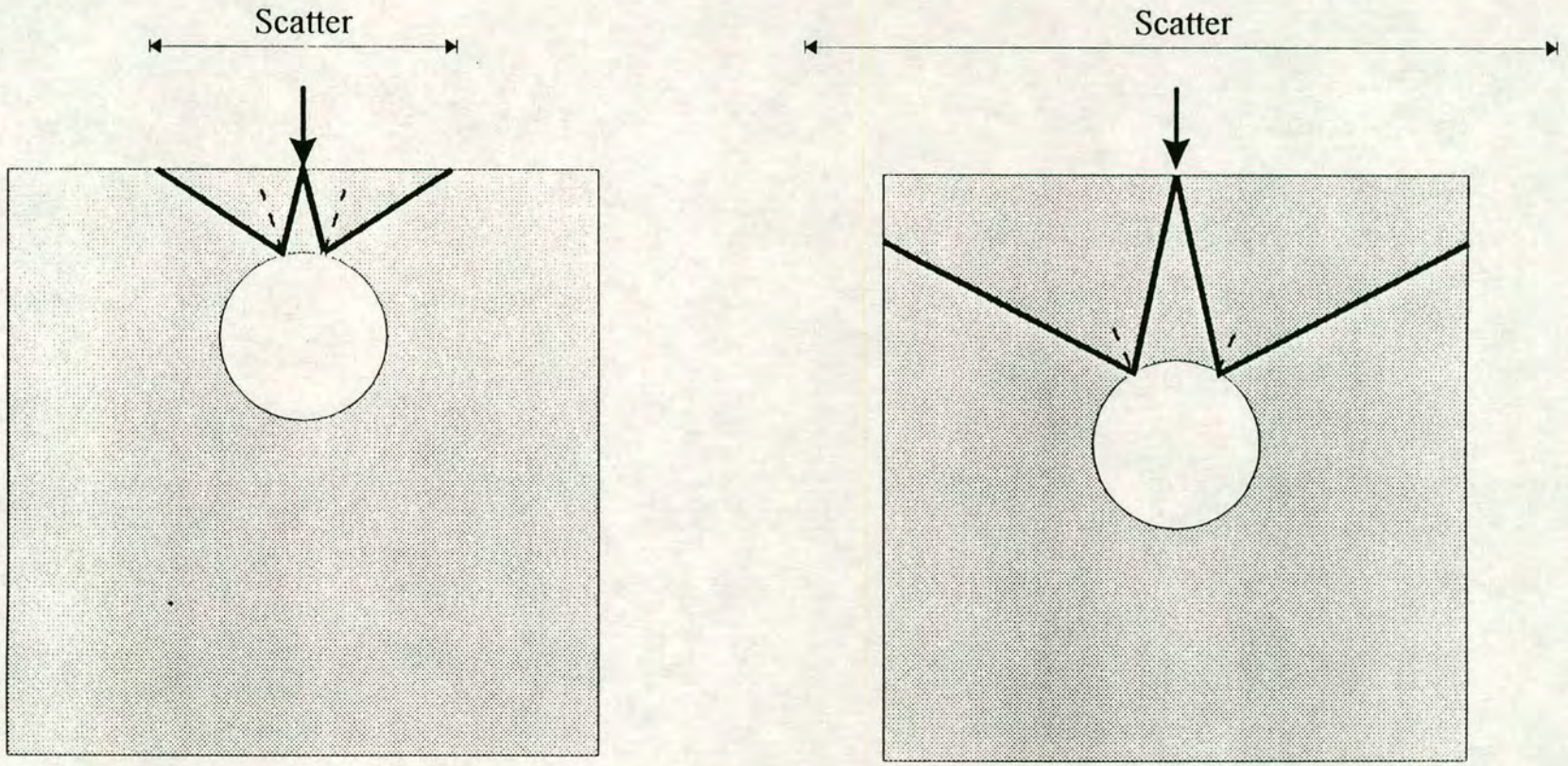

Figure 5.12 Effect of depth to circular defect on reflect and energy scatter

Test	Notes	T_c /μs	f_c /kHz	λ/2 /mm	λ/4 /mm	Defect Profile /mm	Detection
3.1a	100mm dia. at 125mm	30	22	90	45	100	✓
3.1b	100mm dia. at 125mm	50	13	150	75	100	✓
3.1c	100mm dia. at 125mm	70	9.5	210	105	100	?
3.2a	75mm dia at 125mm	30	22	90	45	75	?
3.2b	100mm dia at 125mm	30	22	90	45	100	✓
3.2c	125mm dia at 125mm	30	22	90	45	125	✓
3.3a	100mm dia at 100mm	30	22	90	45	100	×
3.3b	100mm dia at 125mm	30	22	90	45	100	✓
3.3c	100mm dia at 150mm	30	22	90	45	100	?

Table 5.1 Summary of findings from Set 3 and comparison of possible detection limits

5.7 Summary of Discussion

The above results show that the finite element method is a useful way of investigating the range and limitations of the impact-echo method as applied to the investigation of ducted post-tensioned bridges. It is generally assumed that the results expressed in the frequency domain will be more readily interpreted. However, these results show that the displacement-time traces can yield results that are difficult to interpret on the frequency data. As long as a small enough time step is used, the reflections from defects can be determined and the depth to these defects calculated from the time trace. The assumptions made regarding the usable frequency of impact

Chapter VI

Laboratory Investigation

Detailed laboratory testing was carried out to investigate the performance of the developed method and to validate the conclusions drawn from the finite element analysis.

6.1 Introduction

Chapter 5 confirmed that, theoretically, sonic impact-echo techniques might be applied effectively to the non-destructive testing of metal ducted post-tensioned concrete bridge beams. Some limitations regarding the size of void detectable and geometry of the beam were noted and in order to carry out the finite element simulations, a number of major assumptions were made. These are likely to affect the expected results in practice.

It was assumed that concrete is an elastic and homogeneous material and no damping was included for the finite element analysis. The effect of the assumptions are non-conservative, i.e. the results from the finite element simulations will give better, more easily analysed results than a test carried out in practice on a similar model. The finite element analyses are two-dimensional. This means that the voids modelled are of infinite length. In practice, voids contained in beams will be of finite length. The length of void detectable in practice will be investigated.

The contact time of the impact has been shown to be critical in determining the size of defect detectable. The majority of impactors used for the experimental work detailed in this thesis are not instrumented. The impact is therefore not measured directly. However, the results of all the finite element analyses showed that the contact time of the impact could be accurately estimated from the resulting displacement of the beam surface at the impact point. This phenomenon will be investigated in practice. Inaccuracies may arise as the response transducer cannot be placed directly at the impact point. The response transducer must be sufficiently sensitive to detect the amplitude of the response and the displacement of the beam must be measured at a high enough frequency to resolve the displacement trace adequately. However, it should be possible to estimate the contact time from the displacement trace measured by the NIST transducer. This can be compared to the expected contact time for the particular ball bearing diameter calculated using elastic theory. The estimated contact time should be longer than that anticipated as discussed in detail in earlier chapters.

A simple laboratory beam was cast containing a single duct which was ungrouted along half its length. This model was of the same cross-section as one of the finite element models and therefore could be used to validate the finite element results. Once this was done the original laboratory specimen was investigated further using a similar test set-up.

6.2 Response Transducer

The NIST transducer could only be used in a vertical orientation. This created a severe limitation to practical site testing of post-tensioned concrete beams as it is unlikely that the top surface of a beam on a live bridge could be exposed. The most likely test orientation is from the base of a beam. The sides of a beam may also be accessible and these may be sloped in any direction. The transducer was therefore adapted to allow testing to be carried out in any orientation.

The active element of the transducer is in the form of a conical element attatched to a brass mass which is held against the surface of the test specimen by gravity. The mass is connected to an amplifier by a contact resting on a gold wire attatched to the block. This in turn is connected to the metal housing of the transducer. The electrical circuit is completed by connecting the conical element to the transducer housing using a conductive material soft enough to conform to the surface of the transducer and test specimen (NIST Instructions). Thin aluminium foil was initially used to form the connection between the conical element and the housing. A thin layer of clean petroleum jelly was placed between the beam surface and the foil and also the foil and the conical element. The foil was securely clamped to the housing to ensure electrical contact.

6.2.1 Adaptation of NIST Transducer

In order for the transducer to be used in any orientation the brass mass and conical element had to be held in position without making contact with the housing. Contact had to be made between the gold wire connector and the sprung connector arm attatched to the amplifier. The movement of the connector arm could not be impeded.

The whole transducer housing was lined with non-conductive plastic. The base plate was too thick to allow the conical element to contact the test surface through a small hole cut in it so a large section was removed from the base plate of the housing. A thin copper sheet was connected with small holes cut in it for the conical element and feet of the brass mass. This copper sheet also had to be isolated from the base of the mass and the conical element. A very thin brass sheet was then used as a connector between the conical element and the housing, similar to the aluminium foil used previously, figure 6.1. The foil was much harder wearing and did not need to be replaced between tests. However, care had to be taken to ensure that there was

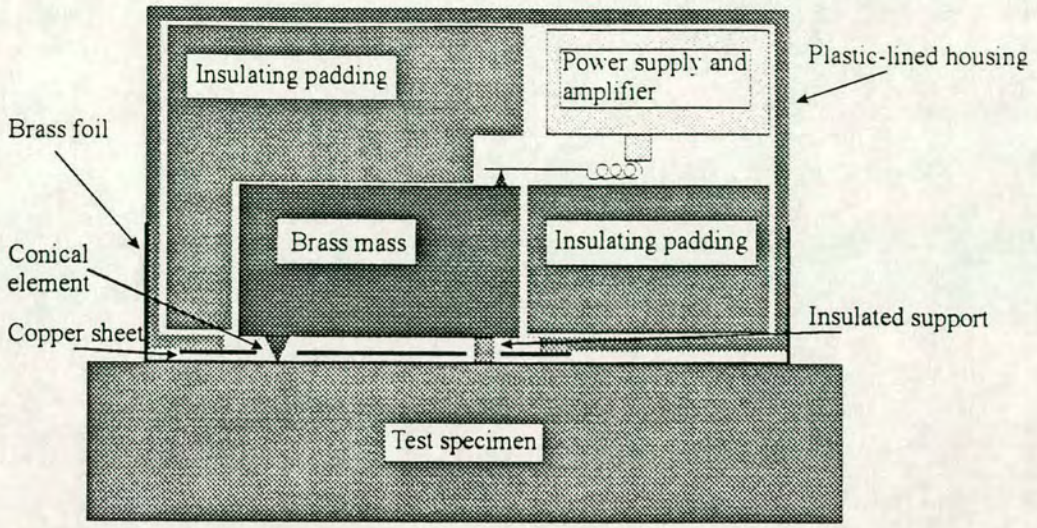

Figure 6.1 NIST displacement transducer adapted for use in any orientation

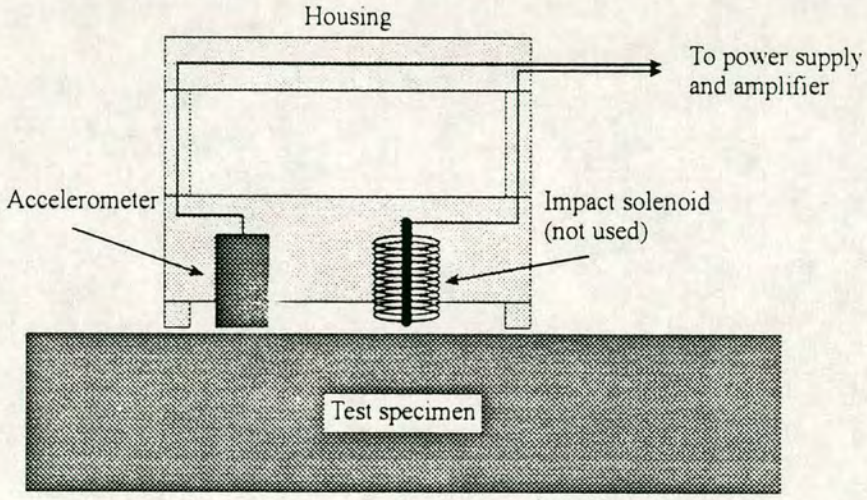

Figure 6.2 OLSON accelerometer

adequate petroleum jelly between the conical element and the brass sheet and the brass sheet and the test specimen. The petroleum jelly between the conical element and the brass sheet did not need to be changed between each test but the petroleum jelly between the test specimen and the brass sheet required cleaning and changing between every test.

6.2.2 OLSON Impact-Echo Instrumentation

The NIST transducer is quite delicate and the testing set-up requires considerable adjustment between tests. This renders the use of the NIST transducer rather cumbersome in the field and extensive remodelling would be required to produce an impact-echo system suitable for rapid testing on site. Two such systems have been produced in the USA, the first is the DOCter as discussed previously which is currently available commercially. OLSON Engineering have produced a prototype impact-echo system, figure 6.2. This system can be applied to the impact echo testing of any structure but work was carried out by the author to determine the suitablilty of the response transducer for use in practical non-destructive testing of metal ducted post-tensioned concrete bridges in the field.

The transducer incorporated into the OLSON system is an accelerometer. Tests have been carried out at the OLSON laboratory which indicate that frequency components of the response up to and beyond 35 kHz can be accurately detected. It is intended to produce a total testing system with a range of impacts being produced by a variety of solenoids. The distance from impact to transducer will be constant and the force of impact will also be more controllable. It is not intended to instrument the impactor initially and so care should again be taken when calculating the cut-off frequency achieved at each impact. At the time of testing only the response transducer could be evaluated.

It is intended to evaluate both transducers in laboratory and field testing.

6.3 Laboratory Test Beam 2

A simple unreinforced concrete beam was constructed of dimensions 300mm wide by 400mm deep by 750mm long. The beam contained a single tendon 100mm in diameter at a depth of 150mm. This was grouted along half its length and totally

ungrouted along the remainder (figure 6.3). The surface of the beam was carefully smoothed off to provide a very flat surface. This creates the best concrete surface condition for testing. This cross-section was modelled using finite element methods as discussed in Chapter V and the test beam was cast to compare the calculated results from finite element simulation to the experimental results found in the laboratory. The finite element analysis indicated that the minimum defect profile detectable may be less than $\lambda/2$ (where λ=minimum wavelength input, assuming an input frequency equalt to $1/t_c$) and that a minimum profile of $\lambda/4$ may be detectable. However, the finite element model gives a very idealised impact signal and assumes a homogeneous material with no signal and measurement system noise. This is likely to lead to better defect detection being predicted. Laboratory testing was carried out using both the NIST and the OLSON transducers.

Research has been carried out at Cornell University investigating the effect of the beam dimensions on the response from impact-echo testing. Distinct modes were measured, the frequency of which depended on the dimensions of the beam. These modes were found to dominate the measured response (Sansalone and Poston, 1992). This affect was also investigated in these tests.

6.3.1 Experimental Procedure

The beam was tested along the centre line of the tendon duct. The majority of the tests were carried out with the NIST transducer but preliminary tests were also carried out with the OLSON accelerometer to ensure similar results were obtained on the simple beam model. A series of different hammers were used to investigate the influence of contact time and then compared to the results found by finite element analysis. The experimental results are detailed below.

6.3.2 Experimental Results

6.3.2.1 Contact time of impact

In the finite element analyses the contact time was discovered to be approximately equal to the inital downwards movement of the beam. The initial downwards movement of the beam could also be seen on the experimental results from test beam 2. Similar results were found over the entire surface of this beam as the surface was carefully prepared before the concrete hardened. The displacement of the beam measured at position A4 is shown in figure 6.4. Four hammers with different ball bearing diameters were

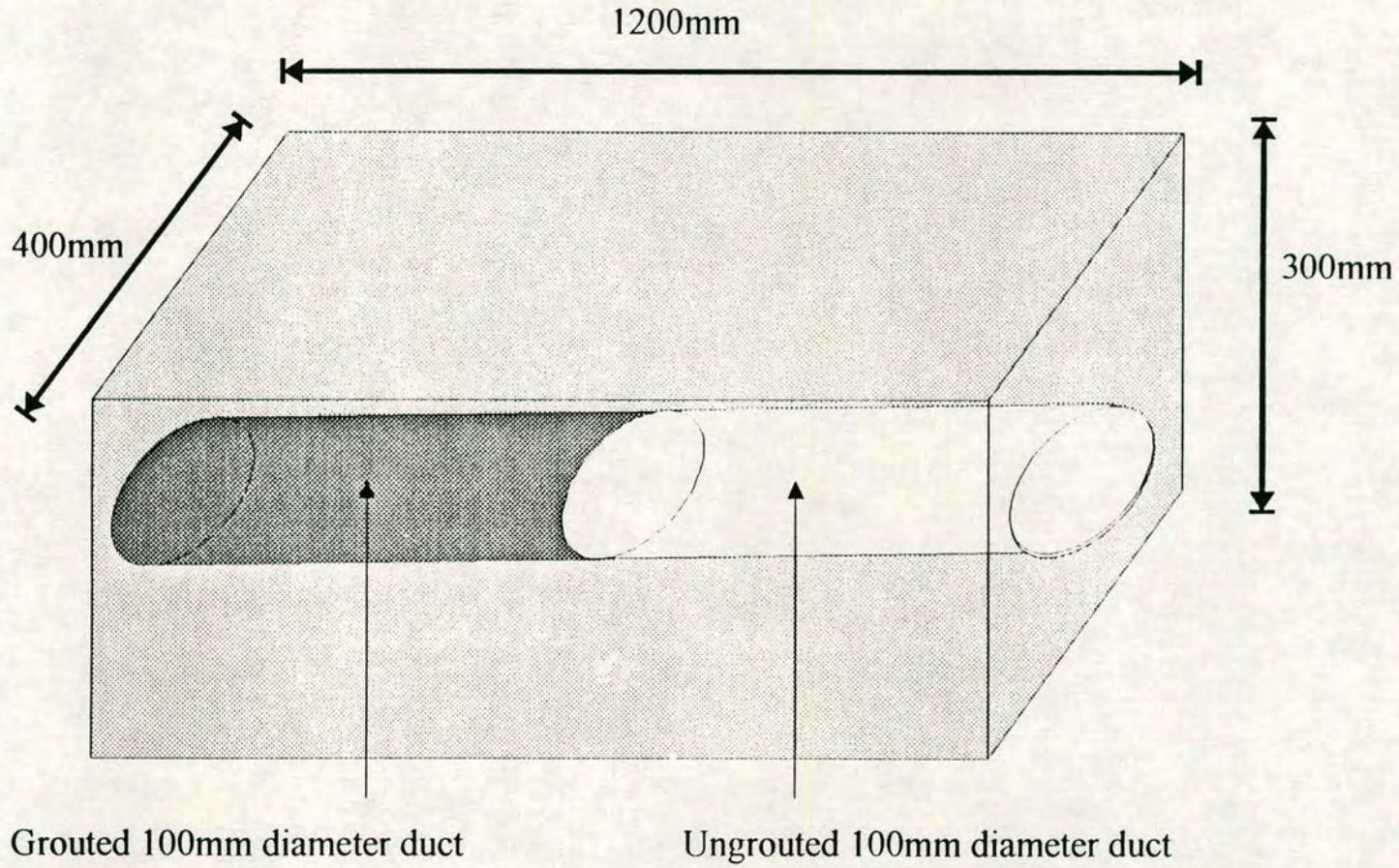

Figure 6.3 Laboratory test beam 2

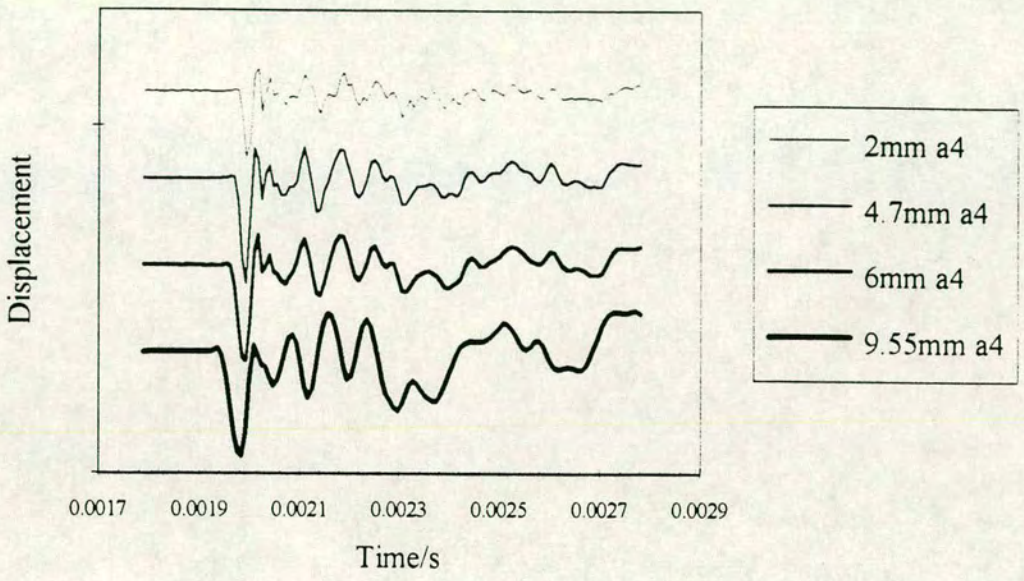

Figure 6.4 Beam displacements at position A4

used. The predicted elastic contact times are shown with the measured estimates of the contact times in table 6.1.

Impact Hammer	Measured T_c	Predicted T_c
9.55mm	70μs	50μs
6.0mm	55μs	30μs
4.7mm	39μs	25μs
2.0mm	31μs	10μs

Table 6.1 Impact contact times

The above table shows that the measured contact times are lower than the expected contact times calculated using elastic theory. It can also be seen that the percentage reduction increases but is constant at approximately 20μs as the expected contact time reduces. This occurs because the impact is not fully elastic, i.e. the concrete surface suffers local crushing at the impact point.

6.3.2.2 Grouted and ungrouted duct using NIST Transducer

A series of tests were carried out on an ungrouted and a grouted section of the test beam. A range of hammers from 2mm diameter ball bearing hammer to 9.55mm diameter ball bearing hammer were used. The results from the ungrouted section are shown in figure 6.5 and from the grouted section in figure 6.6. The expected frequency components of the beam cross-section with an aspect ratio (depth/width) equal to 1.33 are shown in table 6.2.

No. of Frequency Mode	Frequency/kHz
Fundamental	2.5
Mode 2	3.7
Mode 3	5
Mode 4	5.1
Mode 5	6.1
Mode 6	6.6

Table 6.2 Expected frequency components of beam cross-section

The results from the grouted section (figure 6.6) show the dominant peak at 3.625 kHz. This corresponds well with beam mode 2 as shown on table 6.2. A

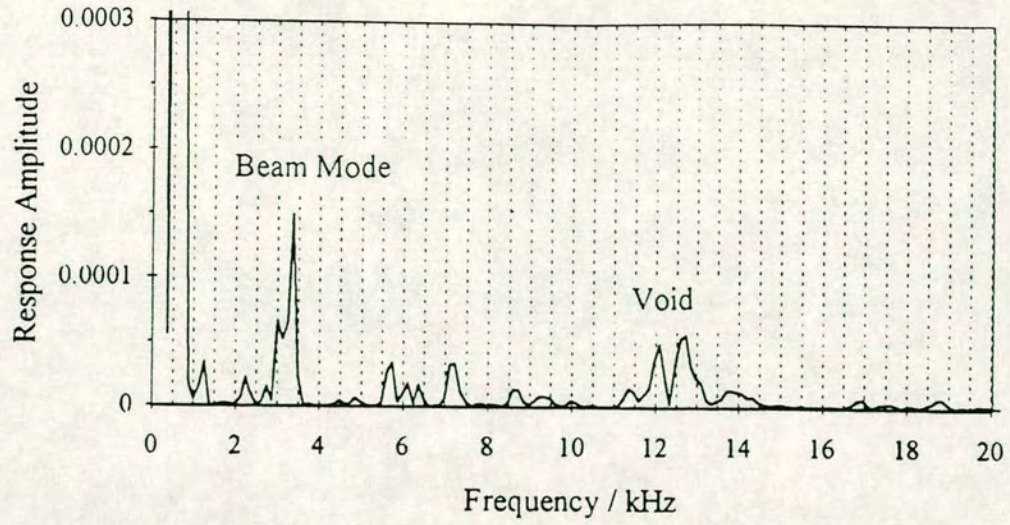

Fig6.5a 2mm hammer on voided section

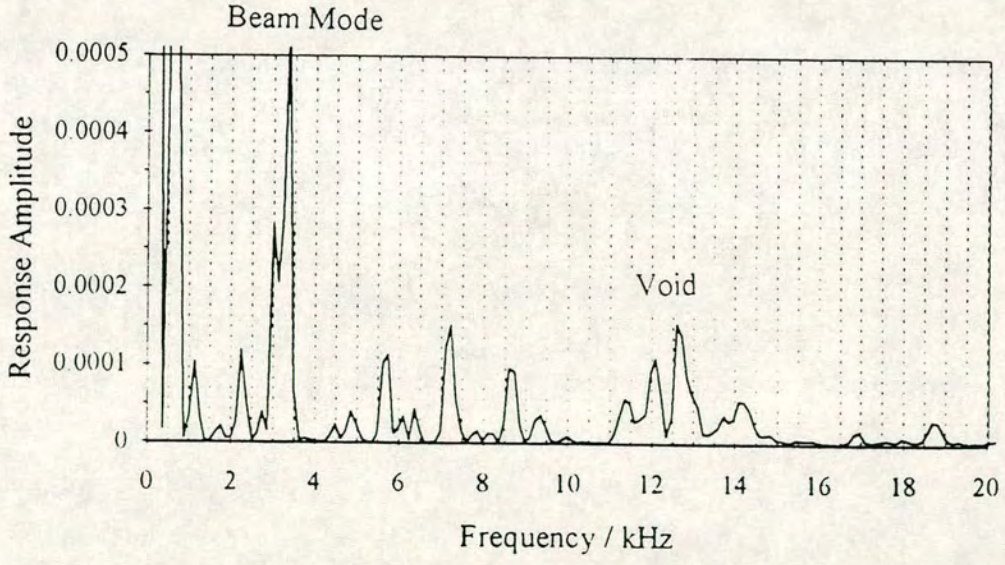

Fig6.5b 4.7mm hammer on voided section

Figure 6.5 Ungrouted frequency spectra (test beam 2)

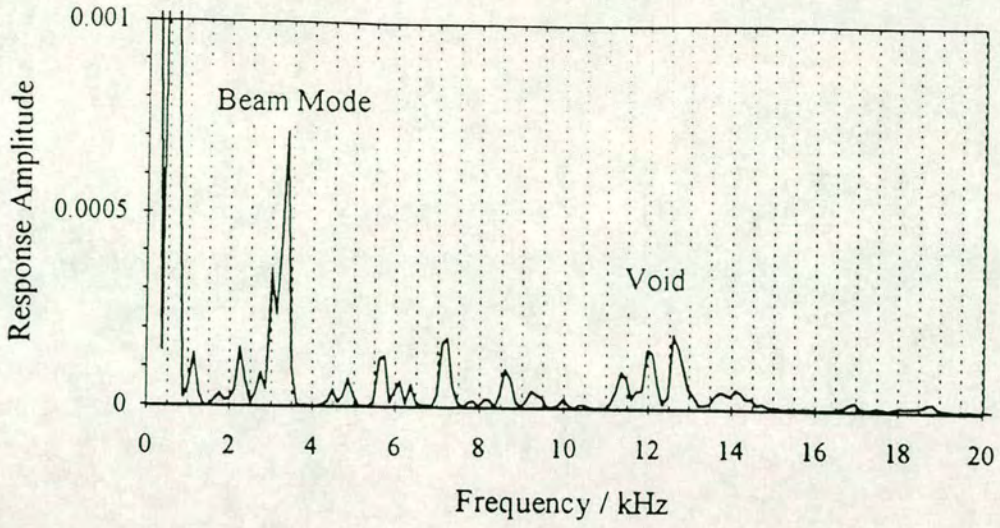

Fig 6.5c 6mm hammer on voided section

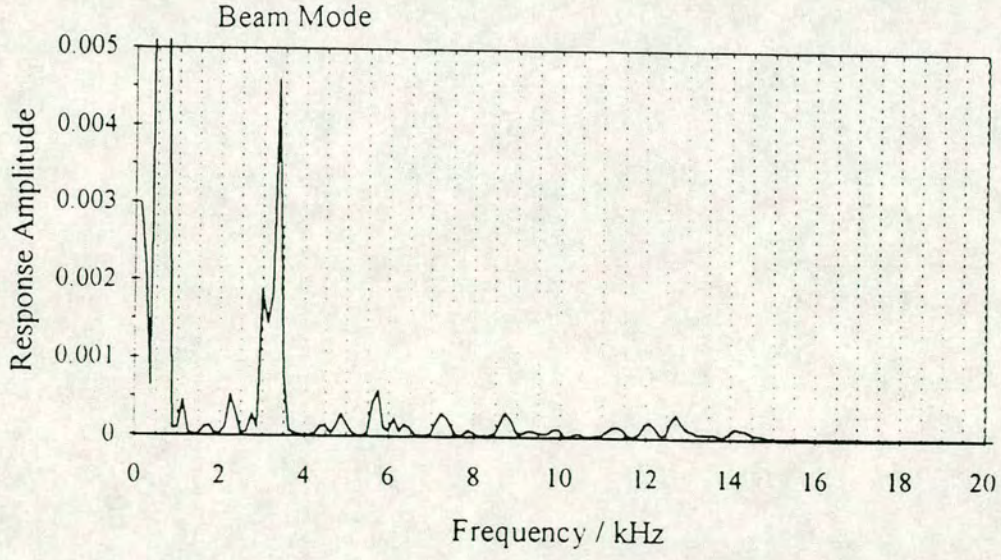

Fig 6.5d 9.55mm hammer on voided section

Figure 6.5 (cont.) Ungrouted frequency spectra (test beam 2)

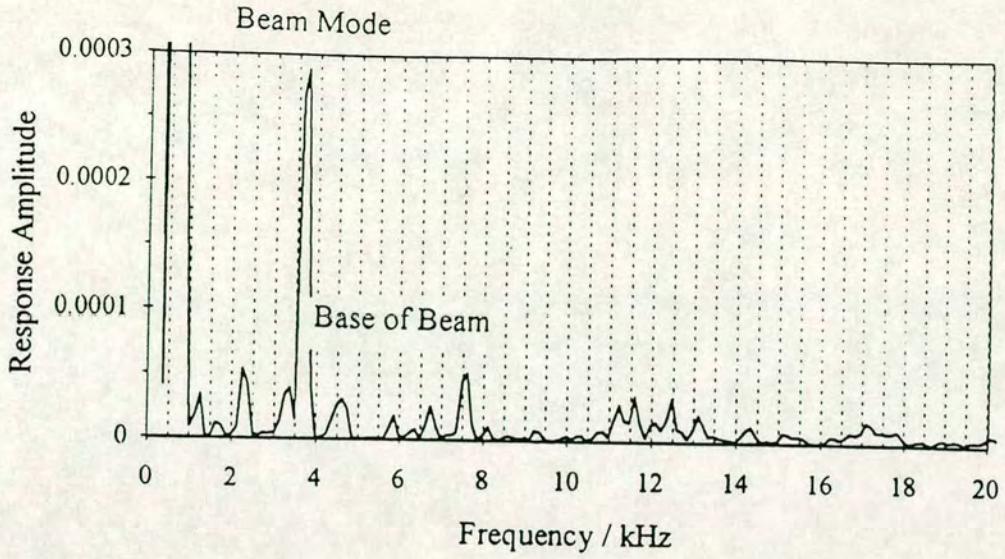

Fig 6.6a 2mm hammer on grouted section

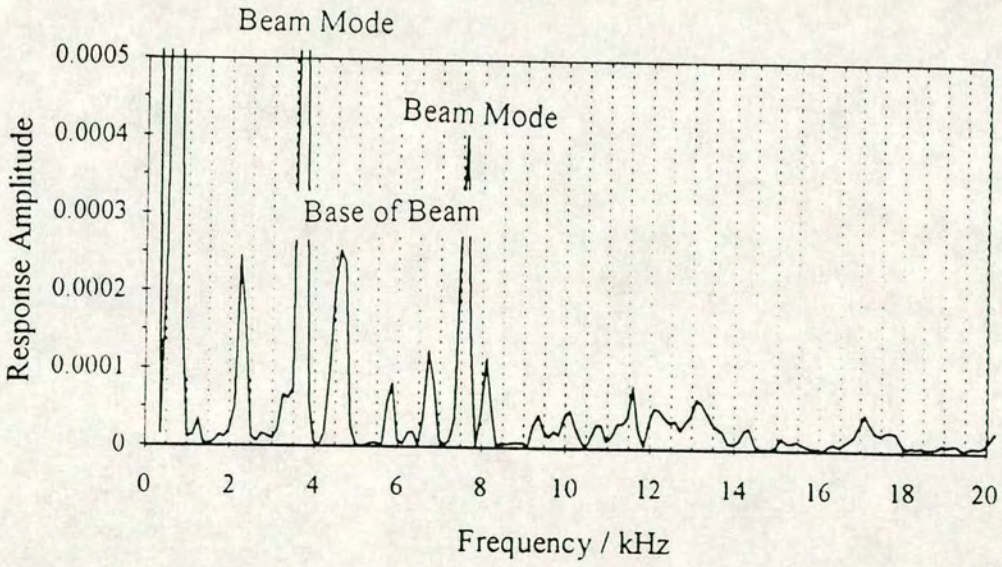

Fig 6.6b 4.7mm hammer on grouted section

Figure 6.6 Grouted frequency spectra (test beam 2)

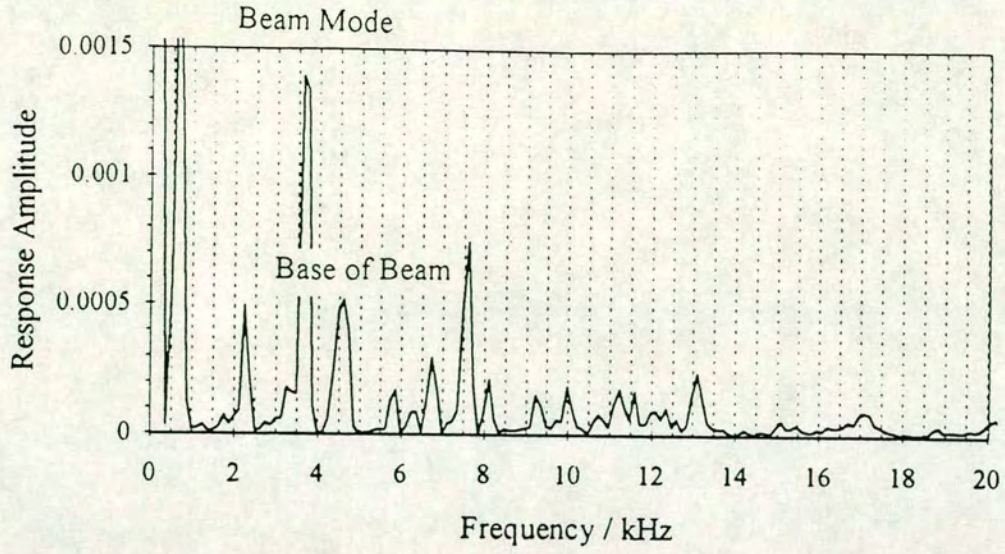

Fig 6.6c 6mm hammer on grouted section

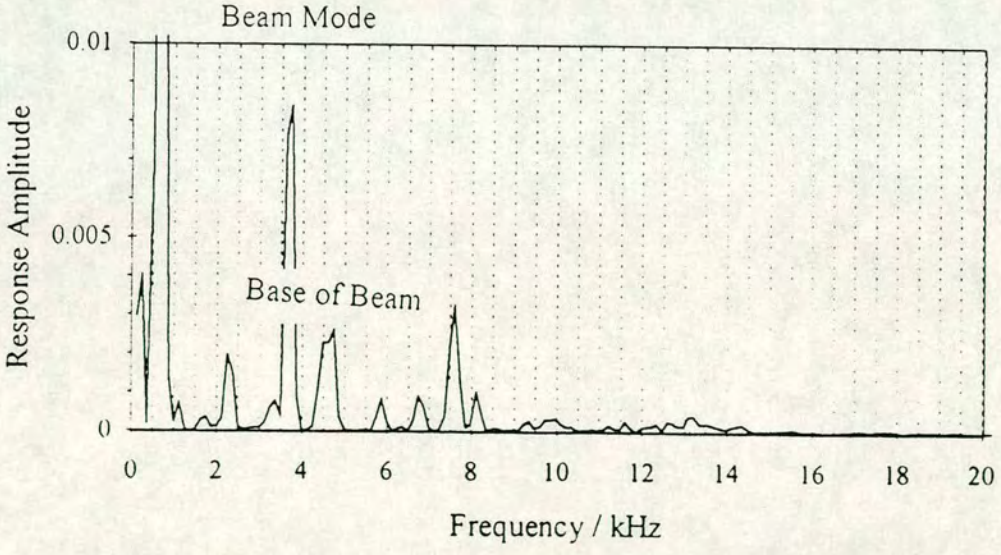

Fig 6.6d 9mm hammer on grouted section

Figure 6.6 (cont.) Grouted frequency spectra (test beam 2)

further reflection at 4.6 kHz can also been seen on each spectrum. This is likely to correspond to a reflection from the base of the beam. The peak at 4.6 kHz on Figure 6.6a is of a relatively low amplitude. The 2mm hammer inputs much less energy into the beam and, with attenuation, the signal reflected from the base is of a very low amplitude and is difficult to detect. A base reflecion at 4.6 kHz corresponds to a compression wave velocity of 3700m/s. This value is relatively low for concrete but the beam will not have developed full strength at the time of testing and was not vibrated at casting. This will result in a low velocity compression wave developing.

Other smaller peaks can seen on each trace. These will be due to the modes of the beam and from the testing system. Each response measured at the grouted section has a frequency component at 7.6 kHz. This component does not correspond very well with the results expected from the work carried out at Cornell (Sansalone and Poston, 1992). This beam was very short (750mm) and it is likely the natural modes of the beam that are excited would be those occuring at higher frequencies than those for a longer beam.

The large low frequency peak corresponds to the fundamental mode of the whole beam - the whole body mode. The beam is 750mm in length and is supported at either end. This mode would be at a much lower frequency on a real beam as the length of the beam would be much longer than 750mm.

The results from the voided section of the beam are shown in figure 6.5. Again a distinct reflection can be seen on each trace at 3.25 kHz. This is at a lower frequency than the corresponding reflections on the spectra from the grouted duct, at 3.625 kHz. This is as expected since the voided beam is less stiff and the frequency modes occur at lower values than the corresponding modes on a solid concrete beam section. No frequency component corresponding to a reflection from the base is apparent on any trace in figure 6.5. The beam is quite narrow, 300mm wide, and it is not be possible for a wave to refract around the void, be reflected from the base and again refract around the void to be measured at the top surface. Base reflections were measured on the finite element spectra but the model in these cases was 1000mm wide and no wave attenuation was modelled. It was therefore possible for sufficient energy to be reflected and refracted to the measurement point.

An obvious reflection from the voided duct is apparent on the traces resulting from impact with the 2mm, 4.7mm and 6.0mm diameter ball bearing hammers at approximately 12.5 kHz. The traces do not show a distinct frequency component as the duct does not offer a plane profile to the wave. The resulting peak on the spectrum is shown over a range of frequencies. The spectrum corresponding to an impact with the 9.55mm diameter ball bearing hammer contains frequency components similar to those shown in the other traces from the voided section. However, the amplitude of the components corresponding to reflections from the voided duct are very low and are difficult to distinguish on the spectrum.

The contact time of this hammer is just over 70μs giving a minimum input wavelength, λ, of 390mm assuming a wave velocity of 3700m/s with a critical input frequency of 1/(1.5*Contact time). The finite element analysis concluded that defects with a profile of λ/4 could be detected. However, the finite element analysis also showed that the depth to a defect was also critical and at a depth of 150mm it was unlikely to be possible to detect a cylindrical defect 100mm in diameter. These experimental results show that it is possible to detect defects at a depth of 150mm but that a target of λ/4 is difficult to distinguish on the response spectrum. As mentioned previously the results from the finite element analysis are thought to be non-conservative, the extent of which was unknown. However, this result shows that the conclusions drawn from the finite element analysis give results which are very close to those found experimentally. These results are summarised in table 6.3.

Hammer Diameter /mm	**T_c /μs**	**f_c /kHz**	**λ /mm**	**λ/2 /mm**	**λ/4 /mm**	**Detection**
9.55	70	9.5	390	195	97	?
6.0	55	12.1	306	153	76	✓
4.7	39	17.1	216	108	54	✓
2.0	31	21.5	172	86	43	✓

Table 6.3 Effect of contact time on the detection of a 100mm diameter void at a depth of 150mm

Other peaks are shown in all four traces from the voided section. The peak at 7 kHz is dominant and corresponds to the same mode shape as the peak at 7.6 kHz found on the response spectra measured at the grouted section. The frequency is reduced as the voided section is less stiff.

6.3.2.3 Conclusions NIST Transducer

The above results show that impact-echo testing can be used to detect ungrouted ducts in metal ducted post-tensioned concrete bridge beams. The model tested was very simple and similar situations are unlikely to occur in practice. However, this test was important in that it showed the method to be reliable and also acted to validate the results found from the finite element analysis.

6.3.2.4 Evaluation of OLSON Transducer

Tests were carried out using the OLSON transducer on the simple beam to allow comparison with the results gained from the NIST transducer. The OLSON transducer is much quicker and simpler to use. Many tests can be carried out in a few minutes as minimum surface preparation and accelerometer preparation is required. These same tests would take considerably longer with the NIST transducer.

The contact time is estimated in the same way as discussed previously. Figure 6.7 shows two examples of the response of the OLSON transducer to impact, displayed in the time domain. The contact times as estimated using the OLSON and the NIST transducers are shown in table 6.4. It can be seen that each estimate agrees exactly but it should be noted that the resolution of the measuring equipment was 7μs.

Hammer Diameter /mm	NIST T_c Estimate /μs	OLSON T_c Estimate /μs	Theoretical T_c /μs
9.55	70	70	50
4.7	39	39	25

Table 6.4 Comparison of estimated contact times using NIST and OLSON transducers

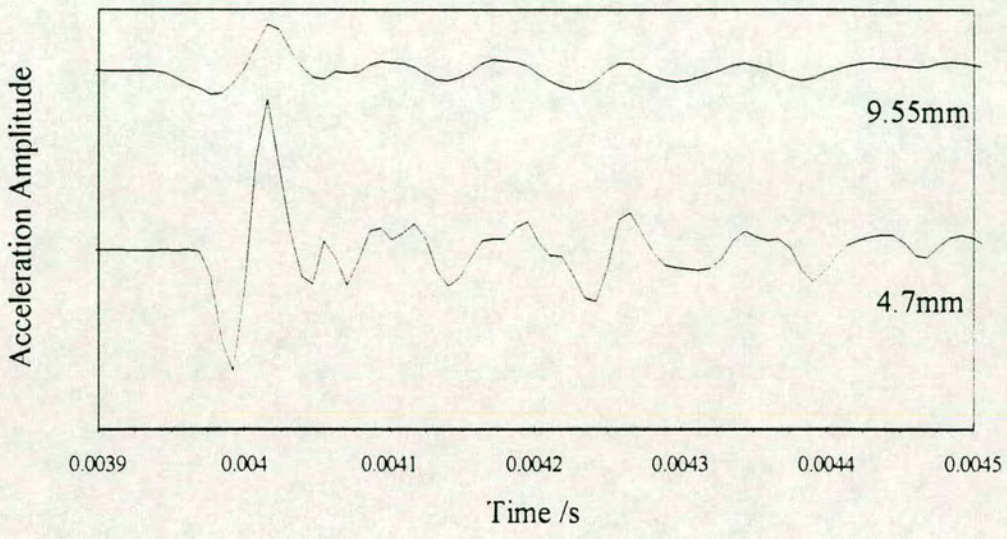

Figure 6.7 Time Domain response using OLSON Accelerometer

The frequency spectra obtained from grouted and ungrouted sections of the beam are shown in figure 6.8. Figure 6.8a and 6.8b show spectra from the voided position using a 4.7mm and a 9.55mm diameter ball bearing hammer respectively. Both traces are similar and the reflection from the voided tendon duct is apparent on each. No low frequency components are apparent on either trace which would suggest that either the amplitude band width of the OLSON accelerometer is lower than that of the NIST transducer or that the performance of the OLSON transducer is poorer at lower frequencies. However, the void is detected using both impact hammers even though the contact time is at the upper limit of contact time required to detect the void. Figures 6.8c and 6.8d show the results from a grouted section of the beam. Again, similarities with the traces recorded using the NIST transducer can be identified. Mode reflections occur at 3.65 kHz and 7.6 kHz on both traces as measured using the NIST transducer. A reflection from the base can also be identified of each spectra. However, these traces are more difficult to interpret than those from the NIST transducer.

The OLSON transducer measures acceleration, $\ddot{x}$ and the NIST transducer measures displacement, x. Performing a Fast Fourier Transform on the measured data gives the response in the frequency domain as a series of sinusoidal signals with different frequencies, amplitudes and initial phases. Acceleration and displacement can be expressed as shown below;

If $x = X\sin\omega t$

then $\ddot{x} = -\omega^2 X\sin\omega t$ (6.1)

Therefore, for a given amplitude of vibration, X, the measured acceleration at high frequency is much higher than the measured displacement for a similar amplitude. At lower response frequencies, the accelerometer will measure a much smaller response than the displacement transducer.

Higher frequency peaks occur which were absent on the traces from the NIST transducer. These peaks are more dominant on the response gained from impact with the smaller hammer. This is as expected as this hammer produces an impact of shorter contact time and therefore higher cut-off frequency. An

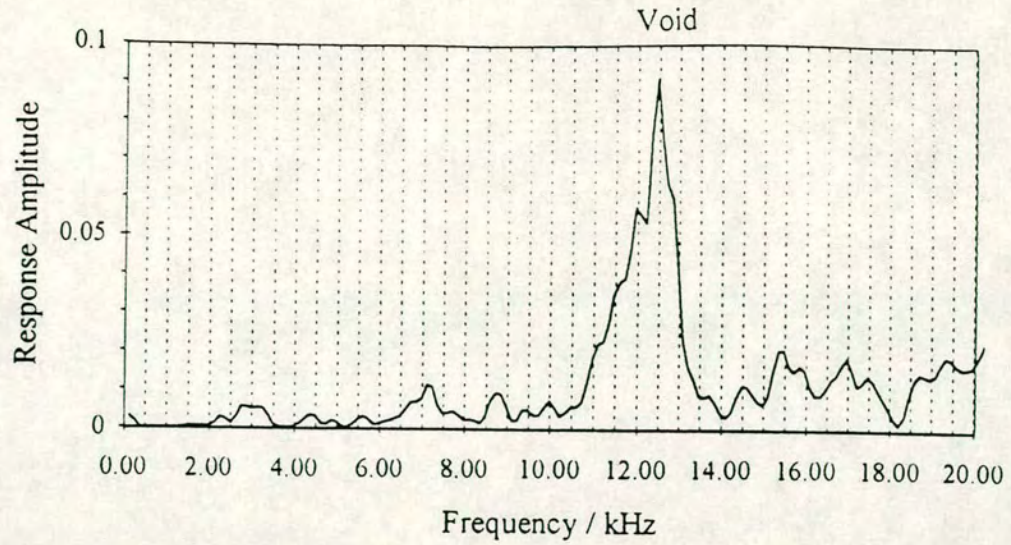

Fig 6.8a 4.7mm hammer on voided section

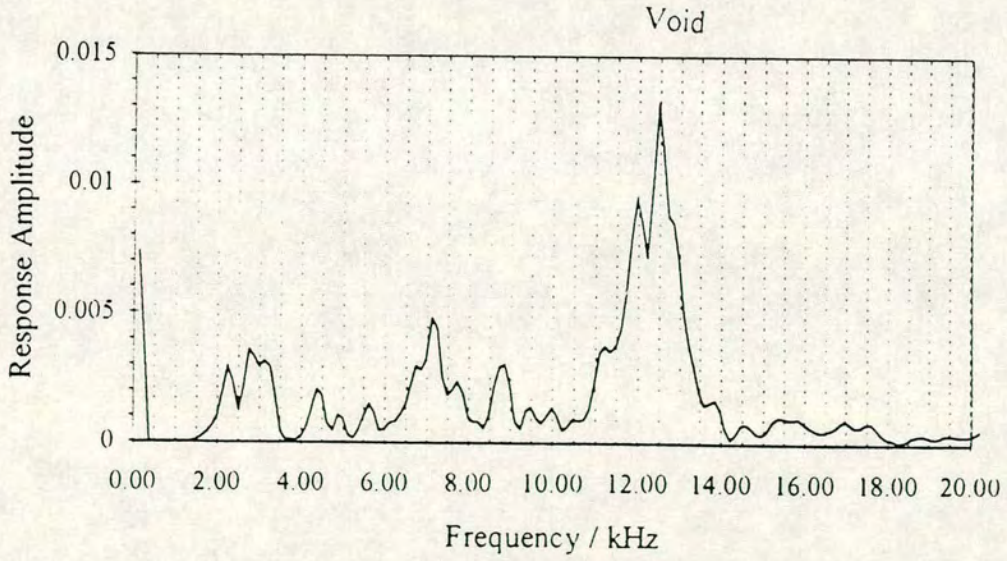

Fig 6.8b 9.55mm hammer on voided section

Figure 6.8 Frequency spectra using OLSON Accelerometer

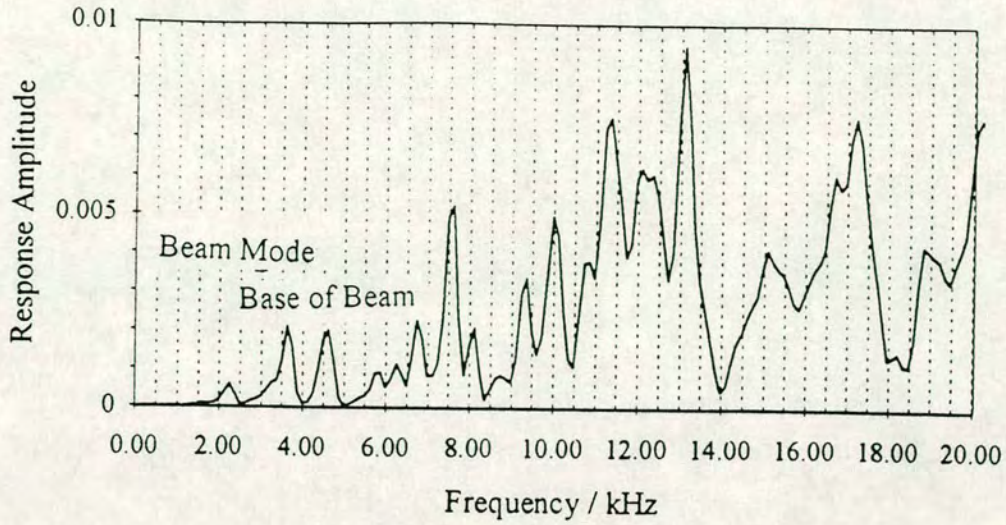

Fig 6.8c 4.7mm hammer on grouted section

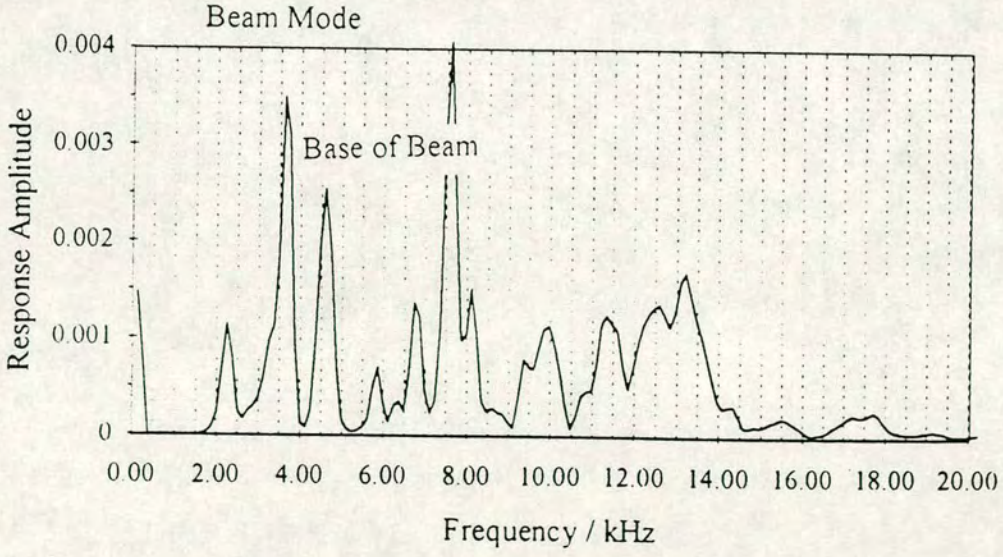

Fig 6.8d 9.55mm hammer on grouted section

Figure 6.8 (cont.) Frequency spectra using OLSON Accelerometer

indistinct peak can be seen at around 12 kHz on each trace. This may be due to a reflection from the grouted duct. The elastic properties of grout are slightly different to those of concrete. However, other peaks occur at high frequencies and it is likely that all these peaks occur due to vibrational modes of the beam and test instrumentation set-up. These peaks are not obvious on the spectra obtained with the NIST transducer but some can be identified by changing the scale of the y-axis. A peak at around 12 kHz can be identified on all the traces. The relative amplitude is very much smaller on the tests carried out at the ungrouted section. This would suggest that the position of the duct could be identified using impact-echo methods provided a close test grid was used. The other reflections which are common to all the tests (with a high enough cut-off frequency) occur at approximately 17.5 kHz. This will be due to a beam vibrational mode. The fact that these higher frequency peaks are dominated by the lower frequency reflections on the results using the NIST transducer but are dominant on the results using the OLSON transducer would again suggest that the response of the OLSON accelerometer is poorer at lower frequency. This response was improved by coupling the accelerometer to the beam surface using petroleum jelly.

6.3.2.5 Conclusions on OLSON Transducer

1. The NIST transducer performs better than the OLSON accelerometer at lower frequencies as it measures displacement rather than acceleration. However, with better coupling, the OLSON accelerometer performs adequately at lower frequencies and is much more practical for use on site as the preparation required between tests is minimal.

2. The contact time of the impact, although not as clear as that measured by the NIST transducer, can be estimated from the acceleration trace measured by the OLSON accelerometer.

3. The OLSON accelerometer provides a quick method of measuring the response of a specimen to impact. The contact surface is much larger than that of the NIST transducer and so, although much easier to couple than the NIST transducer, care must still be taken to ensure adequate coupling. It was considered worthwhile to check the response obtained with each transducer at a few points on the surface of a new test

specimen to ensure similar responses were being measured by each transducer.

6.4 Laboratory Test Beam 1

Laboratory test beam 1, as described in Chapter 4, see figure 4.17, was used to carry out a more detailed investigation of the developed testing method.

6.4.1 Aims

This laboratory specimen was extensively tested during the development of the testing instrumentation and procedure. The beam was then retested using the same method as that used on Test Beam 2. Various test parameters were then investigated as follows:

1. Defect detection using the frequency of the base reflection

2. Effect of contact time

3. Effect of defect shape

4. Effect of depth to void

5. The use of the OLSON transducer was investigated and the results compared to those found using the NIST transducer. The OLSON transducer was found to be suitable for use on Test Beam 2 but coupling effects on a less smooth surface also needed to be investigated.

6. Frequencies of beam vibration

6.5 Frequency of base reflection

6.5.1 Test series 1

The laboratory specimen was tested across the middle section of the beam - see Figure 6.9 using the NIST transducer and a 6.0mm hammer. The analyser resolution was 0.125kHz. Figures 6.10a to 6.10g show the measured frequency spectra for each test point with the corresponding estimated contact time being given in Table 6.5. These contact times were estimated as discussed in section 6.3.2.1. The tested section included a 75mm diameter

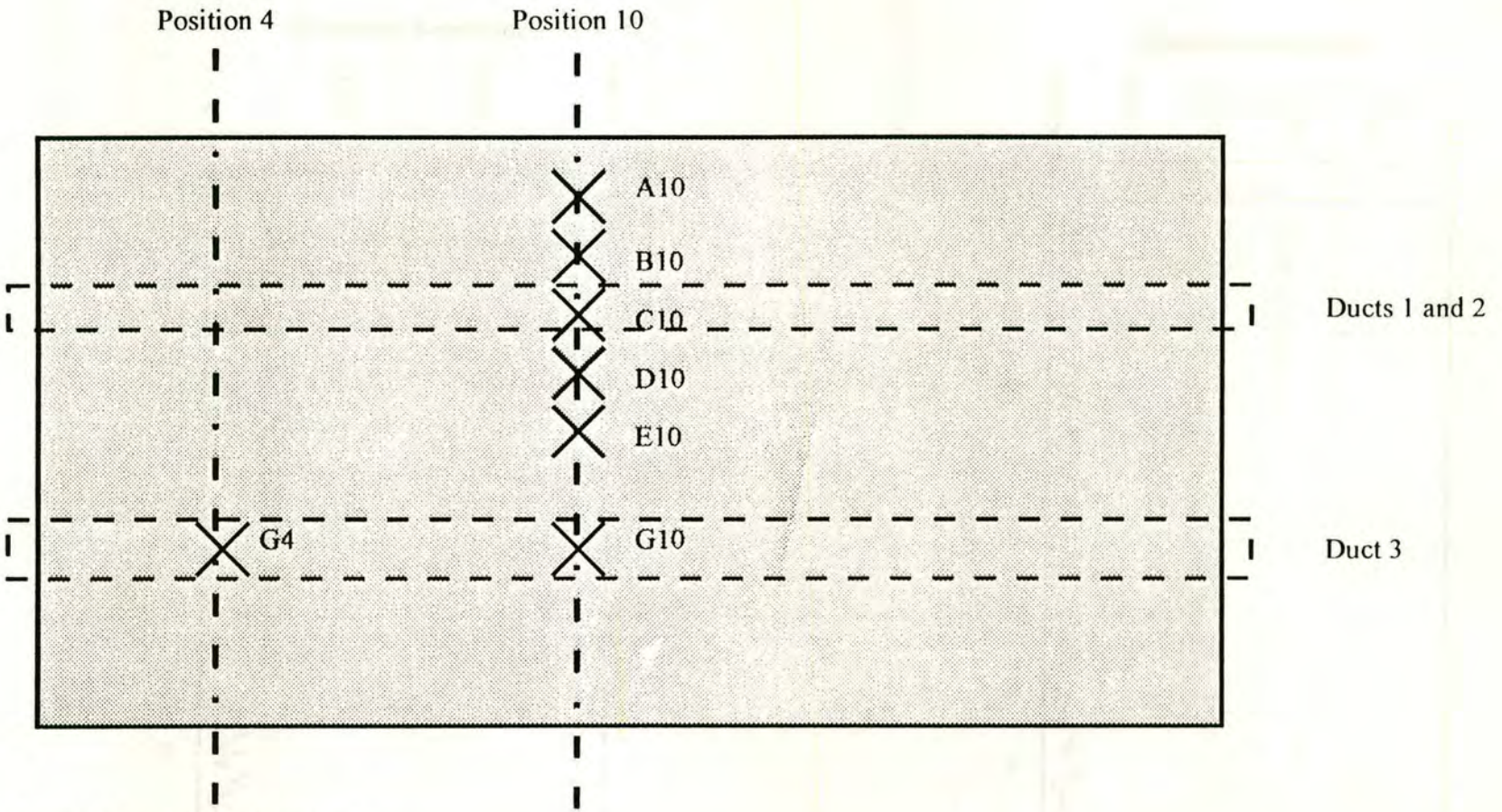

Figure 6.9 Test series 1 - impact positions

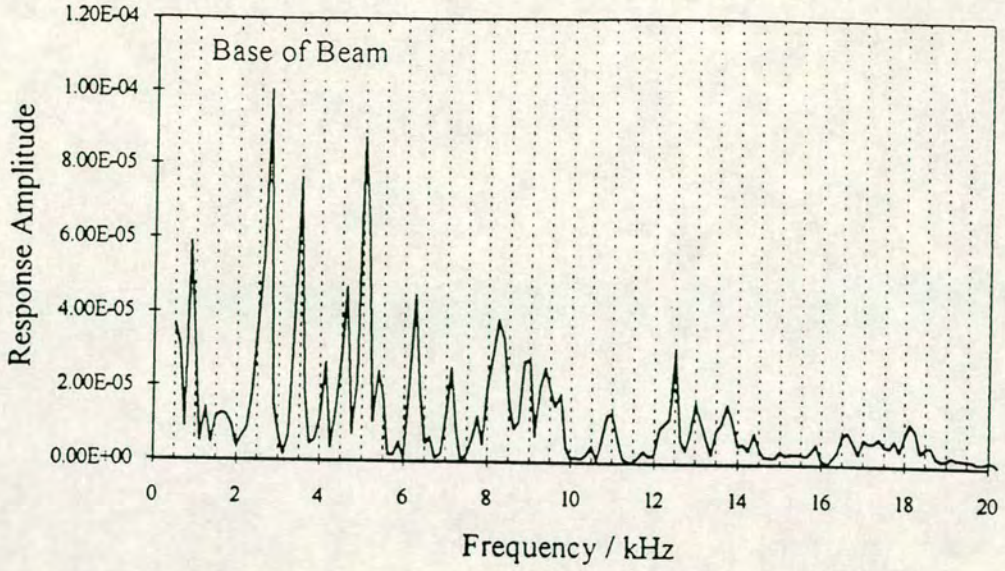

Fig 6.10c Position 10C

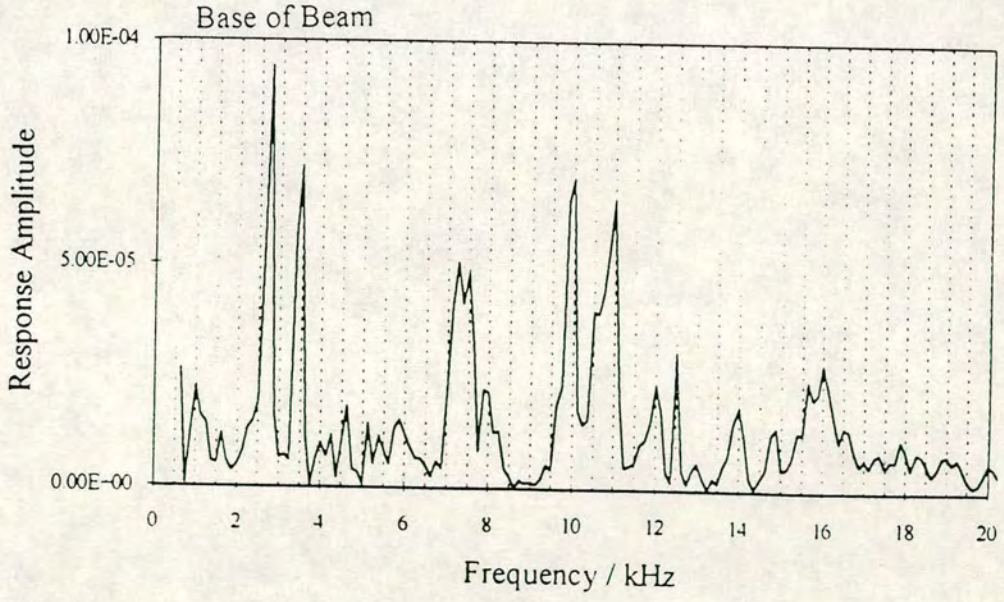

Fig 6.10d Position D10

Figure 6.10 (cont.) Base reflection investigation

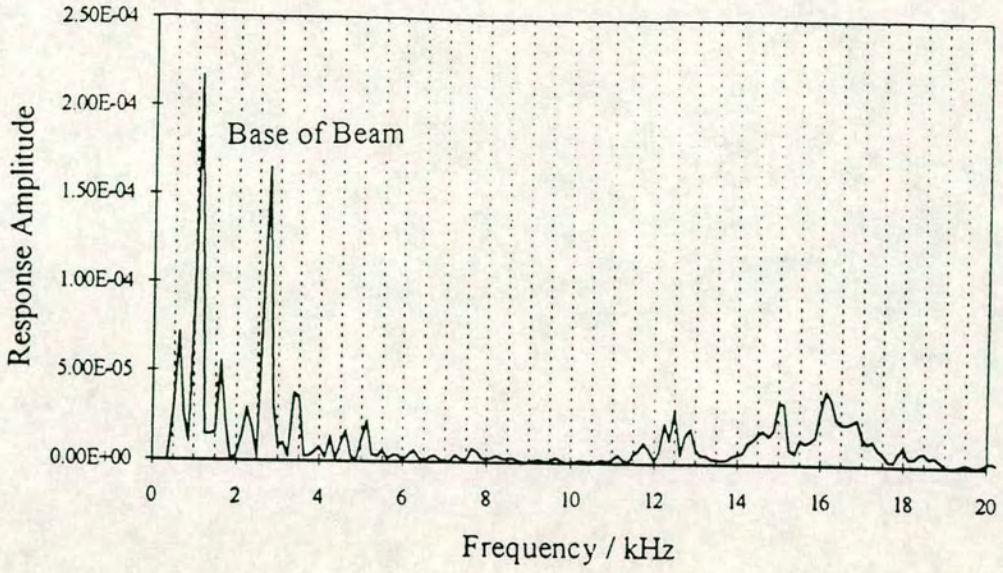

Fig 6.10e Position E10

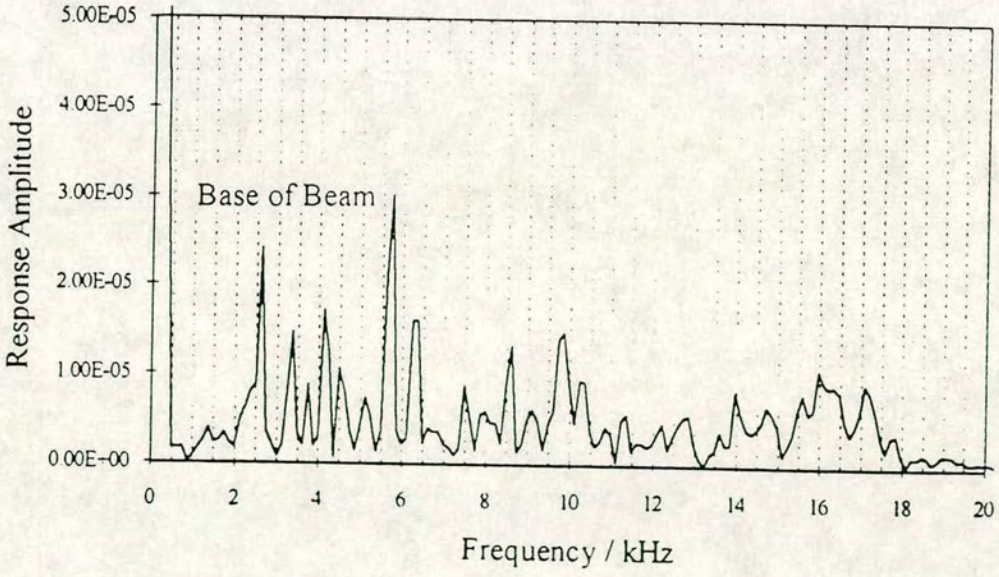

Fig 6.10f Position G10

Figure 6.10 (cont.) Base reflection investigation

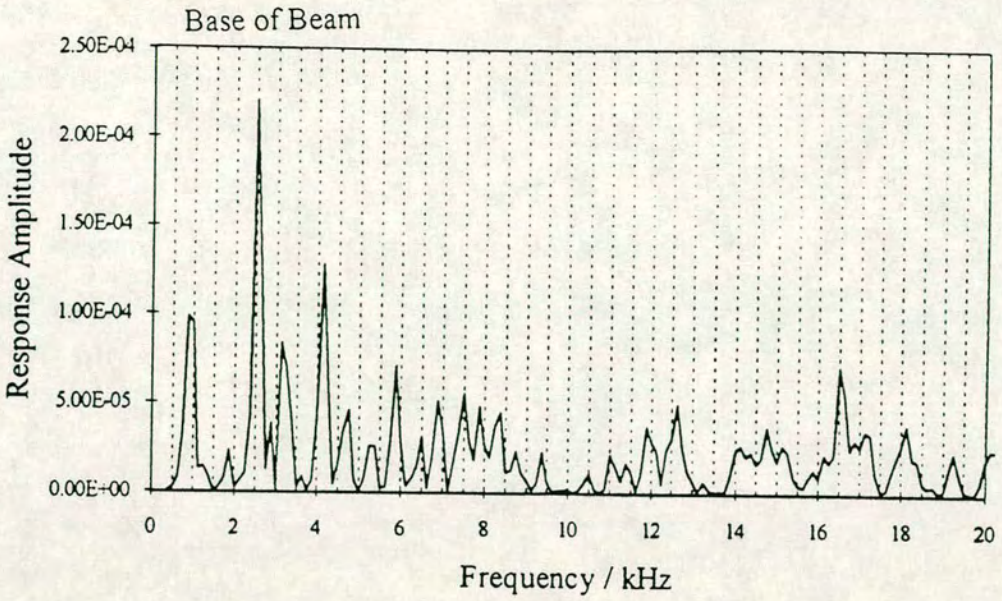

Fig 6.10g Position G4

Figure 6.10 (cont.) Base reflection investigation

void at a depth of 100mm and a fully grouted 100mm diameter duct at a depth of 150mm. A further test was undertaken at position G4. Duct 3 contains a void in the lower half of the duct, again at a depth of 150mm at this position. A summary of the measured frequency of the base reflection at each point is also given in Table 6.5. The values estimated are much lower than those found using the same hammers on test beam 2. The surface of test beam 1 was much rougher and extensive preliminary testing had led to some deterioration of the surface. This explains the increase in contact time as the extent of local concrete crushing would be much greater on this beam.

Test Position	Contact Time/ μs	Base Reflection / kHz
A10	70	2.625
B10	78	2.625
C10	78	2.625
D10	70	2.625
E10	70	2.625
G10	55	2.625
G4	86	2.375

Table 6.5 Time of contact and base reflection frequency of impact-echo test across the middle of test beam 1

Other peaks can be seen on the frequency spectra, the implications of which will be discussed in later sections.

Table 6.5 shows a standard beam reflection at 2.625 kHz. This corresponds to a compression wave velocity of 3675 m/s. This value is quite low for concrete but was expected as the specimen was made in the laboratory and adequate vibration was unlikely. The slump measured at pouring was also quite high (135mm) resulting in a weaker and thus less dense concrete than expected with a correspondingly lower compression wave velocity.

No reduction in base reflection can be seen on Figure 6.10c corresponding to an increase in travel time due to the wave propagating round the void in the 75mm diameter duct. This method of defect detection is not sufficiently

accurate to resolve defects of this size. The reasons for this include the resolution of the analyser which is 0.125kHz on this frequency range. A frequency range of 50kHz was chosen as it gave the best compromise of frequency resolution and time scale resolution. Variations in the concrete strength and condition can result in slight changes in the measured frequency of the base reflection. If the target is small any slight effect on the frequency reflection may be masked by slight irregularities in the concrete. Figure 6.10g shows a reduced frequency of base reflection. The partially grouted 100mm diameter duct results in an increased travel time that is detectable by the measurement system. The test carried out at a fully grouted section of the 100mm diameter duct (figure 6.10f) resulted in a base reflection at 2.625kHz. The compression wave travels through the thin steel liner without any significant change of velocity. This result is in agreement with that found using finite element analysis and previous conclusions by Sansalone et al - see Chapters 4 and 5.

The above tests showed that it was possible to detect sizeable defects in steel lined ducts in concrete using impact-echo techniques and measuring the base reflection only. A further series of tests were carried out along the line of duct 3 (see figure 6.11) to ensure the reliability of this test and to determine whether the size of a defect could be estimated using this technique.

6.5.2 Test series 2

Duct three contains partial voiding at each end of the duct, in the top half of the duct at the front end (positions 1 to 6) and in the lower half of the duct at the back end of the model (positions 14 to 20). The voids were formed by polystyrene blocks, shaped by halving polystyrene sections which were bored out using the steel ducting. The polystyrene was quite difficult to half accurately and it is likely that the voids in each section of the duct are of a slightly different size. Figure 6.12 shows the measured frequency response at points along the line of duct 3 at the surface of the model. The frequency of each base reflection was measured and the contact time estimated as in previous tests. As in Test series 1 the resolution on the analyser was 0.125kHz on a 50kHz frequency range and 7.5μs on a 8ms time scale. A summary of the results are shown in Table 6.6 below.

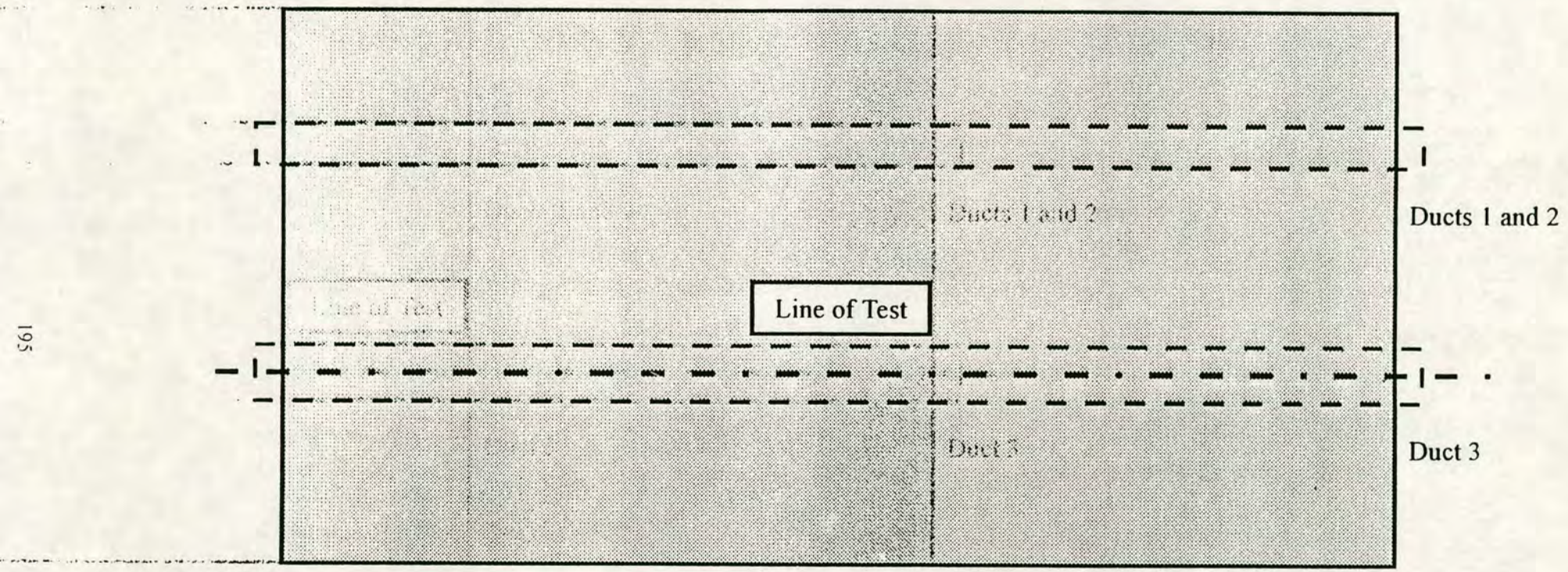

Plan of laboratory test beam 1

Figure 6.11 Test series 2 - impact positions

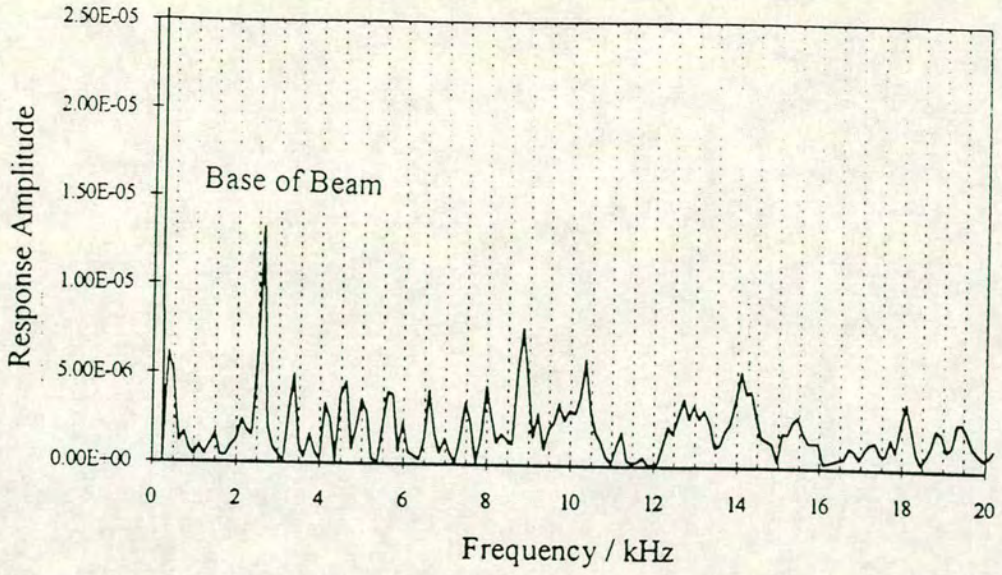

Fig 6.12a Fully grouted section

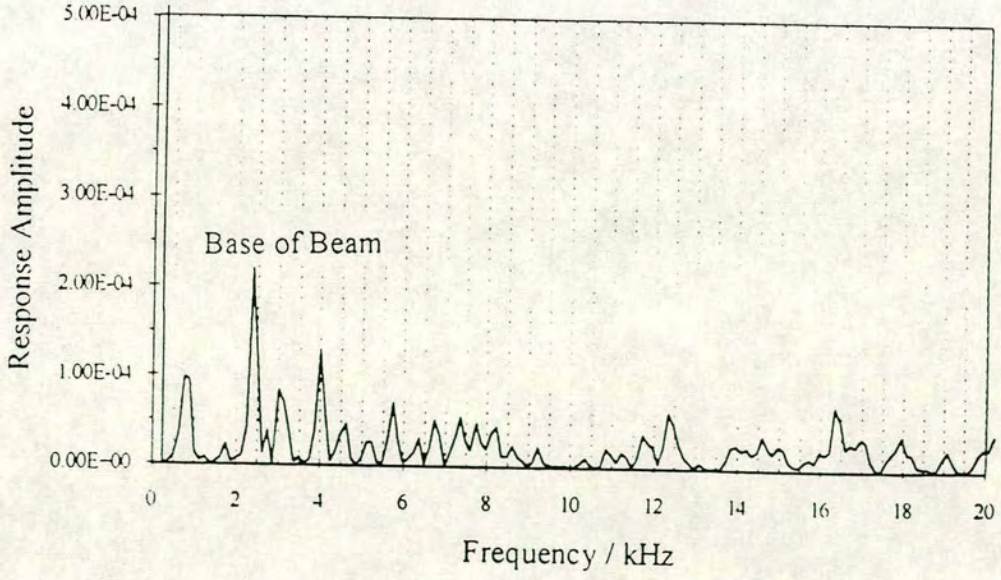

Fig6.12b Void in top section of duct

Figure 6.12 Base reflection spectra for 100mm diameter duct

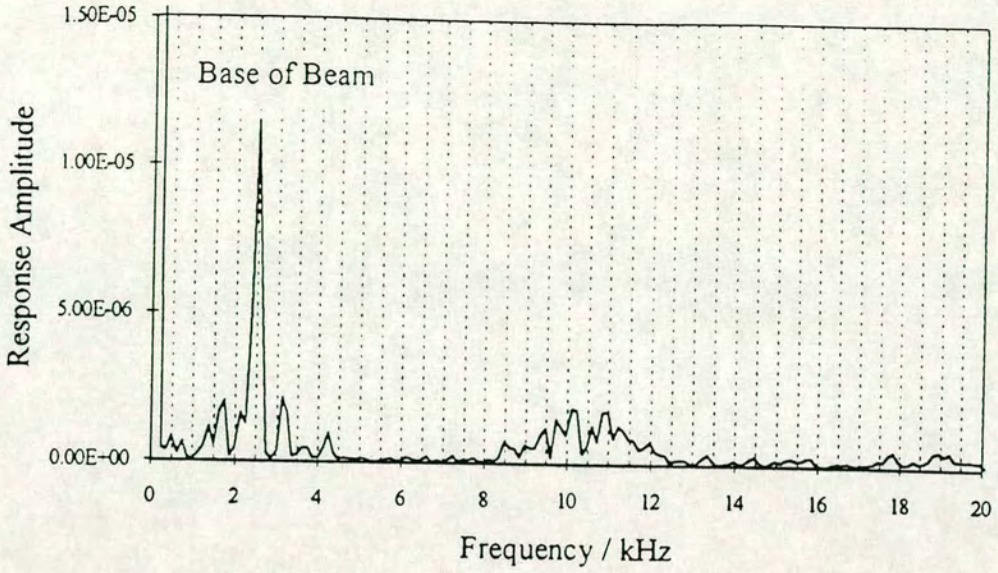

Fig 6.12c Void in lower half of duct

Figure 6.12 (cont.) Base reflection spectra for 100mm diameter duct

Position	Contact time / μs	Frequency of Base Reflection / kHz
G2	55	2.375
G3	62	2.375
G4	70	2.375
G5	62	2.375
G6	62	2.5
G7	55	2.5
G8	47	2.625
G10	55	2.625
G11	47	2.625
G12	70	2.625
G13	62	2.5
G14	62	2.625
G15	47	2.5
G16	70	2.5
G17	63	2.5
G18	63	2.5

Table 6.6 Estimated time of contact and measured base reflection frequency for impact-echo test along the line of duct 3

The above table clearly shows that sizeable voiding can be successfully detected using this method. Voiding is present in the top section of duct three at positions G1 to G6 and in the bottom section at positions G14 to G20. The duct is fully grouted along the middle section. The frequencies of base reflection show this pattern with the base reflection at positions G2 to G5 being measured at 2.375kHz, the central section measured at 2.625 kHz and positions G15 to G18 at 2.5kHz. A slight difference in the void size would account for the difference in frequency of base reflection, however, other slight irregularities in the concrete section could also give rise to this effect.

Other reflections at higher frequencies can be seen on Figure 6.12. These reflections will be discussed further in a later section. No dominant mode shapes are apparent on the spectra obtained on this test specimen. This specimen is much larger than test beam 2 and insufficient energy is input to excite the beam modes to give dominant responses.

6.5.3 Conclusion on Frequency of Base Reflection

Measurement of the base reflection can successfully detect voiding in a duct providing the voiding is sizeable in comparison with the expected travel time of the base reflection. The resolution of the testing system is also very important in determining the success of a test as voiding will decrease the frequency of the base reflection but this may not be detected if the resolution of the measurement system is inadequate.

6.6 Effect of Contact Time and Input Frequency

Chapter V included an investigation into the effect of the contact time of the impactor with the model using finite element analysis. The results of this investigation indicated that it would be possible to detect voiding in a 100mm diameter duct providing the minimum input wavelength, λ, was less than 400mm. The detection of a 75mm diameter void would require a correspondingly shorter minimum wavelength. The finite element analyses also showed that defect identification of a smaller diameter void was more difficult as scattering effects further reduced the reflected energy measured at the surface. These effects were investigated experimentally on laboratory test beam 1.

6.6.1 Test 1 - 100mm diameter void at 150mm depth

A voided section of duct three was tested using a series of different hammers as impactors. The hammers used were the B&K (280g), PCB mini-hammer (1.25g), 6.0mm diameter ball-bearing hammer and a 4.7mm diameter ball-bearing hammer. The contact times of each are shown in Table 6.7 below. It should be noted that the contact times of the ball-bearing hammers are lower than the corresponding contact times for ball-bearing hammer impact on test beam 2. The surface of test beam 2 was purposefully levelled at pouring to ensure as smooth a finish as possible. This was not the case with test beam 1 as the finish on this model was intended to simulate a deteriorated concrete surface such as could be found on a twenty year old bridge beam. Also, extensive preliminary testing had caused some further deterioration of the surface.

Impact Hammer Type	Contact time /μs	Assumed critical frequency (=1/1.5T_c) /kHz	Assumed minimum λ (v=3675m/s) /mm	Proposed critical frequency (=1/T_c) /kHz	Proposed minimum λ (v=3675m/s) /mm
B&K	352	1.9	1934	2.8	1312
PCB	98	6.8	540	10.2	360
6.0mm dia. ball-bearing	70	9.5	387	14.3	257
4.7mm dia. ball-bearing	47	14.2	259	21.3	173

Table 6.7 Contact time on surface of Test Beam 1

Figure 6.13 shows the frequency spectra resulting from each test. A reflection from the voided duct would occur at a frequency of 12.25kHz, assuming a compression wave velocity of 3675m/s. This velocity was calculated using the maximum base reflection of 2.65 kHz. Laboratory testing of a simple concrete beam (test beam 2) showed a minimum input frequency resulting in a wavelength approximately 4 times the diameter of the void was not quite able to convincingly detect the void. Higher frequency inputs, resulting in shorter minimum wavelengths, could detect a void in a 100mm diameter duct at a depth of 150mm in a simple beam. The input frequency required to detect voiding in the ducts in test beam 1 was investigated and then compared to the fidings from the simple beam.

As discussed in section 6.5 a 100mm diameter void results in a reduction in base reflection - this can be seen on all the traces as expected. Figure 6.13a shows the frequency trace resulting from an impact-echo test using the B&K hammer. This hammer inputs a large energy pulse at low frequency resulting in a very clear response as any system noise or other random frequency source occurs at a much lower energy magnitude than reflections from the beam. However, the frequency input is much too low to detect defects in this concrete specimen.

It has previously been assumed that the usable maximum frequency of impact was equal to 1/(1.5*contact time). A contact time of 352μs would therefore

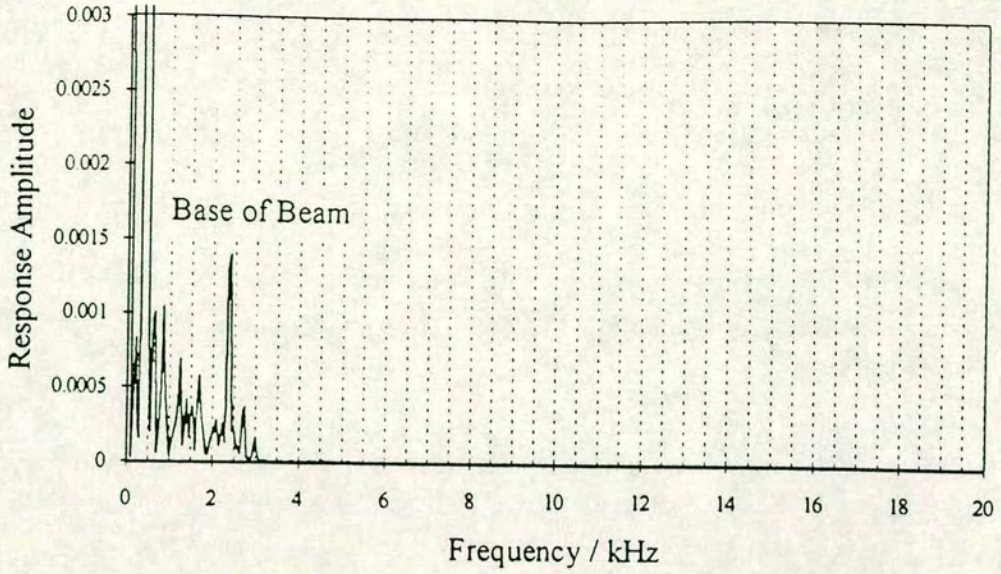

Fig 6.13a Response spectra from B&K hammer

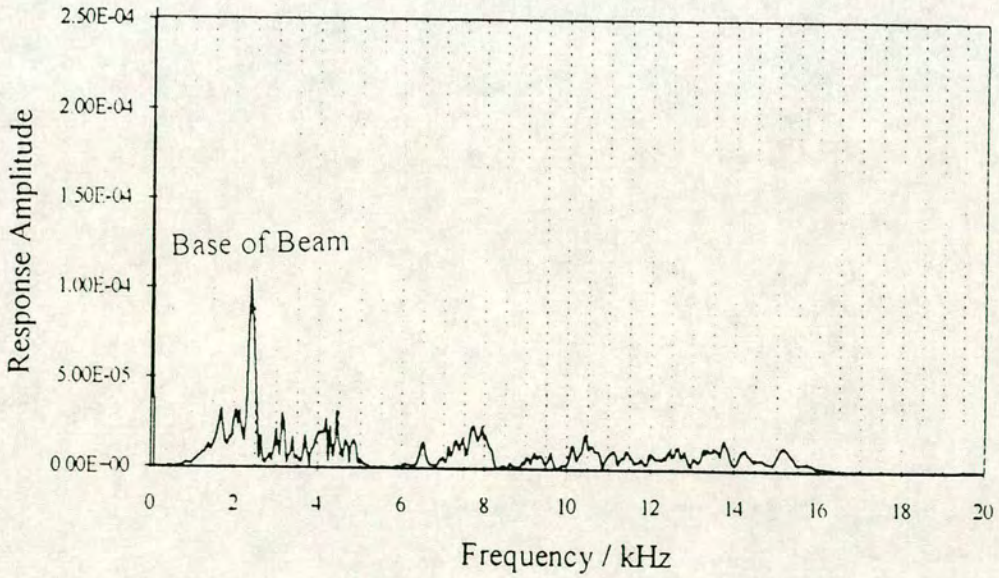

Fig 6.13b Response spectrum from PCB mini-hammer

Figure 6.13 Contact time frequency spectra for 100mm diameter void

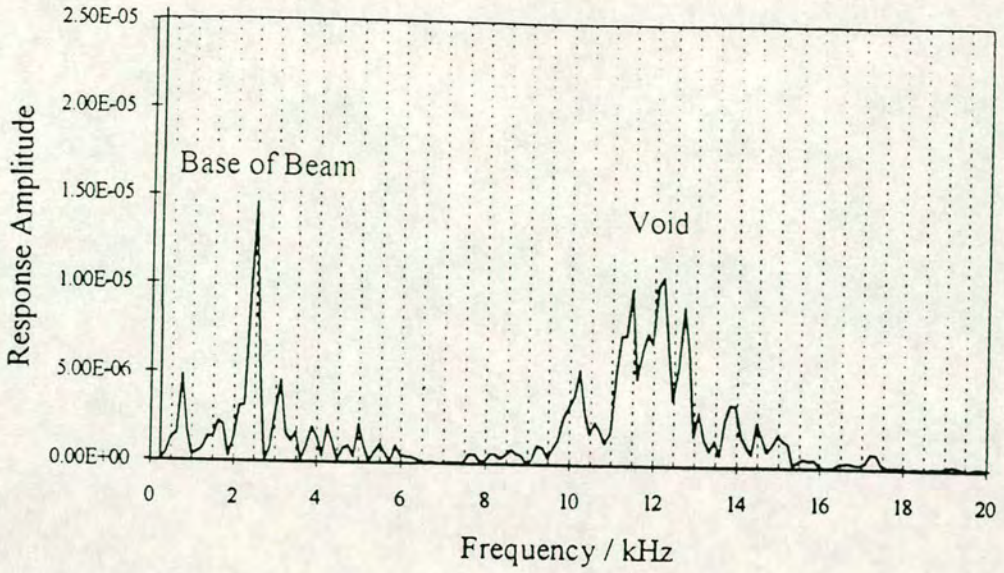

Fig 6.13c Response spectrum from 6.0 mm hammer

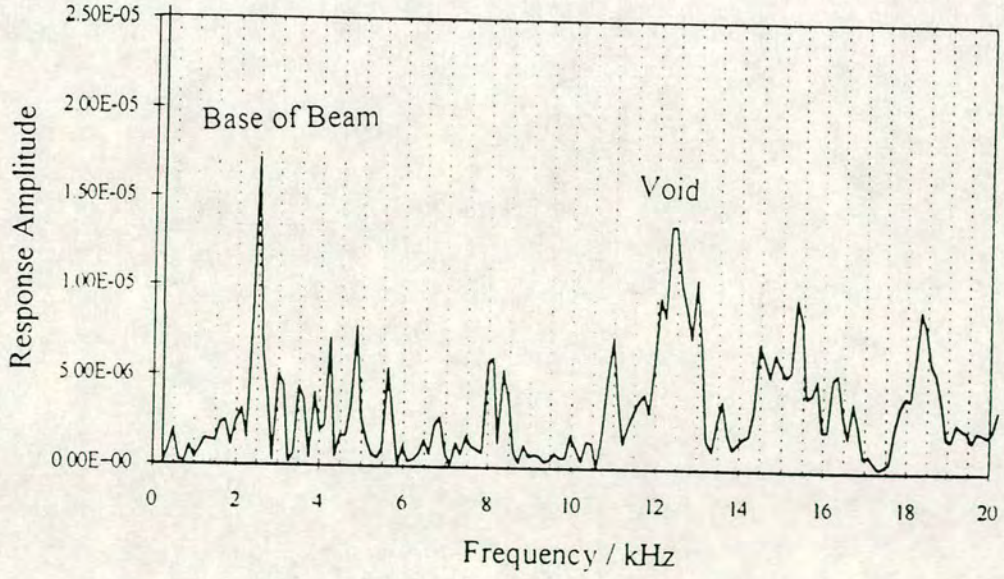

Fig 6.13d Response spectrum from 4.7mm hammer

Figure 6.13 (cont.) Contact time frequency spectra for 100mm diameter void

result in a frequency trace containing components up to a frequency of 1.9kHz and, in this case it would not be possible to detect the base of the beam as it occurs at a frequency of 2.625kHz. However, if it is assumed that a usable frequency equal to 1/contact time is input, a contact time of 352μs would result in a usable frequency up to 2.8kHz and the base reflection should therefore be identified. This can be clearly seen on the trace and indicates that the assumed critical input frequency is under-estimated. Table 6.7 shows the assumed frequencies and associated wavelengths and the difference in minimum wavelength if the proposed usable frequency is used. This will affect the conclusions reached previously relating percentage of input wavelength required to identify defects.

The frequency trace resulting from impact using the PCB mini-hammer again shows a clear peak corresponding to the base reflection. In this case the cut-off frequency of 98μs corresponds to a usable frequency range of 10.2kHz and therefore a minimum input wavelength of 360mm. This is again too long to detect a 100mm diameter defect at a depth of 150mm. A response at frequencies greater than 10.2kHz can be seen on the figure 6.13b. This hammer inputs a higher frequency pulse at a much lower energy level. The base peak can still be clearly seen but other reflections at higher frequencies are detected due to system noise and internal inhomogeneities of the beam.

The two ball-bearing hammers result in much shorter contact times, 70μs and 47μs respectively. Base reflections are still easily seen (see figure 6.13c and d) but the relative magnitude of higher frequency peaks gets progressively larger as the contact time or impact energy reduce. A contact time of 70μs should result in frequencies up to approximately 14kHz being detected. Figure 6.13c shows a series of frequency peaks at 12kHz which relate to the expected frequency peak from the void. This result gives the clearest indication than there is a void in the duct at a depth of 150mm. Figure 6.13d also contains a frequency peak at approximately 12.3kHz again corresponding to a reflection from the void in the duct. In this test the contact time was estimated as 47μs giving an expected frequency response up to 21kHz. Responses can be seen at higher frequencies than that from the duct on this trace. These may be from noise or inhomogeneities within the beam. The energy level input from the 4.7mm diameter ball-bearing hammer is relatively low and so internal inhomogeneity reflections and random

frequencies can give rise to misleading results. This effect can be reduced by repeating the test and comparing the results.

The above series of tests showed it is possible to detect a 100mm diameter void at a depth of 150mm.

6.6.2 Test 2 - 75mm diameter void at 100mm depth

A similar series of tests to those discussed above were carried out over a voided section of duct 1, i.e. at a section containing a 75mm diameter void at a depth of 100mm. The Finite element analyses of this scenario did not give rise to positive defect detection. However, some previous experimental findings have shown the F.E. conclusions to be slightly conservative and so this test was carried out to investigate the possibility of detecting 75mm voids using this impact-echo testing system. The respective estimated contact times and maximum usable frequency responses are shown in Table 6.8.

	Hammer Diameter	Contact time	Max. Usable Frequency	Min. Input Wavelength
a)	9.00mm	100μs	10kHz	370mm
b)	6.00mm	63μs	16kHz	230mm
c)	4.70mm	55μs	18kHz	200mm
d)	2.00mm	40μs	25kHz	150mm

Table 6.8 Estimated contact time and corresponding maximum usable frequency and minimum wavelength for impact-echo test above 75mm diameter duct.

The expected frequency of reflection is 18.4kHz assuming a compression wave velocity of 3675m/s. Table 6.8 indicates that only results c) and d) could give a positive identification of the void as the contact time of the other impacts is too great to allow detection at 18kHz. Figure 6.14 shows the resulting frequency traces from each impact.

The frequency of base reflection in each case is measured at 2.625kHz, i.e. it gives no indication of voiding. Tests a) to c) were carried out at position C10, at the centre of the beam. Each trace shows distinct peaks at 3.3kHz, 4.9kHz

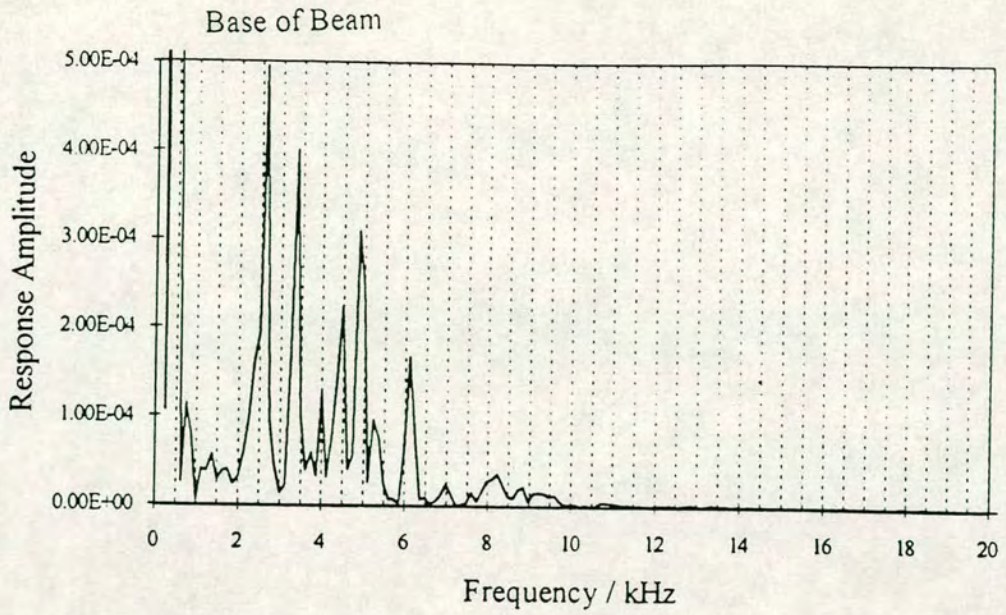

Fig 6.14a Contact time = 100 μs

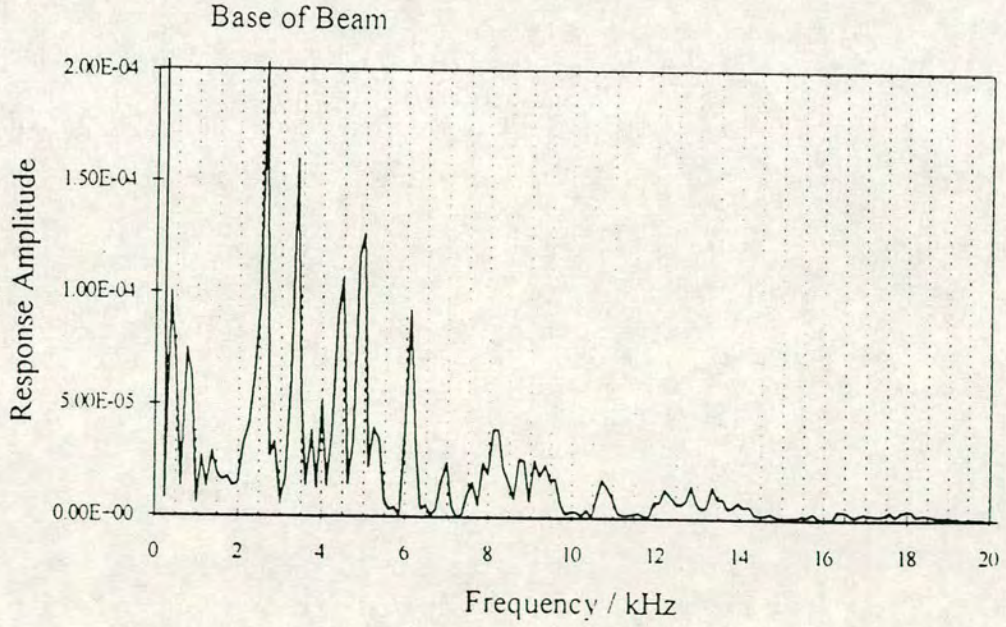

Fig 6.14b Contact time = 63 μs

Figure 6.14 Contact time frequency spectra: 75mm diameter void at 100mm depth

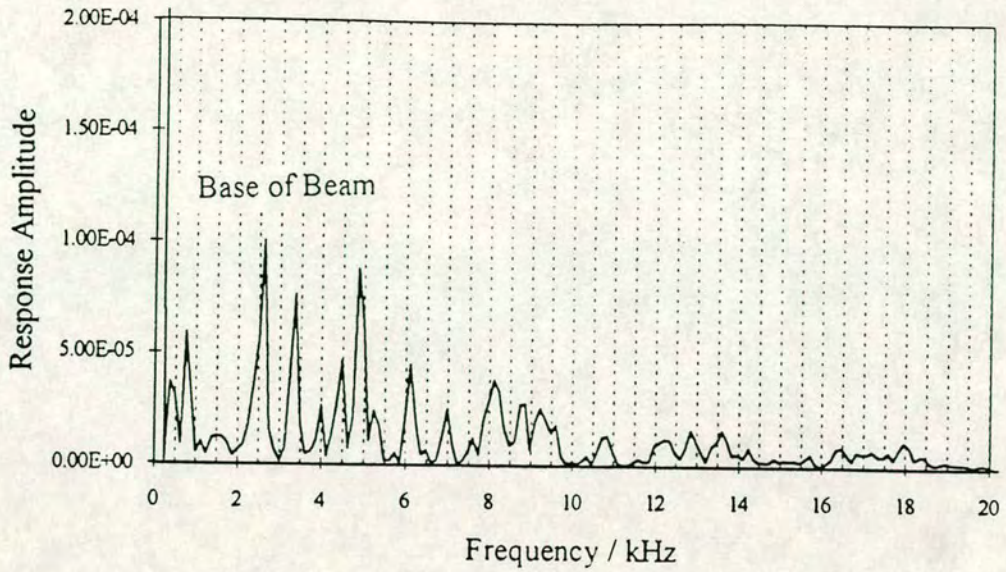

Fig 6.14c Contact time = 55 μs

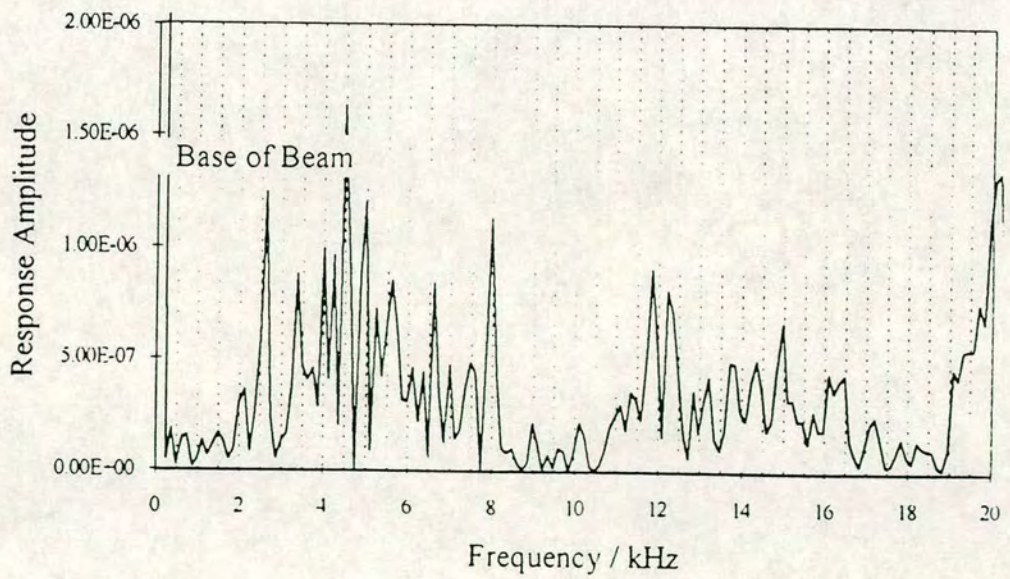

Fig 6.14d Contact time = 40 μs

Figure 6.14 (cont.) Contact time frequency spectra; 75mm diameter void at 100mm depth

and 6.1kHz. These peaks will be investigated in a later section. Test d) was carried out at position C11 (100mm from C10) and a slightly different pattern of frequency peaks can be seen.

No distinct peaks corresponding to a reflection from the voided duct can be seen on either trace a) or b). This is as expected as both contact times were too long to resolve reflections at 18kHz. Figure c) shows a slight peak at 18kHz corresponding to a reflection from the void. The relative magnitude of the peak is very low and it is unlikely to be detected in a real test. The spectrum obtained using a 2.0mm hammer (figure d)) is rather difficult to analyse as the energy input by the small hammer is very low. This results in system noise, etc. becoming more dominant and it is likely to overshadow any useful reflection in the trace.

6.6.3 Conclusions on Effect of Contact Time

The above results show that the assumption that the usable frequency input is equal to 1/1.5*contact time is conservative. Using an input frequency equal to 1/contact time will affect previous conclusions relating size of defect detectable to input wavelength. It was assumed that cylindrical defects with a profile of $\lambda/4$ were detected. By altering the assumed input frequency, it should now be possible to detect cylindrical defects with a profile of $\lambda/2.6$. The depth to a defect is also critical. It is not possible to detect a defect at a depth which results in a reflection at a higher frequency than the input frequency.

6.7 Effect of depth to and shape of defect

Previous results have shown that it is possible to detect defects in 100mm diameter ducts at depths of 150mm with the developed testing system. The minimum repeatable contact time possible with the available impact hammers is approximately 47μs which results in a minimum wavelength of 175mm in this test beam. The minimum defect detectable would have a profile of 175/2.6 = 67mm. This implies that it should be possible to detect defects in a duct 75mm in diameter. However, it has been shown that scattering effects can cause the smaller cylindrical defects to be undetected. Further tests were carried out to investigate this effect.

Impact-echo tests were undertaken at three sections of the 75mm diameter duct 1 using a 4.7mm diameter ball bearing hammer with an average minimum input

wavelength of 200mm. The condition of the duct in the first test, at position C16, is fully grouted. In the second test, at position C18 the duct contains a void in the top section and in the final test, at position C2, the duct contains a void in the lower half of the section. The different void positions present a different depth to and shape of the void. At position C18 the void occurs at a depth of 100mm and offers a cylindrical profile to the incident wave. At position C2 the void occurs at a depth of approximately 140mm and offers a flatter profile to the incident wave. The resulting frequency traces are shown in Figure 6J5 and the results are summarised in Table 6.9..

The base reflections on each trace occur at 2.5kHz and, as expected, give no indication of voiding. Trace a) at the fully grouted section contains no significant peaks other than the base peak. This would seem to indicate a fully grouted duct. Trace b) at the section containing a void in the top portion of the beam contains a slight peak at 17.25kHz. This compares well to the expected frequency peak at 18.3kHz corresponding to a reflection from the void. However, as in previous cases, the peak on the frequency trace is not particularly clear and could easily be overlooked in a field test. Trace c) at the section containing the void in the lower portion of the duct contains distinct peaks at frequencies of 12.3kHz and 14.4kHz. These peaks compare well to the expected frequency peak corresponding to a reflection from voiding in the lower half of the duct, a reflection from a defect at a depth of 140mm would occur at a frequency of 13.1kHz. The void was formed using polystyrene and corrugated cardboard and its profile could easily have been slightly changed during pouring resulting in a change in the depth from the surface of the beam to the top of the void. The void in this case presents a flatter profile to the incident compression wave, resulting in a reduction in the scattering effect. The waves returning to the measurement point therefore contain more energy and so the peak on the frequency trace has a higher relative magnitude.

Test position	Frequency of response /kHz	Possible target
Fully grouted duct	2.5	Base
Partially grouted duct -	2.5	Base
voided in upper section	17.25	Void - Slight peak
Partially grouted duct -	2.5	Base
voided in lower section	12.3	Void
	14.4	"

Table 6.9 Effect of shape of defect in a 75mm diameter duct at 100mm depth

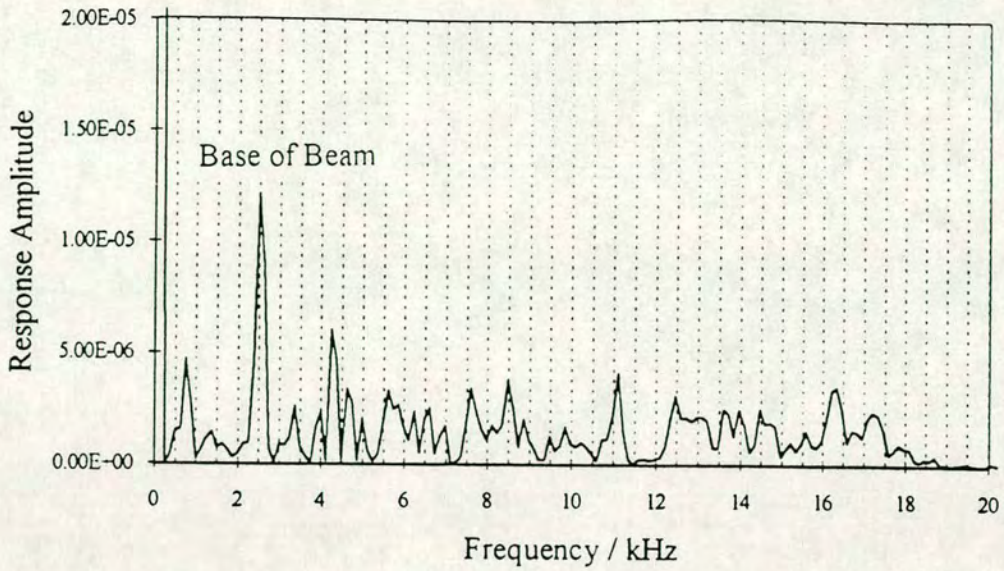

Fig 6.15a Fully grouted 75mm duct

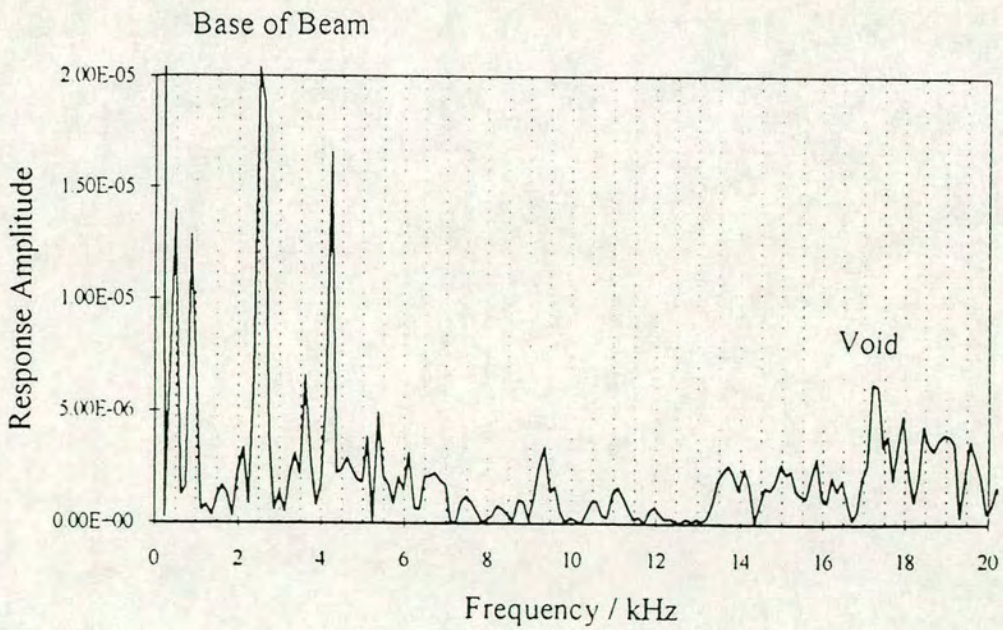

Fig 6.15b Partially grouted 75mm diameter duct with void in upper section

Figure 6.15 Frequency spectra for shape of defect effect

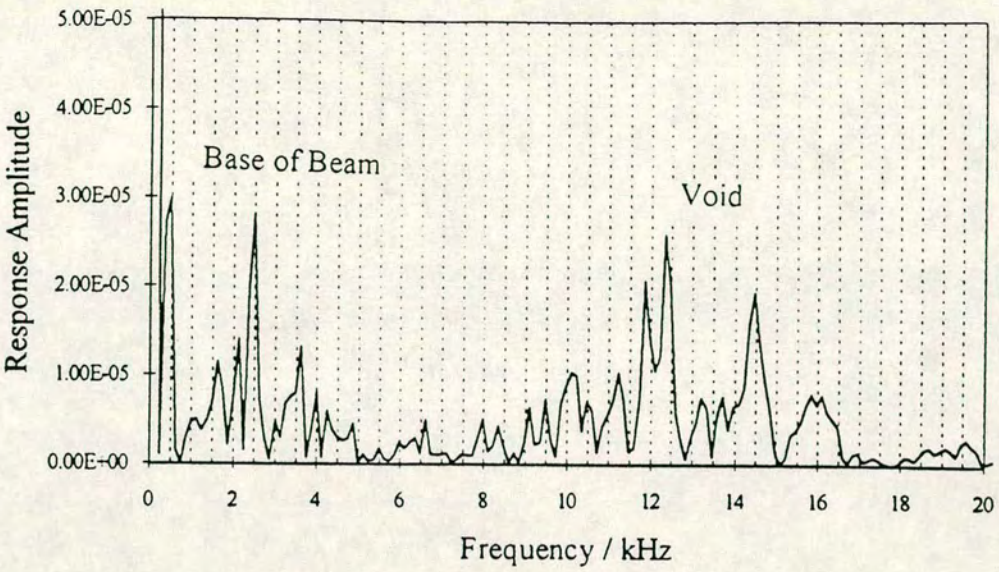

Fig 6.15c Partially grouted 75mm duct with void in lower section

Figure 6.15 (cont.) Frequency spectra for shape of defect effect

6.7.1 Conclusions on Effect of depth to and shape of defect

The assumption that the minimum defect detectable must have a profile of half the minimum wavelength of the incident wave is slightly conservative. Smaller defects can be detected and the critical parameter is the depth to the defect. The input pulse must contain frequencies up to the expected frequency of the reflection from the defect, ie. $F \geq (v/2d)$ - See Chapter 3. The shape of the profile of the defect presented to the incident wavefront is also important in determining the success of a test. The flatter the profile the more likely successful detection will occur. This is as expected and agrees with other experimental findings and the finite element analyses.

The above tests indicate that the developed method can be successful in detecting smaller voids than those concluded from the finite element analyses. However, analysing results from the field will be more difficult and this must be investigated before final conclusions can be drawn.

6.8 Evaluation of OLSON transducer on rough concrete surfaces

The OLSON transducer was shown to provide an efficient method of measuring the response of a specimen with a smooth concrete surface. The instrument is quick and simple to use allowing many more tests to be performed than the NIST transducer. However, the effects of using the OLSON transducer on a rougher concrete surface needed to be investigated before the transducer could be used with confidence in the field.

Tests were undertaken using both the OLSON transducer and the NIST transducer at a number of points on test beam 1 and the frequency traces obtained compared. The results from two of these tests are shown in Figures 6.16 and 6.17. The tests undertaken at position G3 show very good correlation. A good bond was made between the beam surface and the OLSON transducer in this case. However, the results from the test carried out at position G5 do not compare well. The higher frequency components are exaggerated (because the transducer measure acceleration) but the OLSON transducer was unable to measure the lower frequencies in this case.

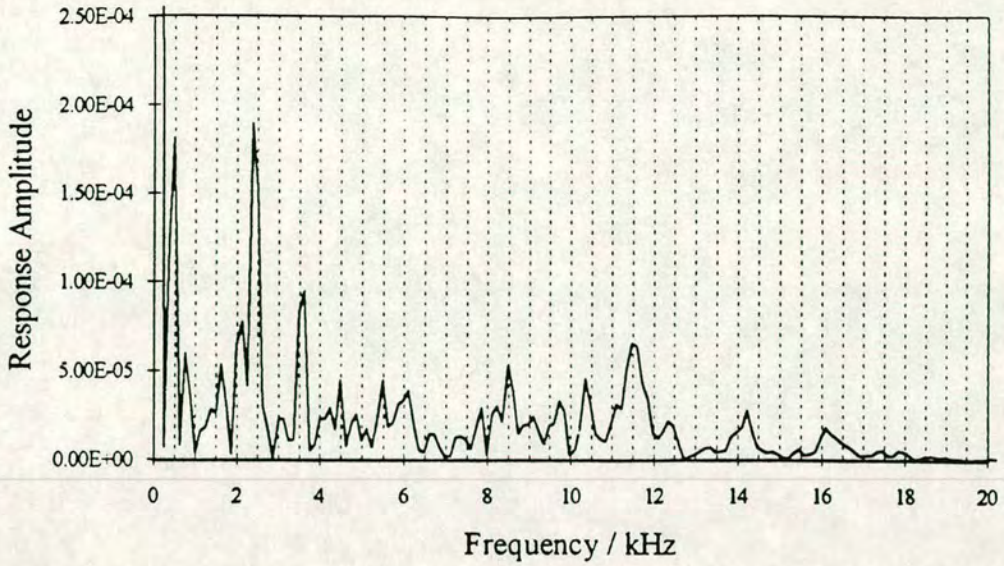

Fig 6.16a Response spectrum using OLSON transducer, position G3

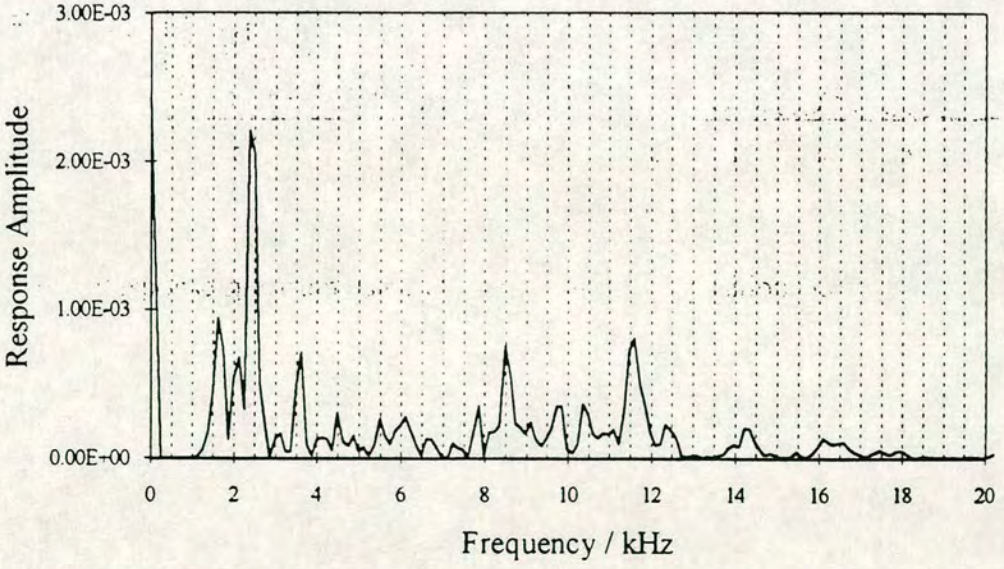

Fig 6.16b Response spectrum using NIST transducer, position G3

Figure 6.16 Transducer comparison 1: good comparison

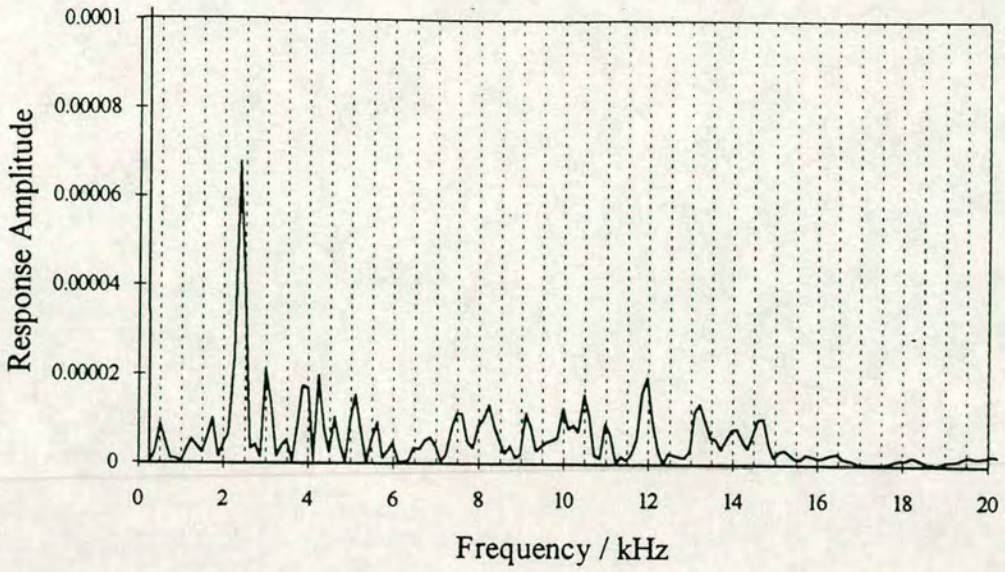

Fig 6.17a Response spectrum using NIST transducer, position G5

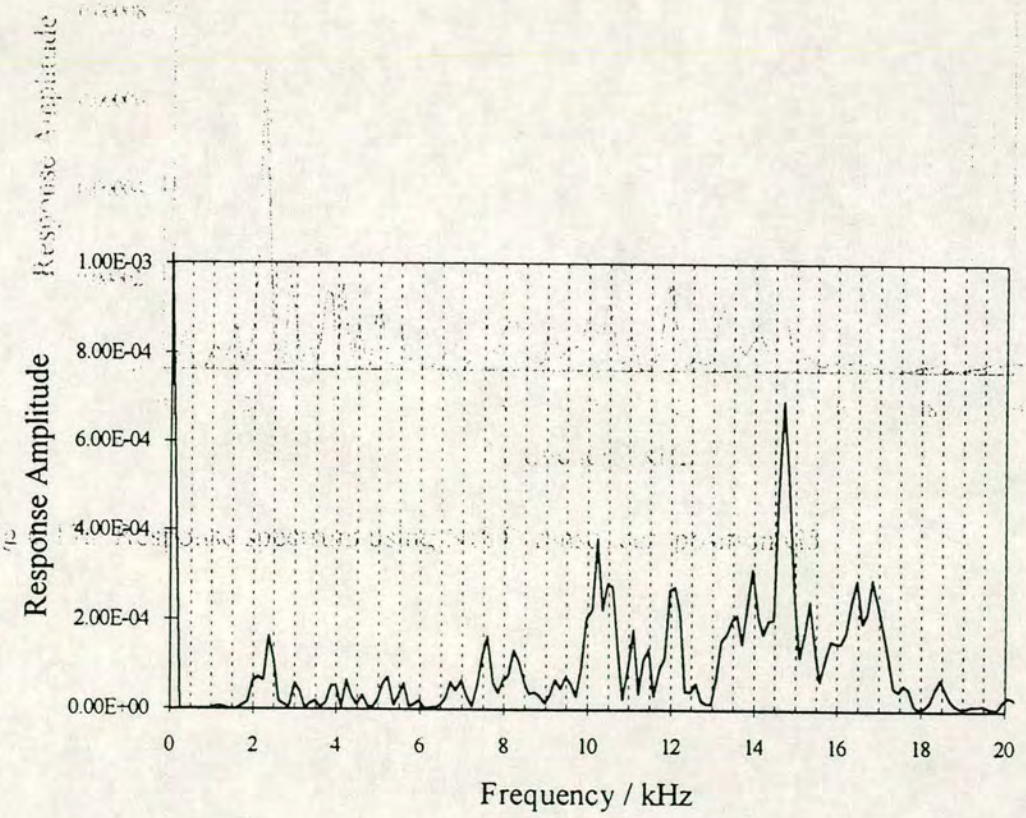

Fig 6.17b Response spectrum using OLSON transducer, position G5

Figure 6.17 Transducer Comparison 2: bad comparison

6.8.1 Conclusions on evaluation of OLSON transducer on rough concrete surfaces

The OLSON transducer provides a quick and simple means of performing impact-echo tests. It is suitable for use on different concrete surface conditions but care must be taken to ensure an adequate bond with the surface is formed.

The above tests resulted in the OLSON transducer being the predominant measuring device used throughout the field testing (as discussed in Chapter 7 of this thesis) as it provided an efficient testing set-up. However, a few tests were carried out with the NIST displacement transducer on each structure to ensure similar, and therefore reliable responses were being measured.

6.9 Conclusions

1. Contact time can be estimated from the response time trace by measuring the initial downward pulse on the diplacement/time trace measured using the NIST displacement transducer. The accuracy of this estimate is dependent on the sensitivity of the transducer and the resolution of the measuring system. On the tests carried out this was 7μs.

2. The smallest impact hammer, 2mm diameter ball-bearing, inputs sufficient energy for the measurement system to detect a reflection from the base of a beam 300mm in depth. However, the relative magnitude of the reflection is small and so 300mm penetration was considered to be at the limit for this hammer.

3. It is possible to detect voiding in a 100mm diameter duct in a simple beam using the developed impact-echo system. This contact time required compares well to that found during the finite element analyses.

4. Frequency of base reflection measurements can successfully detect voiding in duct of 100mm diameter if the line of the duct and the surrounding condition of the concrete are known. If the surrounding concrete condition is not known the frequency of base reflection can give an indication of a defect within the tested section.

5. The developed impact-echo method can be used to detect voiding in ducts at depths of 150mm in beams up to 700mm deep. The 2mm diameter hammer in these tests does not provide a high enough energy input to allow sufficient energy reflection from the base of the beam. Spurious frequency reflections from system noise, internal inhomogeneities in the concrete, etc. become apparent on the traces. These reflections may mask any informative reflections from defects within the beam. As the beam becomes more complex reflections from other defects, not directly beneath the test location, begin to confuse interpretation of the response.

6. The assumption that the maximum usable frequency is $1/(1.5*T_c)$ is conservative. Values up to $1/T_c$ are easily identified and so this value has been assumed for the remainder of this thesis. Previous findings relating the defect profile detectable to the minimum input wavelength therefore change. A value of $\lambda/4$ was concluded from the finite element analyses. This will change to $\lambda/2.6$ if the assumed wavelength relates to $1/T_c$.

7. It is possible to detect voiding in 75mm diameter ducts but the results are difficult to analyse and could easily be misinterpreted in field tests. Detection of defects improves if the depth to the void is greater than 100mm, up to approximately 150mm for a cylindrical defect profile. The defect becomes easier to detect as the void profile flattens, e.g. if the lower half of the duct is voided, and so the scattering effect is reduced.

8. The NIST displacement transducer provides a more accurate measuring device than the OLSON accelerometer. However, implementation on site is much quicker and more straightforward using the OLSON accelerometer. This transducer should be carefully coupled to the beam between each test and some check tests carried out using the NIST transducer to ensure similar responses are being measured. This enables the OLSON accelerometer to be used on site efficiently and with confidence. An estimate of hammer contact time is also possible with the OLSON accelerometer but the time trace is more difficult to analyse than that gained using the NIST transducer.

Chapter VII

Field Validation of Developed Testing Method

Field studies were carried out to investigate the practical application of the developed testing methods. This chapter outlines the background to these investigations, the beams studied and some results obtained.

7.1 Introduction

Laboratory testing had shown that impact-echo testing methods could be successfully used to detect voids within concrete. The range of application and limitations with the test method as applied under laboratory conditions were noted and these needed to be investigated in a more realistic setting. Post-tensioned bridge beams had been tested previously at TRL, see chapter 4. The New beam was available for further testing. This beam had been extensively tested in the intervening three years since the original tests were carried out and had suffered some deterioration. However it was considered worthwhile to test this beam to investigate the effect of the improvements to the test method. A laboratory specimen had also been constructed at TBV-Stanger. This beam was also to be tested.

The ducts in the test beam constructed at TRL were 40mm diameter which is small for post-tensioned ducts. A more usual duct size would be 100mm to 110mm diameter with a cover of approximately 125mm (M40 bridge beams, Ove Arup Partnership). The developed impact-echo system had been shown capable of detecting voids in 100mm diameter tendon ducts but it would be difficult to detect defects in the TRL ducts by the direct reflection method used previously. However, research into impact-echo testing of beams carried out at Cornell University has found that the natural frequencies of beams are detected by impact-echo testing techniques. These frequencies are dependent on the geometry of the beam and the condition of the concrete. Defects within tested sections will therefore give rise to a change in the natural frequencies of that section. If the natural modes of vibration can be identified on some traces, it may be possible to identify areas where further investigation would be recommended. One method of further investigation available is time of flight tomography. This method involves measuring the time of flight of an ultrasonic pulse along many ray paths through a section of the beam. The data is then processed using tomographic software (MIGRATOM was used for this study) and the results given as a velocity plot across the section.

The second test beam at TBV Stanger, Elstree contained 100mm diameter ducts. This model was also tested using both impact-echo and tomographic techniques. The test beams have the same cross-section - See figures 7.1 and 7.2 - and so many of beam modes will be of similar frequency assuming the concrete in each has similar properties.

Figure 7.1 TRL test beam

Figure 7.2 TBV Stanger test beam

7.2 Impact-Echo Testing Instrumentation and Procedure

The typical impact-echo testing system was used as in the laboratory tests. The same analyser was used in these tests, the A & D Dual channel FFT Analyser set to a frequency range of 50kHz. This range gives a frequency resolution of 0.125kHz which was considered acceptable for this investigation. The frequency of impact required to investigate post-tensioned bridge beams is higher than that which can be produced on concrete by available instrumented hammers. Ball bearings of different diameters were attached to wire and used as impactors. Earlier research had concluded that the time of contact, and hence the peak frequency of excitation, could be estimated from the time trace of the response, allowing the usable frequency range of the response to be estimated, see earlier chapters.

Two response trandsucers were used during the field investigations as in the laboratory tests, a NIST displacement transducer which had been modified in the laboratory to allow testing in any orientation, and a prototype impact-echo accelerometer developed by OLSON Engineering in the USA. The NIST transducer has been widely used and provides a reliable measuring device. However, as discussed previously, it is very cumbersome to use in the field, mounting the transducer is complicated and its surfaces require cleaning after almost every test. In contrast, the OLSON accelerometer is very simple and quick to mount on the test surface allowing many tests to be carried out efficiently. The prototype was fitted with an impactor which was to be triggered at the same time as the transducer started recording. The impactor was fitted on the accelerometer housing and would ensure a standard distance between the impact and response recording positions. Unfortuneately the ROM chip controlling this trigger was not robust and had been damaged during the importation of the transducer necessitating the use of the ball-bearing hammers. A number of tests were carried out at each test site and a representative response recorded thus reducing the possibility of a random result being saved. The results were saved onto floppy disk and transferred to a PC for post-processing and printing.

7.3 Tomographic Survey

7.3.1 Basic Tomography Theory

Tomography, from the Greek root, *"tomos"* meaning slice, involves the reconstruction of a two-dimensional section of the test specimen. This slice is constructed using measurements of pulse velocity through the specimen made

outside its perimeter. The mathematical theory was established by Radon in 1917 (Radon, 1917) in which it is shown that the internal characteristics of an object can be exactly reconstructed by a complete set of projections through the object. This theory has been used extensively in modern medicine.

For the surveys carried out in this thesis, transmission tomography is used, ie. energy transmitted through the specimen is measured and the section constructed. This is the simplest form of tomography and can be simply performed by measuring the times of flight of a series of stress pulses along different paths through the specimen. The basic concept is that the stress pulse on each projection travels through the specimen and interacts with its internal construction. Variations in the internal conditions result in different times of flight being measured. The tomographic software reconstructs the section by combining the information contained in a series of these projections, obtained at different angles through the section. Sophisticated reconstruction is available using information contained in each projection, eg amplitude. However, for the initial surveys undertaken the travel time alone was measured and the section reconstructed using the information contained in these times alone.

The travel time depends upon the path length and the velocity of the pulse through the material encountered along the projection. Travel times can be inverted to produce a two dimensional model of the velocities encountered within the section. Figure 7.3 shows a possible ray path from source position, S, to receiver position, R. The time of flight from S to R is measured and represents the average velocity along that particular projection. Mathematically, each time of flight, t, represents a line integral of the wave slowness (the inverse of velocity), p, along the ray path;

$$t = \int_S^R \frac{1}{v} \cdot dl = \int_S^R p \cdot dl \qquad (7.1)$$

where dl is the path length increment.

There exist two main categories for reconstruction of the slowness distribution across a section from a series of line integrals, the first is widely used in medicine and utilises elegant mathematical processes. These are rapid

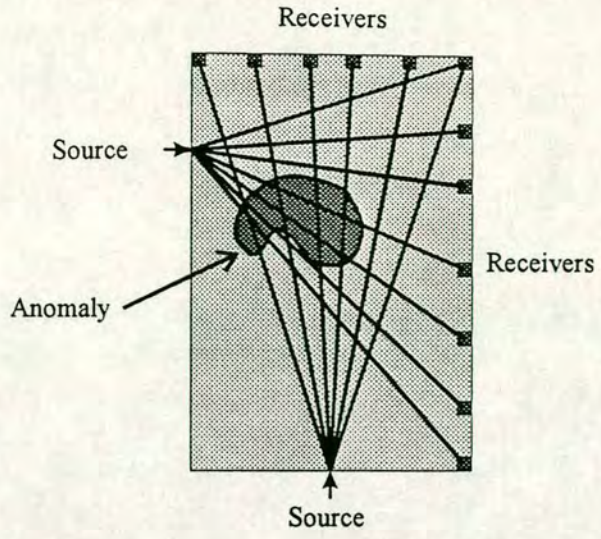

Figure 7.3 Tomographic ray paths

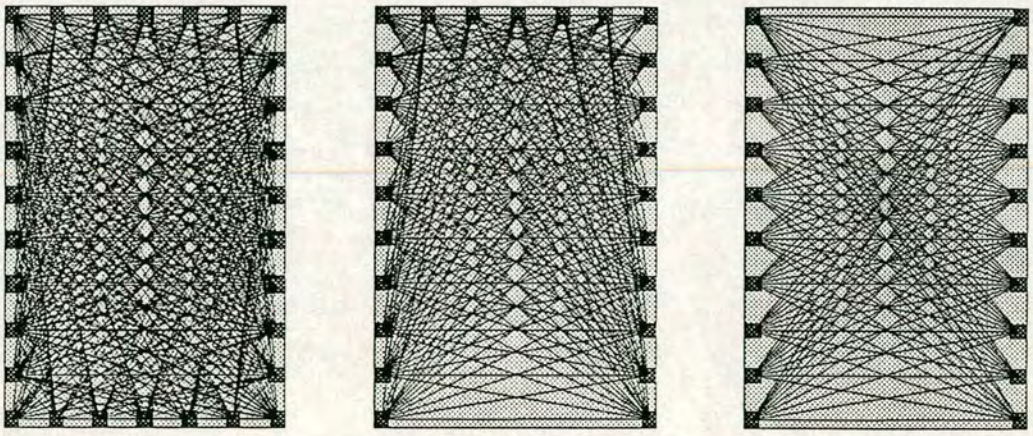

a) Complete coverage b) Surface and side coverage c) Side coverage only

Figure 7.4 Ray path coverage for different transducer arrangements

and exact but require strict geometrical constraints which are not usually possible for structural testing. The reconstruction method used for this study involves series expansion techniques in which the continuous section is modelled as a set of discrete elements, pixels, each with a uniform slowness, p_j (j = 1 to M where M is the number of pixels). The integral corresponding to travel time, t_i (i = 1 to N where N is the number of travel time measurements) is therefore;

$$t_i = \sum_{j=1}^{M} p_j d_{ij} \quad (i = 1..N) \tag{7.2}$$

where d_{ij} is the distance travelled by the ray within the pixel. The above equation can be expressed for a complete set of rays in matrix form as shown below;

$$T = D\,P \tag{7.4}$$

where T and P are column vectors of length N and M, D is an N by M matrix.

Tomography involves solving (7.4) for P, the slowness vector, given the travel time matrix. The matrix of path lengths, D, must therefore be calculated. This is relatively straightforward if straight ray paths are assumed, as D follows from simple geometry. In this study straight ray paths were assumed. The slowness vector, P can then be calculated by inverting D;

$$P = D^{-1}T \tag{7.5}$$

Direct matrix inversion methods incur high computational cost. The tomography software used, MIGRATOM uses a more efficient alternative, algebraic reconstruction techniques, ART. In this iterative reconstruction, an assumed initial velocity model is refined until it converges to a solution according to the travel time data (Migratom manual). The process can be summarised as follows:

1. An initial slowness model is specified and used to calculate a set of model travel times:

$$T' = D\,P' \tag{7.5}$$

2. The model travel times are subtracted from the measured times to obtain the residuals:

$$dT = T - T' \tag{7.6}$$

3. These residuals are then 'back-projected' to obtain a set of correction factors:

$$dP' = D^{*T}\, dT \tag{7.7}$$

4. The model is then updated with the calculated correction factors and the process repeated until suitable convergence occurs;

$$P'' = P' + dP' \tag{7.8}$$

Radon showed that an object could be exactly reconstructed from a complete set of projections. However, this is not practical on site as the time required to provide a complete set would be prohibitive. The best practical arrangement for testing would be to measure travel times on all the beam surfaces but this is unlikely to be possible on a birdge beam. A more likely scenario is that three sides of the beam would be available for testing. A compromise needs to be made between practical testing times and resolution of the test. The higher the resolution needed the larger the number of measurements required with a correspondingly closer mesh (see Figure 7.4). It should be noted that there is a lesser number of ray paths at the edges of the tested section. this can give rise to spurious results in these regions and it is generally recommended that the velocities calculated in the first layer of pixels are disregarded.

7.3.2 Tomographic Survey Instrumentation and Procedure

The travel times for these investigations were measured using an ultrasonic digital tester, PUNDIT. This instrumentation has been widely used to non-destructively test concrete and is robust and therefore suitable for use on site. The testing set-up is shown in Figure 7.5. A test grid was set up at the section

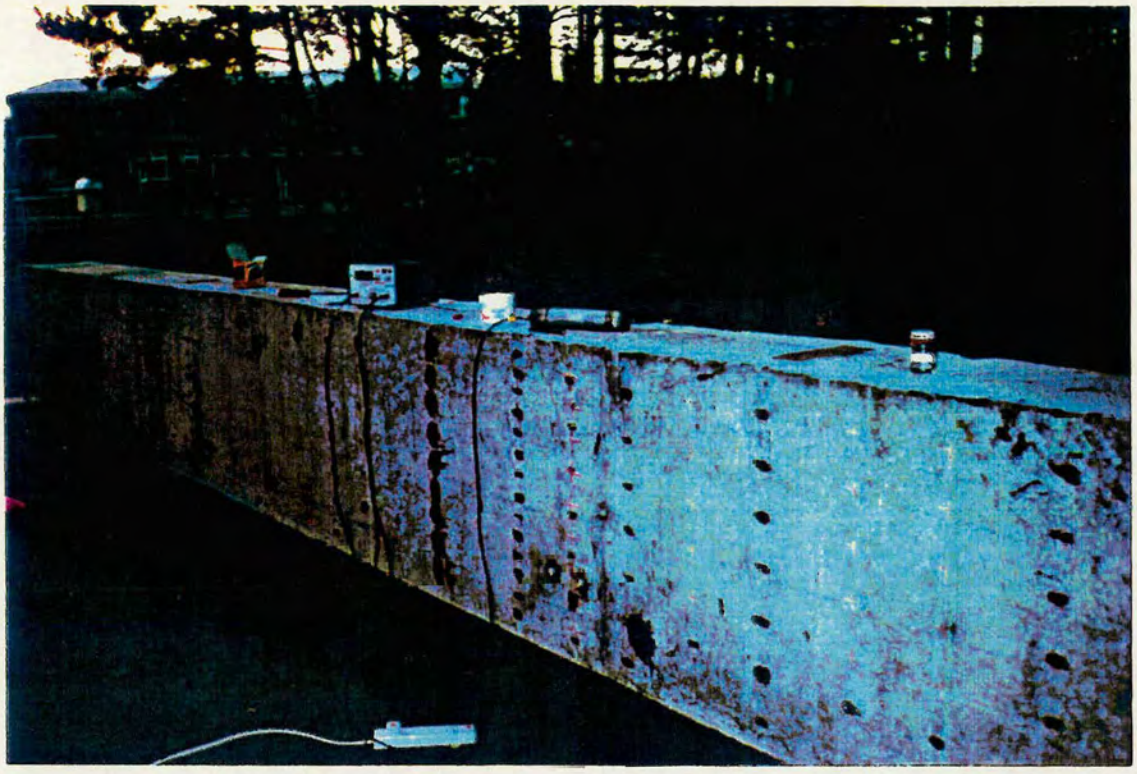

Figure 7.5 Test set-up for tomographic testing (on TRL test beam)

to be investigated using a similar distance between test points on all test surfaces. Each transducer location and corresponding time of flight was noted and subsequently input into a model to be analysed by MIGRATOM software. The internal wave velocities calculated were then presented as a contour plot across the section.

7.4 Testing at TRL

7.4.1. Impact-Echo Testing and Results

The beam was marked up and tested as shown in Figure 7.6. As discussed previously, it was unlikely that defects within the ducts would be detected directly and so typical responses were looked for. The expected frequencies of modes one and two were estimated as approximately 4.5 kHz (Sansalone and Poston, 1992) and almost all of the measured results traces contained a frequency component between 4.25 and 4.625 kHz - See Figure 7.7. The resolution of the testing system is 0.125 kHz and so the above results largely agree with those expected. A distinct response pattern was recorded at position D, 400mm down the side of the beam. The responses at these positions contained a peak at a slightly lower frequency than that expected from beam vibration mode 1, ie around 4.3kHz and a second peak at 6.0kHz. This pattern must arise due to the geometry of the beam and the fact that the impact is carrried out at almost halfway down the beam.

A reflection from the far side of the beam can also be detected on many traces. A reduction in the frequency of this reflection can indicate a defect within the tested section. However, the change in the frequency of the base reflection due to a void in a 40mm diameter duct is very unlikely to alter the base reflection significantly enough to be resolved by the testing system. Other reflections can be seen on the responses. These may be due to simple reflection from defects, higher modes of beam frequency or additional frequency modes produced by defects within the beam. The testing system also produces noise which may affect the response depending upon the relative amplitudes of the signal produced from the beam's response and that of the noise.

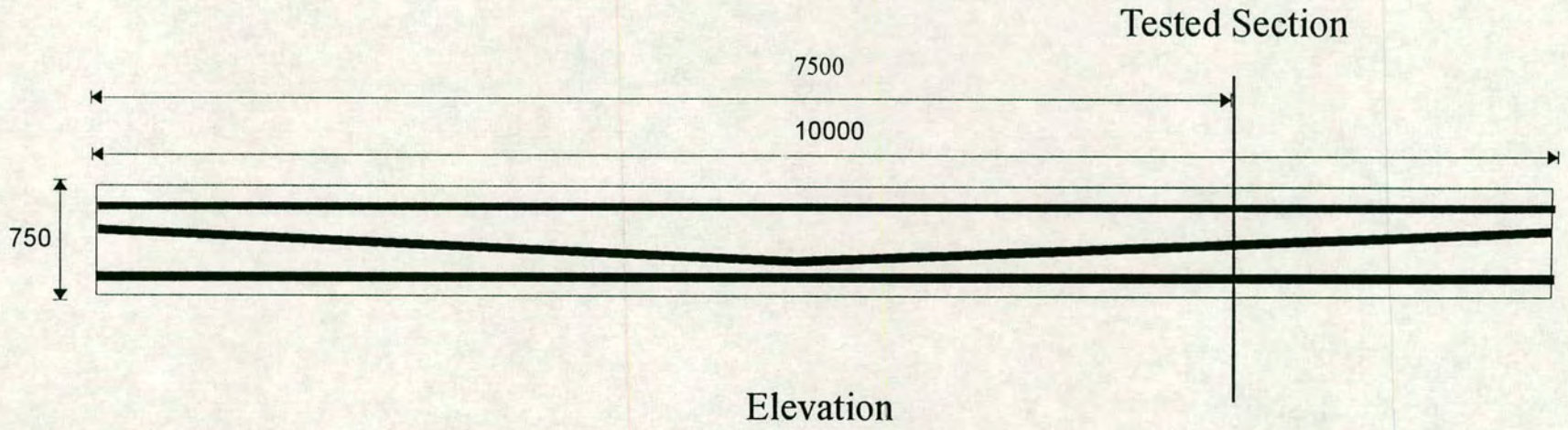

Figure 7.6 TRL beam showing location of the tested section

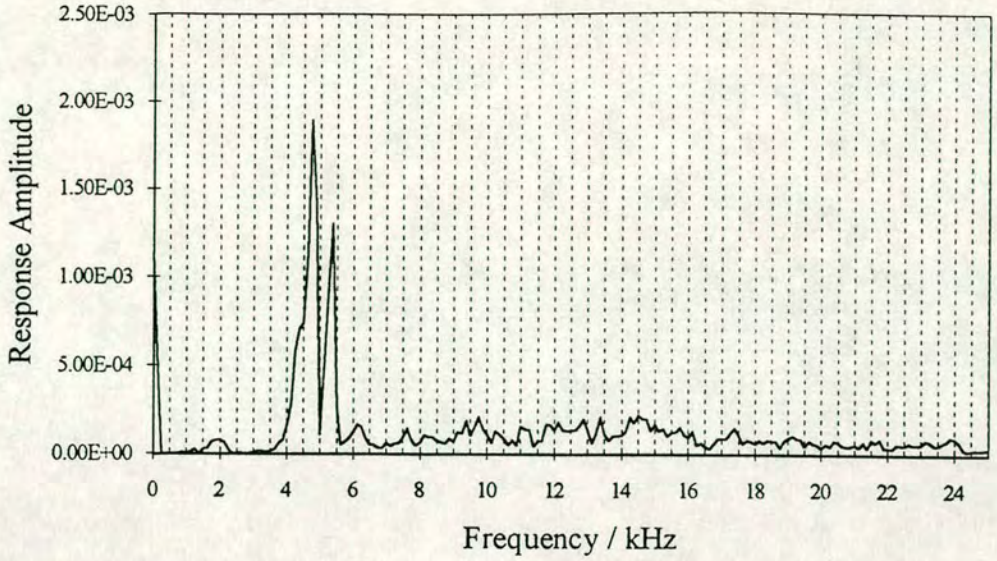

Fig 7.7a 0.2m from top surface

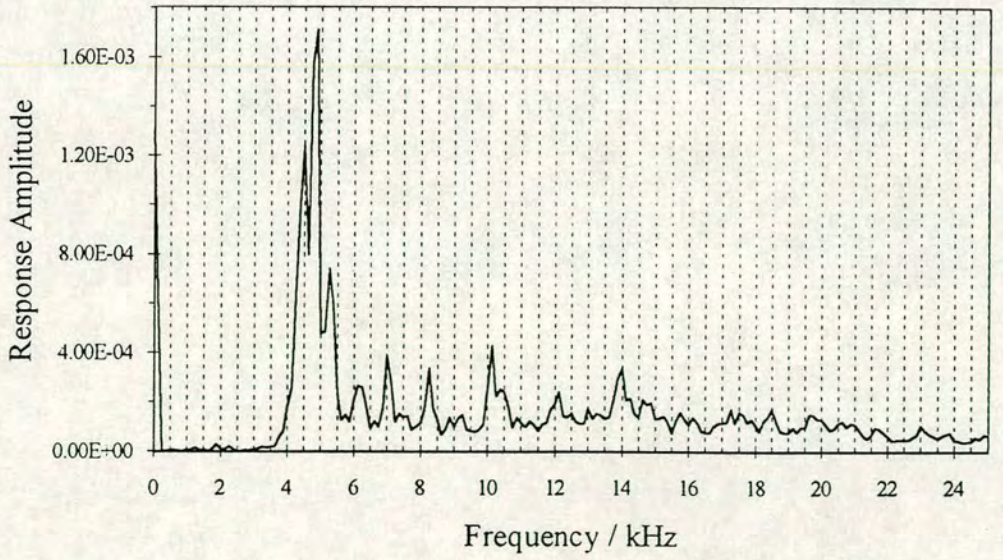

Fig 7.7b 0.3m from top surface

Figure 7.7 TRL Beam. Section 7.75m from end 1

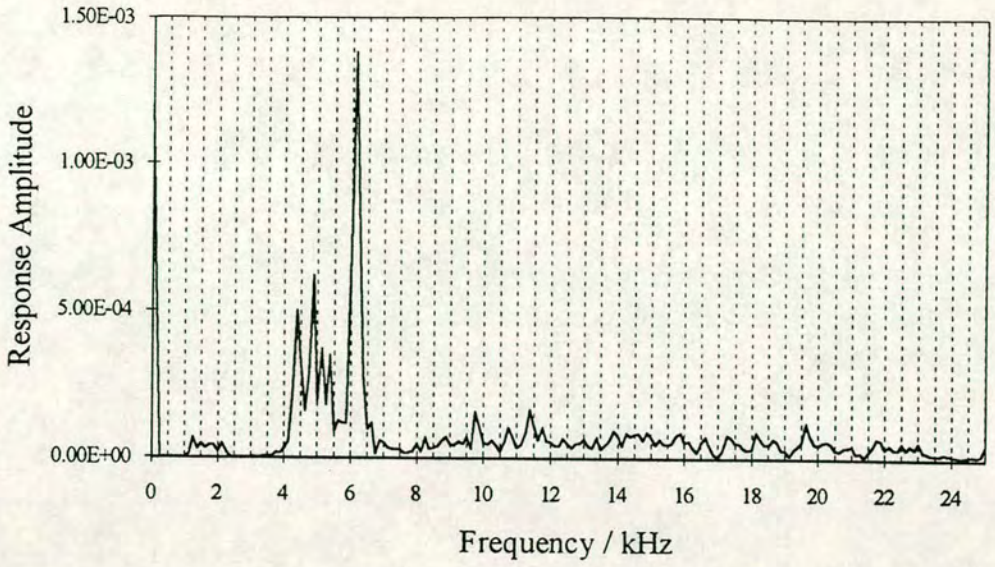

Fig 7.7c 0.4m from top surface

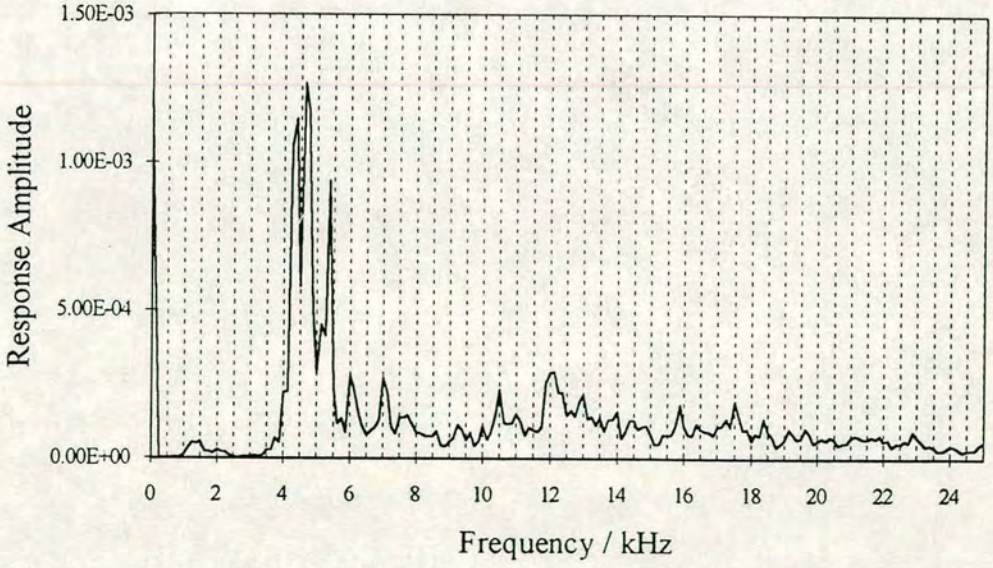

Fig 7.7d 0.5m from top surface

Figure 7.7 (cont.) TRL Beam. Section 7.75m from end 1

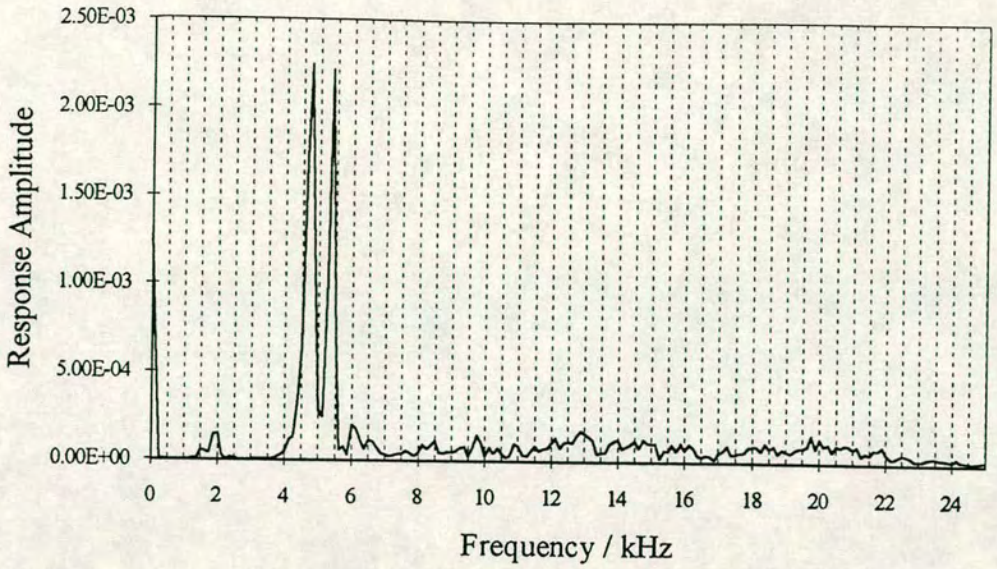

Fig 7.7e 0.6m from top surface

Figure 7.7 (cont.) TRL Beam. Section 7.75m from end 1

With the testing system at present it is not possible to measure the input from the hammer. The response signal can therefore not be normalised and then compared directly with other responses. The amplitudes of the different frequency components on each response cannot be compared with those found at other test positions thus making interpretation of the results more difficult. The response is firstly analysed in the time domain at each test to ensure that a good hammer impact has occured, figure 7.8 shows a good and a poor hammer impact. If a poor impact has occured the test is repeated. This reduces random effects and allows a better comparison of results, but the observations made above still apply. Further work is required to allow confident interpretation of test results from beams with small diameter ducts.

7.4.2. Tomographic Survey

A tomographic survey was carried out at position 22 on the beam (ie. 4.4m from one end) and the results are shown in figure 7.9. The grid spacing used was 75mm vertically and 80mm horizontally. In retrospect this was not a fine enough grid to allow detailed investigation of 40mm diameter ducts. However, the contour plot does seem to indicate the location of the ducts and it seems likely that time of flight tomography offers a very useful testing method for post-tensioned concrete beams.

7.5 Testing at TBV Stanger

7.5.1 Impact-Echo Testing and Results

The ducts in the test beam constructed at TBV Stanger were 100mm in diameter and defects should therefore be detectable using the impact-echo system. The beam was marked up as shown and tests were carried out along the line of duct A and along the line of duct B. These results were briefly analysed on site and then a more detailed investigation was carried out at two sections, 0.4m and 0.8m from the front end of the beam. At these sections impacts were carried out at 0.1m intervals down each side of the beam. It should therefore be possible to compare the measured responses from either side of the section and identify the main beam frequency modes. Other reflections can be compared and a more accurate determination of defect location made by triangulation. In each case the time trace was briefly

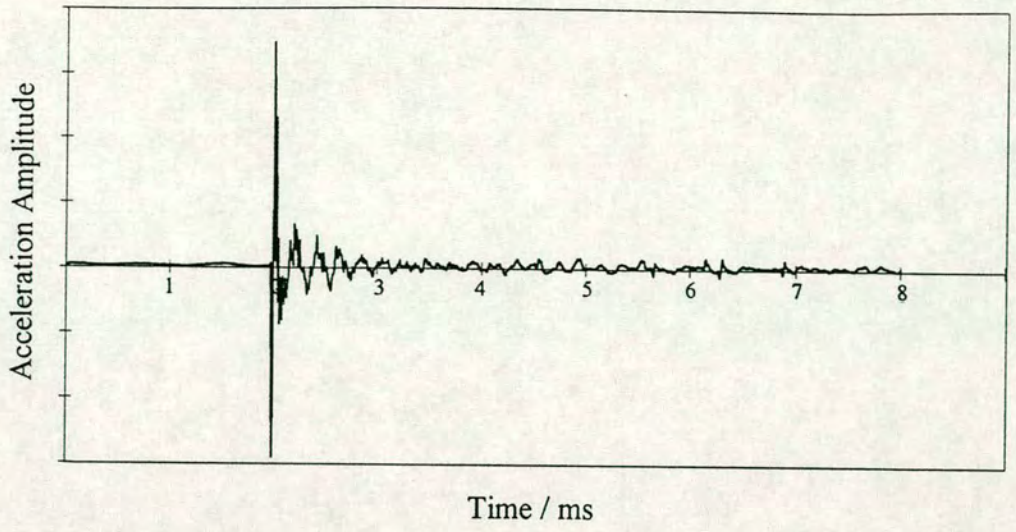

Fig 7.8a Good test response

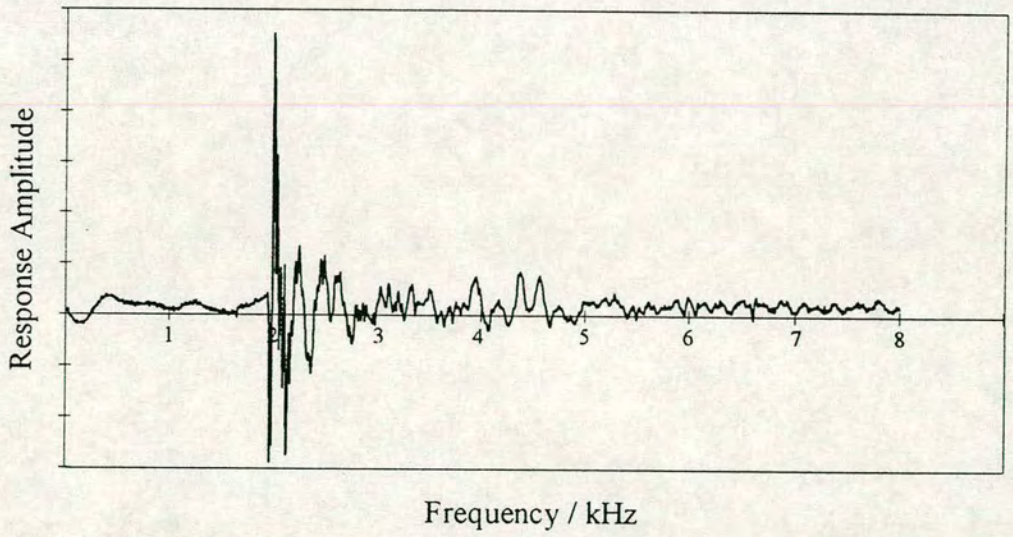

Fig 7.8b Poor test response

Figure 7.8 TRL beam. Good and poor response for hammer impact - time domain

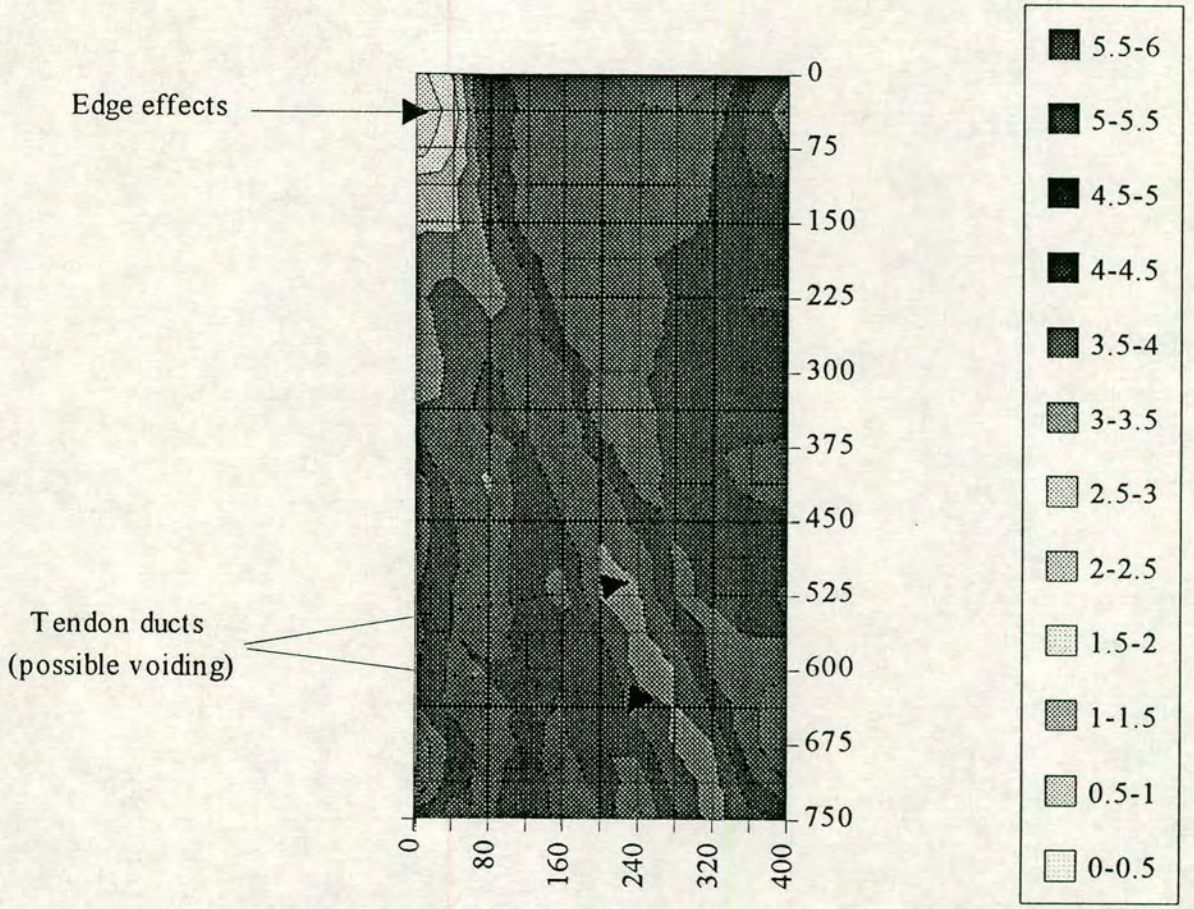

Fig 7.9 TRL Tomographic survey - Position 4.4m from track end

analysed to ensure a clean impact had occured and a usable response had been measured. In some areas of the beam the concrete surface was in a very poor condition and so at these points the response measured gave very little information regarding the internal condition of the beam.

Figure 7.10(a-k) shows the frequency components of the responses measured along the line of duct A. Duct A was orientated horizontally halfway down the beam, with a concrete cover of 100mm. Beam vibration modes of around 4.6kHz, largely agreeing with frequency components measured on the TRL beams, can be detected at many locations. A second frequency component that is present on most of the responses in figure 7.10 occurs at 6.0kHz. This corresponds to the frequency component measured on the TRL beams halfway down the side. These tests were also carried out halfway down the side of the beam, reinforcing the conclusion that the frequency component at 6.0kHz occurs due to the geometry of the beam at the test location. The base reflection is measured on some traces at around 5.2kHz, giving a compression wave velocity of 4200m/s. This reflection is not detected in all cases as the first beam mode of vibration can dominate the response. Other frequency components are detected and the conclusions drawn are summarised in table 7.1.

Figure 7.11(a-k) shows the frequency response of tests carried out along the line of duct B. In this case the duct slopes upwards towards the back of the test beam and again has a concrete cover of 100mm. The first beam mode of vibration is detected on most traces at around 4.6kHz. A frequency component at 6.0kHz is not readily detectable on these traces. These traces are not carried out halfway down the side of the beam as the line of the duct slopes upwards. Other frequency components can be detected and the results are again summarised in table 7.1.

As mentioned previously, the impact is not measured and so the response can not be normalised and then compared directly to other measured responses, however, much information regarding the internal condition of the beam can be obtained.

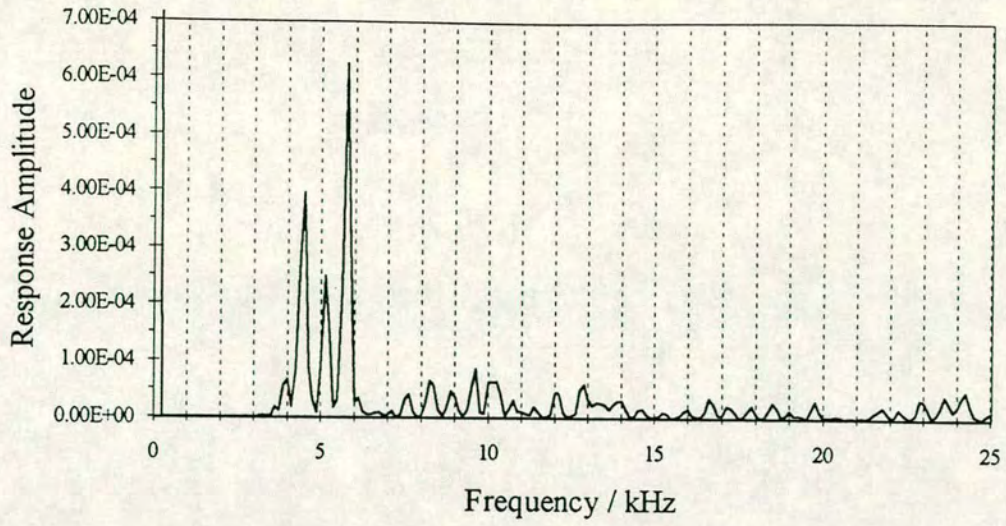

Fig7.10a 0.1m from front end

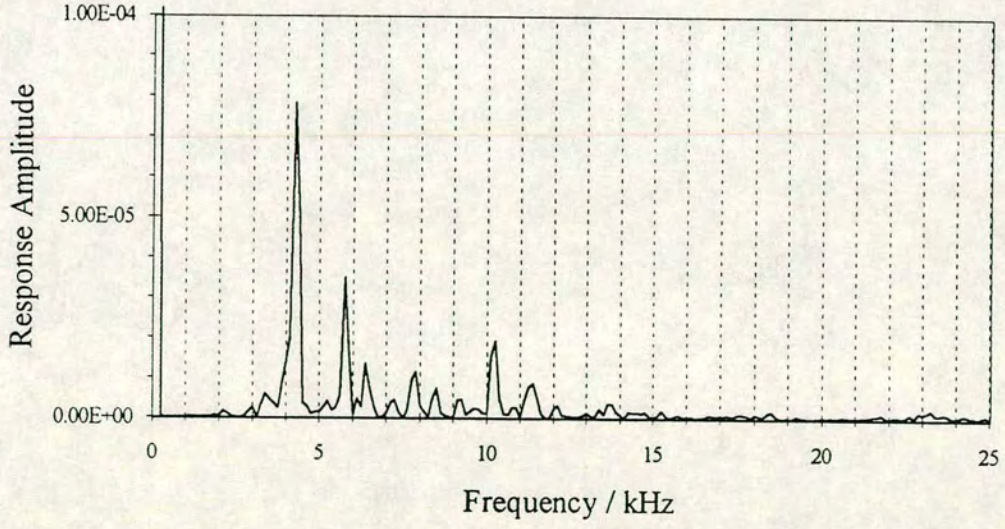

Fig 7.10b 0.2m from front end

Figure 7.10 TBV Stanger beam. Test along duct A on side A

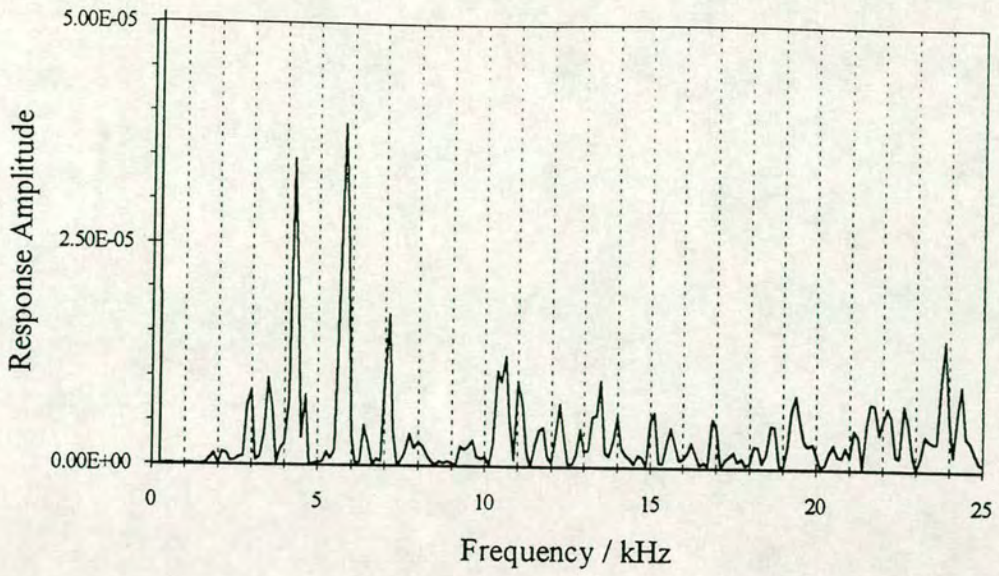

Fig 7.10c 0.3m from front end

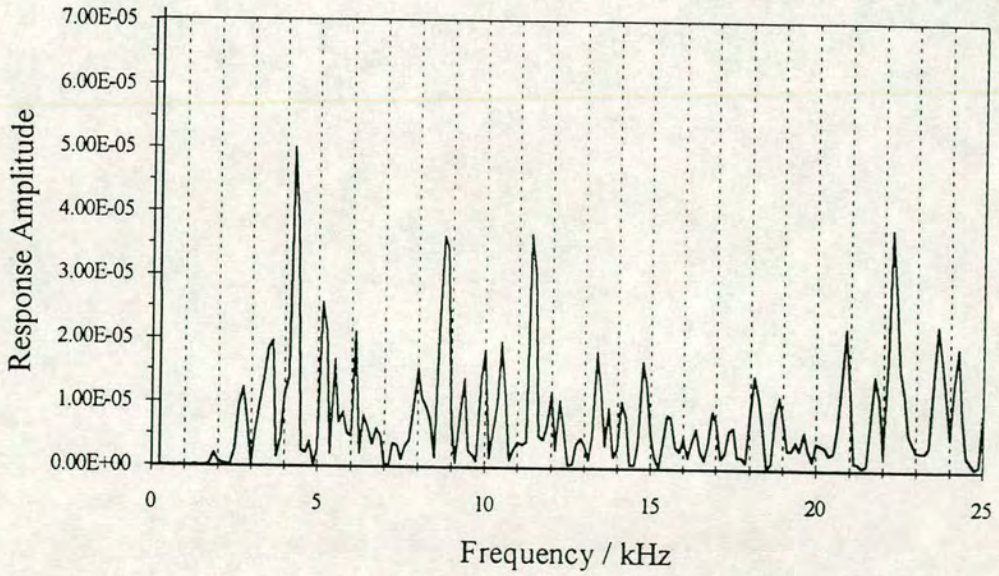

Fig 7.10d 0.4m from front end

Figure 7.10 (cont.) TBV Stanger beam. Test along duct A on side A

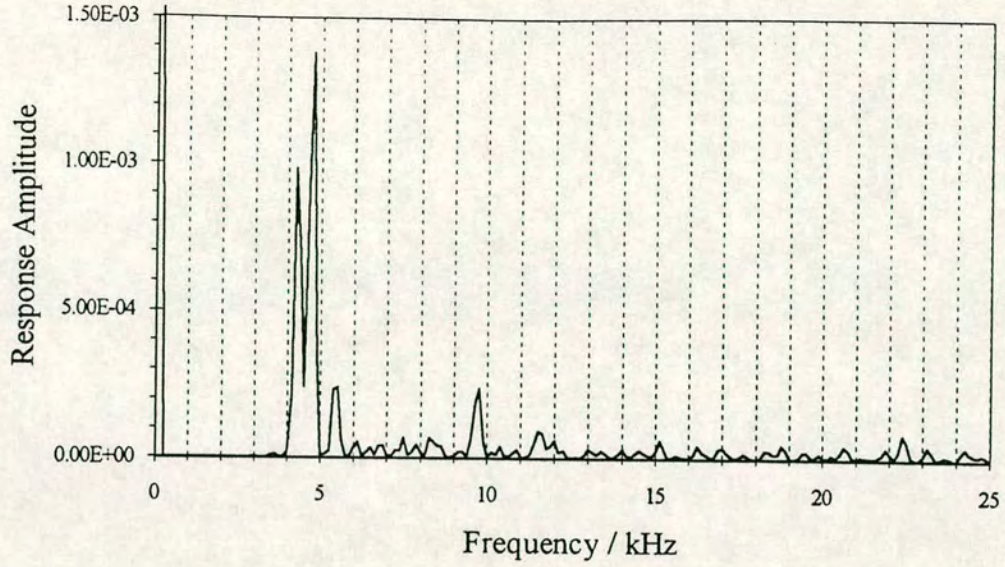

Fig 7.10e 0.5m from front end

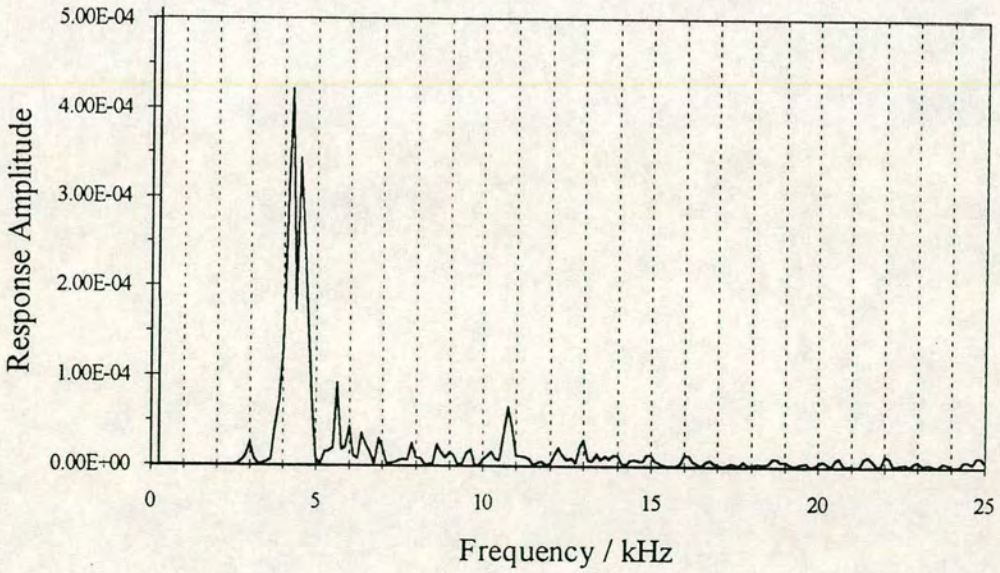

Fig 7.10f 0.6m from front end

Figure 7.10 (cont.) TBV Stanger beam. Test along duct A on side A

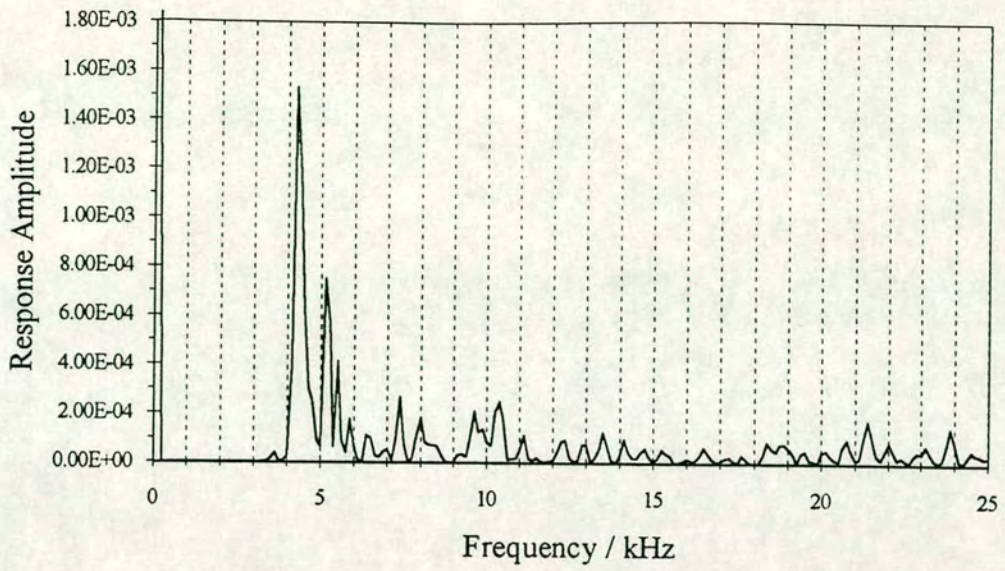

Fig 7.10g 0.7m from front end

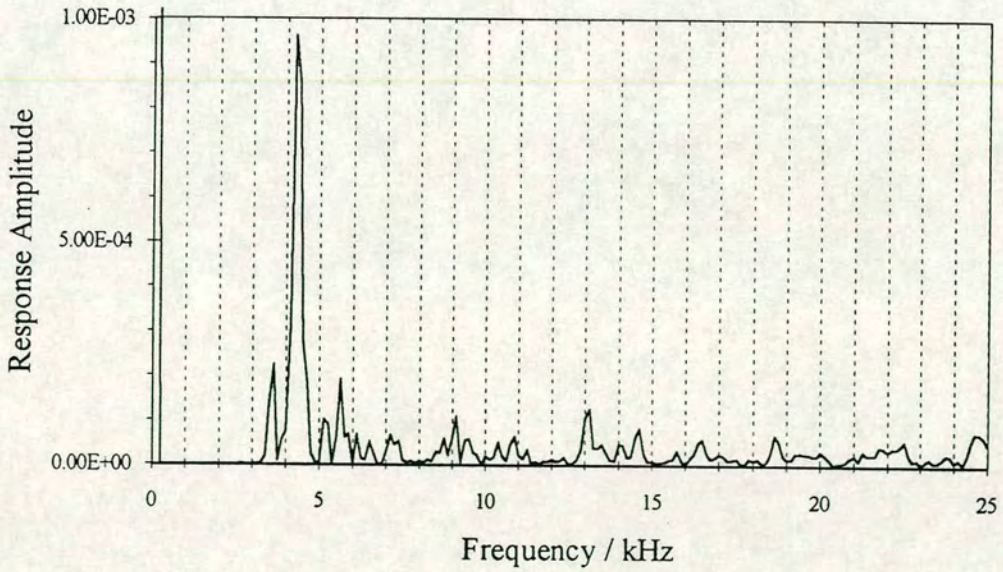

Fig 7.10h 0.8m from front end

Figure 7.10 (cont.) TBV Stanger beam. Test along duct A on side A

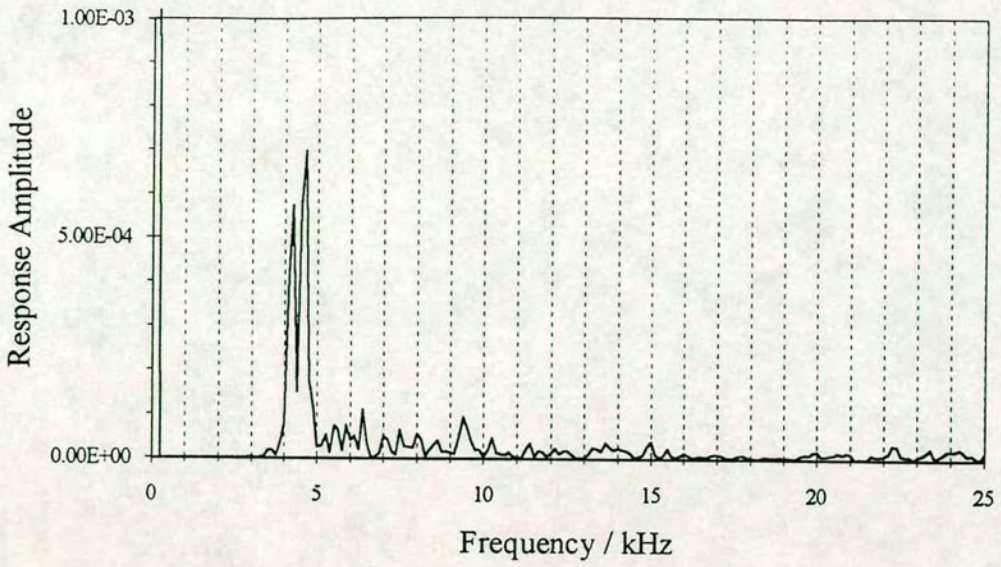

Fig 7.10i 0.9m from front end

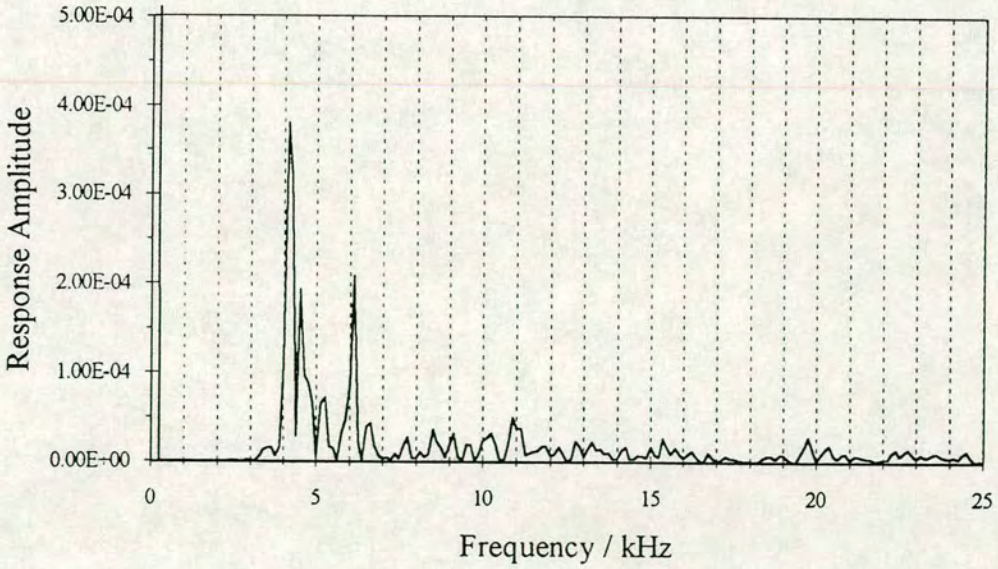

Fig 7.10j 1.0m from front end

Figure 7.10 (cont.) TBV Stanger beam. Test along duct A on side A

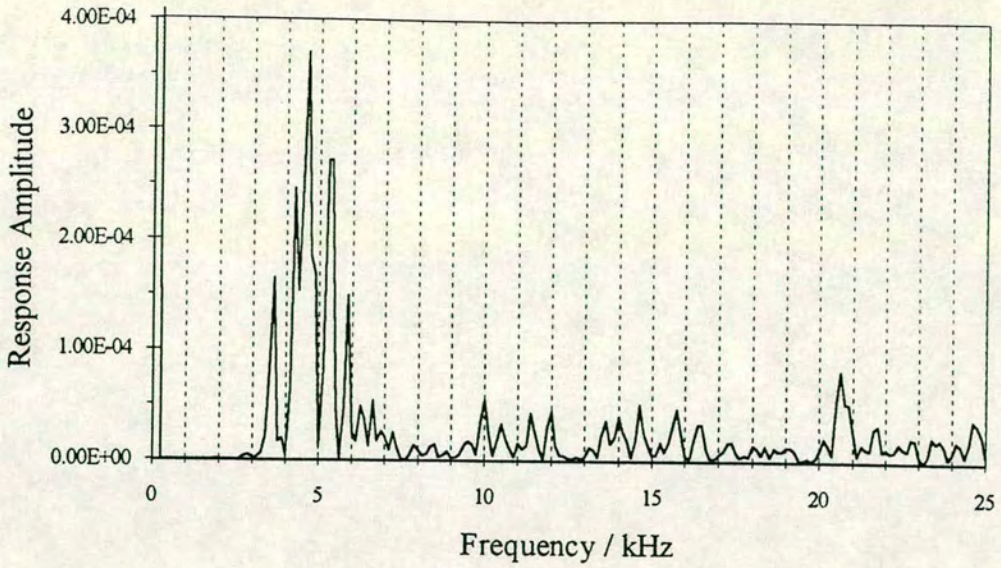

Fig 7.10k 1.1m from front end

Figure 7.10 (cont.) TBV Stanger beam. Test along duct A on side A

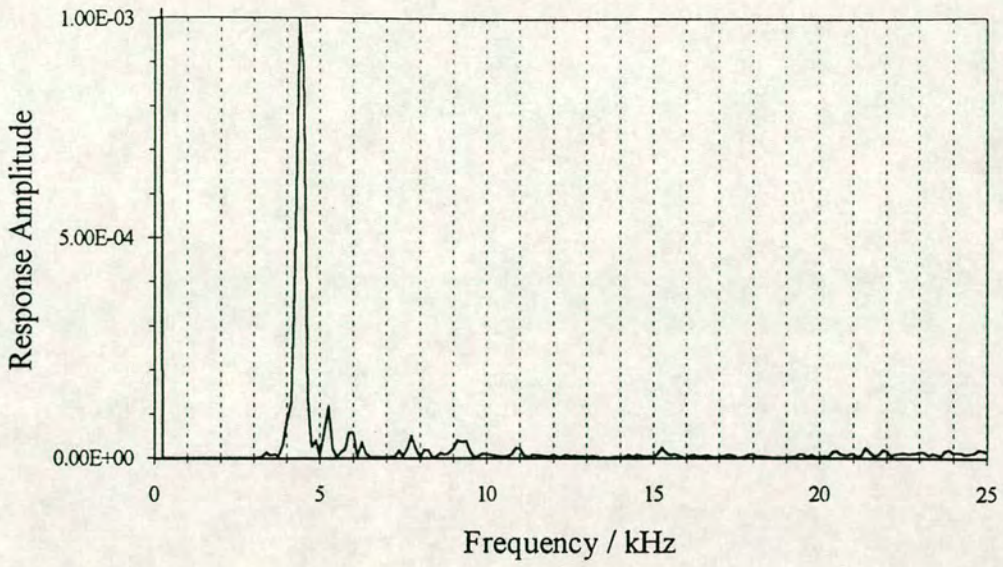

Fig 7.11a 0.1m from front end

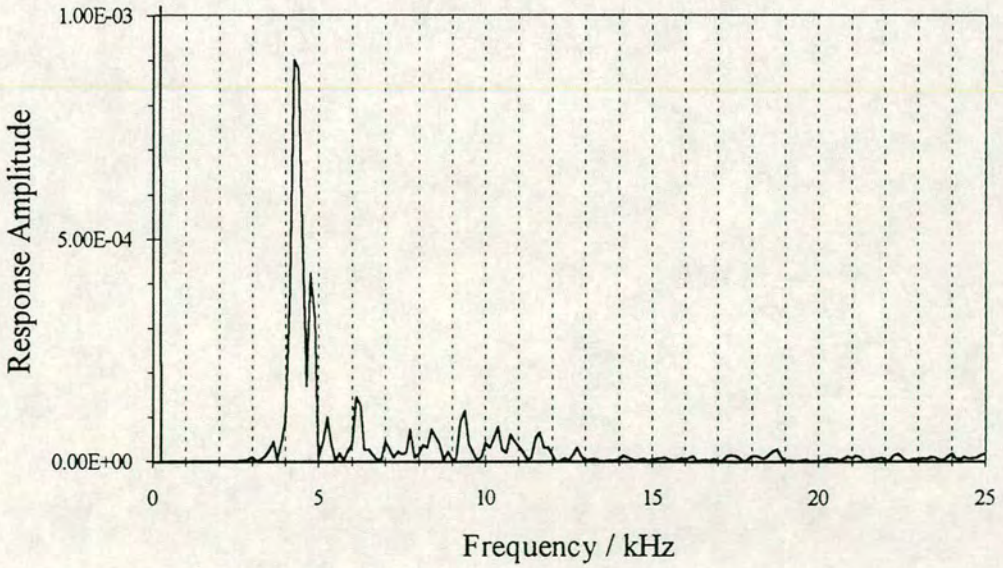

Fig 7.11b 0.2m from front end

Figure 7.11 TBV Stanger beam. Test along duct B on side B

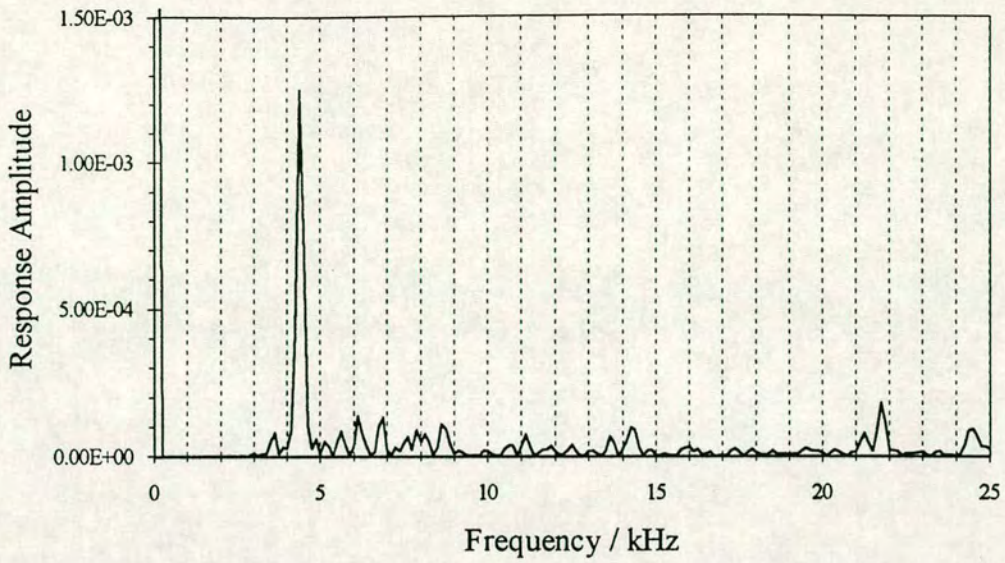

Fig 7.11c 0.3m from front end

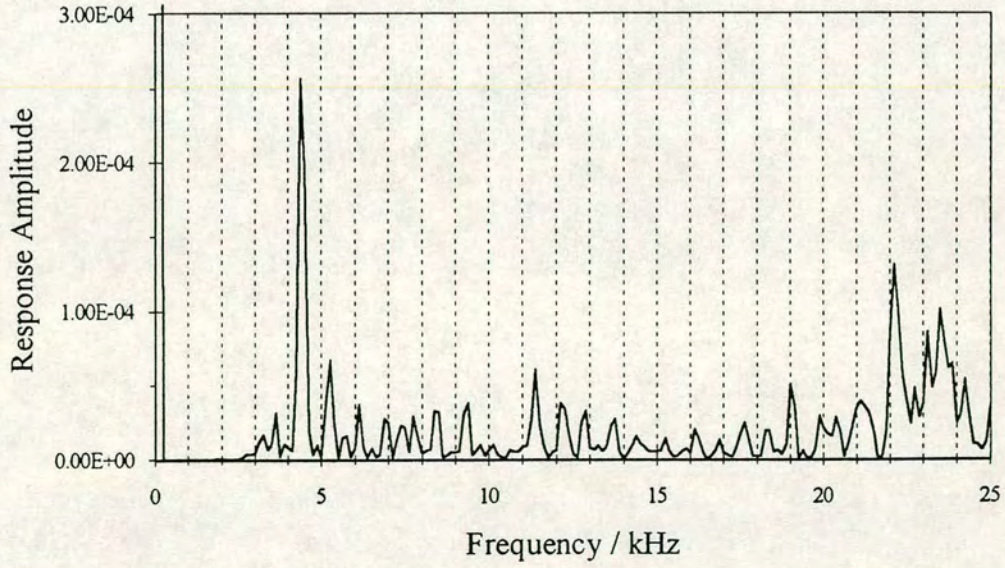

Fig 7.11d 0.4m from front end

Figure 7.11 (cont.) TBV Stanger beam. Test along duct B on side B

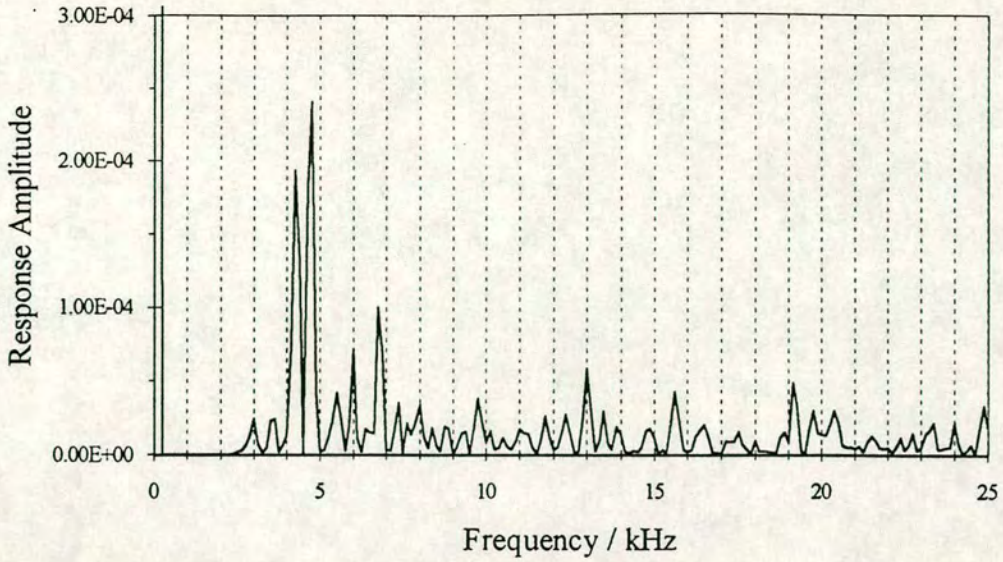

Fig 7.11e 0.5m from front end

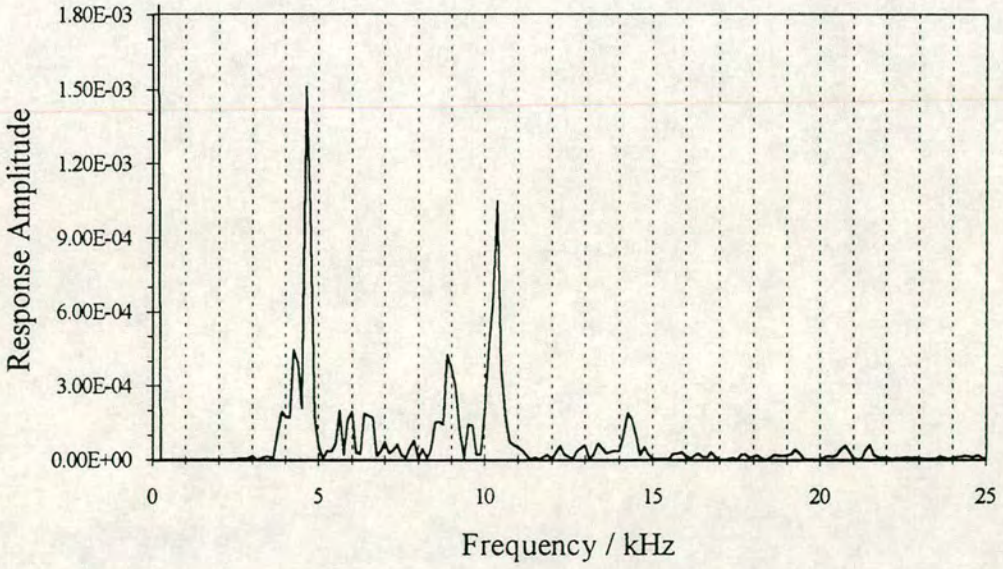

Fig 7.11f 0.6m from front end

Figure 7.11 (cont.) TBV Stanger beam. Test along duct B on side B

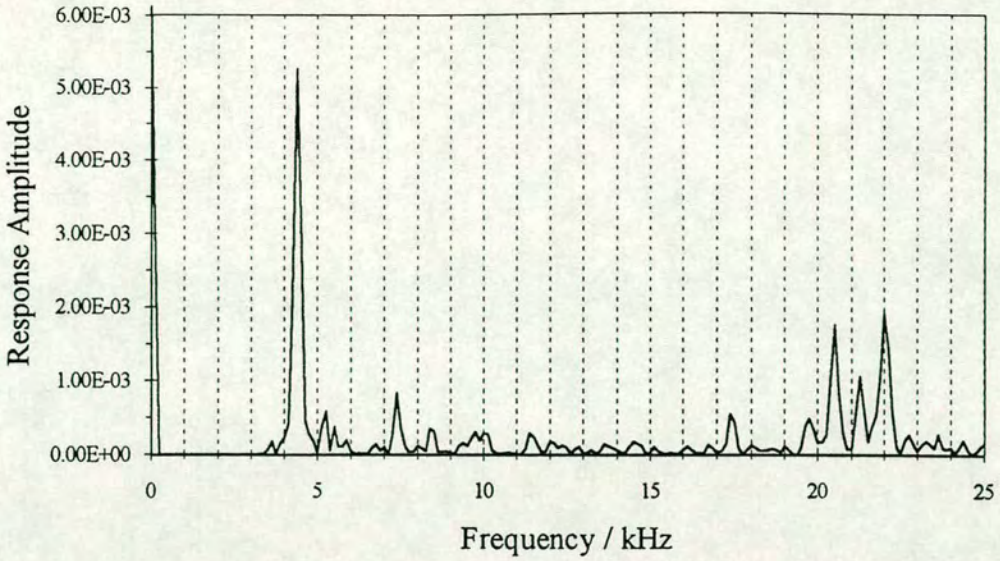

Fig 7.11g 0.7m from front end

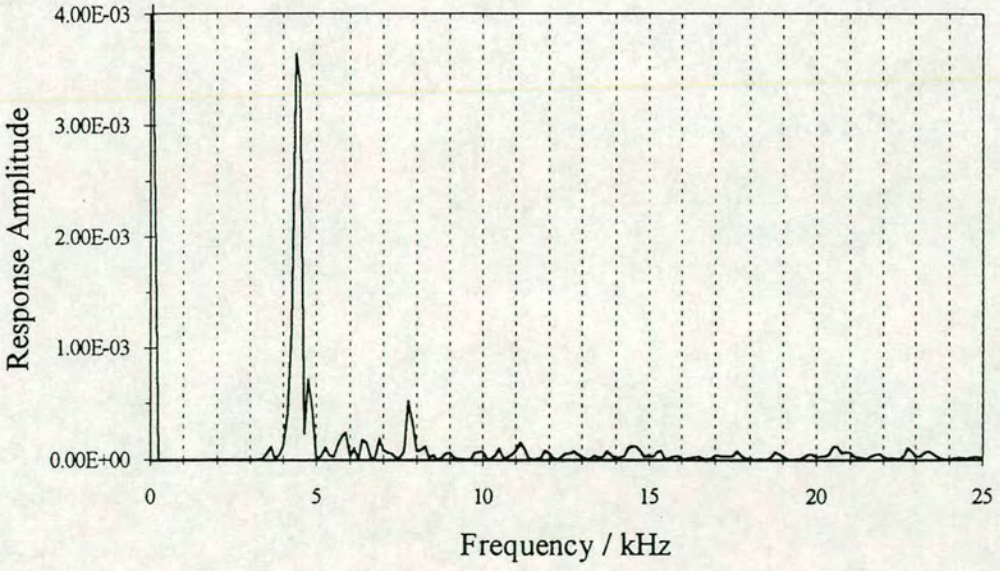

Fig 7.11h 0.8m from front end

Figure 7.11 (cont.) TBV Stanger beam. Test along duct B on side B

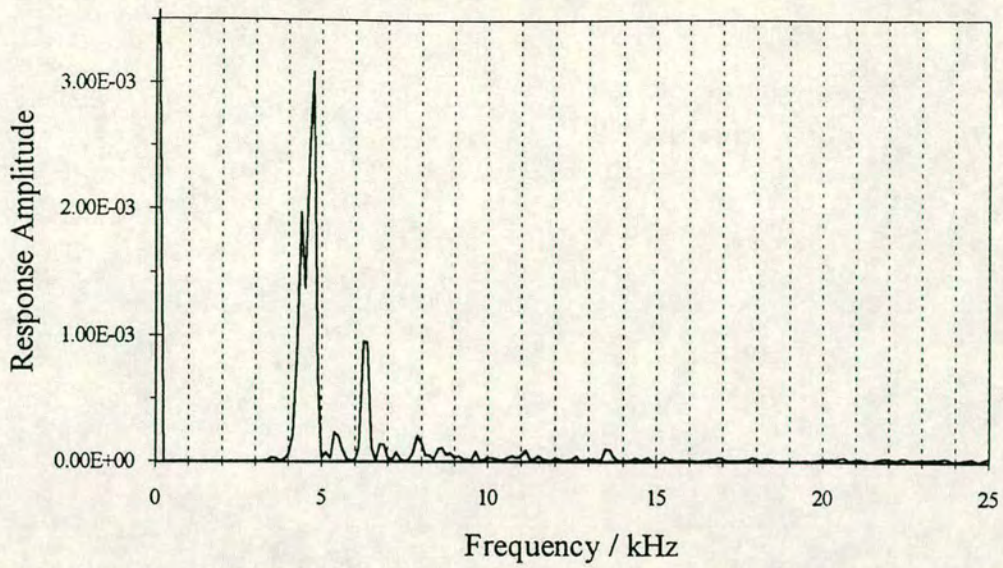

Fig 7.11i 0.9m from front end

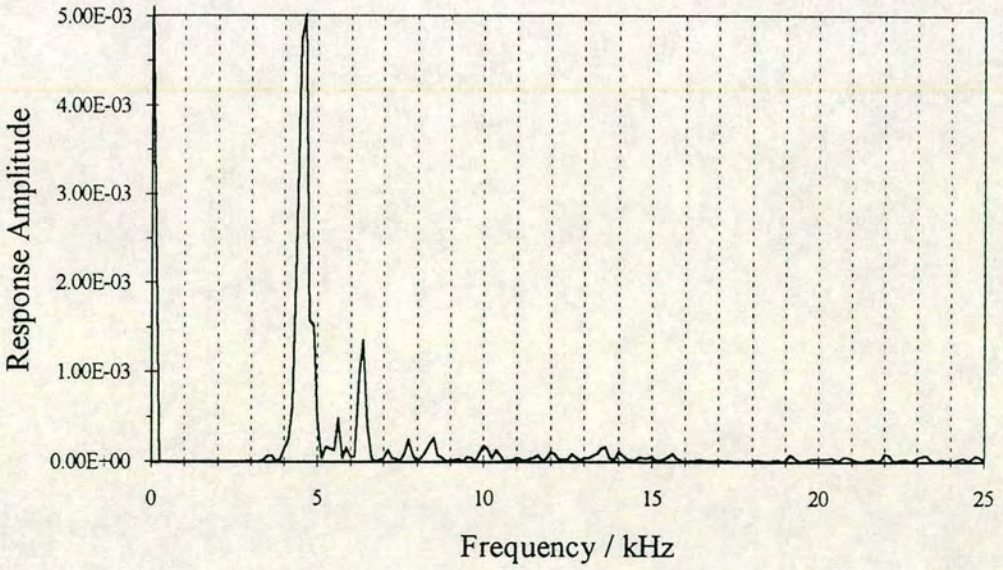

Fig 7.11j 1.0m from front end

Figure 7.11 (cont.) TBV Stanger beam. Test along duct B on side B

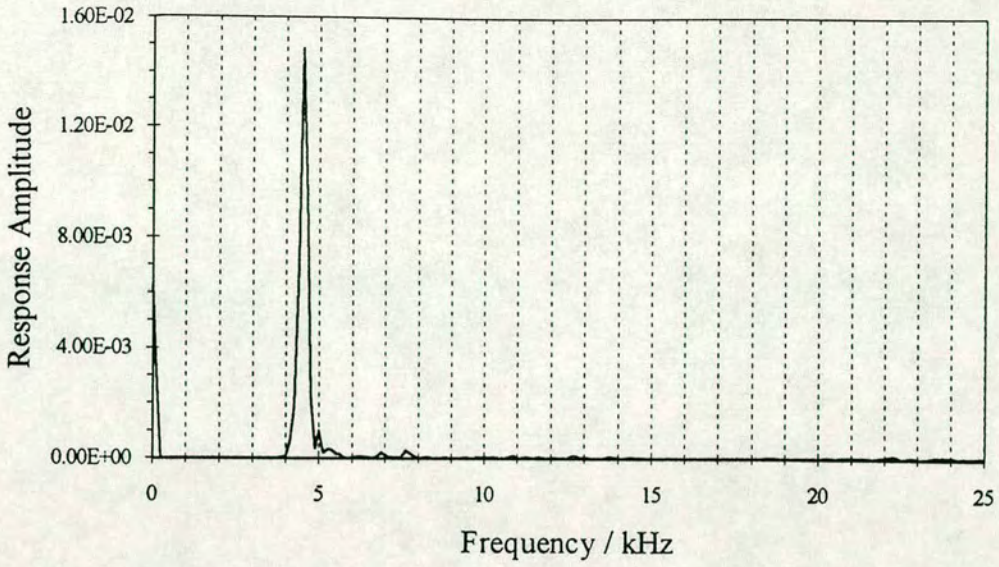

Fig 7.11k 1.1m from front end

Figure 7.11 (cont.) TBV Stanger beam. Test along duct B on side B

Test Position	Possible Targets - Tests from Duct A side	Possible Targets - Tests from Duct B side
0.1m	-	-
0.2m	void in duct B	-
0.3m	void in duct B, near void in duct A	void in duct B
0.4m	void in duct A, other targets within beam	void in duct B
0.5m	possible void in duct A, near void in duct B	-
0.6m	void in duct B	void in duct A
0.7m	void in duct B, void in duct A	Void in duct B
0.8m	edge of void in duct A, other targets within beam	target within beam
0.9m	-	reflection at 6.3kHz
1.0m	-	reflection at 6.3kHz
1.1m	-	-

Table 7.1 Summary of results from tests along the line of each duct

Table 7.1 shows a fairly good correlation of results. The conclusions reached at position 4 are ambiguous as are those reached at position 8. A more detailed test was undertaken at these positions to try to resolve this. The results from these tests are shown in figures 7.12 - 7.15.

The results found from tests carried out on both side faces at position 4 are shown in figures 7.12 and 7.13. These results seem to indicate that a void is present in Duct A and that Duct B is not voided at this point. The results are not always clear. Any frequency components measured could relate to a defect at a distance from the test location corresponding to the measured frequency but in any direction as sonic waves from a point impact have an almost hemispherical wavefront. Therefore, a reflection from a defect at an angle to the test location could easily be misinterpreted as a reflection from a a duct at a greater depth horizontally.

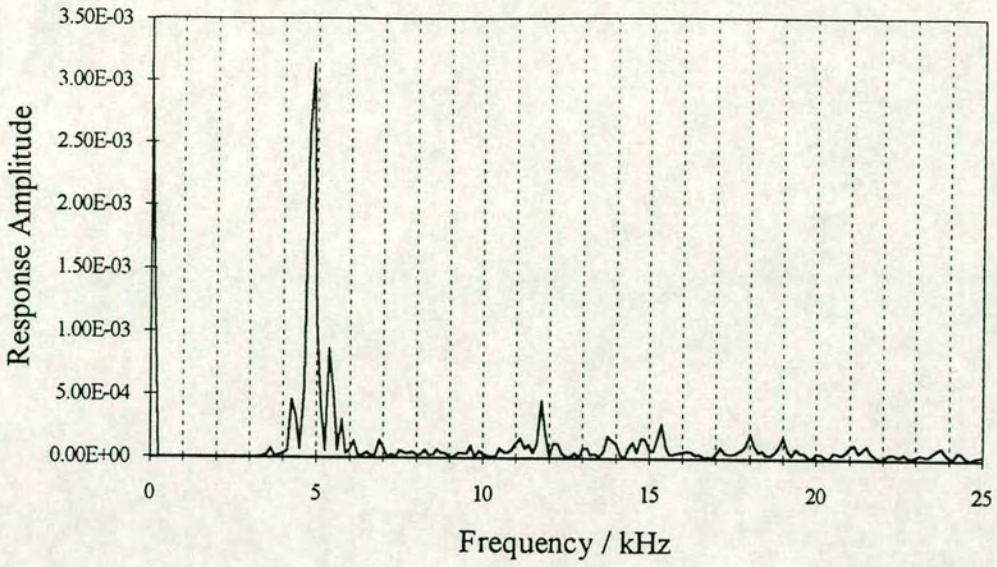

Fig 7.12a 0.1m from top surface

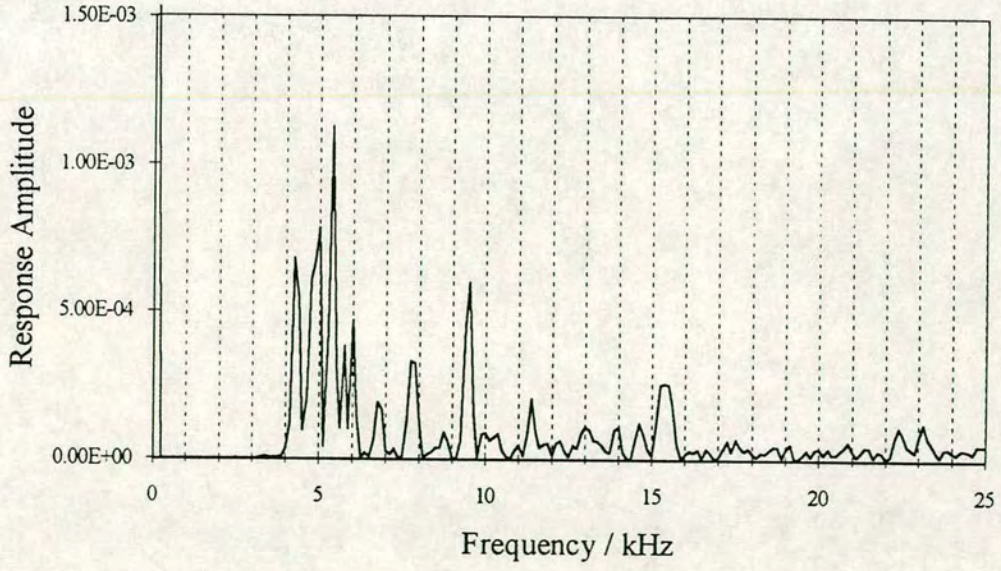

Fig 7.12b 0.2m from top surface

Figure 7.12 TBV Stanger beam, section 0.4m, side A

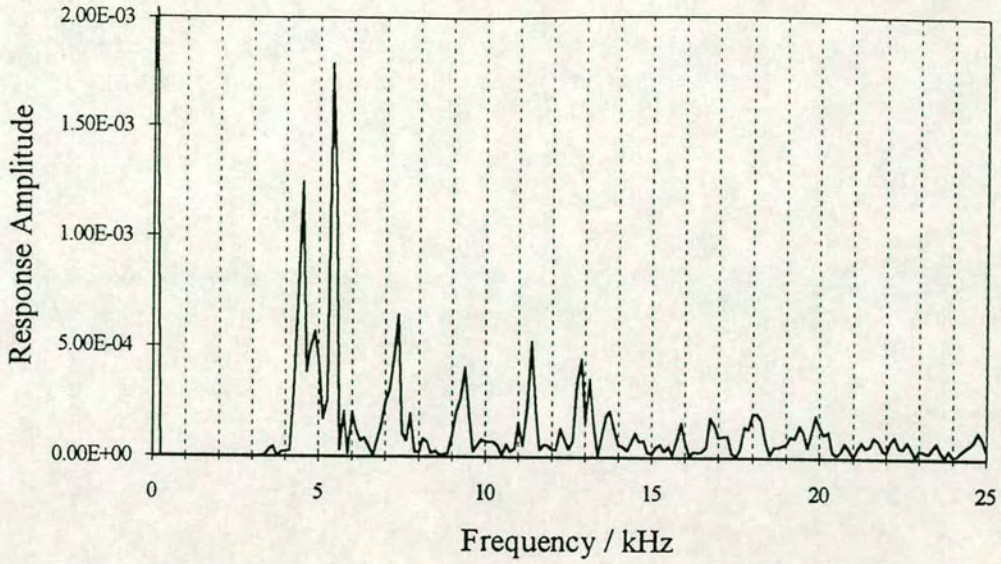

Fig 7.12c 0.3m from top surface

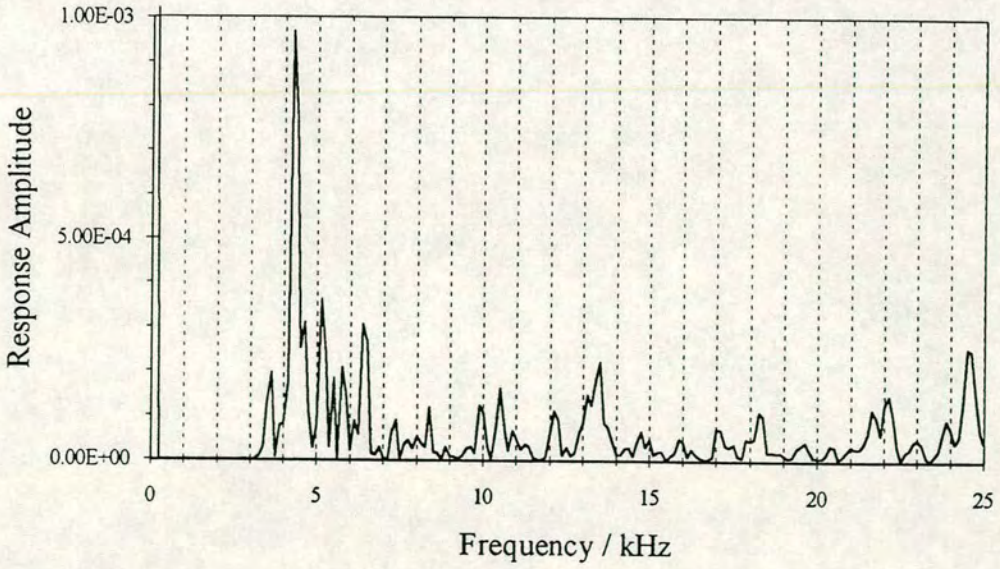

Fig 7.12d 0.4m from top surface

Figure 7.12 (cont.) TBV Stanger beam, section 0.4m, side A

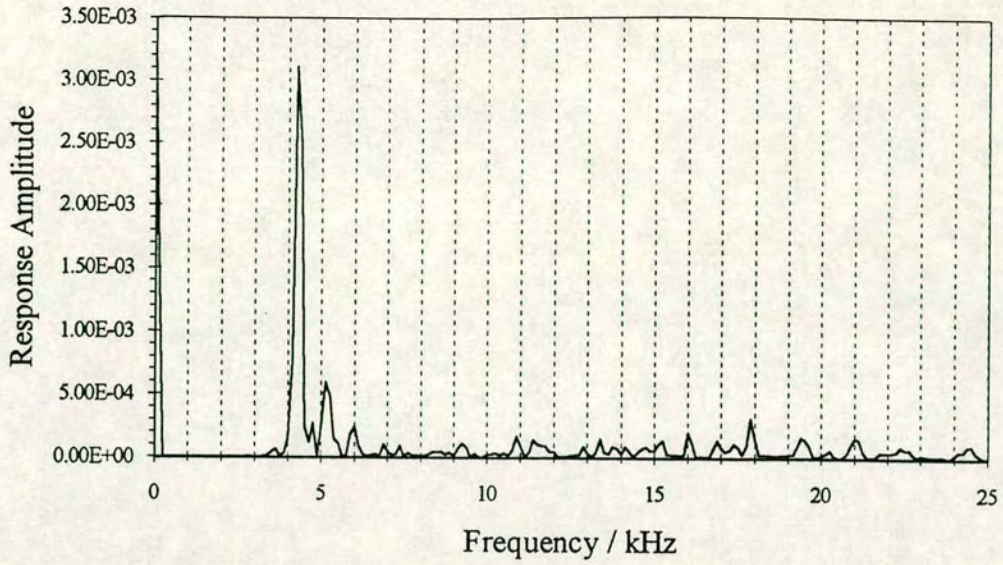

Fig 7.12e 0.5m from top surface

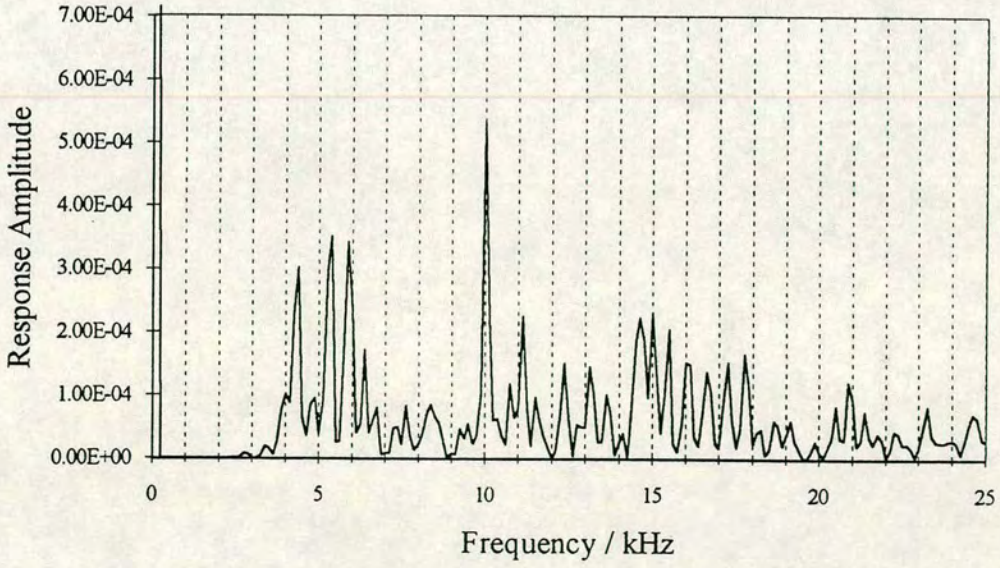

Fig 7.12f 0.6m from top surface

Figure 7.12 (cont.) TBV Stanger beam, section 0.4m, side A

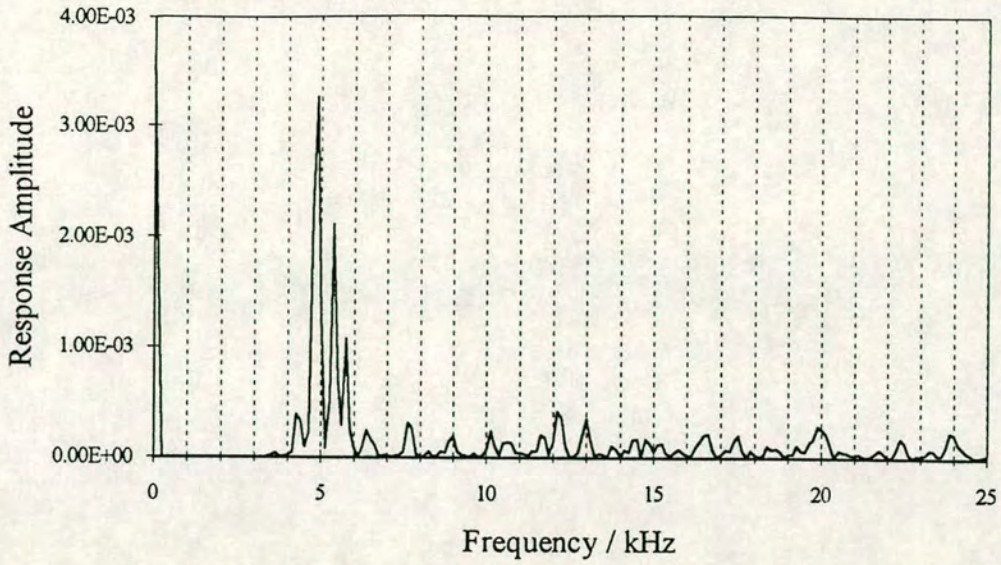

Fig 7.13a 0.1m from top surface

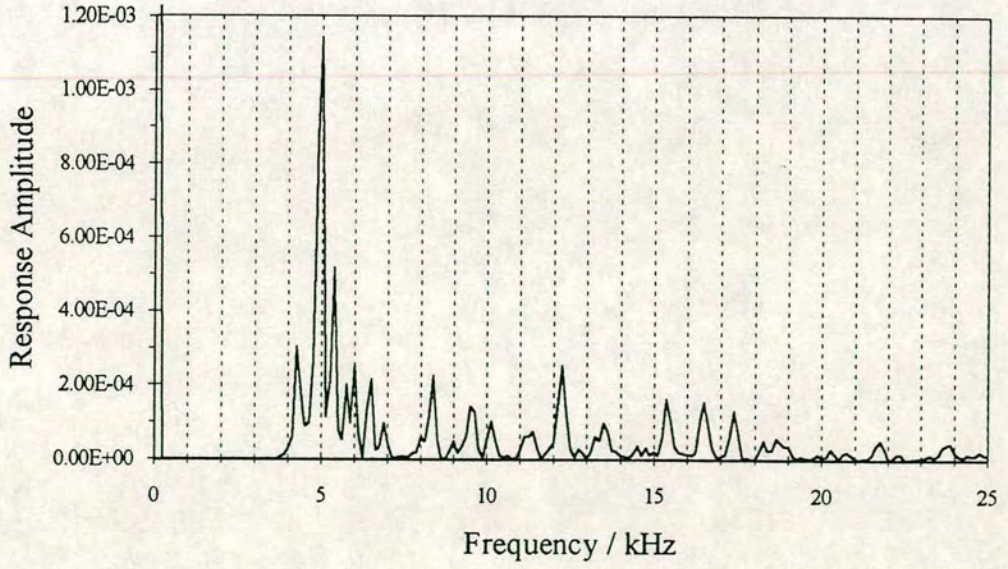

Fig 7.13b 0.2m from top surface

Figure 7.13 TBV Stanger beam, section 0.4m, side B

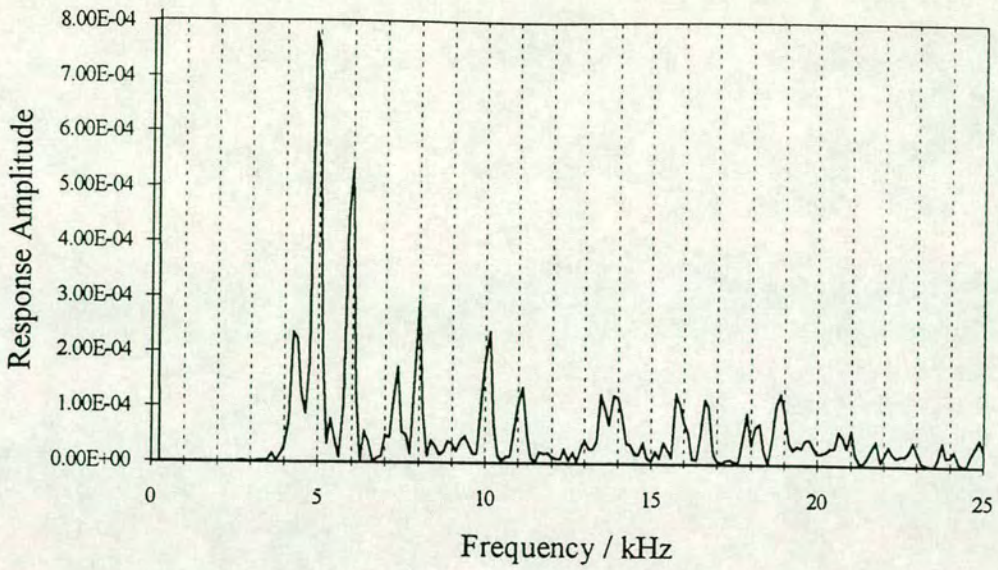

Fig 7.13c 0.3m from top surface

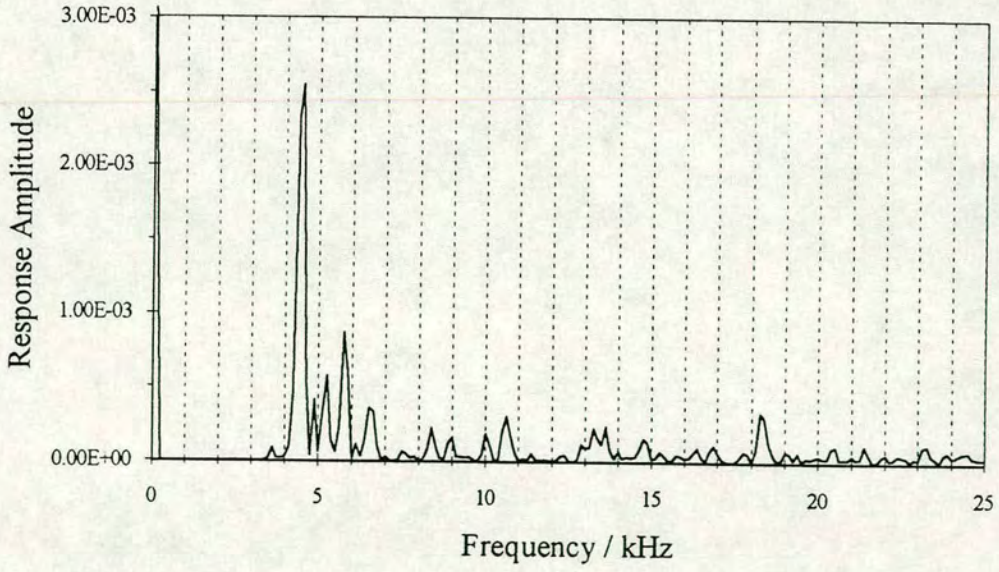

Fig 7.13d 0.4m from top surface

Figure 7.13 (cont.) TBV Stanger beam, section 0.4m, side B

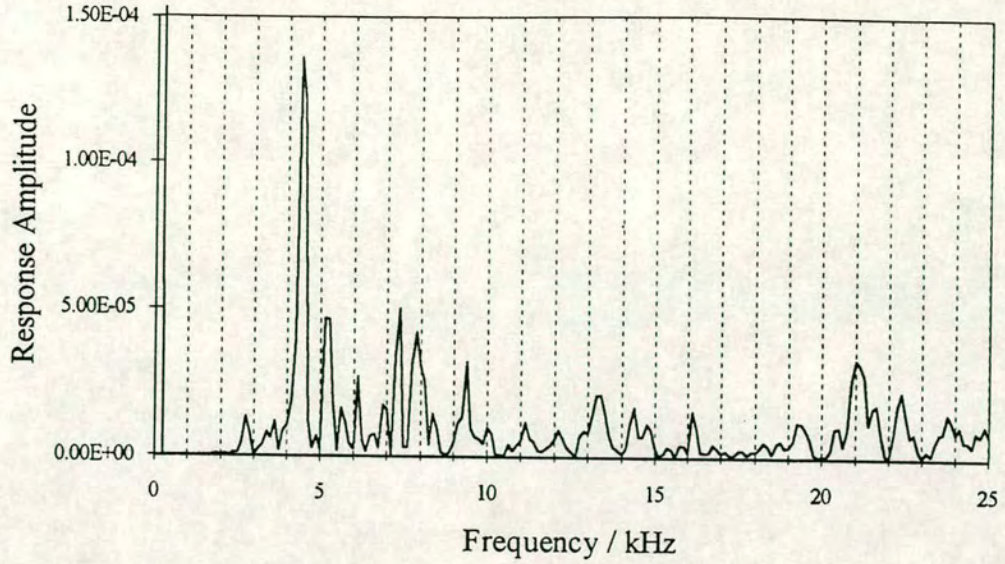

Fig 7.13e 0.5m from top surface

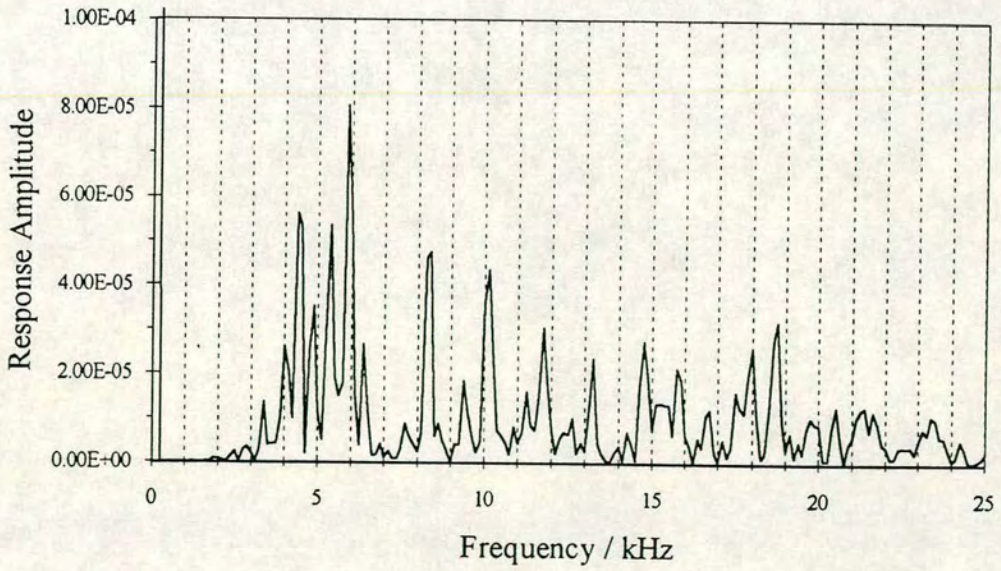

Fig 7.13f 0.6m from top surface

Figure 7.13 (cont.) TBV Stanger beam, section 0.4m, side B

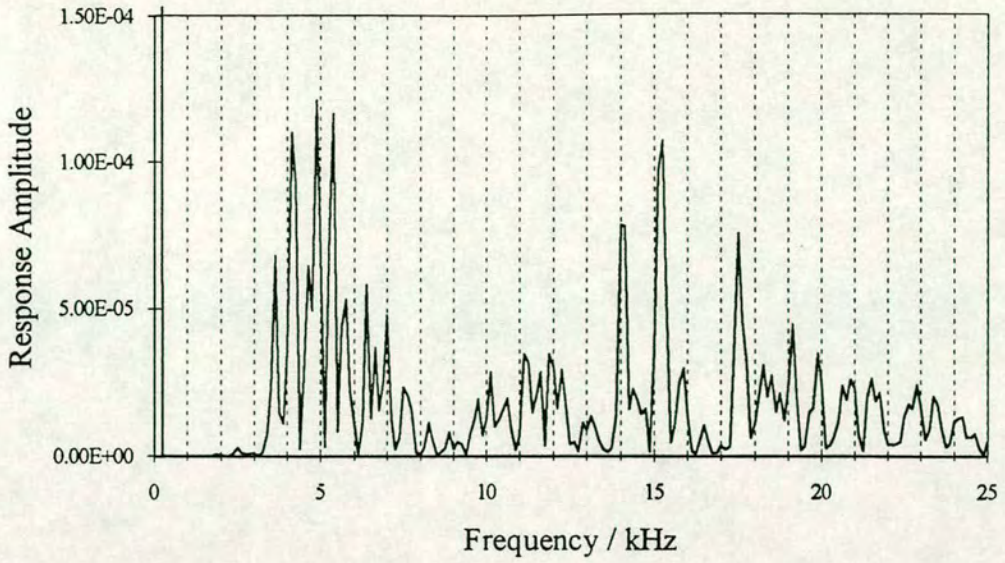

Fig 7.14a 0.1m from top surface

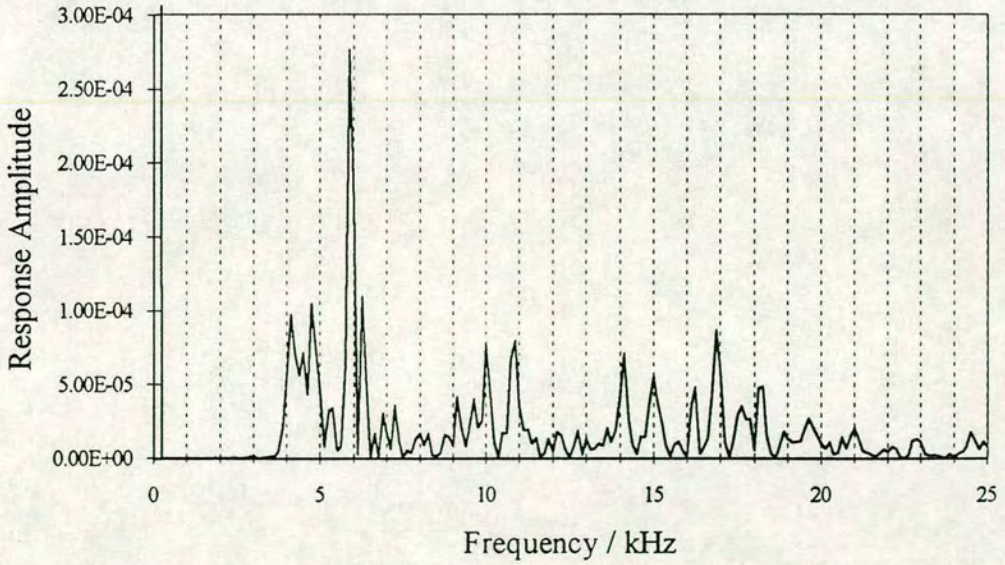

Fig 7.14b 0.2m from top surface

Figure 7.14 TBV Stanger beam, section 0.8, side A

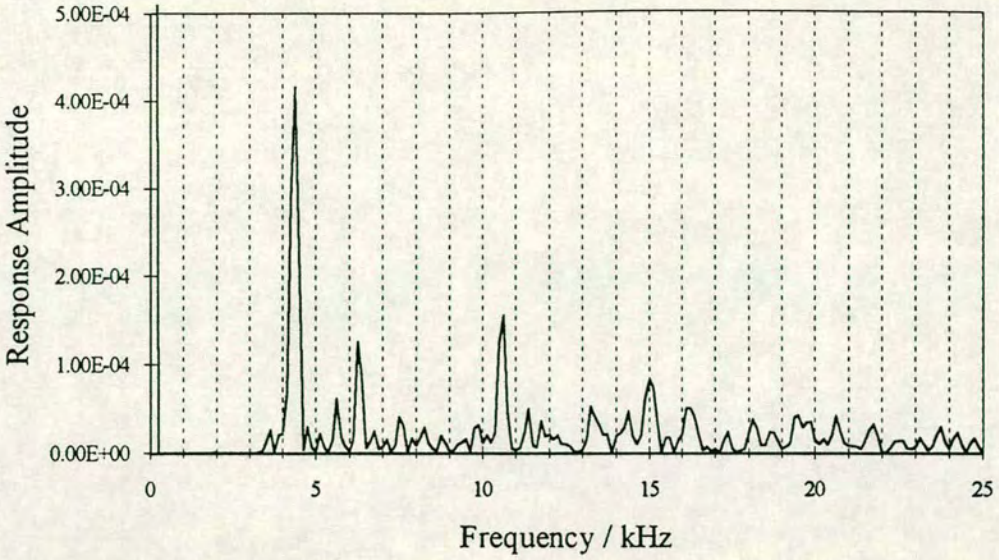

Fig 7.14c 0.3m from top surface

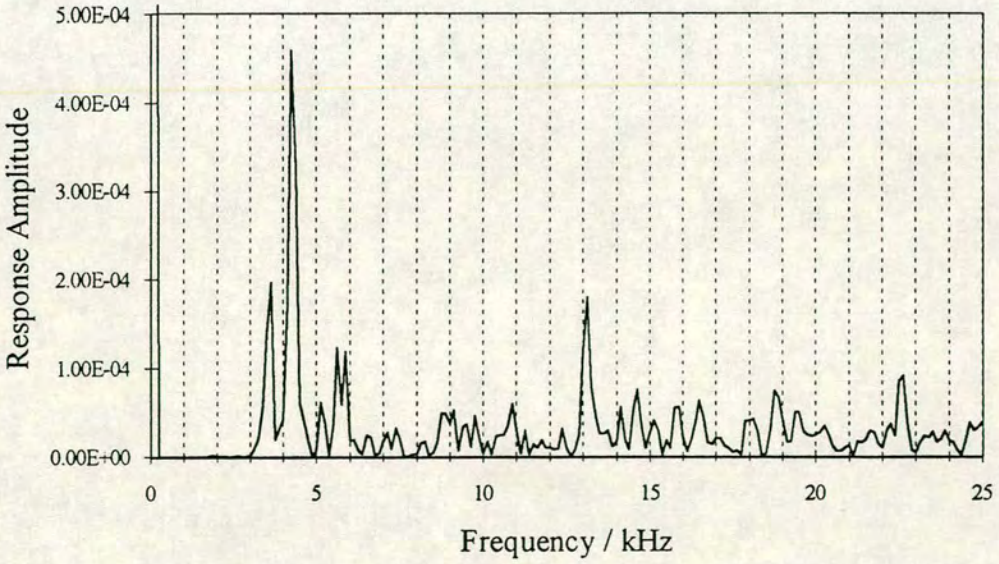

Fig7.14d 0.4m from top surface

Figure 7.14 (cont.) TBV Stanger beam, section 0.8, side A

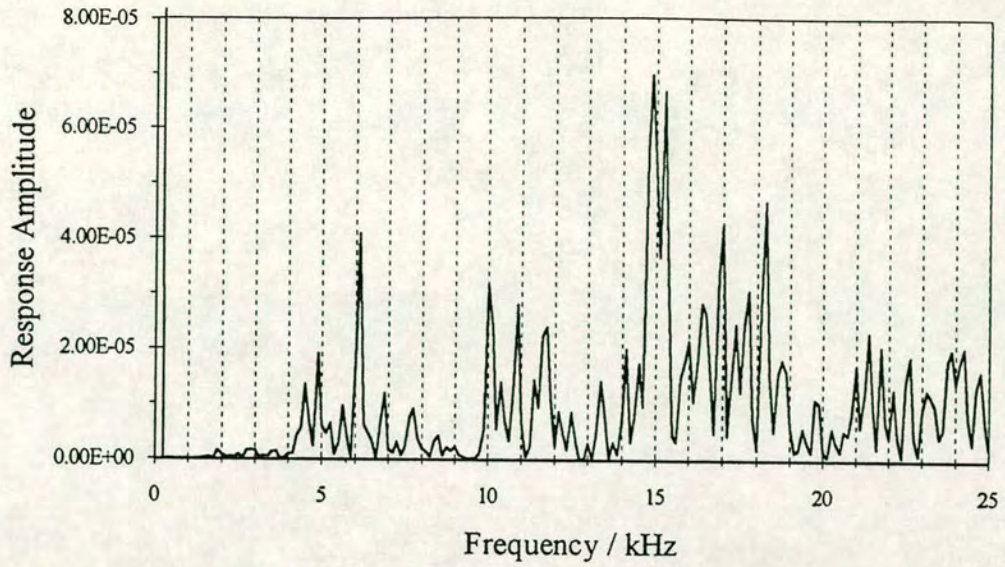

Fig 7.14e 0.5m from top surface

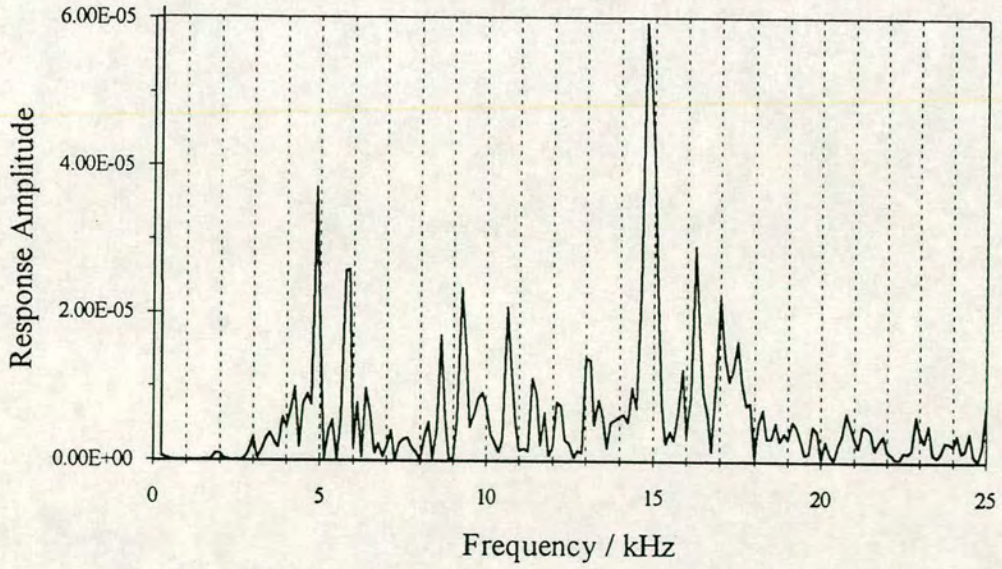

Fig 7.14f 0.6m from top surface

Figure 7.14 (cont.) TBV Stanger beam, section 0.8, side A

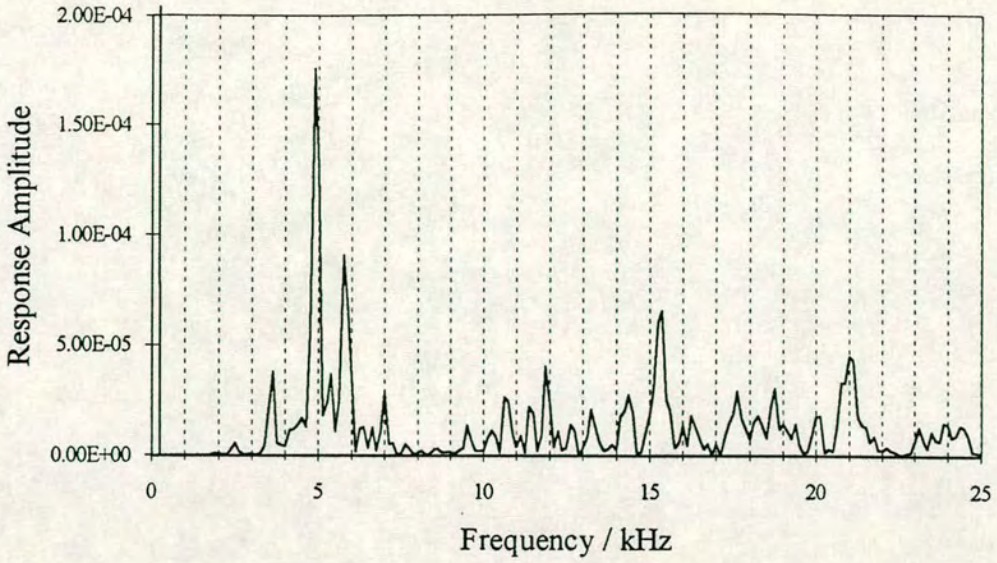

Fig 7.15a 0.1m from top surface

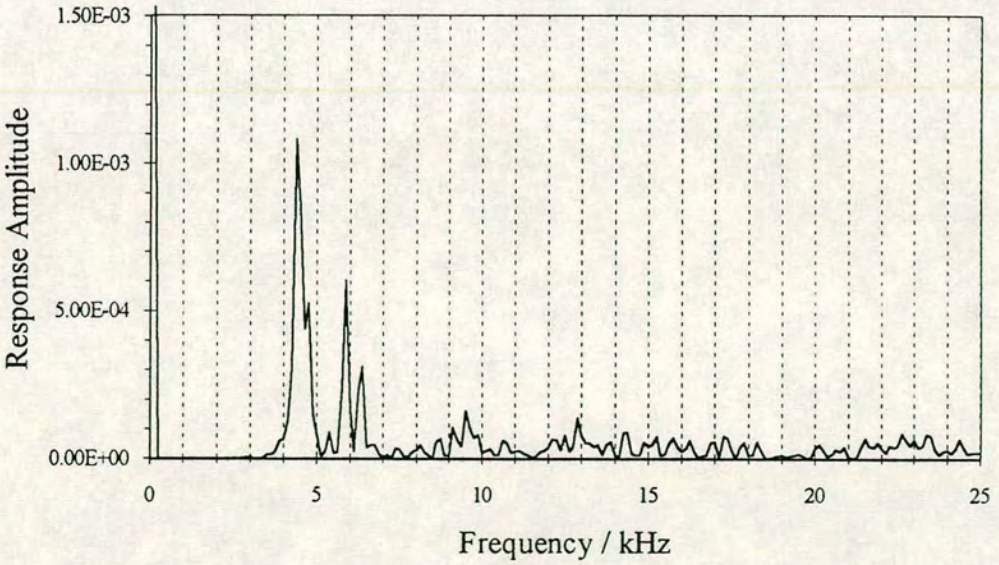

Fig 7.15b 0.2m from top surface

Figure 7.15 TBV Stanger beam, section 0.8m, side B

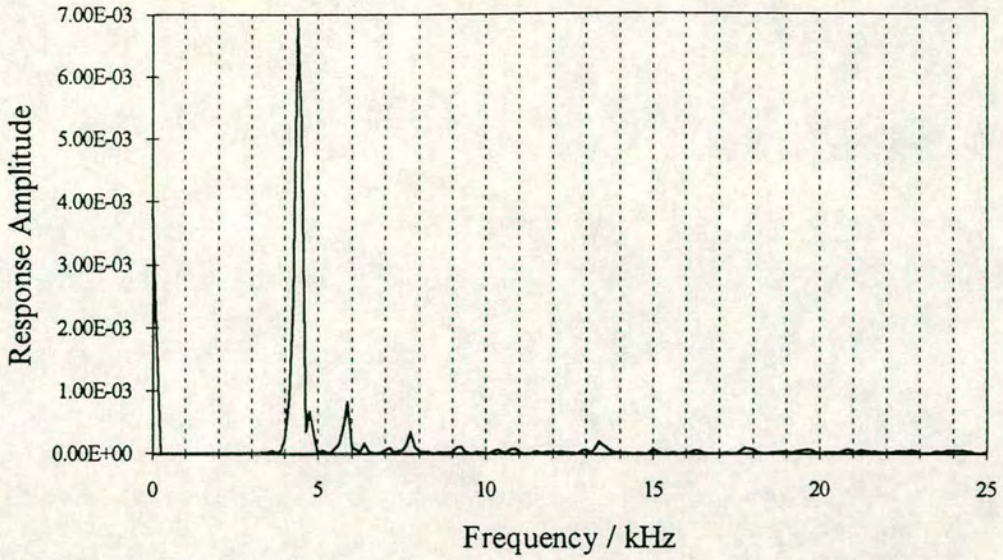

Fig 7.15c 0.3m from top surface

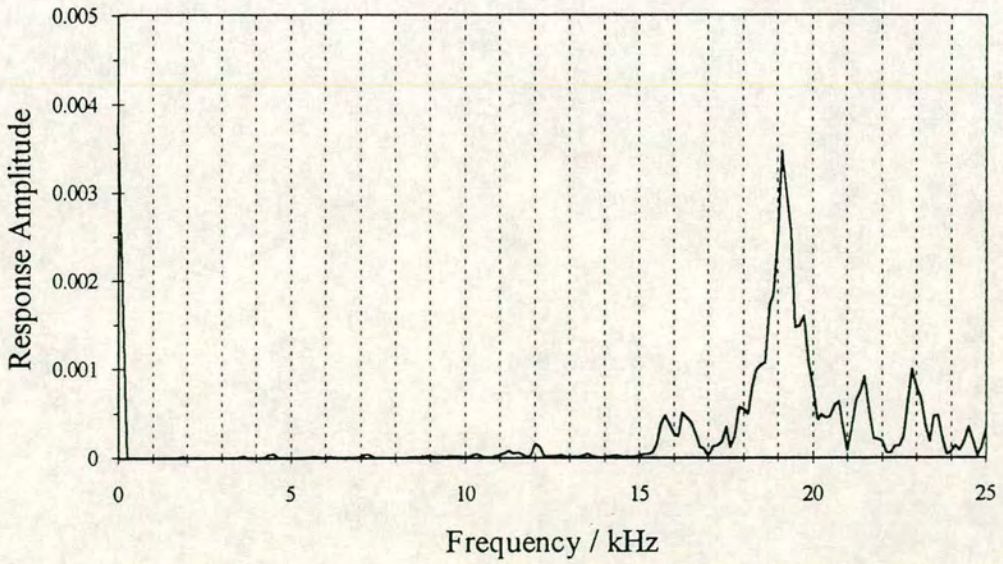

Fig 7.15d 0.4m from top surface

Figure 7.15 (cont.) TBV Stanger beam, section 0.8m, side B

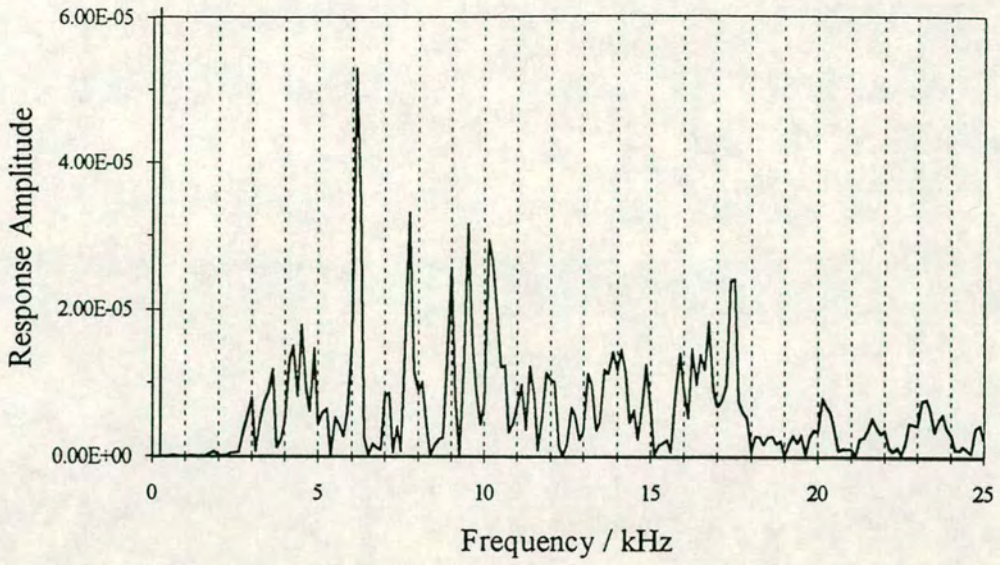

Fig 7.15e 0.5m from top surface

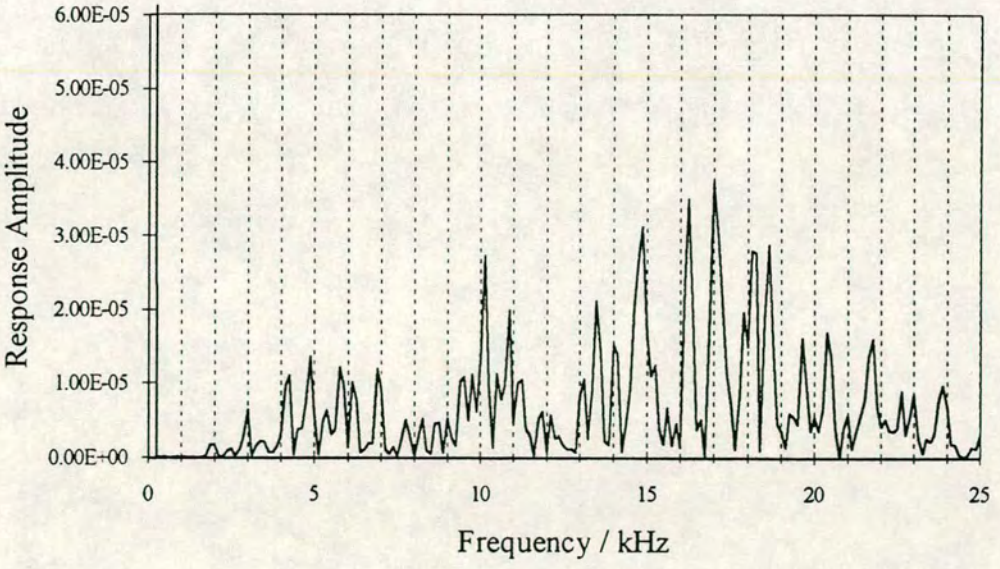

Fig 7.15f 0.6m from top surface

Figure 7.15 (cont.) TBV Stanger beam, section 0.8m, side B

The results from a section at 0.8m are shown in figures 7.14 and 7.15. The surface of the concrete on duct B side was in a poor condition in the lower half of the beam. In these areas the first beam mode of vibration has not been detected. This effect is more obvious on the tests undertaken on side B. The overall interpretation of the results at this position is that duct A may be voided, duct B is likely to be voided but that the general condition of the concrete is poor, especially towards side B.

The above results show that conclusions as to the condition of the beam and the individual tendons can be made using impact-echo testing. As with other non-destructive testing techniques the results are open to some interpretation and the confidence in any conclusions made will be greatly improved if they can be verified using another testing technique. As with the testing carried out at TRL, tomographic surveys were carried on sections of the beam.

7.5.2. Tomographic testing and results

Tomographic surveys were carried out at positions 0.4m, 0.8m and 0.9m from the front of the beam. The surveys at position 0.4m and 0.8m were undertaken to aid interpretation of the impact-echo results. A further test was carried out at position 0.9m in order that a comparison could be made to that undertaken at the section 0.8m from the front.

The tomographic investigation grid was set up on the sides and top surface of the beam with test points at a spacing of 100mm. The test set-up and analysis was similar to that used on the section on the TRL beam. The results for each section are shown in figure 7.16. The velocity contour plot from section 0.4m shows a clear reduction in velocity at the position of duct A. This, taken with the impact-echo results indicates that duct A is voided at this point. No clear indication of voiding in duct B is seen. An area of low velocity is shown in the lower right hand corner, however, this low velocity section is largely confined to the outer layer of pixels. The number of ray paths in these areas are small and unreliable results are to be expected.

Figure 7.16b shows a velocity plot at section 0.8m. Impact-echo results indicated possible voiding in both ducts, with Duct B being more likely to be voided and poor concrete in the lower section of the beam. These results are

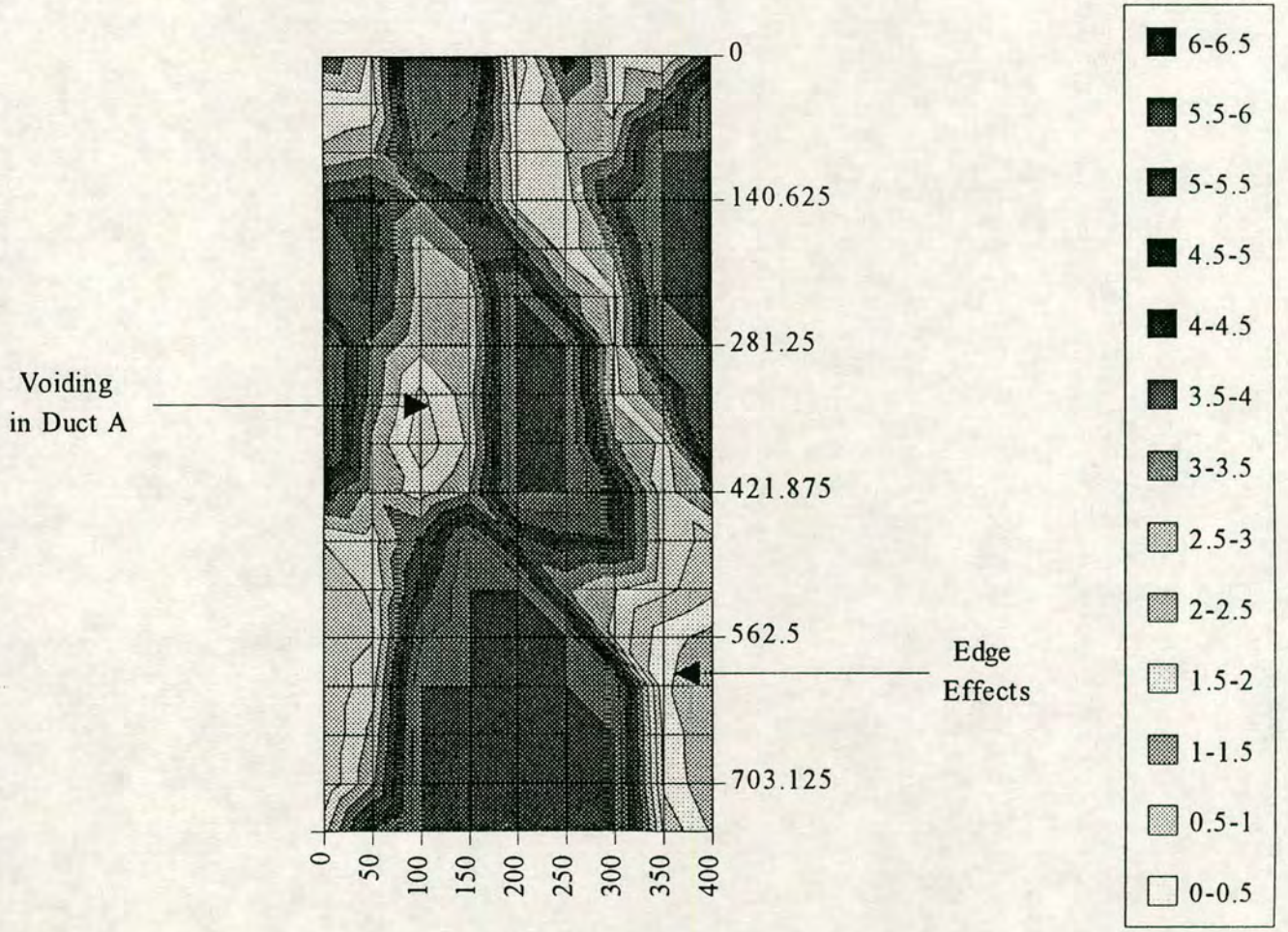

Figure 7.16a TBV Stanger beam Tomographic Survey. Position 0.4m from front end

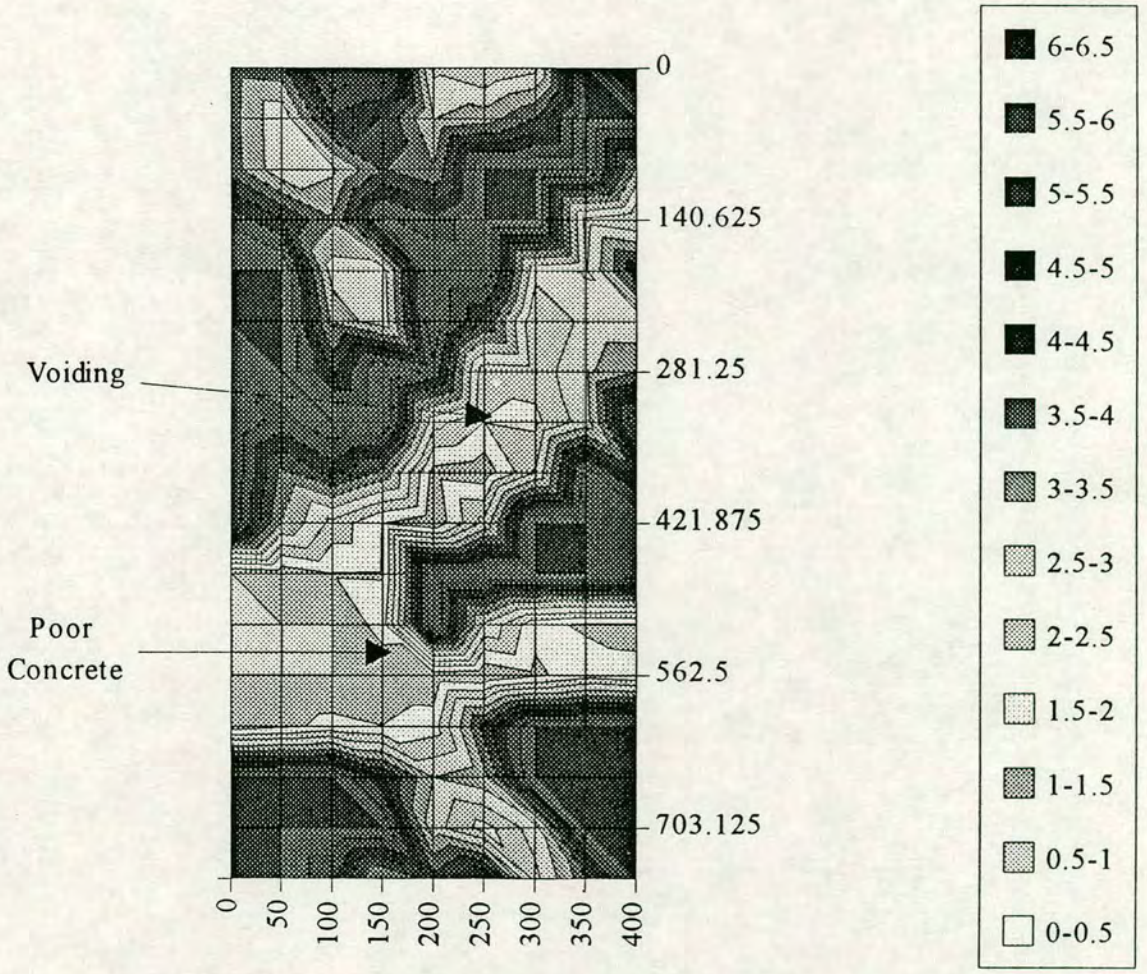

Figure 7.16b TBV Stanger beam Tomographic Survey. Position 0.8m from front end

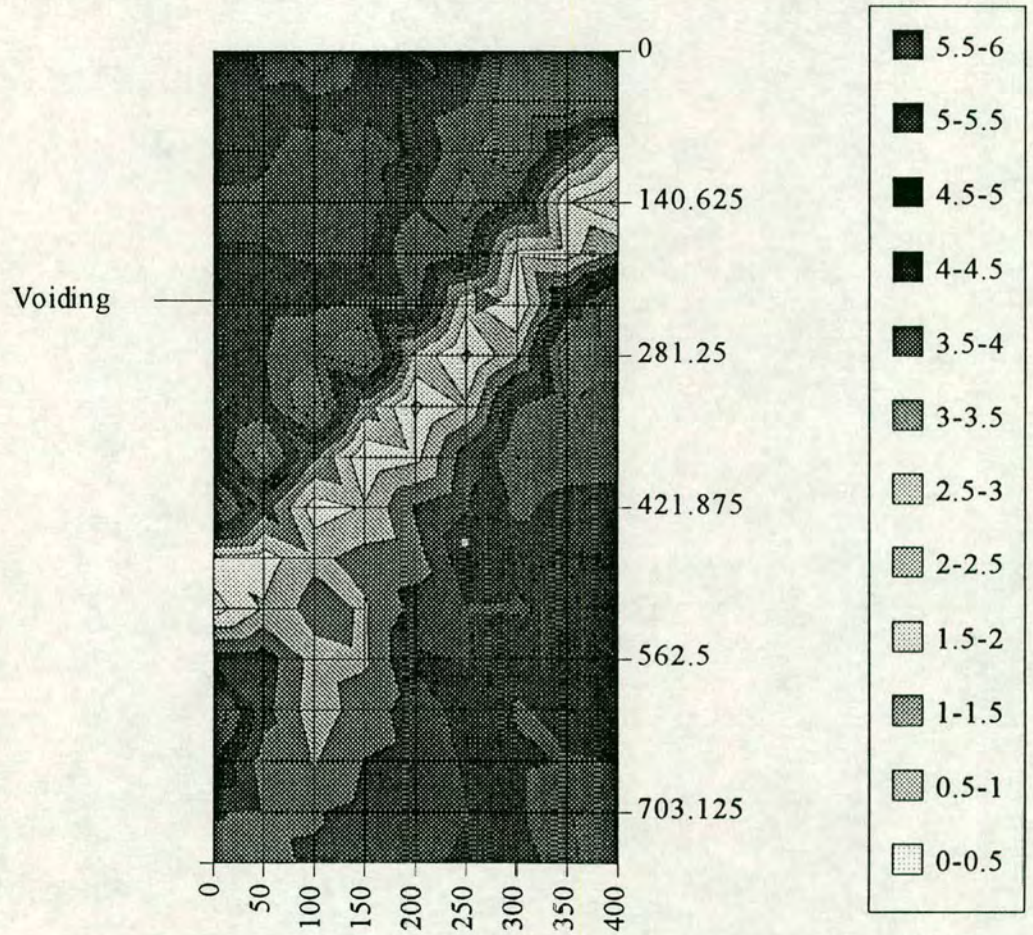

Figure 7.16c TBV Stanger beam Tomographic Survey. Position 0.9m from front end

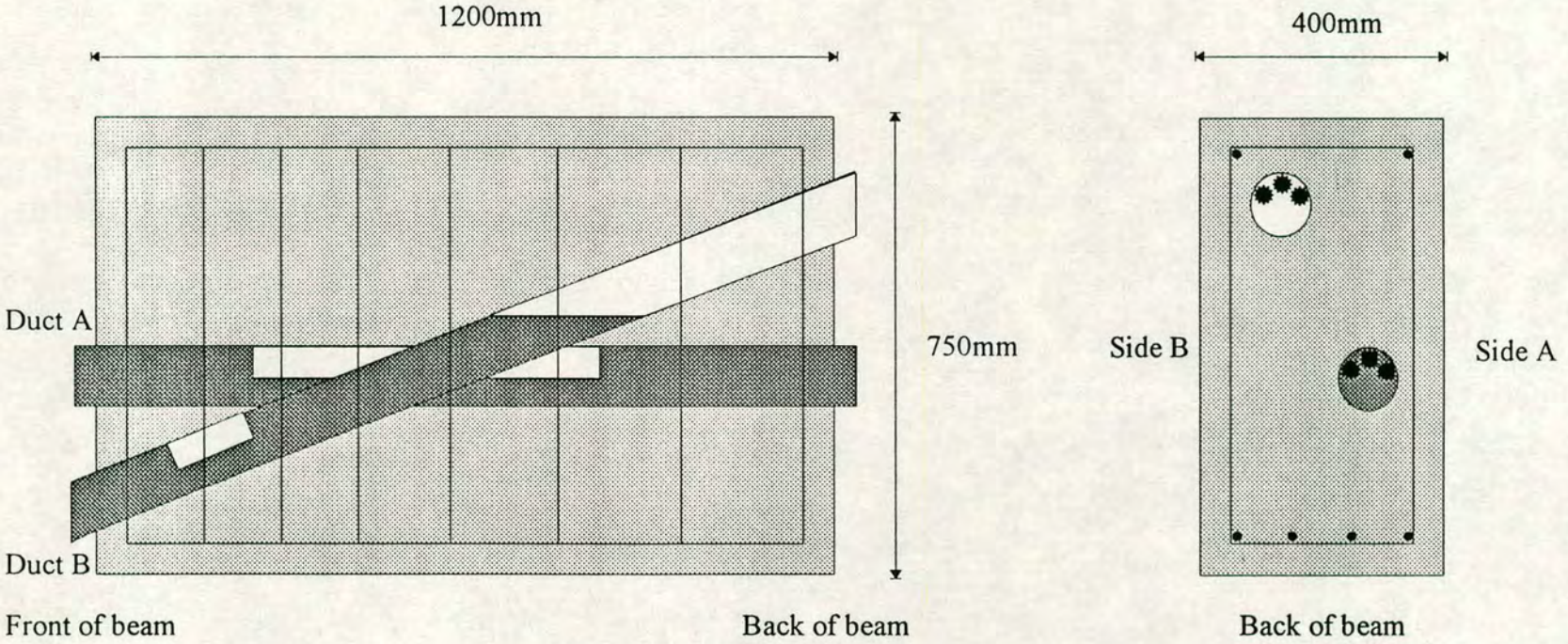

Note: The voids are formed by an air gap or a polystyrene box-out

Figure 7.17 TBV Stanger model with included defects shown

generally confirmed by the tomographic survey. A low velocity area can be seen in the lower part of the beam corresponding to poor concrete. The calculated velocity at the position of duct B (slightly above the centre and to the right) is reduced indicating voiding in this duct. The velocity calculated at the position of duct A seems similar to that of the surrounding concrete but lower velocity areas are clearly visible below this. Voiding in the concrete beneath the duct would give this tomographic response and could also give rise to the reflections measured using the impact-echo techniques. The velocity plot calculated at section 0.9m again indicates probable voiding in duct B and possible voiding in Duct A. The condition of the concrete surrounding the ducts appears fine at this section. The 100mm grid used is rather coarse for resolving the two ducts as they are lying next to each other at this section.

The constructed section of the test beam showing the planned defects is given in figure 7.17. From this diagram it can be seen that in general the non-destructive evaluation was succesful in determining the condition of the beam and tendon ducts. The tomographic surveys were particularly useful in confirming the condition of the beam at sections where the impact-echo testing had given ambiguous results.

7.6 Conclusions

1. Impact-echo techniques can be used to detect voiding in ducts of 100mm diameter at depths of 100mm to 200mm by the measuring of simple reflections from the defects. The testing method is most successful on simply reonforced rectangular beams.

2. The results from I-E testing are improved if a constant impact to measurement position separation is used. The problem of a variation in distance can be improved by repeating the test a number of times and recording a representative trace. This however, does not aid the comparison of tests at different positions. The OLSON transducer is set up to produce the impact and, once the reliability problems are sorted out, this transducer will provide a constant impact to receiver separation.

3. With further work it should be possible to investigate ducts of smaller diameter by analysing the relative frequencies of the modes of vibration of the beam. Response patterns could be identified and any deviation would indicate an area requiring further investigation.

4. As with other NDT techniques the use of impact-echo testing alone can be slightly unreliable. The reliability would be improved if the impact was measured and signals from different locations could then be directly compared. At present this is not possible and so another NDT technique can be applied at positions of interest to further investigate the impact-echo findings. One such technique in time of flight tomography.

5. Time of flight tomography provides a highly successful method of investigating post-tensioned concrete beams. The method is somewhat time consuming and so should be used in conjunction with a simpler testing method, eg. sonic impact-echo, which identifies areas of interest. The smaller the ducts to be investigated, the smaller the required distances between testing stations. This therefore significantly increases the testing time. However, array systems could be developed which would greatly reduce the testing time.

Chapter VIII

Discussion and Recommended Testing Procedure

The results and conclusions formed in previous chapters are discussed with particular reference to their practical applications. A recommended testing procedure using sonic impact-echo techniques is proposed.

8.1 Possible Testing Techniques and Reasons for developing I-E method

Many non-destructive investigation methods are currently commercially available to investigate concrete structures (Bungey, 1992). The method most suited to each testing situation depends upon the size of the structure and the 'target' to be investigated. Another important factor in deciding upon which investigation technique to be used is the required accuracy of the investigation. Very accurate methods are available to test concrete, e.g. radiographic techniques, but these can be very expensive to implement on a wide scale, can cause harmful radiation which requires sheilding or possible evacuation of the area surrounding the test site, and are best suited to thin concrete sections with good access.

Post-tensioned design methods have been widely implemented for the design of the United Kingdom's motorway and trunk road system. Widescale testing is therefore required necessitating the development of a rapid, straightforward but accurate testing system. Traffic disruption must also be kept to a minimum as motorway or trunk road closures can be very expensive. The above reasons generally result in radiographic techniques being unsuitable for all but the most critical bridge inspections. There is no doubt that these methods offer an accurate testing procedure but the expense, disruption and health risks outweigh its use for most post-tensioned bridge inspections.

The ducting used on many post-tensioned bridges is metallic. This forms a highly reflective barrier to electromagnetic raditation of all but the shortest wavelengths, (X-rays and Gamma rays). Electromagnetic investigation techniques utilising radiation of longer wavelengths, e.g. ground penetrating radar, GPR, cannot be applied successfully to investigate the internal condition of metal ducted tendons as most of the energy in the incident wave is reflected at the concrete-metal boundary. It is therefore not possible to investigate the internal condition, and therefore the tendon state, of metallic ducts using GPR.

Sonic Impact-echo techniques have been used extensively to commercially, non-destructively test piles. Recent research carried out at Cornell University in Ithaca, USA has resulted in the development of an impact-echo test system which is now available commercially. This has been used to carry out initial testing of ducts within concrete with some success. A similar testing technique was used at the University of Milwaukee-Wisconsin, USA to investigate voided ducts. The conclusions drawn from each test series conflicted in some areas and although neither set provided a

analysis of the testing method it was shown to be a possible investigation method for the investigation of metal ducted post-tensioned bridge beams.

8.2 Location of ducts for impact-echo testing

The sonic impact-echo method can detect voids within ducts as the difference in the acoustic properties at a concrete/air interface results in a large reflection of energy. This is then measured at the surface of the specimen. However, at a grouted section of a duct, no reflection is measured since the acoustic properties of concrete and grout are very similar. The thin metal duct (usually 1 to 2mm thick) is not detected by the passing wave as its wavelength is too long. This is discussed in a later section where the lack of reflection from the metal duct is shown using finite element techniques. The acoustic properties of grout differ slightly from those of concrete. A slight reflection can therefore occasionally be detected but generally sonic impact-echo techniques are not suitable to determine the location of the ducts.

It is important to locate the ducts accurately as interpretation of impact-echo results becomes much more informative if any 'targets' found can be shown to be within the duct rather than in the surrounding concrete. Ducts can usually be located using any available construction drawings. However, a GPR survey can show any deviations from these drawings and also give an indication of voiding or other defects in the concrete section, outside the tendons. Voiding in these regions is unlikely to be as detrimental to the strength of the beam as voiding within the ducts. A GPR survey will also give an indication of the position and density of reinforcement in the section. A sonic impact-echo survey is unlikely to locate the reinforcement accurately for the similar reasons to why it cannot detect the metal ducting.

When carrying out an investigation into post-tensioned bridge beams it is beneficial to perform an initial GPR survey. Much research has been caried out into the application of this technique to concrete and there is therefore considerable literature available.

8.3 The expected size of tendon ducts in post-tensioned bridge beams

The size of defect detectable is the principal element in a sonic impact-echo test. This is controlled partially by the test configuration and instrumentation but the most important limiting factor is the maximum frequency of excitation. For impact-echo tests with planar targets, the size of the minimum target detectable is of the order of 1/2.6 of the wavelength of the highest frequency of excitation, where $f = 1/T_c$. The method developed has a minimum, repeatable time of contact of 47μs on good quality concrete, using a 4.7mm diameter ball-bearing hammer. This corresponds to a

method developed has a minimum, repeatable time of contact of 47μs on good quality concrete, using a 4.7mm diameter ball-bearing hammer. This corresponds to a frequency of excitation of approximately 21kHz giving the smallest target detectable of 73mm (assuming a compression wave velocity of 4000m/s). The minimum depth at which a target can be detected repeatably is half the minimum input wavelength. Targets which present a smaller profile to the incident compression wave than $\lambda/2.6$ or which lie at a depth lower than half the minimum wavelength may be detected but, if a reflection is not present on the measured response, it cannot be stated with confidence that no defect smaller than that specified or at a closer depth to the surface is present in the test specimen.

Post tensioned bridge beams contain ducts of different diameters. It is more economical to provide fewer, larger diameter tendon ducts containing more tendons than many small diameter ducts with fewer tendons. The tensioning procedure is more straightforward with smaller numbers of ducts and grouting is also easier within a larger duct. A normal size of duct is therefore approximately 100mm in diameter or greater (M40 bridges). The test beam at TRL contained ducts which were 40mm in diameter. This beam was only 10m in length and the tendons were tensioned to allow the application of different testing methods. However, the developed sonic impact-echo method is unlikely to be able to confidently determine the condition of tendons within 40mm diameter ducts. The results found at TRL are therefore inconclusive. However, tests carried out on 100mm diameter ducts show the method to be applicable on beams with ducts of this size.

8.4 The Use of Finite Element Analysis as an investigation tool

The construction of many concrete specimens to test the limitations of the proposed method would be very time consuming and uneconomical. It was important to determine early in the research whether the proposed method could be developed successfully. The finite element method offered an economic and efficient method of determining this and also the range and limitations of application. Much research and development was required to produce instrumentation capable of carrying out a sonic impact-echo survey of a concrete bridge beam. If a simple finite element model of an impact on a two dimensional concrete section containing a large void showed the method incapable of detecting the void, it would be highly unlikely that the practical impact-echo test procedure would be successful.

Finite element analysis offers a method of investigating an idealised situation. The materials are assumed to be ideal, e.g. homogeneous, and coupling problems are not measured as the displacement of the beam is calculated directly during the analysis. No signal noise is modelled and the impact can be modelled as a perfect half sine wave of up to infinite energy and with a contact time of any length. The majority of the analyses carried out for this thesis involved two dimensional finite element models. Any effects resulting from a three-dimensional defect or beam component are not shown on the results, thus again simplifying the result. More complex analyses can be carried out modelling actual impacts, including signal attenuation and realistic input energy levels.

For the work discussed in this thesis, the finite element method was used to carry out an initial investigation into the method to determine whether it could possibly be developed into a suitable testing technique. A laboratory model was constructed to aid the practical development of the technique for use in the field and further, more detailed finite element analyses carried to determine the likely range of application of the method. These results were verified in the laboratory by constructing a simple model similar to one of those modelled mathematically.

It can be concluded that simple finite element analysis offers an excellent method for the initial examination of a proposed test method and also an efficient method of investigating the range of application of the method.

8.5 Use of time and frequency domain traces in mathematical and experimental analyses

8.5.1 Time domain analysis

The time/response trace was initially measured during the practical and mathematical tests. This trace gives valuable information regarding the quality of the impact. If a poor quality or a double impact has occured, it can easily be seen on the time trace. A poor quality impact would occur if the concrete at the impact point crumbled or the surface was irregular. This would show on the time trace as a change in the initial trough, e.g. the trough could become irregular and contain further dips, etc. A double impact can easily be seen on the time trace as a high amplitude response at a time after the initial impact response. It occurs when the hammer is held too rigidly and vibrates on the test specimen.

Irregularities in the measured response of a structure to an impact also occur due to problems with the measurement instrumentation. Signal noise can cause inaccuracies of interpretation and is especially deleterious when the impact signal is of a small amplitude, e.g. with the smaller impact hammers. This is dificult to identify on a frequency domain trace but can usually be seen on the time domain trace as the amplitude of the noise does not attenuate.

If any of the above faults are noted in the time domain trace, the impact-echo test should be repeated.

8.5.1.1 Estimation of contact time from response time trace

The impacts used for the finite element analyses were modelled as half sine waves of predetermined duration and amplitude. The resulting displacement/time trace was closely analysed in each case and it was discovered that the initial trough on each trace corresponded to the time of contact of the impact and is discussed in Chapter V. This phenomenon was investigated on the displacement/time traces measured using the NIST transducer and a similar initial dip was noted on each one as is discussed in Chapter VI. These estimated contact times were checked against the expected contact time for each ball-bearing hammer and tests using instrumented hammers were carried out to allow a direct comparison of the contact time estimated using the response displacement/time trace and the contact time measured using the load cell on the instrumented hammer.

The above tests show that it is possible to estimate the contact time of an impact from a measured displacement/time trace. Similarly, an estimate of contact time can be made from the acceleration/time trace measured using the OLSON transducer from the initial trough and peak on the acceleration/time trace corresponding to the trough in the displacement/time trace.

8.5.2 Frequency domain analysis

Performing a Fast Fourier Transformation (FFT) on the time trace data gives the beam response in the frequency domain. This domain is generally much easier to analyse than the time domain as frequency domain responses are shown as a single peak at a discrete frequency rather than being presented as a continuous displacement or acceleration. Therefore most of the analysis

carried out for this thesis is undertaken on data presented in the frequency domain.

8.6 The use of variations in base reflection

Research carried out at the University of Wisconsin-Milwaukee suggested that the frequency component corresponding to a reflection from the far side of the test specimen, the base reflection, could be used to determine the internal condition. A reduction in the frequency of base reflection occurs at a voided section as the wave must travel around the void, thus increasing the travel time and reducing the frequency of the reflection. This effect was noted on the results from the finite element analyses and, to a lesser degree, on the results from practical tests carried out on voids within 100mm diameter ducts.

Reductions in the base reflections can be seen clearly on the finite element frequency traces as the resolution on these traces is much greater than on the practical tests. The finite element software used for the detailed modelling had the capacity for any time step to be modelled and the concrete surrounding the void is modelled as a homogeneous material. The only factor affecting the frequency of the base reflection is therefore the path length of the wave and so any difference in the measured frequency must be due to the void. Practical testing involves real, inhomogeneous concrete. Variations in the condition of the concrete will give rise to slightly different propagation velocities and can lead to slight differences in the reflection frequency. The analyser averages the time data during the FFT thus reducing the resolution. The resolution on a 50kHz frequency range is 125Hz and is only just sufficient to detect the difference in path length caused by a void in a 100mm diameter duct. Larger variations in the condition of the concrete could also lead to a reduction in the frequency of the base reflection.

A reduction in the frequency of the base reflection across a test specimen can be used to give an indication of voiding in the duct. This reduction may also indicate voiding in another portion of the section and so more detailed analyses should be carried out to determine if a direct reflection from the voided section can be measured. The size of defect detectable depends upon the frequency of excitation, as discussed previously, and more critically, on the resolution of the testing system.

8.7 Effect on impact echo test of beam breathing modes

Research carried out at the University of Cornell, Ithaca, into impact-echo testing of beams found that the geometry of the beam had a considerable effect on the frequency response (Sansalone and Poston, 1992). A chart was produced giving expected frequencies of the beam breathing modes relating to the depth and breadth of the test beams. These expected frequency components were checked on the experimental responses from all the beams tested.

Laboratory test beam 1 has a depth/breadth ratio of 0.7 and so, according to the Cornell research, breathing modes would be expected. However, this beam has a much larger section than a normal bridge beam and the impact contains insufficient energy to excite the breathing modes of a beam of this size.

The smaller laboratory specimen, test beam 2, has a depth/breadth ratio of 1.3 and is of the size that beam breathing modes would be expected on the response. Frequency components were present on the spectra that did not relate to a reflection from any known inclusion. These frequency components related reasonably well to those expected. This beam was of a very simple geometry and contained a large void along half its length. Reflections from the void are likely to dominate the response and the presence of such a large void in a small beam is likely to change the frequency of the beam breathing modes.

Analysis of the different responses measured at grouted and voided sections of test beam 2 show a shift in beam breathing modes. The responses measured at the voided section contain frequency components similar to those measured at the grouted section but shifted to slightly lower frequencies. This is to be expected as the beam modes would be expected to be lower at a less stiff section.

8.8 Limits and range of current I-E method

The research reported in this thesis has shown that sonic impact-echo techniques can be successfully applied to the non-destructive investigation of simply reinforced beams containing voided ducts of 100mm diameter or greater. Critical factors to the

success of an investigation are the measurement of the beam response and the frequency of impact. These factors determine the smallest defect detectable and the range at which it can be detected. Currently, voids of 100mm diameter can confidently be detected at depths of between 100mm and 150mm. Many post-tensioned bridge beams contain ducts of 100mm diameter or greater with a cover of 100mm to 140mm and are of the order of 300mm to 400mm in width. The developed method is therefore well suited to testing these beams.

The system at present is unable to measure the impact directly. An estimate of contact time is possible from the time domain response and this greatly improves the conclusions made from the analysis. However, it is not possible to directly compare results from different tests as individual responses cannot be 'normalised' since the impact is not measured. Instrumented hammers are commercially available which can measure the impact and therefore allow 'normalising' of the signal. These hammers, however do not input energy at a high enough frequency. The ball-bearing hammers constructed for the developed method are not very robust. It is unlikely to be economical to fit a load cell to these hammers as they are designed at present as a number of hammers are required to complete a beam investigation. However, improvements in the connection of the hammer could result in a more robust impactor, thus allowing a load cell to be attatched, similar to the load cell on the PCB mini-hammer. This would improve the analysis as much more detailed signal processing could be carried out.

The OLSON transducer does not contain a load cell at present and the impactor housing is not robust enough for transportation and field testing. However, with small adjustments it is likely that this transducer could be made significantly more robust and a load cell could be attatched to the impactor, again allowing impact measurement and therefore signal normalisation.

The distance between impact and response transducer is not fixed at present. This causes variations in the frequency components of reflections as the distance travelled by the wave will change if the impact and measurement positions change. It is not possible to average a number of measurements taken at the same measurement transducer location as a difference in impact position may cause a change in the frequency component. Averaging these traces may then cause the loss of a reflection from a defect. If the impact to measurement transducer separation was fixed it would be possible to take an average of a few readings taken at that point. Any spurious

reflection would then be minimised as would the effect of random signal noise. The OLSON transducer has this capability at the moment. The use of solenoids as impactors, attached to the transducer housing creates a constant separation. Again an improvement in the robustness of the system would enable better investigations to be carried out.

The tests carried out were on simply reinforced or unreinforced beams. Post-tensioned bridge beams are unlikely to be heavily reinforced as the flexural strength of the beam is provided by the tendons. Many post-tensioned bridges are of segmental construction and so there is no reason to heavily reinforce the concrete. However, heavily reinforced sections are likely to be found at the anchorages of the tendons. These positions can be critical and therefore require testing. Further investigation is required into the developed method to ensure its suitability for testing the anchorage sections of the beam.

Research carried out at Cornell into the effect of reinforcement on impact-echo signals suggests that reflections from reinforcement can be measured. These reflections occur at lower frequencies than expected due to the phase change of the signal, voids have a higher acoustic impedance than concrete and steel has a lower acoustic impedance (Cheng and Sansalone, 1993). However, the developed impact-echo method cannot detect targets within approximately 100mm of the surface and most reinforcement will be closer to the surface than this. The diameter of the reinforcement is unlikely to be greater than 32mm, this presents a small profile to the wavefront and so is unlikely to be detected. Problems caused by reflections from reinforcing bars are likely only to occur where the steel is placed at close centres and presents an almost continuous steel profile to the wave. In this case the expected reflection from this should be calculated and then the response checked for such a frequency component.

8.9 The use of ultrasonic time of flight tomography for the investigation of post-tensioned bridge beams

As with most non-destructive testing techniques, the impact-echo method requires signal interpretation. There is therefore scope for misinterpretation of signals and it is possible that incorrect conclusions regarding the condition of the beam may be drawn. One particular problem with carrying out single point impact-echo tests is that reflections may be measured corresponding to a target at any position on a

spherical surface. Cross checking at different test locations greatly improves the analysis but this becomes complicated and time consuming if a small test grid is required. Confidence in the conclusions drawn from an impact-echo test is greatly increased if a second test method can be utilised to confirm the findings of the tests. This is not necessary at all test locations but a representative sample should be carried out. Ambiguous results from an impact-echo test can also be investigated further using a different technique.

Ultrasonic time-of-flight tomography was used to further investigate a number of ambiguous sections on the test beams. This method was shown to be relatively straightforward to implement. Tomographic techniques were not researched in detail for this thesis but the initial analysis carried out showed the technique offered a powerful investigation technique and could possibly be used to investigate post-tensioned bridge beams with tendon ducts smaller than 100mm in diameter.

Voids in tendon ducts have a much lower wave propagation velocity than concrete. The analyses carried out for this research used straight ray techniques for modelling the velocity contours within the test sections. This technique is straightforward and requires little processing time. However, better techniques are available implementing curved ray tracing and continuous wavefront migration (Jackson and Tweeton, 1994). These methods are likely to be more suitable for post-tensioned beam investigation as the larger variations in propagation velocity are modelled more successfully.

The testing method implemented for these investigations used a simple ultrasonic digital tester with one source and one receiving transducer. The testing is therefore straighforward but time consuming. The use of arrays of transducers would greatly speed up the testing procedure. A datalogger could be used to measure the times-of flight and simple programming could allow the model goemetry to be input. A rapid straight ray analysis of each section could then be carried out on site and any ambiguities investigated further.

8.10 Recommendations for future construction methods of post-tensioned bridges

The post-tensioned design method offers the engineer a flexible and aesthetic bridge design option. It is in the interest of freedom of engineering design to allow post-tensioned techniques to be used on bridges. New construction materials and methods have been researched since the imposition of the moratorium by the DoT in 1992 in order to reduce the development of tendon corrosion. The use plastic ducts would reduce corrosion as electron transfer along plastic ducts is not possible. GPR could also be implemented to test the internal condition of plastic ducts and, as there are many commercial GPR practitioners available, this testing procedure should be economically viable for most bridge inspections. Ducting with a flatter profile is often used in post-tensioned slab construction. Impact-echo testing of this duct profile would be more straighforward as the wave scatter due to the cylindrical profile is much reduced allowing a higher energy reflection to be measured at the receiver location.

8.11 Recommended testing procedure for metal-ducted post-tensioned concrete bridge beams

The testing methods available at present are suitable for use on beams with ducts of 100mm diameter or greater. Future improvements in the instrumentation could result in this investigation method being suitable for testing smaller diameter ducts. However, at present the recommendations for testing post-tensioned bridges with metal ducts using impact-echo techniques are as follows:

1. Investigate all available details of the structure to be tested. This method is most suitable for investigating structures which are lightly reinforced. Carry out a visual inspection of the structure to determine any likely problem areas.

2. If the position of the ducts is unknown, ground penetrating radar can be used for location.

3. Carry out impact-echo tests along the lines of the ducts noting any areas of interest as the test proceeds.

4. Carry out more detailed impact-echo tests at any areas of interest identified during step 3.

5. If the results from step 4 are still ambiguous carry out a tomographic survey. The spacing of the grid should be small enough to resolve the tendons.

6. If possible confirm major findings with intrusive testing.

Chapter IX

Conclusions and Recommendations for Future Work

Individual conclusions are given at the end of each chapter. However, the separate chapters should be considered together to provide an overall conclusion to the research presented. The investigation method developed can be used in its current form but recommendations for future work are included which would improve site implementation.

9.1 General Conclusions

The post-tensioned design method offers an effective and economic way of constructing medium span bridges. However, the problem of voiding in the grouted ducts can lead to corrosion of the tendons due to water ingress. The presence of chlorides from deicing salts can increase the rate of corrosion of the tendons.

Existing non-destructive investigation techniques are inadequate to efficiently test the many existing post-tensioned bridges. A sonic impact-echo technique has been developed which is suitable to investigate the internal condition of the ducts in most post-tensioned bridges. The results from these investigations are more easily interpreted if the tendon ducts are accurately located. Ground penetrating radar, GPR, offers an efficient method for duct location and can also give an indication of the condition of the concrete surrounding the ducts.

A recommended testing procedure for the investigation of post-tensioned bridges using sonic impact-echo techniques has been produced. Confidence in the interpretation is increased if a number of test sections are investigated using ultrasonic time-of-flight tomography. This relatively straightforward technique offers a powerful detailed investigation method. Further research of this method could lead to the development of a more efficient investigation technique.

9.2 Specific Conclusions

9.2.1 Investigation Techniques

- Possible investigation techniques were assessed for the investigation of post-tensioned bridges, namely, visual inspection and endoscopy, ground penetrating radar, radiography, ultrasonic investigation and sonic impact-echo. The investigation technique judged most promising for widespread and economical application was sonic impact-echo.

- The majority of ducting used during construction of post-tensioned bridges was cylindrical steel. Difficulties may therefore arise during sonic investigation as incident waves will be scattered when reflected. This results in less energy being returned to the response transducer than would be measured from a reflection created by a plane material boundary.

- The frequency component of the base reflection can be used in many cases to detect voiding within the tested section. This method is most useful in detecting voids in large diameter ducts within relatively small beams. Problems arise if the beam frequency modes are also measured on the response as these may dominate the trace. It is more difficult to detect voiding in smaller ducts as the relative increase in path length of the base reflection may not be resolved by the testing instrumentation. Variations in the condition of the concrete at discrete sections will also cause a change in the base frequency. It is therefore preferable that direct reflections from voided ducts are measured.

9.2.2 Preliminary investigations

- The condition and mix design of concrete determines the cut-off frequency that can be obtained by an impactor. The cut-off frequency obtained can vary across a single specimen depending on local inhomogeneities within the specimen. Specifically, for newly cast concrete:
  i. The cut-off frequency increases as the concrete cures
  ii. The higher the expected cut-off frequency expected the greater the influence of mix proportions and condition on the actual cut-off frequency obtained.
  iii. The pulse velocity increases as the concrete cures and is higher for concrete and mortar with higher percentages of aggregate.
  iv. The pulse velocity is related to the cut-off frequency obtainable.
  v. There is a linear relationship between the compressive strength and the cut-off frequency obtainable. This could easily investigate the strength of concrete on site and be used to determine formwork striking times.

- Testing from the exposed ends of tendons can lead to successful defect identification. This testing procedure has the following applications and limitations.
  i. This test configuration can successfully detect the nearest one or two defects.
  ii. A major disadvantage of this method is the impracticality of exposing the ends of the tendon ducts.

- The optimum testing set-up was formulated as follows:

i. The Zonic A and D dual channel FFT analyser is suitable for sonic impact-echo testing of concrete.
ii. The NIST displacement transducer was considered the most suitable response transducer.
iii. Ball bearing wire hammers provided the most efficient and versatile impactors.

9.2.3 Finite Element Analyses

- Thin steel ducting does not affect the detectability of voids inside. Simple finite element analyses on models with and without thin steel ducting gave the same result.

- Planar defects are more readily detected than circular defects. Wave scattering from a cylindrical surface reduces the level of energy reflected back to the measurement point.

- The cut-off frequency can be estimated from the diplacement/time response of a finite element analysis. The initial trough on the displacement/time trace gives an estimate of the contact time and therefore the expected cut-off frequency.

- The base reflection, if distinguishable, can be used to determine the approximate size of a defect providing the expected frequency of the base reflection is known. The larger the amount lower than expected, the larger the defect.

- Circular defects can be detected but care must be taken in deciding upon contact time of impulse and measurement time step (this is important for both numerical simulation and field experimentation). The choice of element size and type is also important for finite element simulation.

- Analysis of the results in the frequency domain is usually more straightforward. However, the first reflection from a defect can also be clearly seen on the displacement-time trace if the experiment is well conditioned.

9.2.4 Laboratory testing

- The NIST transducer performs better than the OLSON accelerometer at lower frequencies. However, with better coupling, the OLSON accelerometer performs adequately and is much more practical for use on site as the preparation required between tests is minimal.

- The contact time of the impact can be estimated from the displacement/time trace measured by the NIST transducer. The accuracy of this estimate is dependent on the resolution of the testing system. The contact time can also be estimated from the acceleration/time response as measured using the OLSON transducer, although this is not as clear as that produced by the NIST transducer.

- The OLSON accelerometer provides a quick method of measuring the response of a specimen to impact. The contact surface is much larger than that of the NIST transducer and so care must be taken to ensure adequate coupling. It was considered worthwhile to check the response obtained with each transducer at a few points on the surface of a new test specimen to ensure similar responses were being measured by each transducer.

- The minimum depth to defect detectable is $\lambda/2$ where λ = minimum input wavelength (max input frequency = $1/T_c$). The minimum profile detectable is approximately equal to $\lambda/2.6$.

9.2.5 Field Investigations

- The OLSON transducer is suitable for use in the field. However, the NIST transducer should be used to carry out a few tests on each new structure and the responses from each transducer compared to ensure the results are similar.

- Impact-echo techniques can be used to detect voiding in ducts of 100mm diameter and above at depths of 100mm to 150mm by the measuring of simple reflections from the defects. The testing method is most successful on simply reinforced rectangular beams.

- The results from I-E testing are improved if a constant impact to measurement position separation is used. The problem of a variation in distance can be improved by repeating the test a number of times and recording a representative trace. This however, does not aid the comparison of tests at different positions. The OLSON transducer is set up to produce the impact and, once the reliability problems are sorted out, this transducer will provide a constant impact to receiver separation.

- With further work it should be possible to investigate ducts of smaller diameter by analysing the relative frequencies of the modes of vibration of the beam. Response patterns could be identified and any deviation would indicate an area requiring further investigation.

- As with other NDT techniques the use of impact-echo testing alone can be slightly unreliable. The reliability would be improved if the impact was measured and signals from different locations could then be directly compared. At present this is not possible and so another NDT technique can be applied at positions of interest to further investigate the impact-echo findings. One such technique in time of flight tomography.

- Time of flight tomography provides a highly successful method of investigating post-tensioned concrete beams. The method is somewhat time consuming and so should be used in conjunction with a simpler testing method, eg. sonic impact-echo, which identifies areas of interest. The smaller the ducts to be investigated, the smaller the required distances between testing stations. This therefore significantly increases the testing time. However, array systems could be developed which would greatly reduce the testing time.

9.3 Recommendations for Future Work

9.3.1 Improvements to testing method

The test set-up would be improved if the separation between impact and response measurement positions was kept constant. This could involve attatching more robust hammers to the transducer housing and allowing impact without compromising the energy input. A number of impacts could then be carried out at a test position and the responses averaged, thus

reducing the effects of random signal noise and any other non-repeatable reflections.

Another improvement to the testing system would be the measurement of the impact by adding a load cell to the impactor. This would allow normalisation of the response at different locations by calculating the Frequency Response Function. Responses at different locations could then be compared directly and the relative amplitudes of reflection would give more detailed information regarding the size and location of a target.

9.3.2 Coupling of the impact-echo system to the test specimen

The developed impact-echo system offers a reliable but cumbersome method of coupling the response transducer to the test specimen. It is very time-consuming to implement and is rather delicate for use on site. The OLSON transducer provides a much simpler method of coupling which is robust enough for site work. However, the accelerometer used in this transducer does not perform quite as well as the NIST displacement transducer and so improvements to the coupling of this would improve practical implementation of the sonic impact-echo method.

9.3.3 Ultrasonic time-of-flight tomography

Initial trials of this method gave very promising results. The method at present is time consuming but the test rate would improve dramatically if arrays of receiving transducers were used. The use of tomographic techniques on post-tensioned bridges should be researched further as more powerful ray tracing techniques are available which would improve the resulting velocity models. It should be possible to develop a site testing system which creates inital velocity contour plots for each tested section as the investigation is being carried out. Sections giving ambiguous information could then be retested using a more detailed test grid.

9.3.4 Three-dimensional finite element analyses

Powerful three-dimensional finite element codes are available and could be used to investigate the effects of the total defect size on the measured response. These methods could also be used to produce a more effective method of presentation of the results as the current method of comparing many frequency spectra becomes rather cumbersome.

References

Ansys 5.0 User's Manual Vol. IV, Theory, Ed. Kohnke, P. Swanson Analysis Systems Inc. Houston, USA.

B.S. 1881, Part 4 Methods of Testing Concrete for Strength, BSI, London

B.S. 4408, Part 5, 1974 Non-destructive methods of Tesing for Concrete - Measurement of the Velocity of Ultrasonic Pulses in Concrete, BSI, London

Becker, E.B. Carey, G.F. and Oden, J.T. Finite Elements - An Introduction. Vol. 1, Prentice-Hall Inc. New Jersey, 1981. 258pp.

Beckett, Derrick Concrete Bridges- An Introduction to Structural Design (1), Surrey University Press, Oxfordshire, 1973

Blake, R.J. and Bond, L.J. Rayleigh Wave Scattering from Surface Features, Wedges and Downsteps. Ultrasonics, Vol. 28, No. 4. July 1990, 214-228

Bracewell, R.N. The Fourier Transform and its Application. 2nd Edition. New York, McGraw-Hill, 1986

Bungey, J.H. Testing of Concrete in Structures, 2nd Ed. Surrey University Press, U.K. 1989, pp228.

Bungey, J.H. Millard, S.G. Shaw, M.R. and Thomas, C. Operational Aspects of Radar Investigations. The British Journal of Non-destructive Testing. Vol. 33, No. 12, December 1991, 599-605

Bungey, J.H. Testing Concrete in Structures, CIRIA Technical Note 143, London, 1992. pp 87.

Bungey, J.H. and Madanhoust, R. Evaluation of Non-destructive testing of lightweight concrete. Proc. ICE Structures and Buildings 1994, Vol. 104, August. 275-283

Carino, N.J 1984a Laboratory Study of Flaw Detection in Concrete by the Pulse-Echo Method. In-situ Non-Destructive Testing of Concrete. SP-82, ACI, Detroit 1984, 557-580

Carino, N.J. and Sansalone, M. 1984b Pulse-Echo Method for Flaw Detection in Concrete. NBS Technical note 1199. U.S. Dept. of Commerce/National Bureau of standards. 1984. pp34.

Carino, N.J. Sansalone, M. and Hsu, N.N. 1986a A point source-point receiver, pulse-echo technique for flaw detection in concrete. ACI Journal, March-April 1986. Title no. 83-20

Carino, N.J. Sansalone, M. and Hsu, 1986b N.N. Flaw detection in concrete by frequency spectrum analysis of impact-echo waveforms. International Advances in Non-destructive Testing. 1986, 12, 117-146

Carino, N.J. Jennings, H.J. Hamlin, J.M. & Snell, L.M. Properties of Concrete at Early Ages. Cement, Concrete and Aggregates, V.11 No.2. 1989, 129-131

Cawley, P. The Sensitivity of the Mechanical Impedence Method of Non-Destructive Testing. NDT International, Vol. 20 No. 4. August 1987.

Cawley, P. Non-Destructive Testing of Mass Produced Components by Natural Frequency Measurements. Proceedings of the Institute of Mechanical Engineers. Vol. 199 No. 33. 1985

Chang, C. and Sachse, W. Separation of Spatial and Temporal Effects in an Ultrasonic Transducer. Review of Progress in Quantitative Non-Destructive Evaluation. Vol. 5A and 5B. 1986. 139-147

Cheng, C. and Sansalone, M. 1993a The Impact-Echo Response of Concrete Plates Containing Delaminations - Numerical, Experimental and Field Studies. Materials and Structures. Vol. 26. No. 159, 1993. 274-285

Cheng, C. and Sansalone, M. 1993b Effects on Impact-Echo Signals caused by Steel Reinforcing Bars and Voids around Bars. ACI Materials Journal. Title No. 90. Vol. 5. 1993

Cooke, R.S. Ashurst, D.M. McCavitt, N. and Forde, M.C. Digital radar assessment of Besses o' th' Barn post-tensioned precast concrete segmental rail bridge. Proc. 5th International conference on Structural Faults and Repair, Engineering Technics Press, Edinburgh, UK, 1993. Vol. 1, 305-311.

Corelli, D. and Brown, D.L. Impact Testing Considerations. Proceeding of the International Modal Analysis Conference, 1984, Vol. 2. 735-742

Daniels, P. Gunta, D. and Scott, H. Introduction to Sub-surface Radar, IEE Proceedings, Vol. 135, Pt F, No. 4, August 1988

Davis, A.G. and Dunn, C.S. From Theory to Field Experience with the Non-destructive vibration testing of piles. Proceedings of the Institution of Civil Engineers, Part 2, 1974, Vol. 57, Dec., 571-593

Desai, C.S. Elementary Finite Elements. Prentice-Hall Inc. Englewood Cliffs, N.J. 1979. 434pp.

Dowling, A.P. and Ffowcs Williams, J.E. Sound and Sources of Sound. Ellis Horwood Ltd. Chichester 1983. 321pp.

DTP Press Notice No. 260. Publiched by DTP, Londom 1992.

Ewins, D.J. Modal Testing: Theory and Practice, Research Studies Press Ltd. Letchworth, UK. John Wiley and Sons Inc. Chichester, UK. 1984. 269pp.

Farrier, C.R. Baker, W.E. and Dove, R.C. Dynamic Parameter Similitude for Concrete Models. ACI Structural Journal. Titile no. 91. Vol. 1, 1994

Fegen, I. Forde, M.C. and Whittington, H.W. The Detection of Voids in Concrete Piles using Sonic Methods. Proc. 4 colloque International sur les methodes de controle non destrucif, Grenoble, Sept 1979, 40-46.

Filipczynski, L. Pawlowski, Z and Wehr, J. Ultrasonic Methods of Testing Materials, 2nd Edition. London, Butterworth, 1966.

Gaydecki, P. Glossop, K. and Burdekin, F. A prototype inductive scanning system for two-dimensional imaging of metal reinforcing components in concrete: system design and data visualisation. Proc. International Symposium of Non-destructive testing in Civil Engineering, September, 1995, Berlin, Germany. Vol. 1, 745-752

Gheshlaghi, F. Santamarina, C. Wiese, D. Thomas, M. Polak, M. and Caratin, G. Tomographic imaging concrete structures. Proc. International Symposium of Non-destructive testing in Civil Engineering, September, 1995, Berlin, Germany. Vol. 1, 297-304.

Ghorbanpoor, A. Evaluation of Post-tensioned Concrete Bridge Structures by the Impact-Echo Technique. U.S. Department of Transportation. Federal Highway Administration. Publication No. FHWA-RD-92-096. Dec 1993. pp84.

Ghorbanpoor, A.L. McGogney, C.H. and Virmani, Y.P. Recent Developments in NDE of Concrete Bridge Structures. Proceedings of the Non Destructive Evaluation of Civil Structures and Materails. Boulder, Colorado, May 1992.

Goldsmith, W. Impact, The Theory and Physical Behaviour of Colliding Solids, Edward Arnold, London. 1960, 379pp.

Graff, K.F. Wave motion in elastic solids, Ohio State University Press, Columbus, Ohio, USA, 1975

Halabe, U.B. Sotoodehnia, A. Maser, K.R. and Kansel, E.A. Modelling the Electromagnetic Properties of Concrete. ACI Materials Journal, Title No. 90. Vol. 6, 1993.

Hillger, W. Imaging of Defects in Concrete by Ultrasonic Pulse-Echo Techniques. Proceeding of the Fifth International Structural Faults and Repair Conference, Vol.3, 1993.

Hsu, N.N. Chen, G and Sansalone, M. Characterization of a piezoelectric transducer coupled to a solid. IEEE Ultrasonics Symposium, Denver, CO, 1987, 689-692

Hughes, G. and Speirs, D.M. An investigation into the Beam Impact Problem. Cement and Concrete Association. Technical Report 546. April 1982.

Hunter, S.C. Energy Absorbed by Elastic Waves During Impact. Journal of the Mechanics and Physics of Solids, 1957. Vol. 5. Pergamon Press, London, 162-171.

Jackson, N. and Dhir R.K. Civil Engineering Materials 4th ed.MacMillan Education, London. UK. 1988. 429pp.

Johnson, M.A.E. and Fifield, B.E. Remote visual inspection of voids and cavities - practical experience on post-tensioned bridges. Proc. 5th International Conference on Structural Faults and Repair - 93, Engineering Technics Press, Edinburgh, UK, 1993, Vol. 1, 301-304

Jones, R. Non-destructive testing of concrete. Cambridge University Press, Cambridge, UK. 1962, 104pp.

Kaplan, W. Advanced Mathematics for Engineers. Addison-Wesley Publishing Co. Reading, Mass. USA. 1981.

Kear, P. and Leeming, M. Radiographic inspection of post-tensioned concrete bridges. Insight. Journal of the British Institute of NDT, July, 1994.

Kolsky, H. Stress Waves in Solids. Oxford Clarendon Press, 1953.

Komendant, A.E. Prestressed Concrete Structures, 1st Ed. McGraw-Hill, London, 1952.

Komeyli-Birjandi, F. Sonic Investigation of Masonry Structures. PhD Thesis, University of Edinburgh, Edingburgh, 1986.

Langenberg, K. Bärmann, R. Marklein, R. Irmer, S. Müller, H. Brandfaß, M. and Potzkai, B. Electromagnetic and Elastic Wave scattering and inverse scattering applied to Concrete. Proc. International Symposium of Non-destructive testing in Civil Engineering, September, 1995, Berlin, Germany. Vol. 1, 77-84.

Leemig, M.B. Lane, J.S. and Wade, P.J. Post-tensioned bridge investigation - the way forward. Proc. 6th International conference on structural faults and repair, London, UK, 1995. Vol. 1, 193-198.

Leonhardt, F. Prestressed Concrete: Design and Construction. Trans. C. Van Amerongen. 2nd Ed. Berlin. 1964.

Love, A.E.H. The Mathematical Theory of Elasticity. 4th Ed. New York, Dover Publications. 1944.

Lynn, P.A. and Fuerst, W. Introductory Digital Signal Processing with Computer Applications. John Wiley and Sons, UK. 1989, pp371.

McCavitt, N. and Forde, M. C. The Application of the Method of Convolution to the Simulations of the Response of Masonry Arch Bridges to GPR. ICE Bridge Assessment Seminar. October 1992.

Martin, J. and Forde, M.C., 1995 Influence of Concrete Age and Mix Design on Impulse Hammer Spectrum and Compression Wave Velocity.Construction and Building Materials, Vol. 9, No. 4, 1995, Elsevier Science Ltd. UK. 245-255

Martin, J. Hardy, M.S.A. Usmani, A.S. and Forde, M.C., 1995a Quantifying the Defects in Post-tensioned Bridges using Impulse Ultrasonics. Proc. 6th International conference on structural faults and repair, London, UK, 1995. Vol. 1, 209-216.

Martin, J. Hardy, M.S.A. Usmani, A.S. and Forde, M.C., 1995b Influence of Impulse Spectrum on Defect Detection in Post-tensioned Bridges. Proc. International Symposium of Non-destructive testing in Civil Engineering, September, 1995, Berlin, Germany. Vol. 2, 789-796.

Neville, A.M. and Brooks, J.J. Concrete Technology, Longman Scientific and Technical, Essex, UK, 1987, 438pp

Newland, D.E. An Introduction to Random Vibrations and Spectral Analysis. 2nd Edition. Longman, UK. 1984, 377pp.

Olson, L.D. Measurement of Subsurface, Deep Foundation and Slab/Subgrade Conditions with In situ Seismic, Sonic and Vibration Methods. FIND REST OF REF. June 1991.

Owen, D.R.J. and Hinton, E. Finite Elements in Plasticity: Theory and Practice, Pineridge Press Ltd. Swansea, UK. pp594.

Padaratz, I. and Forde, M.C. A theoretical evaluation of impulse radar wave propagation through concrete. Non-destructive Testing and Evaluation, 1995. Vol. X, 1-24.

Papoulis, A. Signal Analysis, McGraw-Hill, Singapore, 1977, pp 431.

Pessiki, S.P. and Carino, N.J. Setting time and strength of concrete using the impact-echo method. ACI Materials Journal. 1988, 85(5), 389-399

Poston, R. and Sansalone, M. Detecting Cracks in the Beams and Columns of a Post-tensioned Parking Garage Structure Using the Impact-Echo Method. Proc. Non-

Destructive Evaluation of Civil Structures and Materials, 1992. Boulder, Colorado, USA. 129-143.

Pratt, D. and Sansalone, M. Impact-Echo Signal Interpretation Using Artificial Intelligence. ACI Materials Journal. March/April 1992. Vol. 89, No. 2, 178-187

Ricketts, N.J. Inspection of Post-tensioned Concrete Bridges. Inspection Methods and Measurements of Stress. Lecture notes for TRL Seminar, Crowthorne. UK. 1993.

Sansalone, M. and Carino, N.J. Impact-Echo: A Method for Flaw Detection in Concrete using Transient Stress Waves. NBSIR86-3452, National Bureau of Standards, Gaithesburg, Maryland, USA. Sept 1986, pp 220.

Sansalone, M. Carino, N.J. and Hsu, N.N. 1987a A Finite Element Study of Transient Wave Propagation in Plates. Journal of Research of the National Bureau of Standards. Vol. 92, No. 4, 1987, 267-278

Sansalone, M. Carino, N.J. and Hsu, N.N. 1987b A Finite Element Study of the Interaction of Transient Stress Waves with Planar Flaws. Journal of Research of the National Bureau of Standards, Vol. 92, No. 4, 1987, 279-290

Sansalone, M. and Carino, N.J. Impact-Echo: Detecting honeycombing, the depth to surface opening cracks and ungrouted ducts. Concrete International, April 1988. 38-46.

Sansalone, M. and Carino, N.J. Detecting delaminations in concrete slabs with and without overlays using the impact-echo method. ACI Journal, March-April 1989. Title no. 86-M18. 175-184.

Sansalone, M. Lin, Y. and Carino, N.J. Finite Element Studies of the Impact-Echo Response of Plates containing Thin Layers and Voids. Journal of Non-Destructive Evaluation. Vol. 9, No. 1, March 1990. 27-47

Sansalone, M. Lin, Y. and Carino, N.J. Impact-Echo Response of Concrete Shafts. Geotechnical Testing Journal. Vol. 14 No. 2. June 1991. 121-137

Sansalone, M. and Carino, N.J. Detection of Voids in Grouted Ducts using the impact-Echo Method. ACI Materials Journal. Vol. 92, No. 3, 1992. 296-303

Sansalone, M. and Lin, Y. Detecting Flaws in Concrete Beams and Columns using the Impact-Echo Method. ACI Materials Journal, July/Aug 1992. pp33

Sattler, F.J. Refresher, Non-Destructive Methods for Finding Below-Surface Defects. Chemical Engineering. NY. Vol. 96. No. 9. Sept 1989. 161-167.

Schickert, M. Towards SAFT-imaging in ultrasonic inspection of concrete. Proc. International Symposium of Non-destructive testing in Civil Engineering, September, 1995, Berlin, Germany. Vol. 1, 411-418.

Schiller, M. Berra, M. Fatticioni, A. Atkinson, R. and Binda, L. Use of Tomography for Diagnosis and Control of Masonry Repairs
Seminar notes. TRL seminar on Investigation of Post-tensioned Beams.

Stain, R.T. and Dixon, S. Inspection of cables in post-tensioning bridge - what techniques are available. Proc. 5th International Conference on Structural Faults and Repair - 93, Engineering Technics Press, Edinburgh, UK, 1993. Vol. 1, 297-306.

Steinbach, J. and Vey, E. Caisson evaluation by stress wave propagation method. Journal of the Geotechnical Engineering Division, ASCE, Vol. 101, No. GT4, April, 1975, 361-378

Sternglass, E.J. and Stuart, D.A. An Experimental Study of the Propagation of Transient Deformation in Elastoplastic Media. Journal of Applied Mechanics, Vol. 20. 1953, 427

Storrar, D.B. The Management of Post-tensioned grouted-duct Bridges owed by the Department of Transport, Proc. 5th International Conference on Structural Faults and Repairs - 93. Engineering Technics Press, Edinburgh, 1993.Vol. 1. 3-7.

Stroud, K.A. Fourier Series and Harmonic Analysis, Stanley Thornes Ltd.Cheltenham, UK. 1984, 204pp.

Tomsett, H. and Millar, R. Comparative and complimentary techniques in bridge surveys. Proc. 6th International Conference on Structural Faults and Repair - 95, London, UK, 1995. Vol. 1, 53-62.

Ulriksen, C. P. F. Application of Impulse Radar to Civil Engineering, Doctoral Thesis, Lund University of Technology, Sweden, 1982

Waldron, P. Inspection of Post-tensioned concrete bridges, Engineering Significance. Lecture notes for TRL Seminar, Crowthorne. UK. 1993.

Woodward, R.J. and Williams, F.W. Collapse of Ynys-y-Gwas bridge, West Glamorgan. Proc. ICE, August 1988. vol.84 635-669

Woodward, R.J. and Wilson, D.L.S. Corrosion of Post-tensioned Tendons, 1991, Transport Research Record 1211, Crowthorne. UK.

Woodward, R.J. Inspection of Post-tensioned Concrete Bridges - Non-Destructive Testing Methods. Lecture notes for TRL Seminar, Crowthorne. UK. 1993.

Zukas, J.A. Nicholas, T. Swift, H.F. Greszczuk, L.B. and Curran, D.R. Impact Dynamics, John Wiley and Sons, New York. 1982, 452pp

Appendix I

Published Journal Papers

BUTTERWORTH HEINEMANN

Construction and Building Materials, Vol. 9, No. 4, pp. 245–255, 1995

0950-0618/95 $10.00+0.00

0950-0618(95)00027-5

Influence of concrete properties on impulse hammer spectrum and compression wave velocity

J. Martin and M. C. Forde

Department of Civil & Environmental Engineering, University of Edinburgh, Crew Building, The Kings Buildings, Edinburgh EH9 3JL, Scotland, UK

Received 13 January 1995; revised 24 February 1995; accepted 27 February 1995

A pilot study was performed to evaluate the influence of different properties of concrete on the contact time of the hammer head and pulse velocity of compression waves produced by two impact hammers of different mass (280 g and 1.25 g). Each impact hammer was instrumented so that the force introduced to the test specimen could be measured. Differences in measured contact time for each hammer showed how significant the influence of the factor under test was in analysing output from impact-echo tests on concrete. The pulse velocity was calculated using an ultrasonic digital tester which gave the velocity of compression waves. Two sets of 100 mm cubes were made with different mix ratio for this pilot study. The contact time and pulse velocity were calculated and the compressive strength measured at different ages. The results showed that the contact time decreased and the pulse velocity increased with age. However, the mix proportions also affected the results. It was established that as the nominal contact time of the impact decreased so the actual contact time achieved was more affected by the mix proportions and general condition of the concrete.

Keywords: concrete; mortar; age

ıbstantial research has recently been carried out into e use of impact-echo techniques in the investigation concrete[1]. *Figure 1* shows a typical instrumentation t-up. A compression wave is introduced to the test ecimen and the response of the specimen is recorded ing a transducer.

For this study, the compression wave was introduced ing instrumented impact hammers. The contact time the hammer and specimen determines the smallest rget that can be located. As the test specimen becomes ore complex the response of the specimen becomes fficult to analyse in the time domain. It is more useful look at the response in the frequency domain. The ıpact can also be analysed in the frequency domain; e shorter the contact time, the higher the maximum equency input. The maximum frequency input into e test object therefore determines the smallest target at can be detected and the smallest depth to target. In is study, the maximum frequency of input was taken the point at which the frequency spectrum of the ıpact had decreased by 10 dB from the 0 Hz value[2]. his value was termed the cut-off frequency. Most ıpactors used in investigations at present are not strumented and so no direct measurement of the ıpact is made. It is therefore not possible to obtain the equency content of the impact at each test. The aximum frequency input by each impactor is deter-ined using elastic theory[3,4]. Some work has been rried out to determine the input force–time function using deconvolution[5]. The displacement of a point on the beam is measured with time: the displacement–time function. This function is considered the convolution of the input force–time function with an impulse response function (corresponding to the beam). The input force–time function, and therefore the cut-off frequency, can then be determined by deconvolution of the measured displacement–time function with the impulse response function. However, no account is taken of the condition of the concrete in determining the impulse response function.

This paper examines the effects that the mix and condition of the concrete have on the cut-off frequency and velocity obtained as the concrete cures over 28 days. The cut-off frequency and pulse velocity are dependent on the density, ρ, elastic modulus, E, and Poisson's ratio, v, of the concrete. Different mixes of concrete will have different values of ρ and E. For example, as the cement:aggregate ratio increases the density will decrease (for most aggregates) and the results will be affected accordingly. Previously work has been carried out[6] using the variation in compression wave (P-wave) velocity as concrete ages to determine setting time and strength. It was considered worthwhile to determine the p-wave velocity for each set of cubes to investigate the relationship between the development of this and the development of the cut-off frequency.

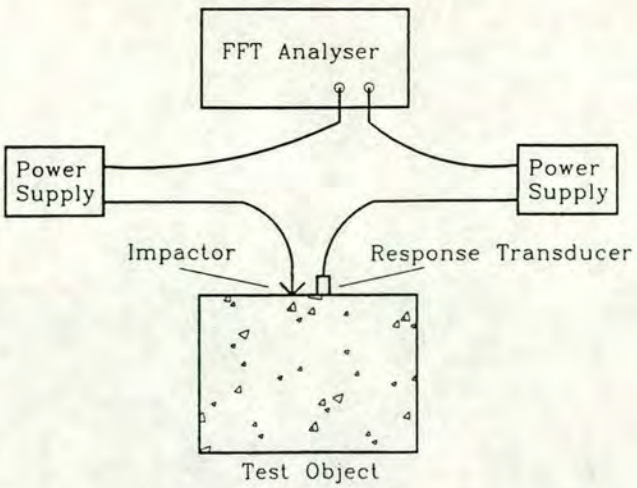

Figure 1 Set up for I-E test

Theoretical background

Stress waves

When carrying out an impact-echo test, a transient stress pulse is introduced into the test object using a mechanical point impact[7]. The pulse propagates through the specimen along spherical wavefronts.

Three types of waves are set up:

- compression waves, P-waves, are dilatational and travel parallel to the direction of propagation;
- shear waves, S-waves, are distortional and travel perpendicular to the direction of propagation;
- surface waves, Rayleigh or R-waves, travel along the surface of the test specimen away from the impact point.

The P and S-waves are partly reflected by material boundaries within the test object. The amount of reflection is dependent on the relative difference in material properties. A large reflection will occur if there is a large difference in material properties and a small reflection will occur if there is a small difference in material properties, see Equation (1)[7]. Total reflection will occur at a boundary with air.

$$A_R = A(r_2C_2 - r_1C_1) / (r_2C_2 + r_1C_1) \quad (1a)$$

and

$$A_T = A(2r_1C_1) / (r_2C_2 + r_1C_1) \quad (1b)$$

where

A = initial wave amplitude
A_R = amplitude of reflected wave
A_T = amplitude of transmitted wave
r_1 = mass density of initial material
r_2 = mass density of second material
C_1 = wavespeed through initial material
C_2 = wavespeed through second material

The movement of the test specimen is measured near to the impact point, see *Figure 1*. This is to give the smallest interference from the surface wave which will pass the measurement transducer before the first reflections from within the test object arrive back at the transducer. Problems may occur if the test object is narrow. The reflection of the surface wave from the edge of the specimen may arrive at the transducer at the same time as reflections from material boundaries within the specimen and distort or swamp the results. P-waves are measured using a displacement, velocity or acceleration transducer.

If the pulse velocity through the specimen is known and the time to the arrival of a reflection from within the specimen is measured, then the distance to the target can be calculated using Equation (2)[1].

$$2d = V_p * t \quad (2)$$

where d = depth to target, V_p = P-wave velocity and t = time to reflection.

As the test object becomes more complex, the time trace of the receiver becomes very difficult to analyse. It is much more straightforward to analyse data from these tests in the frequency domain by carrying out a fast fourier transform (FFT) on the data. See *Figure 2*.

Fast Fourier transform

The Fourier transform is the basis of frequency analysis. The assumption is made that the time signal is made of up to an infinite number of sinusoidal components with various frequencies at different amplitudes and initial phases[8]. Fast Fourier transforms are highly efficient algorithms for computing the discrete Fourier transform and were first developed in the 1960s[9].

The exact relationship between cut-off frequency and smallest target size detectable depends upon the test material, but for concrete the cut-off frequency input will allow the detection of targets that create a profile to the P-wave front of approximately half a wavelength.

$$t = \lambda/2 \quad (3a)$$

and

$$\lambda = V_p/f \quad (3b)$$

where t = smallest target size (m), λ = wavelength (m) and f = cut-off frequency.

Similarly, the minimum depth at which a target can be detected can be calculated from Equation (4).

$$d = V_p/(2f) \quad (4)$$

where d = smallest depth to target (m).

Targets smaller than this may be detected but it is not possible to say that if no reflection is detected, no targets are present. It is therefore important not to overestimate the cut-off frequency input into the test specimen. It would be desirable to measure each impact as

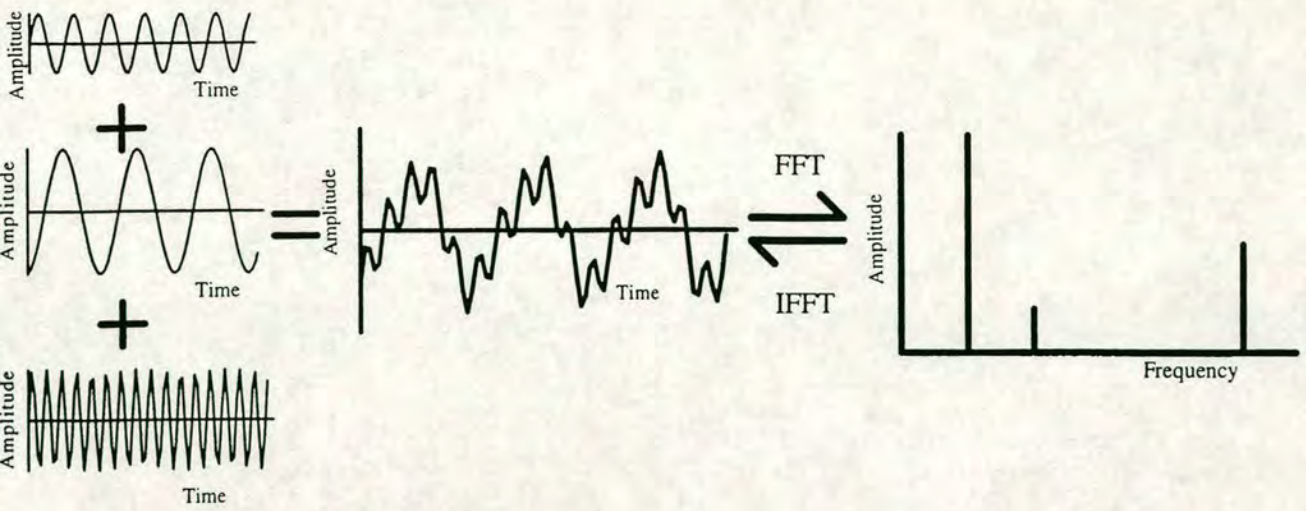

gure 2 Principle of the fast Fourier transform

ıy unusual impact would be instantly detected and the st repeated. An unusual impact would occur if there as a double hit or if there was some localised crushing the concrete. Crushing at impact reduces the cut-off equency considerably.

xperimental procedure

oncrete mixes

wo mixes of concrete were made: one containing sand nd granite (10–20 mm diameter rough granite chips – oncrete) and the other sand only – mortar. The mix oportions are shown in *Table 1*.

Sets of 100 mm cubes were cast. On each testing day ree cubes of each mix were tested.

etermining the pulse velocity

was not possible to accurately measure the P-wave locity of a sonic wave through each cube by impact-ho or transmission test, i.e. by impacting on one side nd measuring the response on the other side. The cut-f frequency was not high enough to pick up the edge the small cubes in an impact echo test. The cubes ere also too small for the time delay to be sufficiently rge to measure on the trace in a transmission test. The lse velocity of an ultrasonic wave was then calculated ing two 54 kHz transducers, see *Figure 3*. The tester calibrated before being used on the cubes by firstly easuring the time of transmission along a calibration linder with a known transmission time and then justing the tester to read the correct time. The 54 kHz

ble 1 Mix proportions

	Concrete (kg)	Mortar (kg)
nd	30	60
avel	37.5	–
ment	15	20
ater	7.5	10

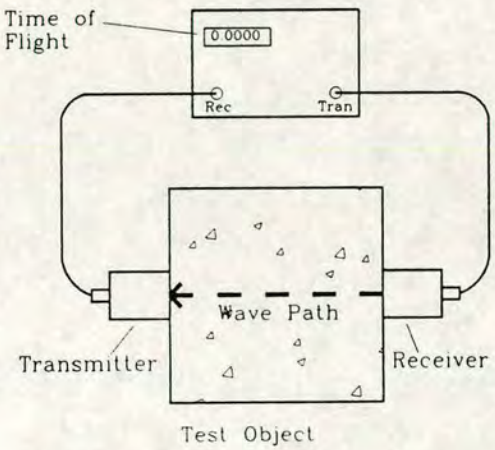

Figure 3 Ultrasonic pulse velocity determination

transducers were placed on opposite sides of the cube, ensuring that both sides were against the smooth sides of the mould when the cubes were cast. This ensured the best coupling. Water pump grease was used to couple the transducers to the cube. One transducer was used as a transmitter and the other as a receiver and the time of flight of the pulse from the transmitter to the receiver, through the concrete, was recorded on the digital tester. This procedure is repeated three times and the average time calculated. The cube is then measured and the ultrasonic pulse velocity calculated. The ultrasonic pulse velocity was then calculated for the other two cubes, from which the average result for that age of concrete was calculated. Previous research[10] has found that compression wave velocities obtained using ultrasonic pulse-velocity methods were higher than those obtained from sonic impulse-echo methods. It was therefore considered necessary to investigate the difference between the ultrasonic pulse velocity calculated through a concrete beam using the same method as described above and the pulse velocity calculated from a transmission test and also an impact-echo test using an impact hammer and receiving transducer.

Converting ultrasonic pulse velocity to sonic pulse velocity

The ultrasonic pulse velocity was calculated through four locations on a 1 m wide concrete beam using the method discussed above. A transmission test and impulse echo test were then carried out at the same locations using the 280 g hammer. This hammer gives a high enough cut-off frequency to pick up the back surface (Equation (3)) and also inputs sufficient energy for the wave to be reflected from the back of the beam and return to the front side for measurement by the accelerometer in the impulse-echo test. See *Figures 1* and *4*.

Impact hammers

Two steel tipped hammers were used. See *Figure 5*. The 280 g hammer has an expected cut-off frequency on steel of 7 kHz and the 1.25 g mini hammer has an expected cut-off frequency on steel of 15 kHz. Both hammers contained a force transducer allowing the force impact to be measured with time.

FFT analyser

A 100 kHz FFT analyser was used. See *Figure 6*. The analyser has built in anti-aliasing filters and so the actual sampling rate is 256 kHz. This gives a good resolution of the impact.

All the tests were performed on a side of the cube that was cast against the smooth metal sides of the cube mould. This ensured similar surface conditions for all the tests. An average of five impacts was taken on each cube with the 1.25 g mini-hammer. The impact was recorded in the time domain (*Figure 7(a)*) initially, as it was then instantly obvious if a mis-hit had occurred. The five impacts were then averaged and an FFT performed which gave the average impact in the frequency domain (*Figure 7(b)*). The cut-off frequency was then noted for each of the three cubes and an average calculated. The above procedure was then repeated using the 280 g hammer (*Figure 8*). The mass, dimensions and compressive strength of the cubes were then measured and the average calculated. This was then repeated on both the concrete and mortar cubes as the cubes aged.

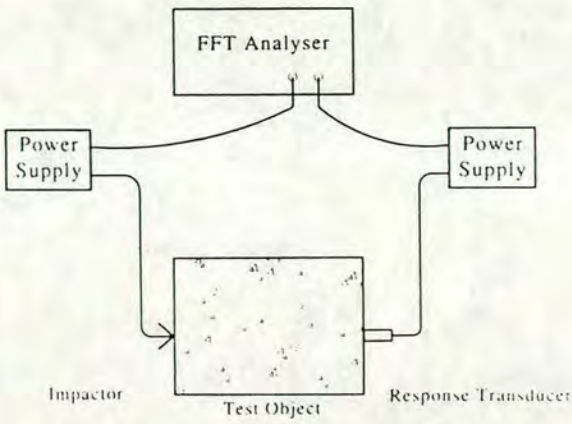

Figure 4 Set-up for sonic transmission test

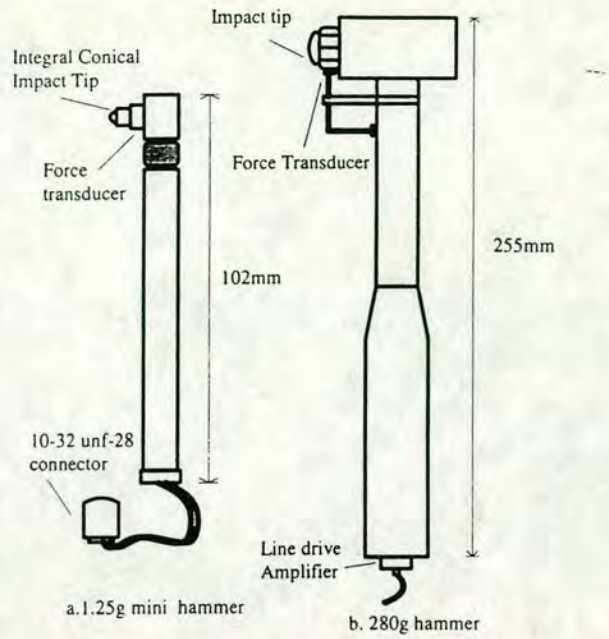

Figure 5 Instrumented hammers

Results

Pulse velocity determination

It was expected that the ultrasonic compression wave speed would be greater than the sonic wave speed. However, this was not found to be the case. The results are shown in *Table 2*.

As can be seen from *Table 2*, the results from the sonic transmission test and the ultrasonic transmission test (54 kHz trans. test) are very similar. The results from the sonic impact echo test (sonic I-E test) are slightly higher than expected. However, there is a considerable spread of calculated velocities within each series. It was therefore not considered worthwhile to factor the velocities calculated on the cubes using the ultrasonic digital tester.

The reason the results were very similar was that the frequency of excitation of the ultrasonic tester was relatively low for ultrasonic testing (54 kHz, whereas most ultrasonic testing is undertaken on metals using transducers with an excitation frequency greater than 200 kHz) and the cut-off frequency of the impulse hammers was relatively high (2–8 kHz, most sonic testing undertaken to date use hammers with a cut-off frequency less than 1.5 kHz). Note:

- Pundit gave an ultrasonic P-wave velocity of 4002 m s^{-1}.
- The transmission tests gave a P-wave velocity of 4000 m s^{-1}.
- The impact-echo test gave a P-wave velocity of 4040 m s^{-1}
- This gives a factor of 1 for velocity results.

Defect identification

Figure 9 shows that there is a significant difference in the cut-off frequency obtained between the concrete and

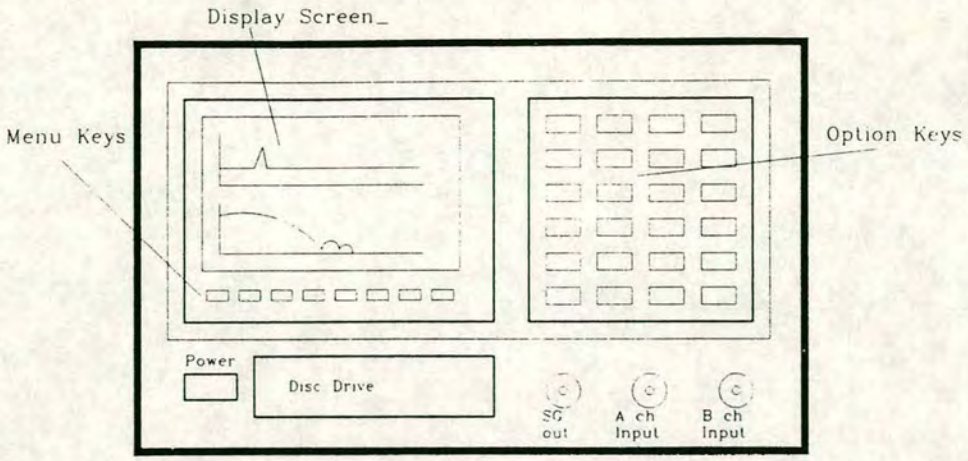

igure 6 Dual channel FFT analyser

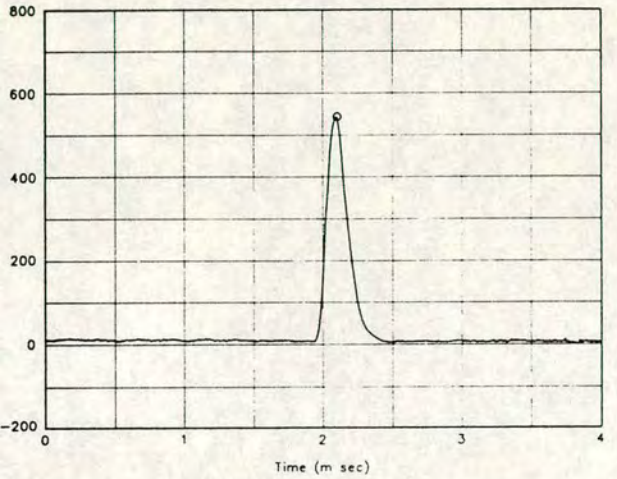

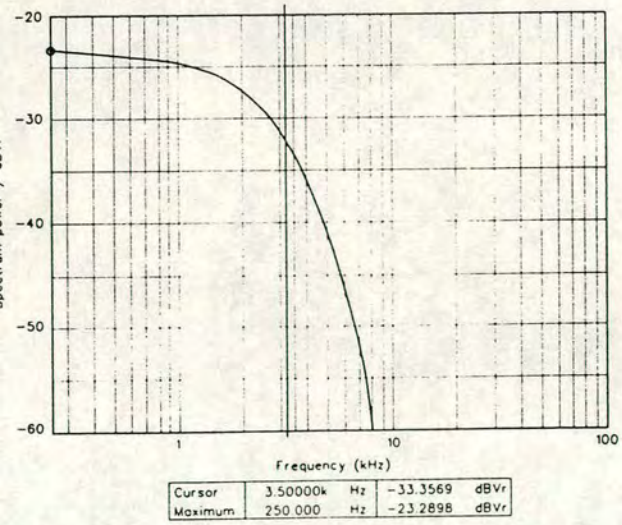

igure 7 (a) 1.25 g hammer impact on 1 day old grout – time omain; (b) FFT of 1.25 g hammer impact on 1 day old grout

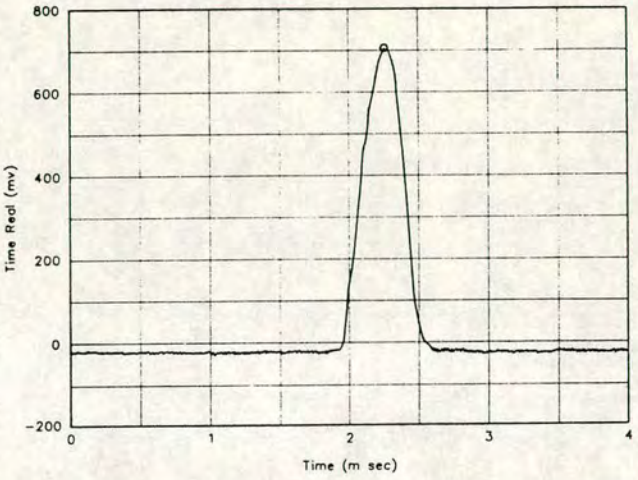

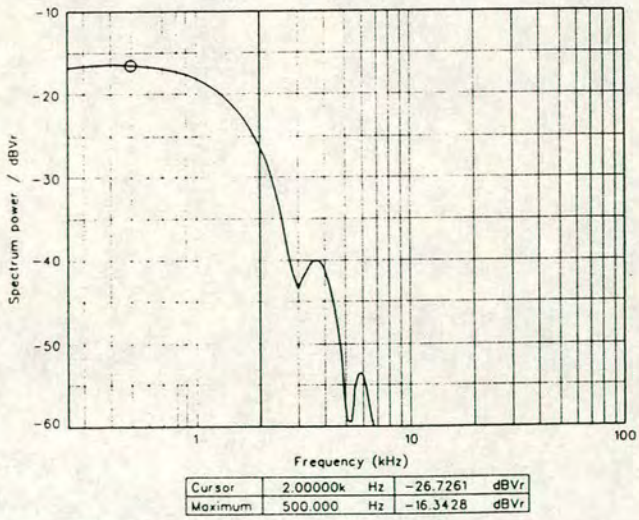

Figure 8 (a) 280 g hammer impact on 1 day old grout cube – time domain; (b) FFT of 280 g hammer impact on 1 day old grout

nortar cubes with the 1.25 g hammer and a detectable difference between the concrete and mortar with the 80 g hammer. These results are an average of readings taken for three test cubes. The results are repeatable and individual cut-off frequencies obtained are shown in *Table 3*. At 28 days the cut-off frequency obtained

Table 2 Transmission test results

	Position	Peak frequency (kHz)	Dist. (m)	Velocity (m s^{-1})
Sonic I-E test	1	2.000	2	4000
	2	1.925	2	3850
	3	2.075	2	4150
	4	2.075	2	4150
			Ave.	4040
	Position	Time ($\times 10^{-6}$s)	Dist. (m)	Velocity (m s^{-1})
Sonic trans. test	1	254	1	3937
	2	260	1	3846
	3	243	1	4115
	4	246	1	4065
			Ave.	3991
54 kHz trans. test	1	248	1	4039
	2	252	1	3971
	3	250	1	3997
	4	250	1	4002
			Ave.	4002

with the 1.25 g hammer is 7 kHz on the concrete cube and 5.25 kHz on the mortar cube – a difference of 25%. The difference in the cut-off frequency obtained with the 280 g hammer on the two sets of cubes is much less (approximately 15%). This would suggest that as the cut-off frequency increases the sensitivity to the concrete mix also increases. A 25% drop in cut-off frequency could have a significant effect on an investigation e.g. a cut-off frequency of 10 kHz is expected when testing a concrete beam. Using Equation (2) and assuming a pulse velocity of 4000 m s^{-1} the profile of the smallest target that should be detectable is 200 mm. However, if the cut-off frequency is actually 7.5 kHz, the profile of the smallest target detectable would be 267 mm. If the investigation is required to find voids greater than 200 mm it could be possible to conclude that the test object was sound when voids were actually present. Impact-echo testing of concrete frequently requires cut-off frequencies much higher than 10 kHz. If an impact generating frequencies up to 50 kHz is expected, the actual cut-off frequency may be very much lower which could have a very serious effect on the results of an investigation if the mix proportions of the specimen have not been investigated. The results indicate that as the expected cut-off frequency increases the influence of concrete mix also increases. The greater the volume and density of aggregate the greater the cut-off frequency obtained using the same impactor.

As can be seen in *Figure 10* the pulse velocity increases with age for both concrete and mortar as the cubes cure. The cubes are hardening over this period and therefore the pulse velocity increases. The pulse velocity is higher through the concrete cubes as expected. The concrete contains granite chips and the pulse velocity through these is higher than that through the sand and the cement paste. As the size of the chips increases it would be expected that the pulse velocity would also increase towards that of solid granite. A difference of 150 m s^{-1} was found. This could lead to a defect being detected in a test specimen but because the assumed velocity was wrong the expected location of the defect would also be wrong – see *Figure 14*.

Figure 11 shows the change in compressive strength for the two sets of cubes over 28 days. These results are quite similar as the water:cement ratio is the same for the mortar and concrete mixes[11]. The concrete has a slightly higher compressive strength. This is expected as it has been found, for a constant water:cement ratio, a mix with proportionately less cement paste has a higher compressive strength. This is due to a reduction in the porosity of the concrete which would give rise to an increased strength (assuming no voids in the aggregate).

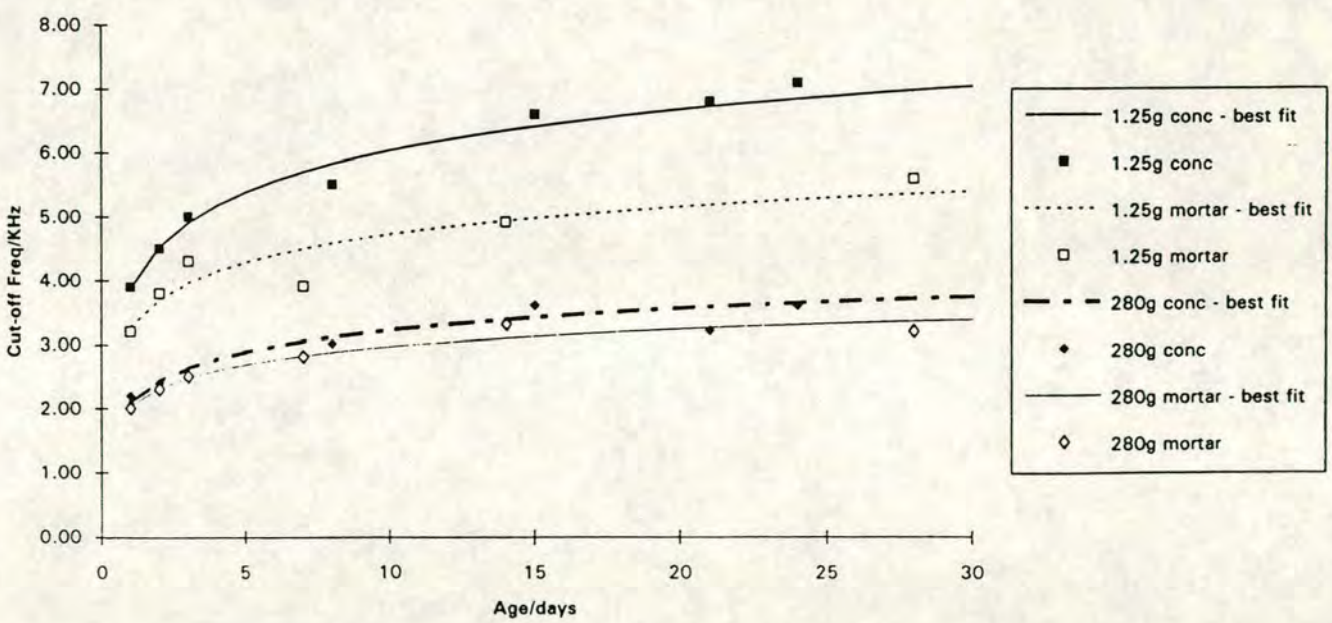

Figure 9 Cut-off frequency data

Table 3 Experimental data

ge ays)	Cube no.	Concrete cube data 280g Hammer Cut-off freq. (kHz)	1.25g Hammer Cut-off Freq. (kHz)	Age (days)	Cube No.	Mortar cube data 280g Hammer Cut-off freq. (kHz)	1.25g Hammer Cut-off freq. (kHz)	Notes
	1	2.375	3.5	1	1	2	2.75	
	2	2.25	4.25		2	2	3.25	
	3	2	4		3	2	3.5	
	1	2.375	4.5	2	1	2.5	3.5	
	2	2.375	4.5		2	2.25	4	
	3	2.5	4.5		3	2.25	4	
	1	2.5	4.75	3	1	2.5	2.5	Ignore
	2	2.5	5		2	2.5	4.5	
	3	2.5	5.25		3	2.5	4	
	1	2.75	4.75	7	1	2.75	4	
	2	3	6		2	2.75	3.5	
	3	3.25	5.75		3	2.75	4.25	
5	1	3.25	6.5	14	1	2.75	3.125	Ignore
	2	2.75	6.75		2	3.5	5.25	
	3	4.875	6.5		3	3.5	4.5	
1	1	3.25	6	28	1	3.25	6.5	
	2	3	7.375		2	3	5.125	
	3	3.275	7		3	3.25	5.25	
4	1	4	7					
	2	3	7.5					
	3	3.875	6.75					
8	1	4	6.25					
	2	4.25	7					
	3	4	6.75					

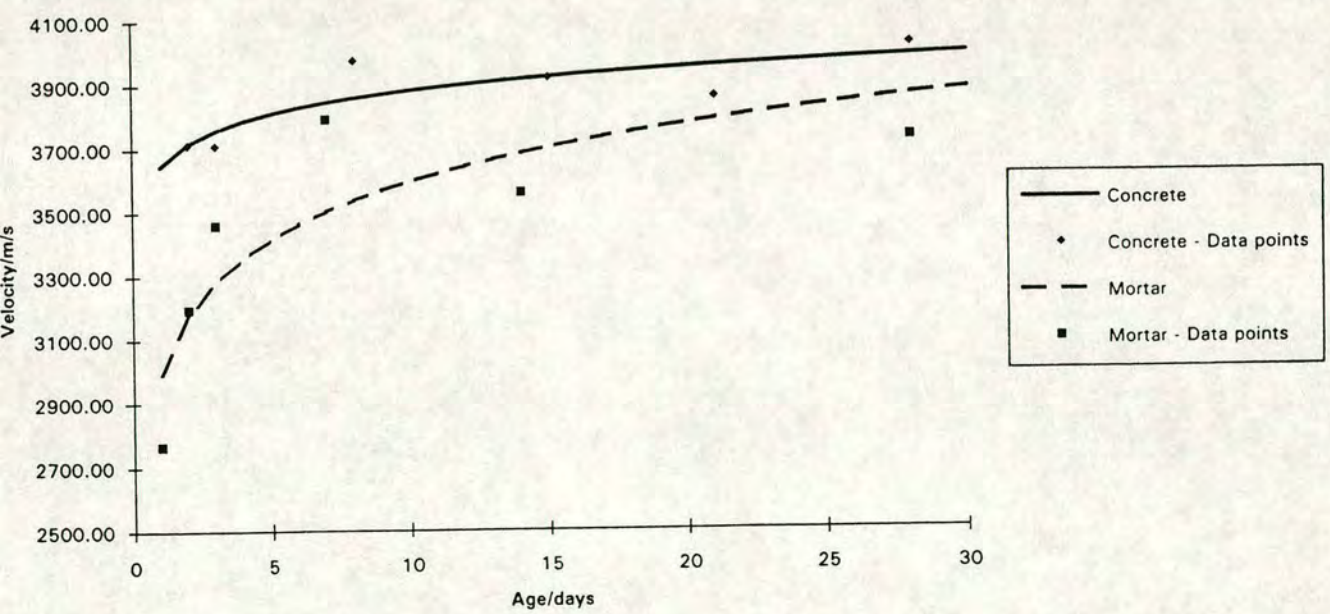

Figure 10 Pulse velocity data

Influence of aggregate on cut-off frequency

The pulse velocity and the cut-off frequency are both related to the elastic modulus, density and Poisson's ratio of the material. The values for each were then compared (*Figure 12*) to determine their relationship. The surface condition also affects the cut-off frequency but is not that important when determining the pulse velocity as the measurement is taken through the whole structure. However, the cubes were constructed in the same way and the tests were carried out to ensure as similar surface conditions as possible.

The graph shows an approximately linear relationship between pulse velocity and cut-off frequency. The mortar cubes seem to give rise to better results with both hammers than the concrete cubes. This could be because the mortar cubes are more homogeneous than the concrete cubes, i.e. there are no granite chips present. With the concrete cubes it would be possible that sometimes a granite chip would be located just under the impact point thus giving a slightly harder surface relative to a point where the granite chip was further from the surface. See *Figure 15*. This would give

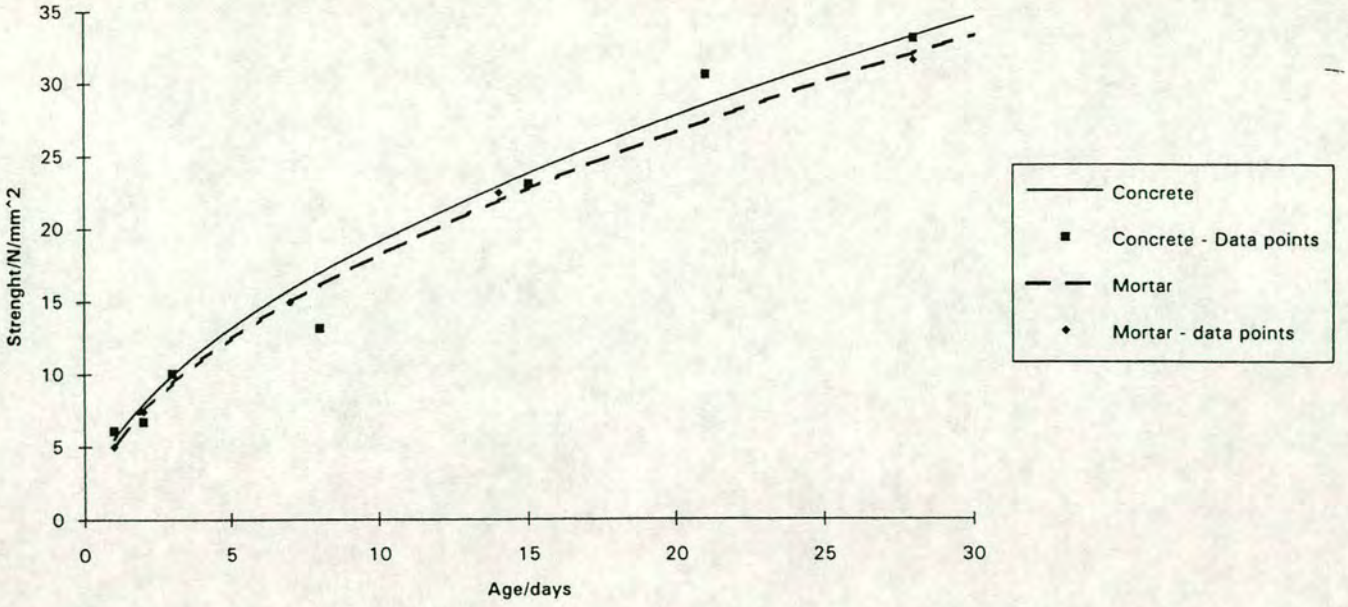

Figure 11 Strength data

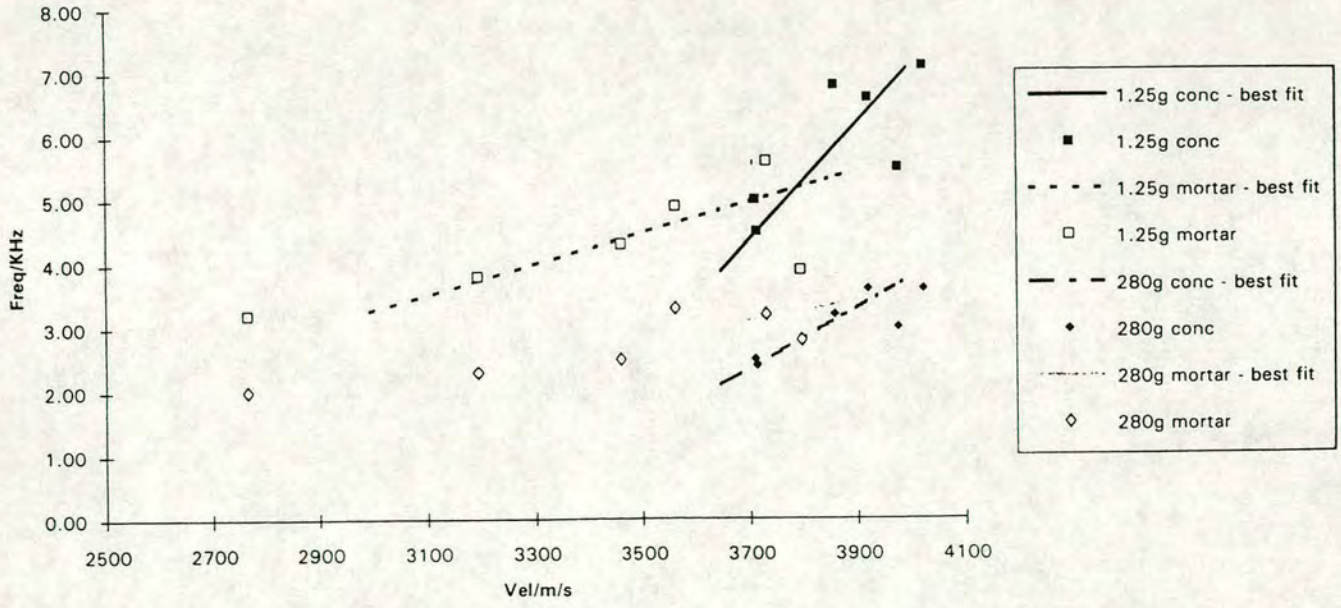

Figure 12 Velocity/cut-off frequency

rise to a higher cut-off frequency. The pulse velocity is calculated through the whole cube and any local variations in granite chip density will be averaged out throughout the whole path length. However, a relationship can be seen and with specific research it may be possible to determine the cut-off frequency obtainable with a certain impactor for a specific mix proportions of concrete.

Implications for assessment of compressive strength

The relationship between strength and cut-off frequency is linear as shown in *Figure 13*. As the strength increases, so the surface hardness and density increase and therefore the cut-off frequency will increase.

The graph indicates that using lower frequency impacts the mix does not greatly affect the cut-off frequency obtained. Also, as the concrete ages and gains strength, the variation in cut-off frequency obtained is not great. Using the 280 g hammer, over a strength gain of 25 N mm^{-2}, the cut-off frequency increases by 1 kHz.

The results from the 1.25 g hammer show a much clearer difference for mix type. With mortar the slope of the line obtained using the 1.25 g hammer is greater than that for the 280 g hammer. For an increase in

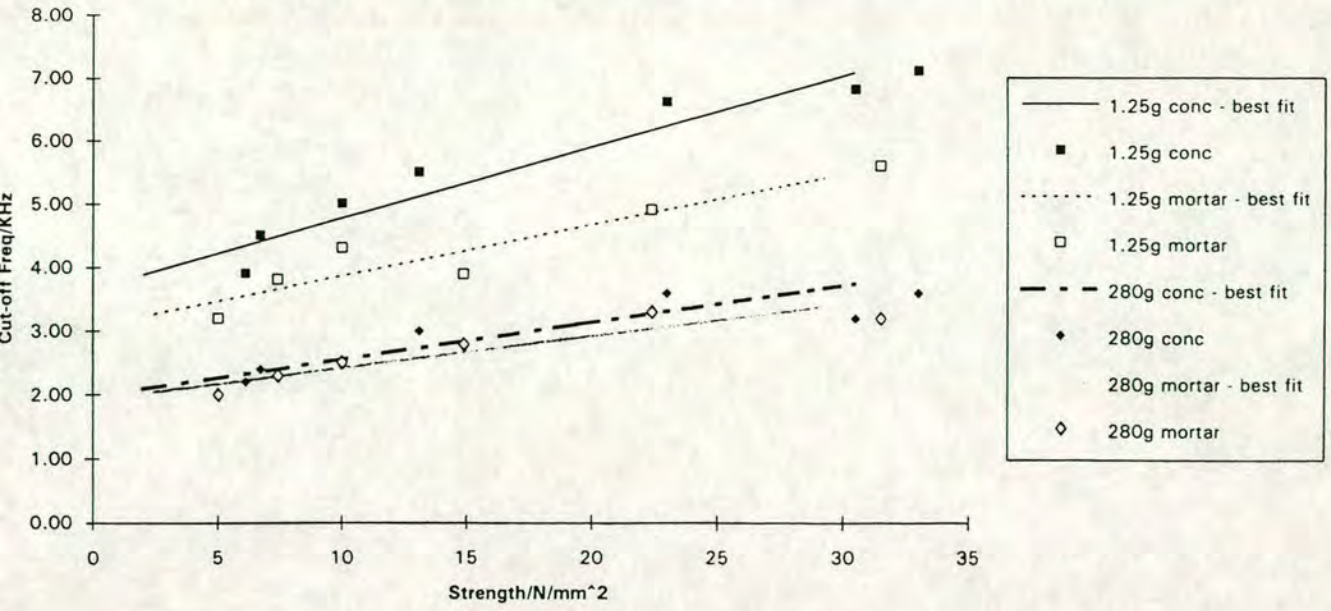

Figure 13 Cut off frequency/strength

strength of 25 N mm^{-2}, the cut-off frequency increases by 2 kHz. The largest slope was found using the 1.25 g hammer on concrete (the hardest material tested). In this case over an increase in strength of 25 N mm^{-2}, the cut-off frequency increases by 3.1 kHz. The above results indicate that an *in situ* testing method for concrete could be developed using high frequency hammers.

A database could be set up with different mixes of concrete and standard curves calculated for each mix of compressive strength against cut-off frequency. The structure could then be tested and the cut-off frequency obtained compared to the curve of strength *versus* frequency for that particular mix of concrete. Alternatively, a more simple approach would be to cast cubes from a delivery of concrete. The cut-off frequency would be measured for, say, three cubes and the compression strength measured at any given age. The cut-off frequency could then be measured at different points on the structure and compared to those obtained on the cubes. Any areas on the structure resulting in a low cut-off frequency would indicate the concrete in that area had a lower strength and care should be taken, e.g. in the removal of formwork. This method would require minimum equipment and many readings could be taken very quickly making this a very economical method for non-destructive testing of concrete structures.

Conclusions

The mix proportions of a concrete and mortar have a significant effect on the cut-off frequency obtained by an impact hammer. The higher the percentage of aggregate, the higher the cut-off frequency obtained. A difference of almost 2 kHz was noted for the same hammer on a mortar and concrete mix.

2 The cut-off frequency obtained increases with age, i.e. as the concrete cures.

3 The higher the modally tuned cut-off frequency of the impactor the greater the effect of mix proportions on the actual cut-off frequency obtained.

4 The pulse velocity increases as the concrete cures. The pulse velocity is higher for concrete and mortar with higher percentages of aggregate. A difference in pulse velocity of 150 m s^{-1} was noted for the mortar and concrete mixes at the same age.

5 The compressive strength of the concrete and mortar increases as the concrete and mortar cure. The compressive strengths of the concrete and mortar are comparable as the water:cement ratio is constant. However, the strength of the concrete is slightly higher as the proportion of paste is lower than that of the mortar.

6 The pulse velocity can be related to the cut-off frequency obtainable for an impulse hammer on a mix of concrete and mortar.

7 There is a linear relationship between compressive strength of a concrete and a mortar mix and the cut-off frequency obtainable. It should be possible to determine the strength of a concrete or mortar mix using an instrumented hammer of high frequency (>5 kHz). This would be simple to carry out on-site and could be used to determine formwork striking times.

8 There is therefore significant potential for the use of instrumented impulse hammer techniques in the non-destructive evaluation of concrete.

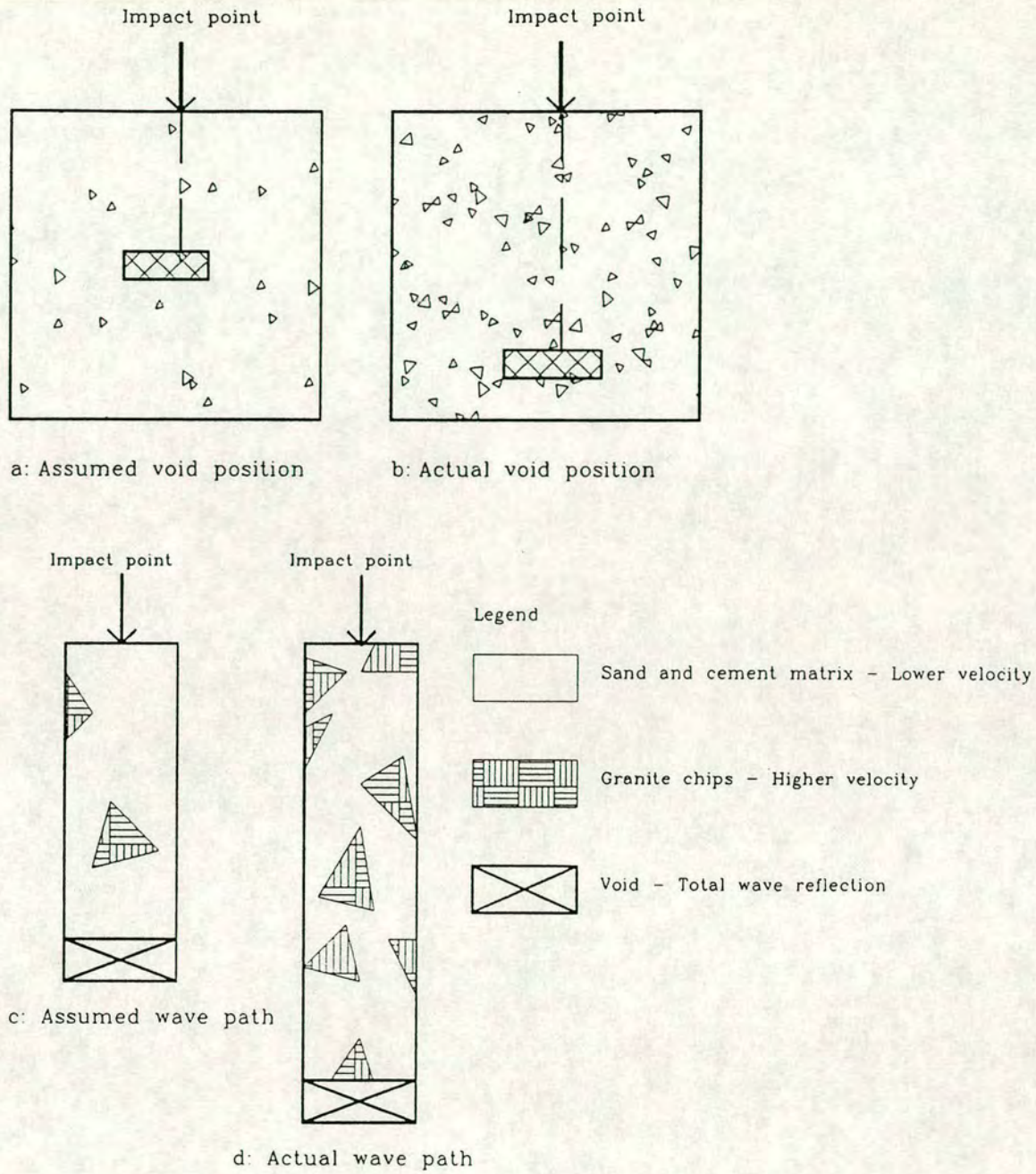

Figure 14 Effect of incorrect assumption of pulse velocity

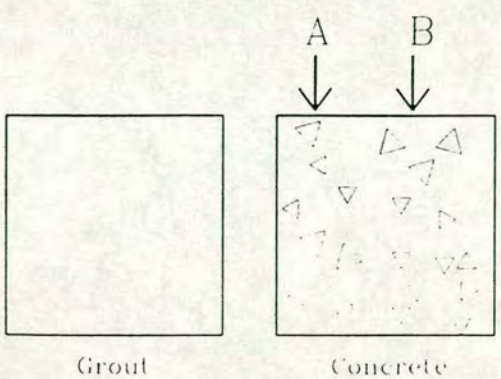

Figure 15 Influence of aggregate on cut-off frequency

Acknowledgements

The authors are grateful to K. Broughton, Dr P. C. Robery and H. A. Tomsett for their helpful input and to undergraduate students David Brookes and Ewan Scott for carrying out the experimental work. Thanks are also due to the University of Edinburgh for providing the facilities necessary to carry out the experimental work, the Engineering and Physical Sciences Research Council and Ove Arup and Partners for providing financial support.

References

1 Carino, N. J. Sansalone, M. and Hsu, N. N. A point source-point receiver, pulse-echo technique for flaw detection in concrete. *ACI. J. Proc.* 1986, 83 (2) 199–208

2 Corelli, D. and Brown. Impact Testing Considerations. *Int. Modal Analysis Conf. Proc.* 1984, Vol. 2, pp. 735–742
3 Love, A. E. *The Mathematical Theory of Elasticity*, 4th edn. Dover Publications, New York, 1944, p. 643
4 Hunter, S. C. Energy absorbed by elastic waves during impact. *J. Mech. Phy. Sol.* 1957, **5**, 162–171
5 Hsu, N. N., Chen, G. and Sansalone, M. Characterization of a piezoeletric transducer coupled to a solid. *IEEE Ultras Symposium, Denver, CO, 1987* pp 689–692
6 Pessiki, S. P. and Carino, N. J. Setting time and strength of concrete using the impact-echo method. *ACI Mater J.* 1988, **85**(5) 389–399
7 Ghorbanpoor, A. *Evaluation of post-tensioned concrete bridge structures by the impact-echo technique.* US Dept. of Transportation, Federal Highway Administration, Pub No. FHWA-RD-92-096, December 1993
8 Papoulis, A. *Signal Analysis*, McGraw-Hill, Singapore, 1977, p. 431
9 Lynn, P. A. and Fuerst, W. *Introductory Digital Signal Processing with Computer Applications*, John Wiley, Chichester, UK, 1989, p. 371
10 Carino, N. J., Sansalone, M. and Hsu, N. N. Flaw detection in concrete by frequency spectrum analysis of impact-echo waveforms, *Intern. Adv. Nondestr. Test.* 1986, **12**, 117–146
11 Neville, A.M. and Brooks, J.J. *Concrete Technology*, Longman Scientific and Technical, Essex, UK, 1987, p. 438

Appendix II

Conference Papers

QUANTIFYING THE DEFECTS IN POST-TENSIONED BRIDGES USING IMPULSE ULTRASONICS

J Martin, Dr M S A Hardy, Dr A S Usmani and Professor M C Forde,
University of Edinburgh, Scotland

Considerable attention has focused on the safety of post-tensioned bridges following the UK Department of Transport/Highways Agency decision to ban the commissioning of any new grouted duct post-tensioned bridges in England. Debate has surrounded the effectiveness of NDT techniques to identify voiding in the ducts. Radar was shown to be effective in identifying the location of the ducts and also in identifying voiding where when non-metallic ducts are used. Further debate surrounds the effectiveness of impulse echo techniques to identify voids in metallic ducts.

This paper aims to indicate the size and position of ducts that should be detectable for a given impulse, using the impulse echo technique. A finite element investigation into the use of impact-echo methods for the investigation of ducted post-tensioned bridge beams is presented. There has been some debate concerning the feasibility of detecting a reflection from a circular duct when measured at a point on the surface. It was concluded that thin steel ducting does not affect the detectability of voids inside; circular defects can be detected but care must be taken in deciding upon contact time of the impulse; and analysis of the results in the frequency domain is usually more straightforward.

1.0 INTRODUCTION

The U.K. Department of Transport issued a press notice in 1992 stating that it would not be commissioning any new grouted duct post-tensioned concrete bridges in England[1,2]. It also announced that existing grouted duct post-tensioned bridges were to undergo detailed inspection.

Many different non-destructive investigation techniques have been applied to post-tensioned bridges with varying degrees of success[3]. Radar has been shown to be effective in identifying the location of the ducts[4] and also in identifying voiding where when non-metallic ducts are used[5]. One of the most promising investigation techniques is the impulse-echo method. Figure 1 shows a typical instrumentation set up for this method.

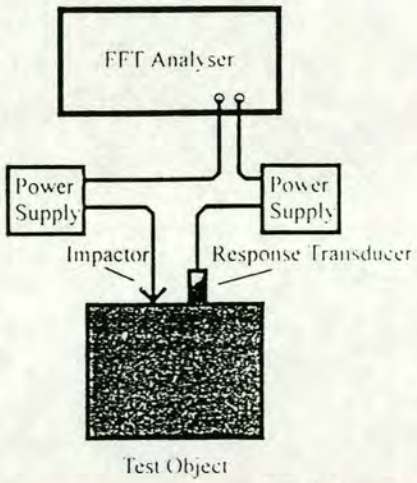

Figure 1: Set-up for Impact-Echo Test

Considerable research has been carried out into the use of impact-echo techniques for the investigation of defects in concrete[6,7]. This technique has also been applied to grouted duct post-tensioned concrete bridge beams[8,9].

The impact-echo method is very successful in detecting planar flaws[10] as the wave-front is reflected back to the surface (see fig. 2a.). Most ducts used in post-tensioned bridge beams are circular in section. This causes scattering of the wave reflection (see fig. 2b); less energy reaches the response transducer and the reflection may not be measured. However, if the duct is voided the base reflection will arrive later than the base reflection for a grouted duct. This occurs as the wave has to propagate around the void.

Figure 2: Circular Defect Causing Wave Scattering

This paper aims to quantify what is achievable with the impact-echo method in the investigation of concrete bridges. A series of finite element simulations has been carried out allowing many different beam configurations to be investigated without the need for time-consuming and expensive laboratory specimen manufacture. In theory, deconvolution methods could be used to clarify these results. However, at present, the impulse cannot be measured with the accuracy required for deconvolution methods to be implemented in practice.

2.0 THEORETICAL BACKGROUND

2.1 Stress Waves

When carrying out an impact-echo test, a transient stress pulse is introduced into the test object using a mechanical point impact[8]. The pulse propagates through the specimen along spherical wave-fronts within the object and cylindrical wave-fronts across the surface of the object.

Three types of waves are set up:

- Compression waves, P-waves, are dilatational and travel parallel to the direction of propagation.
- Shear waves, S-waves, are distortional and travel perpendicular to the direction of propagation.
- Surface waves, Rayleigh or R-waves, travel along the surface of the test specimen away from the impact point.

The P- and S-waves are partly reflected by material boundaries within the test object. The amount of reflection is dependent on the relative difference in material properties across the boundary. A large reflection will occur if there is a large difference in material properties and a small reflection will occur if there is a small difference in material properties. The amount of reflection is given by Ghorbanpoor[8] (Eqn 1). Almost total reflection will occur at a boundary with air.

$$A_R = A\,(\rho_2 C_2 - \rho_1 C_1) / (\rho_2 C_2 + \rho_1 C_1) \quad \text{---------- (1a)}$$

and

$$A_T = A\,(2\ \rho_1 C_1) / (\rho_2 C_2 + \rho_1 C_1) \quad \text{---------- (1b)}$$

where A_R = Amplitude of reflected wave
A = Initial wave amplitude
A_T = Amplitude of transmitted wave
ρ_1 = Mass density of initial material
ρ_2 = Mass density of second material
C_1 = Wave speed through initial material
C_2 = Wave speed through second material

The movement of the test specimen is measured near to the impact point - see figure 1. This is to reduce the interference from the surface wave that will pass the measurement transducer before the first reflections from within the test object arrive back at the transducer. Problems may occur if the test object is narrow. The reflection of the surface wave from the edge of the specimen may arrive at the transducer at the same time as reflections from material boundaries within the specimen and distort or swamp the results. The P-waves can be measured using a displacement, velocity or acceleration transducer.

If the pulse velocity through the specimen is known and the time to the arrival of a reflection from within the specimen is measured, then the distance to the target is given by (eqn. 2)[11]

$$2d = V_p t \quad \text{---------- (2)}$$

where d = depth to target
V_p = P-wave velocity
t = time to reflection

As the test object becomes more complex, the time trace of the receiver becomes very difficult to analyse. It is much more straightforward to analyse data from these tests in the frequency domain by carrying out a Fourier transform on the data. (see figure 3)

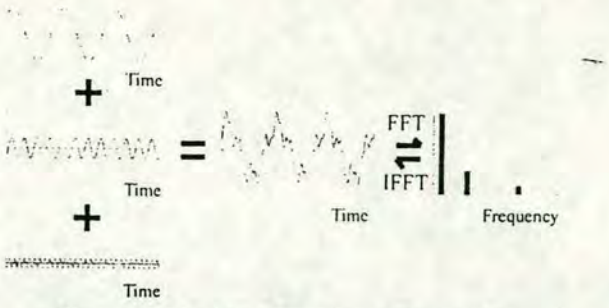

Figure 3. Principle of the Fourier Transform

2.2 Fast Fourier Transform

The Fourier transform is the basis of frequency analysis. The assumption is made that the time signal is made of up to an infinite number of sinusoidal components with various frequencies at different amplitudes and initial phases[12]. The Fast Fourier Transform (FFT) is a highly efficient algorithm for computing the Discrete Fourier Transform and was first developed in the 1960s[13].

The exact relationship between the highest frequency applied by the impact (the *cut-off frequency*) and smallest target size detectable depends upon the test material, but for concrete the cut-off frequency input will allow the detection of targets that create a profile to the p-wave front of approximately half a wavelength[14].

$$L = \lambda/2 \quad \text{------- (3a)}$$

and

$$L = V_p/f_c \quad \text{------- (3b)}$$

where L = smallest target size (m)
λ = wavelength (m)
f_c = cut-off frequency

Similarly, the minimum depth at which a target can theoretically be detected can be calculated from Eqn 4.

$$d = V_p/(2f_c) \quad \text{------- (4)}$$

where d = smallest depth to target (m)

2.3 Finite Element Simulation

The finite element method derives from classical structural analysis techniques. Rather than manipulating the governing equations into differential form and then solving numerically, this method divides the domain of the solution into a finite number of simple sub domains, elements, and constructs an approximation of the solution over the collection of elements[15]. The method has been used with remarkable success in many fields because of the generality of the underlying principles.

The finite element method consists of eight basic steps[16]:

Step 1: Discretise and select element configuration
Step 2: Select approximation models of functions
Step 3: Define strain-displacement and stress-strain relationships
Step 4: Derive element equations
Step 5: Assemble element equations to obtain global or assemblage equations and introduce boundary

conditions
Step 6: Solve for the primary unknowns
Step 7: Solve for derived or secondary quantities
Step 8: Interpretation of results

Two-dimensional finite element analyses have been carried out on concrete with various 'targets' included in the model. Two finite element codes were used. ANSYS version 5.0a, developed by Swanson Analysis Systems, Inc. of Houston, Pennsylvania was used to perform the analysis of plane voids and lined and unlined ducts. DYNPAK[17] was used to perform the analysis of beams with spherical voids.

3.0 EXPERIMENTAL PROCEDURE

3.1 Initial Finite Element Analysis

Two sets of models were constructed to determine whether defects in the beam models could be detected using the finite element method. ANSYS version 5.0a was used for these analyses.

The following assumptions were made throughout the finite element analysis:

* Concrete behaves as a homogeneous, isotropic and elastic material. Modulus of elasticity = 31.9 GN/m^2. Poison's ratio = 0.2. Mass density = 2214 kg/m^3. The concrete grout used in the ducts has the same properties.

* Steel behaves as an homogeneous, isotropic and elastic material. Modulus of elasticity = 210 GN/m^2. Poison's ratio = 0.3. Mass density = 7800 kg/m^3.

The first series models were constructed of a concrete beam of width 1000 mm and depth 300 mm. These are illustrated in figure 4. The first model was of a solid concrete beam, the second containing a 50 mm delamination at 150 mm, the third a 400 mm wide, 50 mm deep void at 150 mm, the fourth a 200 mm wide, 50 mm deep void at 150 mm and the fifth a 150 mm diameter circular void at 125 mm. The time step used was 5μs and the force impulse was a 50μs duration half sine wave. A full transient dynamic analysis was carried out on each model.

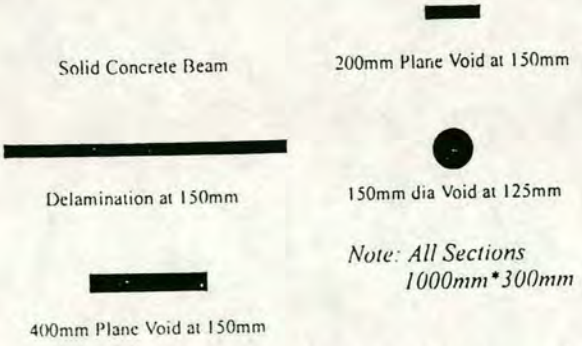

Figure 4. Series 2, Finite Element Models

The second series investigated the effect of a 5 mm steel liner on a 400 mm wide, 50 mm deep plane duct on the results of a finite element analysis. Four models were constructed with the same mesh density. The first model was of a fully grouted unlined duct, the second a fully grouted steel lined duct, the third an ungrouted unlined duct and the fourth model was of an ungrouted steel lined duct. These are illustrated in figure 5. The time step used was 5μs and the force impulse was again a 50μs half sine wave. Again, a full transient dynamic analysis was carried out on each model.

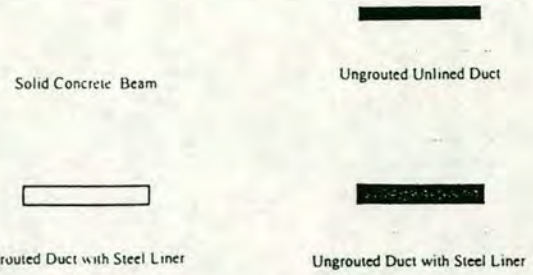

*Notes: 1: All Sections 1000mm * 300mm*

Figure 5. Series 2, Finite Element Models

3.2 More Detailed F.E. Work

The third series of analyses was carried out using DYNPAK. This program allowed a more detailed analysis to be carried out, i.e. a finer mesh and shorter timesteps could be used. Reflections from circular voids were investigated. The dimensions of the beam were again 1000 mm wide by 300 mm deep. The time step used throughout was 0.75 ms and a total of 4096 steps were calculated. This series was divided into three distinct sets:

Set 1: Investigation of contact time of impulse. A model was constructed with a 100 mm diameter void at 125 mm depth. Finite element analyses were carried out with half sine wave impulses of 30 μs, 50 μs and 70 μs duration.

Set 2: Investigation of void size detectable. A half sine wave impulse of 30μs duration was used throughout this set. The top of each void was 125 mm from the top surface of the beam. The first model contained a 75 mm diameter void, the second a 100 mm diameter void and the third a 125 mm diameter void.

Set 3: Investigation of depth to void. As in set 2, a half sine wave impulse of 30 μs duration was used throughout this set. The void in each model was 100 mm in diameter. The first model contained the void at 100 mm from the surface, the second at 125 mm from the surface and the third at 150 mm from the surface.

4.0 RESULTS

4.1 Series 1

Figure 6 shows the vertical displacement-time traces for the first two models - the solid concrete beam and the beam with a delamination at 150 mm. See Fig.6. The traces are quite difficult to analyse and a vertical drift is apparent in each case. This drift is present because the model is unrestrained in the vertical direction. Therefore, the whole model starts moving downwards when the load is applied. The results are more easily analysed if the frequency spectrum is calculated (figure 7). This was done using a 512 point FFT. The spectrum of the

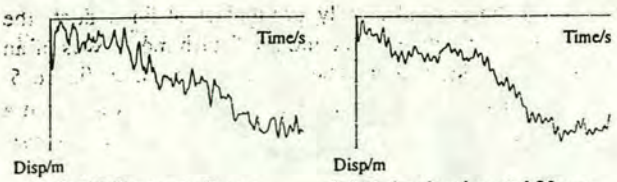

(a) Solid Concrete Beam (b) Delamination at 150mm

Figure 6. Series 1, Vertical Displacement/Time Traces

(a) Solid Concrete Beam (b) Delamination at 150mm

(c) 400mm plane void at 150mm (d) 200mm plane void at 150mm

Figure 7. Series1, Frequency Spectra

solid beam, figure 7a, shows a clear peak at the frequency corresponding to the base of the beam, 6.7 kHz. This peak cannot be seen on the spectrum of the results from the model containing a delamination at 150 mm, figure 7b. This plot shows a peak at the frequency corresponding to the frequency of a reflection from the delamination, 13.3 kHz. Figure 7c shows the spectrum obtained from the model containing a 400 mm wide void at 150 mm depth. Again a peak is clearly visible corresponding to the frequency expected from the void, 13.3 kHz. The peak from the base is difficult to identify on this plot. Figure 7d shows a similar spectrum plot. This was obtained from the model containing a 200 mm wide void at 150 mm depth. The frequency peak corresponding to the reflection from the void is still visible but is not as well defined as in the previous two cases. The frequency peak corresponding to the base reflection is easier to identify than in the previous case. The final plot from series 1 shows the spectrum obtained from the model containing a 150 mm diameter circular void at 125 mm. The base reflection can be identified on this plot and is at a slightly lower frequency than that shown in figure 7a. This is as expected as the wave must travel around the void to reach the base of the beam, thus travelling a greater distance and so reducing the frequency of the reflection. A series of peaks can be seen in the region of the frequency expected from the void but limitations in the finite element method software used prevented more detailed analysis of this.

4.2 Series 2

The vertical displacement-time traces from each analysis are shown in Fig. 8. It can be seen that the presence of the steel liner has little effect on the displacement of the beam surface. Similarly to the first series of models, the traces from the ungrouted ducts (Figs 8b and 8d) show a vertical component of displacement at a higher frequency than the traces from the grouted ducts (Figs 8a and 8c). Fig. 9 shows the frequency spectrum for each of the above models. As expected, the plots from the models with grouted ducts show the base reflection at approximately 6.7 kHz. The base reflection is not visible on the plots from the ungrouted ducts but a peak at the frequency corresponding to the top of the void is clearly visible on both plots.

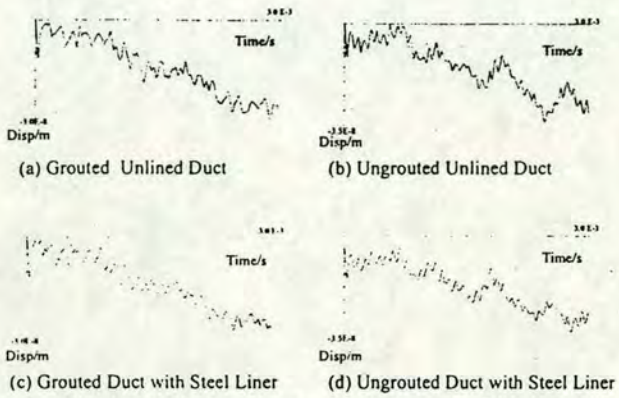

(a) Grouted Unlined Duct (b) Ungrouted Unlined Duct

(c) Grouted Duct with Steel Liner (d) Ungrouted Duct with Steel Liner

Figure 8. Series 2, Vertical Displacement/Time Traces

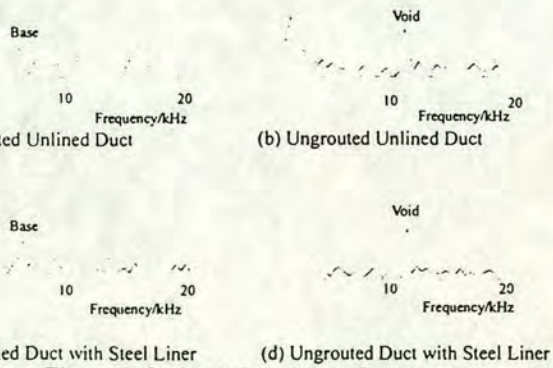

(a) Grouted Unlined Duct (b) Ungrouted Unlined Duct

(c) Grouted Duct with Steel Liner (d) Ungrouted Duct with Steel Liner

Figure 9. Series 2, Frequency Spectra

4.3 Series 3

DYNPAK was used to carry out these analyses. No vertical drift is shown on the displacement/time traces as this program requires the model to be constrained.

Set 1

Figure 10 shows the vertical displacement-time traces for the model containing a 100 mm diameter void at 125 mm from the beam surface - figure 10a with an impulse contact time = 30μs, figure 10b with contact time = 50μs and figure 10c with an impulse of contact time = 70μs. The expected arrival time of the compression wave from the base of the beam is approximately 160μs causing the surface of the beam to drop at this time. This can be seen on each displacement-time trace. A compression wave reflected from the top surface of the void would be expected to reach the surface of the beam at 60μs. This wave arrival would again cause the surface of the beam to

(a) Contact time = 30 us

(b) Contact time = 50us

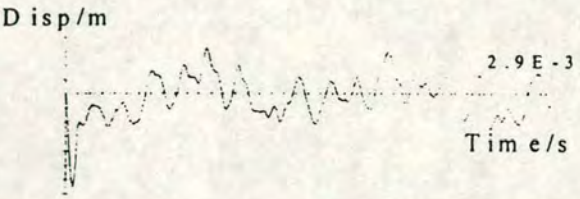

(c) Contact time = 70 us

Figure 10. Series3, Set1, Displacement/Time Traces

rop. The plot shown in figure 10a shows a clear drop in the urface at the expected time. Figure 10b also shows a definite rop in the beam surface but it is not as large as that with a 0μs impulse. The plot shown in figure 10c shows a iscontinuity at about 70μs but the magnitude is much reduced. Frequency spectrum plots were also calculated for this analysis. This was done by performing a four point moving average on he results from the finite element analysis, extracting every 4th oint and performing a 1024 point FFT on the data. The pectrum plots are shown in Figure 11. The frequency peak orresponding to the base reflection can clearly be seen on each lot. The peak corresponding to the reflection from the void an be seen at approximately 14.5 kHz. This peak is clearly een in Figure 11a, can be seen in Figure 11b and is difficult to dentify in Figure 11c. This is because the longer pulse length loes not input sufficient energy at these higher frequencies.

Set 2

The frequency spectra are shown for each of the models constructed for Set 2 (figure 12). The traces were constructed n the same way as those described for Set 1. Figure 12a shows he plot obtained from the model containing a 75 mm void at 125 mm depth. This trace is quite difficult to interpret. The base reflection can be seen at approximately 6.0 kHz. A frequency peak can also be seen at approximately 14.5 kHz but it is difficult to separate from peaks around that value. The plot obtained from the model containing a 100 mm diameter void at 125 mm is shown in figure 12b. The frequency peak corresponding to the base reflection can clearly be identified. This is at a slightly lower frequency than that shown in figure 12a. The peak corresponding to the reflection from the void can also be identified (14.5 kHz). Figure 12c shows the plot obtained from the model containing a 125 mm void at 125 mm.

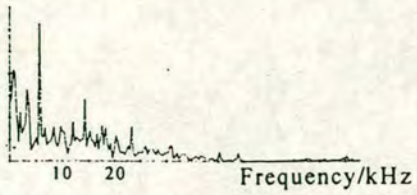

(a) Contact time = 30 us

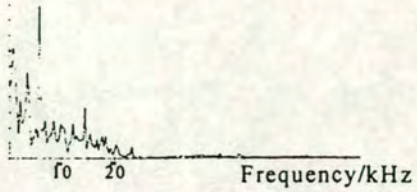

(b) Contact time = 50 us

(c) Contact time = 70 us

Figure 11. Series 3, Set 1, Frequency Spectra

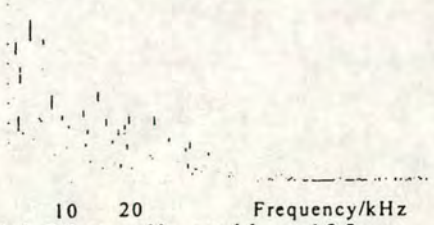

(a) 75mm dia. void at 125mm

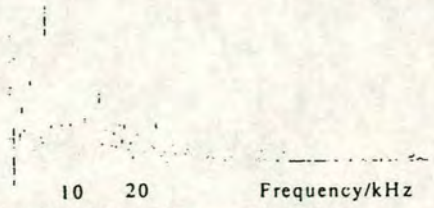

(b) 100mm dia. void at 125..

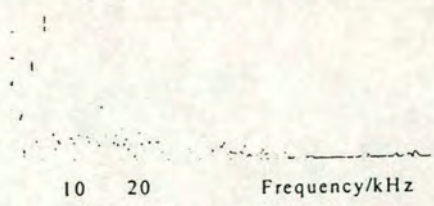

(c) 125mm dia. void at 125mm

Figure 12. Series 3, Set 2, Frequency Spectra

Again the peak from the void can be seen. The peak corresponding to the base reflection is clearly visible, again it is at a slightly lower frequency than that shown in figure 12b.

(a) 100mm dia. void at 100mm

(b) 100mm dia. void at 125mm

(c) 100mm void at 150mm

Figure 13. Series 3, Set 3, Displacement/Time Traces

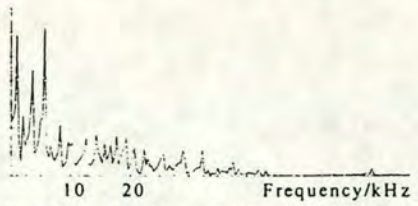

(a) 100mm dia. void at 100mm

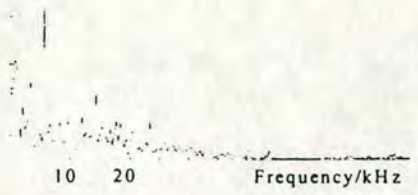

(b) 100mm dia. void at 125mm

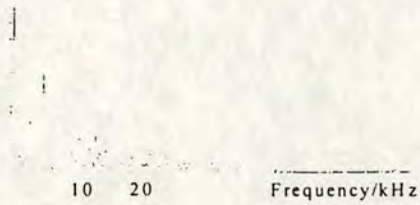

(c) 100mm dia. void at 150mm

Figure 14. Series 3, Set 3, Frequency Spectra

Set 3

The vertical displacement-time traces for Set 3 are shown in figure 13. The downwards displacement of the beam surface due to the arrival of the reflected wave from the void can be seen on each trace. The time of arrival varies as expected. The reflection from the void at a depth of 100 mm arrives at approximately 60μs, the reflection from the void at a depth of 125 mm arrives at approximately 70μs and the reflection from the void at a depth of 150 mm arrives at approximately 85μs. The frequency spectrum plots were constructed as before. The frequency peak corresponding to the reflection from the void at 100 mm is difficult to distinguish in figure 14a. Figure 14b shows a clear peak at approximately 14.5 kHz corresponding to the reflection from the void at 125 mm. The peak on the frequency spectrum corresponding to the reflection from the void at 150 mm can be seen with difficulty in figure 14c.

5.0 ANALYSIS AND DISCUSSION

5.1 Series 1

The finite element method can be used to analyse structures containing planar flaws quickly. The results from series 1 show that even with the limited mesh density available with the software, planar defects can easily be identified. The size of the defect can be estimated by comparing the frequency of the base reflection with that from a solid beam section. The larger the defect, the lower the frequency of the base reflection. Circular voids are more difficult to detect and require a much finer mesh. However, circular voids of a reasonable diameter can be detected. As with a planar void, the base reflection occurs at a lower frequency since the wave must propagate around the void to reach the base. Large circular voids may give rise to peaks on the frequency spectrum. As the diameter of the void increases the amount of scattering reduces since the void provides a flatter profile to the wave-front

5.2 Series 2

Similar results are produced with ducts that are lined and unlined. The frequency spectra for the ungrouted ducts clearly show a peak corresponding to a reflection from the void. This peak is missing from the spectra from the grouted ducts. The thin steel liner has very little effect on the results as the wavelength of the highest frequencies contained in the impulse are much greater than the thickness of the steel. Consider a thin steel layer bonded on to concrete (representing an ungrouted, steel lined duct). No stress occurs at the air-steel interface and, since the steel is thin, virtually no stress will occur at the steel-concrete interface. If the thin steel layer, of greater rigidity, was bonded between two layers of concrete, with the same rigidity, (representing a grouted steel lined duct) the thin layer would not interfere with the stress wave propagation and so the waves will travel directly through the layer[7].

5.3 Series 3

It has been shown that the shorter the contact time, the smaller the defect that can be detected. This is as expected. The assumed maximum frequency input to the beam is shown below:

$$f_c \approx 1/(1.5T_c) \qquad \text{----------} \quad (5)$$

where f_c=Max. frequency input (cut-off frequency) /Hz

T_c=Contact time of impulse /s

From the results obtained this appears to be rather conservative. However, the analyses carried out are on two-dimensional models, with concrete assumed to behave as a linear, isotropic and homogeneous material. This should lead to clearer results than those obtained from real concrete specimens.

Set 1 shows that as the contact time of the impulse increases, the 100 mm void at 125 mm depth becomes more difficult to detect. Using equations 4 and 5, the critical impulse duration would be approximately 40μs. It should therefore be possible to detect the void in model 3 only. However, as mentioned above, the model is a simplified version of a real concrete structure and so the void could be detected with an impulse of 50μs but could not be detected with an impulse of 70μs duration.

The results from Set 2 agree with the expected results. Using equations 3 and 5, the minimum profile that could be detected with an impulse of 30μs duration is 90mm. Therefore it will be possible to detect a 100 mm void and a 125 mm void at a depth of 125 mm but it will not be possible to detect a 75 mm void at the same depth. The frequency of the reflection from the base also reduced as the void diameter increased. This was as expected and could be used to determine the relative size of the voids.

The models constructed in Set 3 investigated the influence of the depth to a void on the resulting displacement-time traces and frequency spectra. If the void is at a depth close to the minimum depth at which defects become detectable the defect may not be detectable, as occurred in figure 14a. Scattering may also adversely affect the detection of a void at greater depth (figure 15). In this case, the deeper the void, the more severe the scattering.

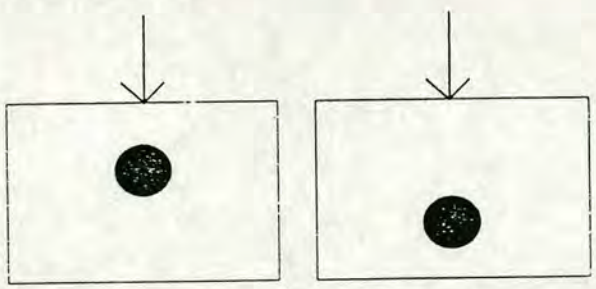

Figure 15. Depth to Circular Defect Affecting Wave Scattering

The above results show that the finite element method is a useful way of investigating the range and limitations of the impact-echo method as applied to the investigation of ducted post-tensioned bridges. It is generally assumed that the results expressed in the frequency domain will be more readily interpreted. However, these results show that the displacement-time traces can yield results that are difficult to interpret on the frequency data. As long as a small enough time step is used, the reflections from defects can be determined and the depth to these defects calculated from the time trace.

6.0 CONCLUSIONS

1. Thin steel ducting does not affect the detectability of voids inside
2. Planar defects are more readily detected than circular defects.
3. The base reflection, if distinguishable, can be used to determine the approximate size of a defect providing the expected frequency of the base reflection is known. The less the amplitude compared with that expected, the larger the defect
4. Circular defects can be detected but care must be taken in deciding upon contact time of impulse and measurement time step (this is important for both numerical simulation and field experimentation). The choice of element size and type is also important for finite element simulation.
5. Analysis of the results in the frequency domain is usually more straightforward. However, the first reflection from a defect can also be clearly seen on the displacement-time trace if the experiment is well conditioned.

7.0 ACKNOWLEDGEMENTS

The authors acknowledge the University of Edinburgh for providing the facilities necessary to carry out the analyses, the Engineering and Physical Sciences Research Council and Ove Arup and Partners for providing financial support.

8.0 REFERENCES

1. Press Notice No. 260. Published by DTP, London, 1992
2. Storrar, D.B. (1993) The management of post-tensioned grouted-duct bridges owned by the Department of Transport, *Proceedings of 5th International Conference on Structural Faults and Repairs-93*, Engineering Technics Press, Edinburgh, Vol 1, 3-7.
3. Woodward, R. J. (1993) Inspection of Post-tensioned Concrete Bridges - Non-destructive Testing Methods. TRL, Crowthorne, UK
4. Stain, R. T. and Dixon, S. (1993) Inspection of Cables in Post-tensioned Bridges - What Techniques are Available. *Proceedings of 5th International Conference on Structural Faults and Repairs-93*, Engineering Technics Press, Edinburgh, Vol 1, 297-300.
5. Cooke, R.S., Ashurst, D.M., McCavitt, N & M.C. Forde (1993) Digital radar assessment of Besses o' th' Barn Post-tensioned precast concrete segmental rail bridge, *Proceedings of 5th International Conference on Structural Faults and Repairs-93*, Engineering Technics Press, Edinburgh, Vol 1, 305-311.
6. Carino, N. J. Sansalone, M. and Hsu, N. N. (1986) A Point Source-point Receiver, Pulse-Echo Technique for Flaw Detection in Concrete. *ACI Journal Proceedings*, March-April 1986, **83**, No. 2, 199-208.
7. Carino, N. J. Sansalone, M. and Hsu, N. N. (1986) Flaw Detection in Concrete by Frequency Spectrum Analysis of Impact-Echo Waveforms. *International Advances in Nondestructive Testing*, **12**, 117-146.
8. Ghorbanpoor, A. (1993) Evaluation of Post-tensioned Concrete Bridge Structures by the Impact-Echo Technique. *U.S. Dept. of Transportation, Federal Highway Administration, Publication No. FHWA-RD-92-096*, Dec. 1993.
9. Sansalone, M. and Carino, N. J. (1988) Detecting Honeycombing, the Depth to Surface Opening Cracks and Ungrouted Ducts using the Impact-Echo Method. *Concrete International*, April 1988.
10. Cheng, C. and Sansalone, M. (1993) The Impact-Echo Response of Concrete Plates Containing Delaminations - Numerical, Experimental and Field studies. *Materials and Structures* 26, No. 159, 274 - 285
11. Fegen, I., Forde, M.C. & Whittington, H.W. (1979) The Detection of Voids in Concrete Piles using Sonic Methods. *Proc. 4ème Colloque International sur les méthodes de contrôle non destructif*, Grenoble, Sept 1979, 40-46.

12. Papoulis, A. (1977) *Signal Analysis*, McGraw-Hill, Singapore, pp 431.
13. Lynn, P. A. and Fuerst, W. (1989) *Introductory Digital Signal Processing with Computer Applications*, John Wiley and Sons, Chichester, England, pp 371.
14. Martin, J & Forde, M.C. (1995) Influence of concrete age and mix design on impulse hammer spectrum and compression wave velocity, *Construction & Building Materials* (in press).
15. Becker, E. B. Carey, G. F. and Oden, J. T. (1981) *Finite Elements - An Introduction*, Vol.1, Prentice - Hall, Inc. Englewood Cliffs, N.J., pp 258.
16. Desai, C. S. (1979) *Elementary Finite Elements*, Englewood Cliffs, N.J. 434pp
17. Owen, D. R. J. and Hinton, E. (1980) *Finite Elements in Plasticity: Theory and Practice*, Pineridge Press limited Swansea, U.K. pp 594.

International Symposium Non-Destructive Testing in Civil Engineering (NDT-CE) 26.-28.09.1995

Influence of impulse spectrum on defect detection in post tensioned bridges

J. Martin, M. Hardy, A. Usmani, M. Forde
University of Edinburgh, Edinburgh (GB)

Keywords: *Bridges, Concrete, Radar, Sonic*

In the UK, the Department of Transport/Highways Agency's decision to ban the commissioning of any new grouted duct post-tensioned bridges in England has generated an increased interest in NDT inspection techniques. Debate has surrounded the effectiveness of NDT techniques to identify voiding in the ducts. Radar is effective in identifying the location of the ducts and also in identifying voiding where non-metallic ducts are used. Further debate surrounds the effectiveness of impulse echo techniques to identify voids in metallic ducts.

This paper aims to indicate the size and position of ducts that should be detectable for a given impulse, using the impulse echo technique. A finite element investigation into the use of impact-echo methods for the investigation of ducted post-tensioned bridge beams is presented. The results of the F.E. model are verified from laboratory experiments

Introduction

In 1992 the UK. Department of Transport stated that it would not be commissioning any new grouted duct post-tensioned concrete bridges in England[1,2]; and that existing grouted duct post-tensioned bridges were to undergo detailed inspection. Many different NDT techniques have been applied to post-tensioned bridges with varying degrees of success[3]: radar is effective in identifying the location of the ducts[4] and in identifying voiding where non-metallic ducts are used[5]. One of the most promising investigation techniques for identifying voids within a metal ducted tendon is the impulse-echo method. Figure 1 shows a typical instrumentation set up for this method.

Research has been carried out into the use of the impulse-echo technique for the investigation of defects in concrete[6,7]. This technique has also been applied to grouted duct post-tensioned concrete bridge beams[8,9]. The impact-echo method is very successful in detecting planar flaws[10], but most ducts used in post-tensioned bridge beams are circular in section. This causes scattering of the reflected wave, less energy reaches the response transducer and the reflection may not be detectable. The impact method is therefore critical.

The objective of this work is to investigate what impact pulses are required to detect flaws in post-tensioned bridge beams. F.E. simulations were carried out and initial experimental verification undertaken.

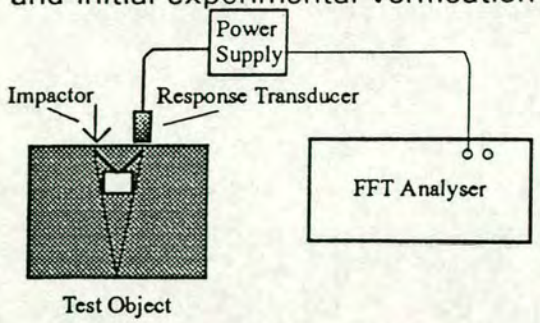

Figure 1: Set-up for Impact-Echo Test

THEORETICAL BACKGROUND

Stress Waves

In an impact-echo test, a transient stress pulse is introduced into the test object using a mechanical point impact[8]. The pulse propagates through the specimen along spherical wave-fronts and along its surface with cylindrical wave-fronts. It is reflected at material boundaries. A large reflection will occur if there is a large difference in material properties and a small reflection will occur if there is a small change. The amount of reflection and transmission is given by Ghorbanpoor[8].(Eqn 1) Almost total reflection will occur at a boundary with air.

$$A_R = A\,(\rho_2 C_2 - \rho_1 C_1) / (\rho_2 C_2 + \rho_1 C_1 \quad \text{---------- (1a)}$$

and

$$A_T = A\,(2\ \rho_1 C_1) / (\rho_2 C_2 + \rho_1 C_1 \quad \text{---------- (1b)}$$

where A_R = Amplitude of reflected wave A = Initial wave amplitude
A_T = Amplitude of transmitted wave ρ = Mass density
C_1, C_2 = Wave speed through initial and second material

If the pulse velocity through the specimen is known and the time to the arrival of a reflection from within the specimen is measured, then the distance to the target is given by Fegen[11] as:

$$2d = V_p t \quad \text{---------- (2)}$$

where d = depth to target V_p = P-wave velocity t = time to reflection

As the test object becomes more complex, the time trace of the receiver becomes very difficult to analyse. It is much more straightforward to analyse data from these tests in the frequency domain by carrying out a Fourier transform on the data. (see figure 3)

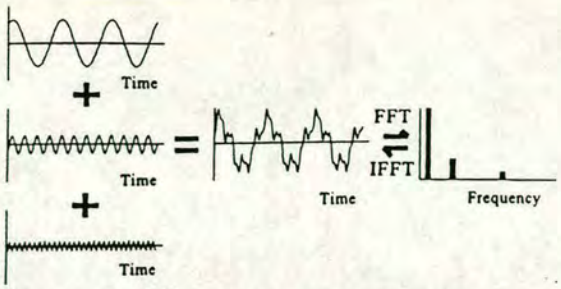

Figure 2. Principle of the Fourier Transform

Fast Fourier Transform

The Fourier transform is the basis of frequency analysis. The assumption is made that the time signal is made of up to an infinite number of sinusoidal components with various frequencies at different amplitudes and initial phases[12]. The Fast Fourier Transform (FFT) is a highly efficient algorithm for computing the Discrete Fourier Transform and was first developed in the 1960s[13].

The exact relationship between the highest frequency applied by the load (the cut-off frequency) and smallest target size detectable depends upon the test material, but for concrete the cut-off frequency input will allow the detection of targets that create a profile to the wave front of approximately half a wavelength[14].

$$L = \lambda/2 \qquad \text{-------} \quad (3a)$$

and $$\lambda = V_p/f_c \qquad \text{-------} \quad (3b)$$

where

L = smallest target size (m) λ = wavelength (m) f_c = cut-off frequency (Hz)

Similarly, the minimum depth at which a target can theoretically be detected can be calculated from:

$$d = V_p/(2f_c) \qquad \text{-------} \quad (4)$$

where d = smallest depth to target (m)

Finite Element Simulation

The finite element method derives from classical structural analysis techniques. Rather than manipulating the governing equations into differential form and then solving numerically, this method divides the domain of the solution into a finite number of simple sub domains, elements, and constructs an approximation of the solution over the collection of elements[15]. The method has been used with remarkable success in many fields because of the generality of the underlying principles.

Two-dimensional finite element analyses were carried out to investigate the effect of time of contact of the impact on the results from a narrow beam. It has been shown that it is possible to detect circular voids in a wide beam using appropriate impacts[16]. DYNPAK[17] was used to perform the analyses.

The use of DYNPAK enabled detailed analyses to be carried out, i.e. a fine mesh and short time steps could be used to minimise any mesh or aliasing effects. A narrow beam model was constructed, 300mm wide by 400mm deep containing a 100mm diameter void at a depth of 150mm. This allowed the effect of the arrival of surface wave reflections to be investigated. The time step used throughout was 0.5μs and a total of 8,192 steps were calculated. The contact times of the impacts were 50μs, 70μs and 100μs.

The following assumptions were made throughout the finite element analysis.

* Concrete behaves as a homogeneous, isotropic and elastic material. Modulus of elasticity = 31.9 GN/m^2, Poisson's ratio = 0.2, Mass density = 2214 kg/m^3.

EXPERIMENTAL PROCEDURE

Laboratory Testing

A concrete beam was cast containing 3 metal ducts with various defects: two ducts were 75mm in diameter and the third was 100mm in diameter, Fig. 3.

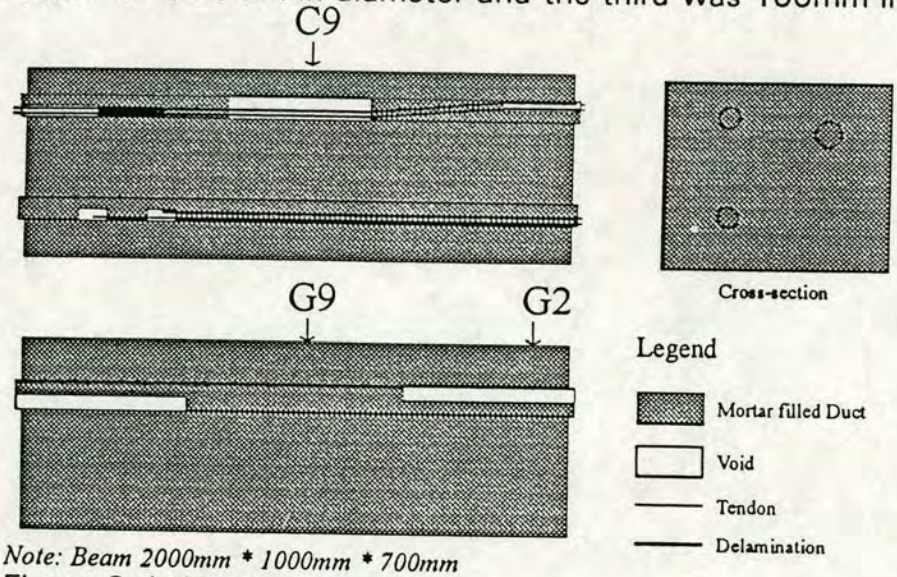

*Note: Beam 2000mm * 1000mm * 700mm*

Figure 3: Laboratory Model

The impulses were produced using different sizes of ball bearings mounted on wire. Three different diameters of ball bearing were used, 9.55mm, 6.0mm and 4.7mm. The expected contact time of each ball bearing on a concrete surface was calculated using elastic theory[18]. However, previous work indicates that the actual contact time would be longer than expected due to local crushing of the concrete[14]. The contact time would also increase due to the mounting of the ball bearings on wire. The displacement of the beam surface was measured using a NBS conical reference transducer connected to a 100kHz 2-channel FFT analyser (figure 1). Measurements were taken at three points: G9, 100mm dia. ungrouted duct at 150mm from the surface; G2, 100mm partially voided duct - void at lower side of duct - at 150mm from the surface; and C9, 75mm ungrouted duct at 100mm from the surface. An average of ten impact responses was taken for each ball bearing at each point and the frequency spectrum calculated.

Finite Element Results

Frequency spectra are shown for each analysis: by taking an 8 point average and extracting every 8th point before performing an FFT. Fig. 4a shows the result of a 50μs contact time, 4b with a 70μs contact time and 4c with a 100 μs contact time. In all the graphs the peaks corresponding to the base reflection and surface wave reflection can be clearly seen: 4a and 4b show a clear reflection at the expected frequency of the void. This reflection is difficult to distinguish on 4c. Fig. 5 shows the displacement trace for the 50μs contact time. The initial trough corresponds to the contact time of the impact.

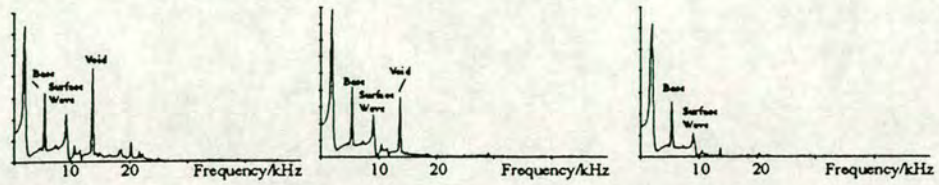

4a. tc = 50 us 4b. tc = 70 us 4c. tc = 100 us

Figure 4. Finite Element Frequency Spectra

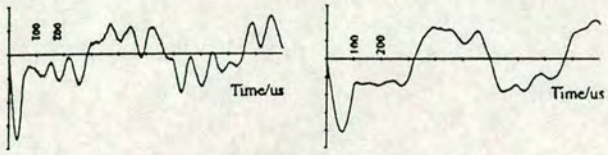

5a: tc = 50 us 5b: tc = 100 us

Figure 5. Finite Element Displacement / Time Traces

Laboratory Results

The displacement results show a similar initial downwards pulse to the results from the F.E. analyses. The contact time of the average hammer impact can then be estimated from the displacement plot. The usable frequency range on the output can then also be estimated. Table 1 shows the estimated contact times.

Impact	Ball bearing	contact time	1/tc
G9	4.7	62	16.2
	6.0	70	14.3
	9.55	100	10.0
G2	4.7	85	11.8
	6.0	117	8.6
	9.55	125	8.0
C9	4.7	62	16.2
	6.0	70	14.3
	9.55	109	9.2

Table 1: Estimated contact times and corresponding usable frequencies.

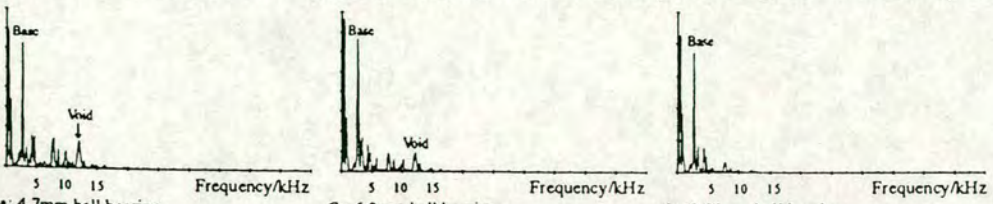

6a: 4.7mm ball bearing 6b: 6.0mm ball bearing 6c: 9.55mm ball bearing

Figure 6. Frequency Spectra from position G9

The frequency traces obtained with each ball bearing are shown in figure 6. The base reflection can clearly be seen in each trace. The expected frequency peak corresponding to the reflection from the voided duct can be seen on traces 6a and 6b (12kHz). This peak cannot be resolved on trace 6c as the 9.55mm ball bearing does not produce sufficient energy at that frequency level.

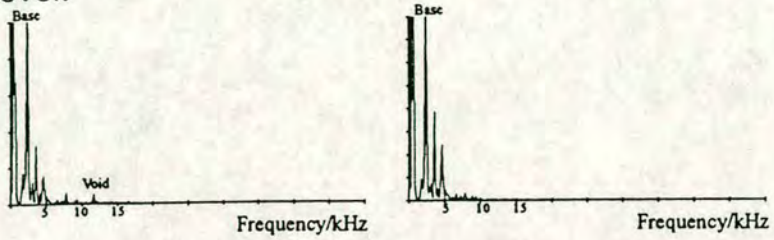

7a: G2, 4.7mm ball bearing 7b: G2, 6.0mm ball bearing

Figure 7. Frequency Spectra from position G2

Fig.7 shows the frequency plots obtained from position G2: 7a using the 4.7mm ball bearing and 7b using the 6.0mm ball bearing. The tendon duct directly below position G2 is: 100mm dia.; depth of 150mm; and is partially grouted with the void in the lower half of the duct. Fig. 7a shows a small peak at 11.5kHz corresponding to a small reflection from the voided duct. Fig. 7b shows no such peak as the 6.0mm dia. ball bearing lacked sufficient energy at that frequency. The results from the 9.55mm dia. ball bearing showed no peak at this frequency.

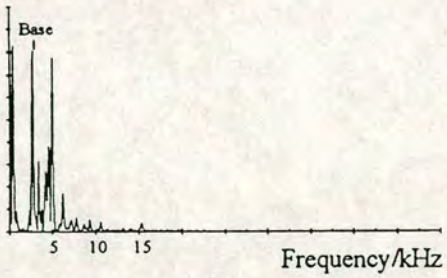

C9, 4.7mm ball bearing

Figure 8. C9 Frequency Spectrum - 4.7mm ball bearing

The frequency trace obtained at position C9 using the 4.77mm diameter ball bearing is shown in Fig. 8. Again the base reflection is evident. However, the expected peak corresponding to the voided tendon duct is at 20 kHz. No peak can be seen on this trace as, again, insufficient energy has been introduced to the beam at this frequency.

DISCUSSION

Results from the F.E. analysis clearly show that, for an idealised concrete beam, defects can be detected. It is possible to detect voiding in narrow beams. The surface wave reflections are detected but can easily be identified. The contact time is important and the highest frequency detectable is approximately equal to 1/contact time. Therefore the void could be detected in the first two analyses (tc = 50 μs, 70 μs) and could not be readily detected in

the final analysis (tc = 100 μs). These results agree with previous F.E. investigations[16]. A 2-D idealised concrete beam was modelled for the F.E. analyses discussed in this paper. The results found must then be related to experimental results from real concrete beams.

The results from position G9 show a distinct peak corresponding to the 100mm diameter voided duct at a depth of 150mm. This peak is evident on the traces produced by the 4.7mm and 6.0mm diameter ball bearings, but cannot be seen on the trace produced by the 9.55mm ball bearing. This agrees with the findings from the F.E. simulation. The maximum frequency introduced to the beam by the 9.55mm ball bearing was too low to detect the void. Defects can be found at frequencies up to 1/contact time - see table 1. Other peaks are apparent on the frequency spectra, due to reflections from other targets within the beam model.

The results at position G2 from the 4.7mm ball bearing show a small peak corresponding to the reflection from the partially filled duct. The amplitude of this reflection is small. The profile of this defect is smaller than that of the void at position G9 - figure 5. The approximate contact time is also higher than that at position G9, resulting in a lower maximum frequency.

Insufficient energy is introduced to the beam by any of the ball bearings to detect the 75mm diameter void at a depth of 100mm.

The results show that defects can be detected in real concrete beams. However, the results from a single test would be difficult to analyse without prior knowledge of the beam components. A more practical method when testing a real concrete beam would be to test an array of points and compare the findings from each point. Detailed plans of the beam would also be very useful where available. Radar could be used to detect the position of the metal ducts.

CONCLUSIONS

1. Cylindrical defects can be detected in idealised narrow beams. The surface wave is shown in the results but can be identified.
2. The contact time can be estimated from the displacement trace for both finite element analysis and experimental testing.
3. The maximum frequency that can be detected by both finite element analysis and experimental testing is approximately 1/contact time.
4. Cylindrical defects can be detected in real concrete models but care must be taken when analysing the results.

ACKNOWLEDGEMENTS

The authors acknowledge the University of Edinburgh for providing the facilities necessary to carry out the analyses, the Engineering and Physical Sciences Research Council and Ove Arup and Partners for providing financial support.

REFERENCES

1. Press Notice No. 260. Published by DTP, London, 1992
2. Storrar, D.B. (1993) The management of post-tensioned grouted-duct bridges owned by the Dept. of Transport, *Proc. 5th Int. Conf. Structural Faults & Repair-93*, Engineering Technics Press, Edinburgh, Vol1, 3-7.
3. Woodward, R. J. (1993) *Inspection of Post-tensioned Concrete Bridges - Non-destructive Testing Methods.* TRL, Crowthorne, UK.
4. Stain, R. T. and Dixon, S. Inspection of Cables in Post-tensioned Bridges - What Techniques are Available. *Proc. 5th Int. Conf. Structural Faults & Repair-93*. Engineering Technics Press, Edinburgh. Vol 1, 297-300.
5. Cooke RS, Ashurst DM, McCavitt N & Forde MC (1993) Digital radar assessment of Besses o' th' Barn Post-tensioned precast concrete segmental rail bridge. *Proc. 5th Int. Conf.: Structural Faults & Repair-93*. Engineering Technics Press, Edinburgh. Vol 1, 305-311.
6. Carino, N. J. Sansalone, M. and Hsu, N. N. (1986) A Point Source-point Receiver, Pulse-Echo Technique for Flaw Detection in Concrete. *ACI Journal* , March-April 1986, Vol. 83, No. 2, 199-208.
7. Carino, N. J. Sansalone, M. and Hsu, N. N.(1986) Flaw Detection in Concrete by Frequency Spectrum Analysis of Impact-Echo Waveforms, *International Advances in Nondestructive Testing*, 1986, Vol. 12, 117-146.
8. Ghorbanpoor, A. (1993) Evaluation of Post-tensioned Concrete Bridge Structures by the Impact-Echo Technique. *U.S. Dept. of Transportation, Federal Highway Administration, Publication No.FHWA-RD-92-096*, Dec.
9. Sansalone, M. and Carino, N. J. (1988) Detecting Honeycombing, the Depth to Surface Opening Cracks and Ungrouted Ducts using the Impact-Echo Method. *Concrete International*, April 1988.
10. Cheng, C. and Sansalone, M. (1993) The Impact-Echo Response of Concrete Plates Containing Delaminations - Numerical, Experimental and Field studies. *Materials and Structures*. Vol. 26, No. 159, 274-285.
11. Fegen, I., Forde, M.C. & Whittington, H.W. (1979) The Detection of Voids in Concrete Piles using Sonic Methods. *Proc. 4eme Colloque International sur les methodes de controle non destructif*, Grenoble, Sept 1979, 40-46.
12. Papoulis, A. (1977) Signal Analysis, McGraw-Hill, Singapore, pp 431.
13. Lynn, PA & Fuerst W (1989) *Introductory Digital Signal Processing with Computer Applications*, John Wiley & Sons, Chichester, England, pp 371.
14. Martin, J. & Forde, M.C. (1995) Influence of concrete age and mix design on impulse hammer spectrum and compression wave velocity. *Construction and Building Materials* (in press) 1995.
15. Becker, E. B. Carey, G. F. and Oden, J. T. (1981) *Finite Elements - An Introduction*, Vol.1, Prentice - Hall, Inc. Englewood Cliffs, N.J., pp 258.
16. Martin, J., Hardy, M. S. A., Usmani, A. S. and Forde, M. C. (1995) Quantifying the defects in post-tensioned bridges using impulse ultrasonics. *Proc 6th Int. Conf.: Structural Faults & Repairs-95*. Engineering Technics Press, Edinburgh. Vol 1. 209 - 216
17. Owen, D. R. J. and Hinton, E. (1980*) Finite Elements in Plasticity: Theory and Practice*, Pineridge Press limited Swansea, U.K. 594pp.
18. Goldsmith, W. (1980) *Impact, the theory and physical behaviour of colliding solids.* Edward Arnold, London, 379pp.